

**ADVANCED TECHNOLOGY FOR
LARGE STRUCTURAL SYSTEMS**

Lehigh University

**Residual Strength and Repair of Damaged and Deteriorated
Offshore Structures**

Area One

**CORROSION DAMAGE -- EFFECT ON STRENGTH
TUBULAR COLUMNS WITH PATCH CORROSION**

By
A. Ostapenko
T. W. Berger
S. L. Chambers
M. F. Hebor

Research Sponsored by

**Exxon Production Research Company
Minerals Management Service (U.S. Dept. of the Interior)
(Technical Assessment and Research Branch)
Mobil Technology Company
Shell Offshore, Inc.**

ATLSS Report No. 96-01

**August 1996
[Distribution restricted until September 1997]**

**ATLSS Engineering Research Center
Lehigh University
117 ATLSS Dr., Imbt Laboratories
Bethlehem, PA 18015-4729
(610) 758-3525**

An NSF Sponsored Engineering Research Center

DISCLAIMER

This report has been reviewed by the Minerals Management Service and other Sponsors and approved for publication. Approval does not signify that the contents necessarily reflect the views and policies of the Sponsors, nor does mention of trade names or commercial products constitute endorsement or recommendation for use.

TABLE OF CONTENTS

	Page
ABSTRACT	ix
1. INTRODUCTION	1-1
1.1 Project Organization	1-1
1.2 Research on Tubular Columns with Patch Corrosion	1-1
1.3 Outline of the Project	1-3
2. MEASUREMENT OF GEOMETRICAL PROPERTIES OF SALVAGED SPECIMENS P1-C1 TO P4-C2	2-1
2.1 Thickness Measurements	2-2
2.1.1 Thickness Measurement Procedure	2-2
2.1.2 Micrometer Readings	2-3
2.1.3 Measurement of Thickness with Ultrasonic Testing Equipment	2-3
2.2 Pre-test Measurements	2-4
2.3 Post-test Measurements	2-5
3. MATERIAL PROPERTIES OF SALVAGED SPECIMENS	3-1
4. TEST PROGRAM OF SALVAGED SPECIMENS P1-C1 TO P4-C2	4-1
4.1 General	4-1
4.2 Instrumentation	4-1
4.2.1 Arrangement of Gages	4-2
4.2.1.1 Instrumentation of P4-C2	4-2
4.2.1.2 Instrumentation of Specimens P2-C1 and P3-C1	4-4
4.3 Epoxied Sleeve Repair of Previous Buckle in Specimen P1-C1	4-6
4.4 Test Setup and Procedure	4-8
4.4.1 Test Setup	4-8

4.4.1.1	Specimens P2-C1 and P3-C1	4-8
4.4.1.2	Specimens P1-C1 and P4-C2	4-9
5.	TESTING OF SALVAGED SPECIMENS (P1-C1 to P4-C2)	5-1
5.1	Description of Individual Tests: Short Columns	5-1
5.1.1	Specimen P2-C1	5-1
5.1.2	Specimen P3-C1	5-2
5.2	Description of Individual Tests: Long Columns	5-2
5.2.1	Specimen P1-C1	5-2
5.2.2	Specimen P4-C2	5-3
6.	BEHAVIOR OF SALVAGED SPECIMENS AND TEST RESULTS	6-1
6.1	Behavior of Specimens P1-C1, P2-C1 and P3-C1	6-1
6.1.1	Specimen P1-C1	6-1
6.1.2	Specimens P2-C1 and P3-C1	6-1
6.2	Behavior of Specimen P4-C2	6-2
6.3	Test Results	6-2
6.3.1	General	6-2
6.3.2	Thickness Variation in Corrosion Patches	6-3
6.3.2.1	Specimen P1-C1	6-3
6.3.2.2	Specimen P2-C1	6-4
6.3.2.3	Specimen P3-C1	6-5
6.3.2.4	Specimen P4-C2	6-5
7.	TESTS ON SPECIMENS WITH SIMULATED CORROSION DAMAGE (P5 TO P15)	7-1
7.1	Introduction	7-1
7.2	Layout of Specimens	7-1
7.3	Preparation of Specimen Ends	7-3
8.	INITIAL GEOMETRY OF SPECIMENS P5 TO P15	8-1

8.1	General	8-1
8.2	Diameter Measurements	8-1
8.2.1	'Pedestal' Method Using Depth Micrometer	8-1
8.2.2	'Pedestal' Method Using Dial Gage Rig	8-2
8.2.3	Six-inch Micrometer	8-3
8.2.4	'Lathe' Method	8-3
8.3	Out-of-Roundness (OOR)	8-4
8.4	Out-of-Straightness (OOS)	8-5
8.5	Conclusions	8-5
9.	CORROSION PATCHES ON TEST SPECIMENS P5 TO P15	9-1
9.1	General	9-1
9.2	Geometry of Corrosion Patches	9-1
9.3	Methods for Measuring Patch Thickness	9-2
9.3.1	Angle Method for Measuring Thickness	9-2
9.3.2	Fork Method for Measuring Thickness	9-3
9.3.3	Ultrasound Method for Measuring Thickness	9-4
9.3.4	Comparison of Methods	9-5
9.4	Patch Grinding Procedure	9-6
10.	TEST SETUP AND INSTRUMENTATION (SPECIMENS P5 TO P15)	10-1
10.1	General	10-1
10.2	End Bearing Fixtures	10-1
10.2.1	Spherical Bearing Fixtures	10-1
10.2.2	Fixed-End Bearing Fixtures	10-2
10.2.3	Cylindrical Bearing Fixtures	10-3
10.3	Strain Gage Instrumentation	10-4
10.4	Dial Gage Instrumentation	10-5
10.4.1	Specimen Dial Gages	10-5
10.4.2	Machine Dial Gages	10-5
10.5	Test Setup	10-5

11. TEST RESPONSE OF SPECIMENS	11-1
11.1 General	11-1
11.2 Static and Dynamic Ultimate Loads	11-2
11.3 Spherical Bearing Tests	11-2
11.3.1 Specimen P5	11-3
11.3.2 Specimen P5a	11-3
11.3.3 Specimen P6	11-4
11.3.4 Specimen P7	11-4
11.3.5 Specimen P8	11-4
11.3.6 Specimen P9	11-5
11.4 Fixed Bearing Tests	11-5
11.4.1 Specimen P10	11-6
11.4.2 Specimen P11	11-6
11.4.3 Specimen P12	11-6
11.5 Cylindrical Bearing Tests	11-7
11.5.1 Specimen P13	11-7
11.5.2 Specimen P14	11-7
11.5.3 Specimen P15	11-8
12. BEHAVIOR OF TEST SPECIMENS P5 TO P15	12-1
12.1 Behavior of Specimens with Spherical Bearings	12-1
12.1.1 Load-Deformation Behavior	12-1
12.1.2 Specimen Behavior from Strain Data	12-2
12.2 Problems with Spherical Bearings	12-4
12.3 Behavior of Specimens with Fixed-end Bearings	12-5
12.3.1 Load-Deformation Behavior	12-5
12.3.2 Specimen Behavior from Strain Data	12-5
12.4 Behavior of Specimens with Cylindrical Bearings	12-6
12.4.1 Load-Deformation Behavior	12-6
12.4.2 Specimen Behavior from Strain Data	12-7

13. FINITE ELEMENT ANALYSIS	13-1
13.1 Introduction	13-1
13.2 General Description of FE Models	13-2
13.2.1 Description of Shell and Beam Elements	13-2
13.2.2 Modeling of the Corrosion Patch	13-3
13.2.3 Solution Process	13-4
13.2.4 Material Properties	13-4
13.3 Finite Element (FE) Models	13-5
13.3.1 FE Models for Specimens P5 to P9	13-5
13.3.2 FE Models for Specimens P10 to P12	13-5
13.3.3 FE Models for Specimens P13 to P15	13-5
13.3.4 Combined FE Models	13-6
13.4 Comparison of Test Results with FE Analysis	13-6
13.4.1 General	13-6
13.4.2 Specimens P5 to P9 (Spherical Bearings)	13-7
13.4.3 Rotation of Spherical Bearings	13-8
13.4.4 Specimens P10 to P12 (Fixed Ends)	13-9
13.4.5 Specimens P13 to P15 (Cylindrical Bearings)	13-9
13.4.6 Combined FE Specimens	13-10
14. APPROXIMATION OF CORRODED SECTIONS	14-1
14.1 Previous Work	14-1
14.1.1 "Shifted Circles" Model	14-1
14.1.2 "Cosine Patch" Model	14-2
14.2 "Constant-Thickness Patch" Model	14-2
14.2.1 Definition of Patch	14-2
14.2.2 Geometrical Properties of Constant-Thickness Patch Model	14-3
14.2.3 Input Parameters and Modeling Considerations	14-6

14.2.4	Comparison of Cross-Sectional Properties: Thickness from "Constant-Thickness Patch" Model vs. Measured Thickness	14-8
14.3	"Linear Segments" Model	14-9
14.3.1	Definition of Model	14-9
14.3.2	Procedure for Modeling	14-10
14.3.3	Cross-Sectional Properties	14-11
15.	RESIDUAL STRENGTH OF MEMBERS WITH PATCH-CORROSION DAMAGE	15-1
15.1	Other Research and Background	15-1
15.1.1	Research at Texas A&M	15-1
15.1.2	Research by Hebor and Ricles	15-1
15.2	Study of Damage Parameters and of Their Effect on Strength	15-3
15.2.1	Selection of Parameters	15-3
15.2.2	Effect on Strength	15-5
15.2.2.1	Effect of Longitudinal Dimension of Constant-Thickness Portion b	15-5
15.2.2.2	Effect of Patch Slenderness D/t_p	15-6
15.2.2.3	Effect of Effective Width of Reduction WR	15-6
15.2.3	Effect of Area Reduction AR -- Initial Study	15-7
15.3	Effect of Relative Area Reduction a_r -- Cubic Formula	15-10
15.4	Recommendations	15-12
16.	LOCAL BUCKLING	16-1
16.1	General	16-1
16.2	Effective Area for Local Buckles	16-1
16.3	Equivalent (Modified) Thickness in Patch	16-2
16.4	Local Buckling Formulas	16-3
16.5	Local Buckling Loads for Specimens P5 to P27 (Specimens with Patch Corrosion)	16-6

17. FORTRAN PROGRAM CXS AND COMPARISON OF METHODS	17-1
17.1 Fortran Program CXS.for	17-1
17.2 Comparison of Methods	17-3
17.3 Comparison with Tests Conducted at Texas A&M	17-3
18. SUMMARY AND RECOMMENDATIONS	18-1
18.1 Summary	18-1
18.2 Recommendations	18-6
18.2.1 Recommendations for Application of Completed Research	18-6
18.2.2 Recommendations for Future Research	18-7
19. ACKNOWLEDGMENTS	19-1
20. REFERENCES	20-1
21. NOMENCLATURE	21-1
TABLES	
FIGURES	
PHOTOGRAPHS	
APPENDIX A. FORTRAN-77 PROGRAM CXS.for	A-1
A1. Introduction	A-1
A2. Input	A-1
A2.1 Input Units	A-2
A2.2 Input from Keyboard	A-2
A2.3 Input from External File	A-3

A3. Output	A-4
A3.1 Output Units	A-4
A3.2 Output to Screen and Separate File	A-4
A3.3 Output to Screen and Cumulative File	A-6
A4. Special Cases	A-6
A4.1 Sections with a Hole or Holes	A-6
A4.2 Undamaged Sections	A-6
A4.2.1 Load Applied at the Center	A-7
A4.2.2 Load Applied with Eccentricities e_x and e_y	A-7
A5. FLOW CHART for Program CXS.for	A-9
A6. Lising of Program CXS.for	A-15

ABSTRACT

Offshore oil production platforms are subject to corrosion damage, and many old platforms have deteriorated to the extent that their capacity has seriously diminished. Corrosion has been observed to be very irregular and to occur mainly on the outside surface. When the corrosion damage is relatively uniform over the surface, the member can be analyzed as a regular tube but with reduced thickness and with the strength controlled by overall column strength or local buckling. However, when the damage is mainly local with the irregular thickness reduction concentrated over a small portion of the tube (patch corrosion), the failure can develop in such a weakened area over the affected cross section leading to the collapse of the whole member. No convenient tools are presently available for analyzing the effects of such damage.

The objective of this study was to formulate a simple engineering procedure for computing the ultimate strength of tubular columns with localized patch corrosion damage. The scope was limited to short columns with one corrosion patch on the outside surface although two long-column tests were also conducted on salvaged members.

The experimental part of the research included the testing of four specimens salvaged from old platforms; two long columns (24.5 and 20.5 ft long with 10.7 and 14 inch diameters, respectively) and two short (3.3 and 6 ft long, both with $D=10.7$ inches). All four had spherical bearings to achieve pinned end conditions. In addition, tests were made on eleven (11) short specimens (12.5 to 28 inch long, all with $D=5.5$ inch) which had corrosion patches simulated by grinding. These simulated patches all had the "Constant-Thickness Patch" pattern with sinusoidal transition to the original thickness. Five specimens had spherical bearings, three cylindrical, and three were fixed-ended.

Geometrically and materially nonlinear finite element analysis (using program ABACUS) was performed on the latter 11 test specimens (with simulated patches), as well as, on additional 12 specimens so that a wider range of patch geometries would be covered. All 23 specimens were analyzed for both pinned and fixed end conditions. Comparison of the computed and the test ultimate loads and the load-deformation relationships indicated that FE analysis was sufficiently accurate, and that the analytical results may be used in parametric studies.

A parametric study using the data base consisting of the 15 experimental and 46(2×23) analytical results of this project, as well as, 18 experimental and 30 analytical results from other previous and concurrent research, led to the conclusion that the most dominant parameter influencing the ultimate strength of such tubular columns with a single corrosion patch is the reduction of the cross-sectional area caused by the patch.

Other parameters, such as, the ratio of the diameter to the reduced thickness in the patch (D/t_p) which would affect the local buckling strength, and the circumferential extent of the patch, appeared to have relatively small effect on the ultimate strength. The longitudinal dimension of the reduced thickness in the patch was found to have essentially no effect as long as it was greater than approximately one-fifth ($1/5$) of the radius.

Regression analysis of the available data with respect to the area reduction resulted in two simple 3-term formulas: one for pinned and the other for fixed ends. Since the actual tubular members are neither pinned nor fixed, a formula corresponding to the ultimate load for pinned ends increased by one-third ($1/3$) of the difference between the loads for fixed and pinned end conditions is proposed as an engineering design formula. In comparison with the available experimental loads, this design formula gives a correlation within approximately 15%.

It was found that the very irregular variation of the thickness in field-corroded (salvaged) members around the circumference can be conveniently represented by a series of segments with linear thickness variation. This idealization was used as the basis for developing an interactive computer program for determining the loads according to the following five criteria:

- (1) Initial yielding anywhere in the cross section.
- (2) Local buckling in the corrosion patch according to the API Specification.
- (3) Local buckling in the corrosion patch according to the DnV Specification.

[The effect of load eccentricity is taken into account for these three cases.]

- (4) The value from the proposed approximation formula for the design load.
- (5) The ultimate load from the approximation formula for pinned ends.

Outside clamped-on sleeves with Epoxy interface were found to be an effective method for repairing tube segments with patch corrosion damage and/or local buckles.

It is recommended that future research address the following topics:

- 1) Extension of the proposed formula to include a refinement for the effect of other parameters besides the area reduction, such as, D/t_p , the mean circumferential extent of the patch, and the degree of damage beyond the maximum of 35% of the area reduction used in the current study.
- 2) The effect of length and end conditions.
- 3) The effect of multiple corrosion patches since they give a more realistic representation of the actual patterns of corrosion damage.

1. INTRODUCTION

1.1 Project Organization

This Joint Industry Project "Residual Strength and Repair of Damaged and Deteriorated Offshore Structures" at Lehigh University covered the following three areas of research:

Area One -

"Corrosion Damage -- Effect on Strength"

with Dr. Alexis Ostapenko, Principal Investigator

Area Two -

"Corrosion Damage -- Assessment in the Field"

with Dr. Stephen P. Pessiki, Principal Investigator

Area Three -

"Repair of Dented Tubular Columns -- Whole Column Approach"

with Dr. James M. Ricles, Principal Investigator

This report describes the research conducted in Area One on the general topic entitled "Tubular Columns with Patch Corrosion".

1.2 Research on Tubular Columns with Patch Corrosion

Tubular circular steel members are used as structural components in offshore structures because they are symmetrical and have equal strength in all directions and offer least resistance to wave action. Exposure to harsh marine environment causes corrosion damage in these members. The effect of this damage is a reduction in strength of the

members which must be determined in order to accurately evaluate the safety of the structure.

It has been found that corrosion damage occurs primarily in two forms: uniform corrosion over the entire surface of the member, and localized, or patch, corrosion which affects only small portions of the tube surface. Prior research on uniformly corroded tubular members indicated that the ultimate load can be readily determined by analyzing them as tubular members with constant, but reduced, thickness according to currently available design procedures.[2,8] It is more difficult, however, to determine the strength of members damaged by patch corrosion, and this is the topic of this study.

Ostapenko found previously that patch corrosion causes a modification in the distribution and magnitude of stresses in the vicinity of the damaged area, and may result in the development of local buckles depending on the effective D/t ratio in the patch, the yield stress and the corrosion patch geometry.[8] It was also found that the post-ultimate strength of members decreases more rapidly if local buckling develops at a stress level below yielding than if the section yields prior to local buckling. The tests of patch corroded members also revealed that local buckling developed only if the damaged area extended sufficiently for forming local buckles.[8]

The tests conducted at Texas A&M University on field-corroded salvaged tubular members included some specimens that failed by local buckling in corrosion patches.[9] Although the reported data are rather sketchy, the results were considered in the study of the current project.

Research by Hebor and Ricles concurrent with this study included tests and FE analysis of short tubular members with patch corrosion of sinusoidal variation simulated by grinding.[5,10] However, the study was limited to the degree of damage which led to the initiation of yielding prior to local buckling. The results of that work were included in the current study to supplement the data base.

The project described here included four tests on corroded tubes salvaged from decommissioned platforms. Two tests were on long columns, while the other two were on short specimens. In addition, eleven short specimens were tested with the corrosion damage simulated by grinding. To provide greater flexibility in modeling the geometry of corrosion patches in actual members, the geometry of the patch was defined by a portion of constant thickness with a sinusoidal transition to undamaged portions. The values of the controlling parameters of the patch were selected to specifically look into the effect of local buckling developing before the ultimate load.

The experimental observations and strain gage readings and the output from finite element analysis were used to pinpoint the initiation of local buckling and its effect on the ultimate load. Finite element analysis was performed on twelve additional cases in order to expand the ranges of patch geometry. The tests and the finite element analysis were used to also evaluate the effect of the end conditions-- pinned or fixed.

A parametric study of all the available results from this project and other sources led to a derivation of an approximate "engineering type" formula for estimating the ultimate capacity of patch corroded tubular columns typical for offshore structures.

A FORTRAN-77 program was prepared to facilitate computation of the capacity of tubular members with patch corrosion using the strength limitations by the following criteria: first yielding in the cross section, local buckling according to the API and DnV Specifications, and the ultimate strength from the formula developed in this study.

1.3 Outline of the Report

Separate groups of chapters deal with the material relevant to salvaged test specimens and test specimens with patch corrosion simulated by grinding.

Chapters 2 to 6 describe the specimens, instrumentation, testing procedure and the results of the four specimens made from field-corroded salvaged tubes.

Chapters 7 to 12 describe the eleven test specimens with the patch corrosion damage simulated by grinding. All of them were made from one original tube. The corrosion damage had the "constant-thickness patch" pattern with various values of patch parameters, and three types of end fixtures were used: spherical, fixed and cylindrical. Preparation of the specimens, instrumentation and test observations are presented.

Chapter 13 gives the details of the finite element analysis of the eleven test specimens and compares the computed values with the test results. Twelve more specimens were analyzed to extend the ranges of damage parameters.

Chapter 14 presents the models that were used for approximating the irregular pattern and thickness variation in field corroded tubular members. Specifically, two thickness variation models for cross sections through the patch are detailed.

Chapter 15 outlines the procedures employed to develop simplified formulas for computing the axial strength of tubular columns with patch corrosion damage.

Chapter 16 addresses the problem of local buckling in the corrosion patches, observations from tests and finite element analysis, and the approach which was found to be convenient for engineering application.

Chapter 17 briefly describes the FORTRAN computer program which was developed for analyzing irregular cross sections idealized with the "linear-segment patch" model. (A more detailed description of this program is given in Appendix A.) The chapter also gives a comparison of various methods with the test results and a discussion of the tests at Texas A&M University.

Finally, Chapter 18 summarizes the work performed in this project and lists the recommendations for the use of the developed procedures and formulas. The chapter also gives the recommendations for future research that is needed to consider extended ranges of damage and to generalize the "engineering" analysis of patch corroded columns.

2. MEASUREMENT OF GEOMETRICAL PROPERTIES OF SALVAGED SPECIMENS P1-C1 TO P4-C2

The four salvaged corroded specimens, P1-C1, P2-C1, P3-C1 and P4-C2, had the original cross-sectional and material properties of Specimens C1 and C2 of Ref. 8, and these are listed in Table 2-1. The extensions '-C1' and '-C2' designate the corresponding source specimens. Specimens P1-C1 and P4-C2 were tested as long columns. The shorter columns, Specimens P2-C1 and P3-C1, were made from Specimen P1-C1 after it was tested, and they had lengths of 40 inches ($\approx 4D$) and 72 inches ($\approx 7D$), respectively. The L/r ratio was not considered to be a factor in these tests due to the short length of the specimens.

All four specimens had local (patch) corrosion. Patch corrosion is "...corrosion only over local portions of the tube surface that limits the member strength by local buckling or an earlier yielding in the areas affected by corrosion..."[8] Patch corrosion is irregular around the circumference and leads to an amplification of stress in the thinnest area(s) where, then, yielding and/or local buckling would initiate. Early yielding may lead to subsequent local buckling in the plastic range.

All of the specimens labeled '-C1' developed local buckles and their strength was limited by localized yielding of the cross section. These three specimens all failed well below the yield load based on the original dimensions of the tube cross section. Specimen P4-C2 failed globally as a column at a larger relative load than the '-C1' specimens since the reduction in thickness of this specimen was not significant enough to induce local buckling.

2.1 Thickness Measurements

2.1.1 Thickness Measurement Procedure

After visual inspection and selection of potentially endangered areas, thickness measurements were taken by means of a micrometer and/or an ultrasonic thickness measuring device. A ± 0.001 -inch micrometer was used to take thickness measurements only in areas near the end, and an ultrasonic unit¹ was used for points away from the ends. The areas were then ranked according to the amount of thickness reduction and the extent of the corroded patch with the most severe patch being labeled 'A'. Six areas were selected for more detailed measurements on Specimen P1-C1 and three areas on Specimen P4-C2. These pre-selected areas were used as a guide for cutting Specimens P2-C1 and P3-C1 from Specimen P1-C1 after it was tested.

At each of the selected areas, a 2.0×2.0 inch grid was drawn completely around the circumference of the tube and centered on the location of minimum thickness. One to three ultrasonic thickness measurements were taken within each square. For each thickness measurement, the distance from End A of the tube (Figs. 2-1, 2-2 and 4-5a and 4-5b) and the location around the circumference from the 0° longitudinal reference line were recorded. Since visual observations and the sample thickness measurements were not fully indicative of the location of potential local buckling, thickness measurements on a more refined grid were made after the test in the area or areas where local buckles did develop.

These thickness measurements were later used to generate contour and surface plots. Program Surfer² matches the measured points exactly and creates a smooth transition surface in-between. Thickness measurements, including their longitudinal ('y' location) and circumferential ('x' location) positions, are entered into the program. Surfer then generates

¹ Epoch Model 2002 Ultrasonic Thickness Gage by Panametrics

² Golden Software Corp., Golden, CO

a function, $t_i = f(x_i, y_i)$, relating thickness, t_i , to the x and y coordinates by the use of splines, so that the thickness at intermediate points for specific x_i and y_i can be computed. Each surface plot in this study is a graphical representation of this function.

2.1.2 Micrometer Readings

Micrometer readings at the ends of the specimen were used to provide calibration of the ultrasonic measurements. To obtain reasonably accurate thickness measurements, fine-grain sandpaper was used to produce a proper "seat" for the micrometer. A proper "seat" allows the micrometer to give measurements of the actual thickness, thus excluding the layers of mill scale, rust and paint. Micrometer readings were taken at approximately two-inch intervals around the circumference. Readings at exactly the same points with ultrasonic equipment served the purpose of calibration. Table 2-2 presents the micrometer and ultrasonic measurements taken at some specific points and then used to calibrate the ultrasonic equipment.

2.1.3 Measurement of Thickness with Ultrasonic Testing Equipment

The primary advantage ultrasonic thickness equipment has over a micrometer is that measurements can be taken at any point along the specimen. A micrometer is limited to taking measurements only near open edges, such as at the ends. Also, a micrometer requires both the inside and outside surfaces of the wall to be clean, whereas the ultrasonic equipment requires only the contact surface (outside) to be clean.

Prior to measuring the thickness of the tubes, four rectangular-shaped pieces of steel, each with a different thickness representing the range of thicknesses expected, were used for calibrating the ultrasonic equipment. A ± 0.001 -inch micrometer was used to measure the thickness of the steel pieces for comparison with the ultrasound measurements. Comparative measurements at the ends of the tubes provided data for adjusting the ultrasonic unit for the type of steel measured.

The ultrasonic transducer requires a flat, smooth contact surface that is free of rust in order to ensure accurate readings. Since the transducer is roughly one-quarter of an inch in diameter, a grinder was used to provide a clean, smooth surface of this dimension at each location where an ultrasonic thickness measurement was made. The surface in areas of heavy corrosion is very irregular and pitted. Since the smallest thickness is often located within these irregular and pitted areas which the ultrasonic transducer cannot reach, the measured and smoothed thickness (Sect. 2.1.1) may actually be an upper bound of the actual smallest thickness.

Previously, the critical areas for Specimens P1-C1 and P4-C2 where the specimen wall was the thinnest were identified visually. They are indicated by the letters 'A' through 'F' and 'A' through 'C' in Figs. 2-1 and 2-2, respectively.[8] For Specimens P2-C1 and P3-C1, additional thickness measurements were taken in order to have more data for the areas susceptible to local buckling. The location of these areas relative to the original length of Specimen C1 together with the areas that were previously established is shown in Fig. 2-1.

2.2 Pre-test Measurements

Prior to the axial tests, thickness measurements were taken in areas where the expectation of local buckling was greatest. The measurement study of each suspected area was made on a 2.0 × 2.0 inch grid, and a point visually representative of the average thickness within each square was ground to a smooth surface to allow for the ultrasonic transducer. In the areas with very irregular pitted surfaces, it was sometimes impossible to grind a smooth surface within the central portion of the square and grinding was done in a more accessible portion. Photo 2-2 shows a typical grid in the vicinity of the area with a hole for Specimen P1-C1.

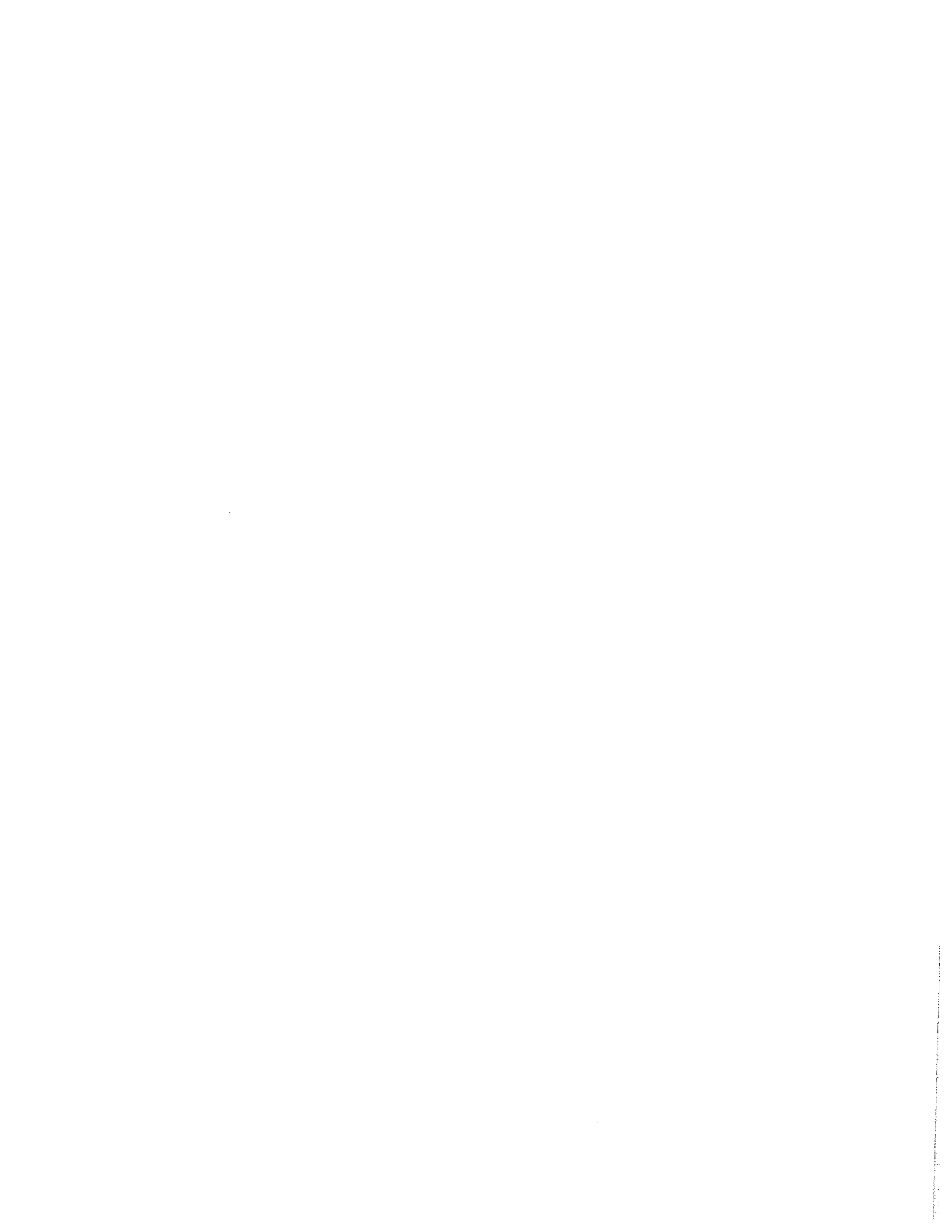
2.3 Post-Test Measurements

A finer grid was used in order to get a more accurate representation of the variation of thickness in the regions that developed local buckles. The original 2.0×2.0 inch grid was subdivided into a 1.0×1.0 inch pattern. The resultant circumferential thickness plots and contour maps of thickness variation in the areas of local buckling are described in Chapter 6.



3. MATERIAL PROPERTIES OF SALVAGED SPECIMENS

Table 2-1 summarizes the material property data previously obtained for the source Specimens C1 and C2 of Ref. 8 and valid for the current Specimens P1-C1, P2-C1, P3-C1 and P4-C2. The methodology for determining these material properties is discussed in that reference.[8] At that time, hardness measurements as well as tensile coupon tests were conducted to obtain the static yield stress and the static ultimate stress.



4. TEST PROGRAM OF SALVAGED SPECIMENS P1-C1 TO P4-C2

4.1 General

Specimens P1-C1 and P4-C2 were tested in the Baldwin 5-million pound universal testing machine.¹ Specimens P2-C1 and P3-C1 were tested in the 800-kip machine.² Spherical bearing end fixtures were used for all specimens, and they are shown in Fig. 4-1 and Photo 4-1. A 2.5 million pound capacity spherical bearing was used at the top while a 1.5 million pound spherical bearing was used at the bottom. These bearings allowed rotation of the specimen ends in any direction. The instrumentation was designed to measure the overall axial shortening, the rotation at the ends and the strain at several locations on the specimen.

4.2 Instrumentation

The labeling scheme identifying each measuring device and its location was based on longitudinal reference lines that had been established in previous tests.[8] The line of maximum convex out-of-straightness was labeled the '180 degree' line and the maximum concave out-of-straightness was labeled the '0 degree' line. The '90 degree' and '270 degree' lines were determined by going clockwise at the specimen end labeled A.(Fig. 4-2) These four longitudinal reference lines at 0, 90, 180 and 270 degrees around the circumference and the distance from the A end of the specimen uniquely identified the position of each gage.

¹Baldwin-Lima-Hamilton Corp., Philadelphia, PA

²Riehlé Testing Machine Corp., 1905

A 16-channel data acquisition system¹ using software written by the Lehigh University Fritz and Imbt Labs personnel was used for the tests of Specimens P2-C1 and P3-C1. This system could not be used for Specimens P1-C1 and P4-C2 since the long column tests required more than 16 channels. The MEGADAC Acquisition Unit² was used for these tests instead.

4.2.1 Arrangement of Gages

This section describes the placement and identification of the instrumentation used to measure strains, rotations, lateral displacement and axial shortening. The instrumentation included the following: strain gages, dial gages, LVDT's (linear voltage displacement transducers), and rotation gages.

4.2.1.1 Instrumentation of Specimens P1-C1 and P4-C2

The general arrangement of the instrumentation for Specimen P1-C1 is shown in Fig. 4-3 and Photo 2-1(a), and for Specimen P4-C2 in Fig. 4-4 and Photo 2-1(d). There were six strain gages for Specimen P1-C1 and four for Specimen P4-C2, two rotation gages, ten lateral LVDT's, two vertical LVDT's, four LVDT's used for measuring rotation at the bottom end, one vertical dial gage and two horizontal dial gages.

The ranges of the instrumentation were as follows:

The maximum stroke for twelve of the LVDT's was ± 2 in. and for the other two ± 3 in. The 3-in. stroke gages were used at Level 2 (mid-height) where most of the lateral deflection was expected. The vertical dial gages had a maximum stroke of ± 2 inches, and the lateral ± 3 inches.

¹Keithley Metrabyte Corporation, Taunton, MA, 1991.

²MEGADAC Data Acquisition Unit, OPTIM Corp., Germantown, MD

Specimen P1-C1 had two sets of three strain gages attached around the circumference at each end of the sleeved repair (see Sect. 4.3 below).(Fig. 4-3) The strain gages were placed at the 0°, 135° and 225° longitudinal reference lines two inches from the ends of the repair. These strain gages were identified by labels SGA1, SGA2, SGA3, SGB1, SGB2 and SGB3. The pattern of designation was the following: **SGA1** indicates **Strain Gage, Level A, Number 1** where **Level A** is at the top of the sleeved repair. The other set of three gages was at **Level B** at the bottom of the sleeved repair.(Fig. 4-3)

The placement of the LVDT's at the five levels along the length of the specimen provided information on the lateral movement of the specimen in any direction.(Figs. 4-3 and 4-4) The LVDT's were labeled according to the following scheme: LVDT **L3E**, for example, indicates LVDT, Level 3, East, and **L0W** indicates LVDT, Level 0, West. Level 0 and Level 4 were one diameter from each end. Levels 1 and 3 were at the quarter points, and Level 2 was at mid-length. Each level had two lateral LVDT's at a 45 degree angle with respect to the 180 degree line (one to the west, the other to the east).

Two LVDT's were used for measuring the axial shortening of the specimens, one on the east side and the other on the west. The labelling scheme for these LVDT's was **LVE** for LVDT, Vertical, East, and **LVW** for LVDT, Vertical, West. The LVDT was attached to a weighted block (to prevent any movement of the LVDT) at the bottom of the specimen. The LVDT was connected directly to the top end plate of the specimen by a small-gauge wire. To assure straightness, the wire was yielded by stretching right before the final connection.

To measure the end rotation of a specimen, two rotation gages were attached at the top. They were five inches from the top of the specimen on both the north and west sides and were labeled Tilt N and Tilt W, respectively.(Figs. 4-3 and 4-4)

Since no more rotation gages were available, four LVDT's (two for the N-S direction, two for the East-West direction) were used at the bottom to measure rotation. They were positioned vertically on the lever arms which were attached directly to the bottom of the specimens on the north and west sides.[8] Two LVDT's were placed on each lever arm, one at the end and the other next to the specimen. The difference in readings of the two LVDT's divided by the distance between them gave the rotation of the specimen in the direction of the arm. These LVDT's were labeled as: TN1, TN2, TW1 and TW2 (LVDT TN1 indicated Tilt, North, Number 1 while LVDT TW2 indicated Tilt, West, Number 2).

Finally, the dial gages were used for two purposes: 1) as a backup for the vertical LVDT measurements in case of malfunction or power failure, and 2) to provide additional data. Three dial gages were used. One 2-inch dial gage was used to measure the machine head displacement from the head to the base of the machine. The dial gage was labeled as DV1, standing for Dial gage, Vertical, Number 1. The other two dial gages had maximum strokes of 6 inches and were placed laterally at the mid-length. Both were connected to the specimen by means of a yielded wire attached to small screws tapped into the specimen wall. These two gages were labeled as LVDT L2W (LVDT at Level 2, West) and L2E (LVDT at Level 2, East).

Prior to testing, all LVDT's were calibrated on a calibration stand. All electronic sensors (strain gages -- P1-C1 only, rotation gages and LVDT's) were read and recorded using the MEGADAC Data Acquisition System and the OPUS 2000 operating software. The MEGADAC system was operated with a backup power supply in case of a power failure. The dial gages were read and recorded manually.

4.2.1.2 Instrumentation of Specimens P2-C1 and P3-C1

The general arrangement of the instrumentation for Specimens P2-C1 and P3-C1 is shown in Figs. 4-5a and 4-5b, and Photos 2-1(b) and 2-1(c). The instrumentation consisted of eight strain gages, two rotation gages, five LVDT's (linear voltage displacement transducers), and two 0.001-inch dial gages. Strain gages, rotation gages and LVDT's were

read and recorded using the data acquisition system listed in Section 4.2. The dial gages were read and recorded manually.

Specimens P2-C1 and P3-C1 used identical labeling schemes for instrumentation. Two sets of four strain gages were located at the 0°, 90°, 180° and 270° reference lines at one diameter away from the ends. These gages were identified as SG1 through SG8.

Four of five LVDT's, labeled LVDT1 through LVDT4, were attached around the bottom of the specimen, at a distance of approximately six inches away from the specimen wall. The fifth LVDT, labeled LVDT5, was used to measure the displacement between the base and head of the machine. Figures 4-5a and 4-5b, and Photos 2-1(b) and 2-1(c) show the location of LVDT5 with respect to the machine head. It was placed approximately 8 inches from the specimen surface. This reading, combined with the dial gage readings, provided the overall shortening of the specimen under load. The LVDT's were attached to the bottom base plate with magnets and connected by very thin wire to the magnets on the top end plate. LVDT5 was attached to the machine head with a C-clamp and Epoxy to ensure it would remain secure during the test.

Two rotation gages were attached to the top end plate, one at the north and the other at the east side of the plate as shown in Figs. 4-5a and 4-5b. The purpose for the placement of the rotation gages at 90° to one another was to measure rotation in any direction.

Finally, two 0.001-inch dial gages were placed on the west and east sides of the specimen as shown in Figs. 4-5a and 4-5b. These dial gages were used as a backup to LVDT5 in case of electrical failure as well as providing additional data. These dial gages were labeled DVE and DVW (DVE - for Dial Vertical East, DVW - for Dial Vertical West). Each gage was secured with a magnet to the bottom end plate and connected with a thin wire to another magnet attached to the top end plate.

4.3 Epoxied Sleeve Repair of Previous Buckle in Specimen P1-C1

Specimen P1-C1 was made from Specimen C1 which was tested in a previous research program and had developed local buckles as shown in Fig. 2-1 and Photo 4-2.[8] These buckles had to be repaired before testing Specimen P1-C1 to be able to reach a higher load than the load that caused the original buckling in Specimen C1. The use of an Epoxied sleeve was selected as the method of repair. In this method, two half circular shells are clamped over the locally-buckled damaged area with the void between the specimen wall and the shells filled with Epoxy. The shells would be bolted to each other on the sides, thus, creating a circular sleeve over the damaged portion of the tube. The sleeve should extend far enough to either side of the local buckles to develop sufficient bond strength for transmitting adequate forces over the buckled area. Photo 4-2 shows the specimen and the two sleeves before application of the Epoxy Repair.

Epoxy PC-7 was chosen because of its zero-slump consistency, ease of handling and ready availability. However, it turned out that no consistent information was available on the bond and shear strength characteristics. Thus, it was necessary to conduct some small-scale tests to determine these material properties before the sleeve could be designed.

The shells (half-sleeves) were made from a 25-inch length (approximately two diameters) of a 3/8-inch thick 12-inch diameter pipe, and the bolting lugs welded at the longitudinal edges. The installation of the repair sleeve consisted of the following five steps:

1) **Surface Preparation.** All bonding surfaces of the specimen and the repair sleeve were sandblasted down to the base metal in order to remove corrosion and paint, and create a rough surface for bonding the Epoxy.(Photo 4-2) It was necessary to keep the sandblasted specimen surface clean by blowing off the dust from sandblasting and cleaning with a solvent (e.g., Denatured Alcohol) any hand smudges or other contaminants.

2) **Test Fitting.** The sleeve was test-fitted to the specimen without Epoxy in order to check dimensions and clearances and define the position. A wooden block was clamped to the specimen to mark the longitudinal position. During the test fitting, spacers (wooden wedges) were inserted between the sleeve and the specimen to establish the proper uniform clearance. The location of the spacers was marked so that the position of the sleeve could be re-established during the final assembly with Epoxy.

3) **Mixing and Application of Epoxy.** The Epoxy was mixed in a 1:1 ratio of the A (white) and B (black) components. The process was found to be done most thoroughly by scraping the mixing board with the putty knife and 'folding' the Epoxy over onto itself until a uniform gray color was developed. To 'wet' the bonding surfaces with the Epoxy, a thin layer of approximately 1/16 to 1/8 inch was smeared to all bonding surfaces. A large mound of Epoxy was then heaped at the center of the bonding area on each half of the sleeve.

4) **Application of Sleeve Shells.** The first shell was pressed onto the surface of the specimen. As the Epoxy mound was compressed and spread out, with the excess squeezing out from the open ends and at the sides, any air pockets would also be pushed out. The small wooden spacers were inserted at their pre-marked locations to maintain the proper gap between the specimen wall and the sleeve. The shell was pressed down with a 'rocking' motion to help squeeze out the excess Epoxy and the spacers had to be checked and kept in their locations. When the first shell of the sleeve was in position, it was fixed in place with a piece of steel angle laid across the back of the shell and clamped to the specimen at both ends of the sleeve.

The second shell was then applied in the same manner. When both shells of the sleeve were matched up, the bolts were inserted and hand tightened. The position and spacers were checked, and the bolts fully tightened. Photo 4-3 shows the specimen in the testing machine with the Epoxy repair.

5) **Hardening of Epoxy.** The Epoxy allows approximately one hour of working time before it starts setting. This provides sufficient time for completing the repair. The nominal strength is reached in approximately twenty-four hours, and the specimen can be tested after this time.

4.4 Test Setup and Procedure

4.4.1 Test Setup

The installation of the specimens into the testing machine followed the same procedure for all of them. The specimen was lifted into the testing machine with the overhead crane. Next, the machine head was lowered and attached to the top of the specimen. Then, the specimen was lifted by the machine head to provide clearance for the placing of the bottom spherical fixture and aligning it. The specimen was centered and lowered onto the bottom spherical fixture. Four-inch square wooden blocks were placed between the test bed and the bottom end plate to prevent any tilting of the specimen as the machine head was lowered. At this point, all instrumentation was checked for proper functioning. Finally, the machine head and the top spherical fixture were lowered into the final position onto the top end plate. Once the top spherical fixture was properly centered on the top end plate, it was secured by driving wooden wedges between it and the lugs welded to the top end plate.

The final step was to connect all wires, LVDT's, gages and dials to the data acquisition unit and check that all were functioning properly before commencing with testing.

4.4.1.1 Specimens P2-C1 and P3-C1

The short specimens, P2-C1 and P3-C1, were tested in the 800-kip Riehlé Testing Machine¹ with one 2.5-million pound capacity spherical end fixture at the bottom and one

¹Riehlé Testing Machine Corp., 1905

with a capacity of 1.5 million pounds at the top. (Figs. 4-5a and 4-5b, and Photo 4-1) Before being placed into the machine, the specimen had a two-inch thick end plate tack welded at each end. These plates had four steel lugs welded to them to keep the spherical fixture in the center of the end plate. Small gaps between the lugs and the round end fixture allowed for minor adjustments for more refined centering.

4.4.1.2 Specimens P1-C1 and P4-C2

Both long specimens, Specimen P1-C1 and P4-C2, were tested in the five-million pound Baldwin¹ universal testing machine.

Specimen P1-C1 was made from the previously tested Specimen C1 from Ref. 8 by repairing the damage due to local buckles as described in Section 4.3. Specimen P1-C1 had a maximum out-of-straightness of 1.25", which was in the area of the buckles. Figures 4-6 to 4-9 show the out-of-straightness of Specimen P1-C1 over the full length.

Specimen P4-C2 was made from the previously tested Specimen C2 of Ref. 8 by cutting off 30 inches at the B end, thus removing the portion with local buckles. Prior to testing, Specimen P4-C2 had limited out-of-straightness as can be seen in the profiles (Figs. 4-10 to 4-13). However, after the specimen failed as a column, the total out-of-straightness became much more pronounced as shown in Fig. 4-13.

¹Baldwin-Lima-Hamilton Corp., Philadelphia, PA



5. TESTING OF SALVAGED SPECIMENS (P1-C1 TO P4-C2)

The testing procedure for the specimens was divided into the pre-ultimate and post-ultimate ranges. The pre-ultimate range was controlled by load increments while the post-ultimate range was controlled by displacement increments.

5.1 Description of Individual Tests: Short Columns

5.1.1 Specimen P2-C1

Figures 5-1 and 5-2 show the plot of load vs. shortening for Specimen P2-C1. The specimen was loaded in 15-kip increments up to a load of 60 kips. Then, the increments were doubled to 30 kips. At 150 kips, it was noticed that there was a slight drop-off of the load when the machine was stopped to take readings. Then, 20-kip load increments were used up to a load of 270 kips. At this point, the specimen had difficulty sustaining the applied loading of 270 kips and the load dropped to a static reading of 260 kips. The load was increased to 265 kips and then to 270 kips. Local buckles began to appear at this point in the area marked 'E' in Fig. 4-5a.(Photo 5-1) An attempt to increase the load up to 280 kips resulted in the static load of 268 kips. Two more attempts were made to increase the load (up to 280 kips). Each time the load immediately dropped to 268 kips, the static ultimate load. At this point, the transition was made from load increments to displacement increments. Displacement increments of 0.03 inches were taken until the total shortening of the specimen was three times that at the ultimate load. At the total shortening of 0.338 inches and the load of 231 kips, the specimen was unloaded in seven displacement decrements using the eastern dial gage as the control with steps of approximately 0.01 inches.

5.1.2 Specimen P3-C1

The load vs. average shortening curve for Specimen P3-C1 is shown in Fig. 5-3. The specimen was loaded in 20-kip increments to a dynamic ultimate load of 280 kips, which stabilized to a static ultimate load of 275 kips. The linear relationship between the load and axial shortening began to deviate at the load of 260 kips. Local buckles were observed developing in the area labeled 'C' at this point. (Fig. 4-5b and Photo 5-2) After reaching the static ultimate load of 275 kips, the specimen gradually lost strength and loading was then controlled by displacement increments of 0.02 inches. Loading continued until the total shortening of the specimen reached three times that at the ultimate condition. At the total shortening of 0.394 inches and a load of 232 kips, the specimen was unloaded in seven steps.

5.2 Description of Individual Tests: Long Columns

5.2.1 Specimen P1-C1

The static load vs. axial shortening curve for Specimen P1-C1 is shown in Fig. 5-4. The specimen was loaded in 15 kip increments to a load of 195 kips. At this point, the curve began to deviate from a straight line and then leveled off, indicating the onset of yielding. Loading continued until a dynamic ultimate load of 232.3 kips was reached. The load stabilized to a static ultimate load of 223.2 kips. Between 150 and 195 kips, 'crackling' of corrosion material could be heard, and it became more prevalent as the load approached the ultimate level. As the test continued past the ultimate load, corroded material began to flake off from the surface, indicating yielding at some locations. After the dynamic load dropped to 221 kips, displacement increments of approximately 0.07 inches were used to control the test. It was at this point that local buckling was first observed at the hole below the repair sleeve. Photo 5-3 shows these buckles near the hole. After three additional displacement increments past this point, the test was stopped at the total axial shortening of 0.29 inches and the load of 150 kips. It was decided that it would be undesirable to deform the specimen excessively since more tests on it were anticipated. The specimen was

unloaded in three decrements of 50 kips each. The tube rebounded elastically 0.2 inches, making the final axial deformation of 0.09 inches.

Figure 5-5 shows the plot of the lateral deflection at all levels for the specimen. The total lateral deflection at mid-length was 0.95 inches in the north-northeast direction. It can be seen from the figure that the largest lateral deflection was at Levels 1 and 2, located approximately 28 and 101 inches above the hole, respectively, and in the direction of the 45° line (north-northeast). The hole was located on the west face (270° line) of the specimen. As a result, it was expected that the specimen would buckle in the 90° direction. However, the specimen had significant initial out-of-straightness in the north-south direction (0°-180° line). (Figs. 4-6 to 4-9) Thus, the initial out-of-straightness of the specimen (OOS=1.23 in. at 18 ft from End A) had a greater effect on the direction of lateral displacement than the centroidal shift due to the thickness reduction in the vicinity of the hole ($e=0.88$ in.).

5.2.2 Specimen P4-C2

The static load vs. axial shortening curve for Specimen P4-C2 is shown in Fig. 5-6. The specimen was loaded in 25-kip increments to a load of 150 kips. Then, the load steps were increased to 50 kips. Between 350 and 450 kips, 'crackling' of corrosion material could be heard, and it became more prevalent as the load continued to increase. The load step was decreased between 450 kips and 575 kips to 25 kips. At this point, the static load vs. axial deflection curve was still linear. However, from 575 to 600 kips, the curve began to flatten out and the drop to the static load began to steadily increase. From 600 to 608 kips the specimen stopped accepting additional load and the flaking off of corrosion material indicated yielding was occurring in corroded areas. Starting at 608 kips, the specimen began to slowly accept more load up to a dynamic ultimate load of 635 kips, which dropped to the static maximum load of 613.65 kips. There was a large amount of flaking during this phase of loading, particularly at the south side and bottom of the specimen. There was no noticeable lateral displacement in any direction. As the load dropped from 552 kips to 500 kips, the total axial shortening grew by 1.04 inches and the southwest lateral deflection at Level 3 grew to a total of 1.91 inches. Then, the specimen was unloaded in five 100-kip

decrements with an elastic rebound of approximately 0.23 inches. Thus, the permanent axial deformation was 0.81 inches.

It was discovered in the post-test observations that a portion of the specimen cross section had ovalized in the upper half of the specimen, and the ovalization was in the southwest direction. Post-test longitudinal profiles, shown in Figures 4-10 to 4-13, indicate that most of the curvature was in the half of the specimen where the cross section had ovalized. It can be concluded that the increase in the axial shortening and lateral deflection as the load dropped from 552 kips to 500 kips was due to extensive yielding in the ovalized areas.

Figures 4-10 and 4-13 show that the initial out-of-straightness was opposite in curvature to the final out-of-straightness. Thus, it can be surmised that the centroidal shift due to thickness reduction had a greater effect on the maximum stress developed in the cross section than the initial out-of-straightness.

Figure 5-7 shows the lateral displacement for Levels 0 through 4. Most of it was in the upper half to two-thirds of the specimen. The specimen failed as a column, deflecting in the southwest direction.

6. BEHAVIOR OF SALVAGED SPECIMENS AND TEST RESULTS

6.1 Behavior of Specimens P1-C1, P2-C1 and P3-C1

Specimens P1-C1, P2-C1 and P3-C1 were all made from the same Specimen C1 tested in a previous research project and are described in Sects. 4.2 and 4.3. Thus, they all had the same material properties and original uncorroded wall thickness and diameter. Ultimate loads are provided in both kips and in non-dimensionalized form with respect to the original uncorroded yield load.

$$P_y = F_y A_{orig} \quad (6-1)$$

6.1.1 Specimen P1-C1

Specimen P1-C1 reached an ultimate static load of 223 kips, that is, at 0.53 of the yield load of the original uncorroded cross section, P_y . The specimen buckled locally around the hole, but only after some yielding had taken place in the reduced cross section. Later, local buckles also developed at the very bottom of the specimen on the east side. Specimen C1 (the source for Specimen P1-C1) reached a static ultimate load of 177 kips ($0.42P_y$). [8] At that time, the load was limited by local buckling in the weakest patch corroded area. After that area was repaired (see Sect. 4.3), Specimen P1-C1 reached a static ultimate load of 232 kips, that is, there was an increase of 31% in ultimate load.

6.1.2 Specimens P2-C1 and P3-C1

Specimens P2-C1 and P3-C1 both reached the same ultimate dynamic load, 280 kips. However, Specimen P3-C1 came down to a static ultimate load of 275 kips ($0.66P_y$) while Specimen P2-C1 had an ultimate static load of 268 kips ($0.64P_y$). The specimens failed by significant yielding of the weakened areas followed by local buckling. Both specimens sustained a higher load than Specimen P1-C1. For Specimen P2-C1, the increase in the

static ultimate load was approximately 17% and for Specimen P3-C1, 23%. In comparison to the original test on Specimen C1 of Ref. 8, the increase in the ultimate load for Specimens P2-C1 and P3-C1 was 51% and 55%, respectively.

Figure 2-1 shows that Specimen P2-C1 had more areas of heavy corrosion than Specimen P3-C1. In comparing the post-ultimate behavior of the specimens, it can be seen that the slopes of both post-ultimate curves were similar (Figs. 5-1 and 5-3).

6.2 Behavior of Specimen P4-C2

Specimen P4-C2 reached an ultimate static load of 614 kips, which is $0.85P_y$. It failed in the column mode, that is, not by local buckling as the other specimens. It appears that the amount of cross-sectional reduction in any one area was not severe enough to make local buckling govern the strength.

Specimen C2 (from which Specimen P4-C2 was made) reached a static ultimate load of 556 kips ($0.77P_y$). [8] It failed by local buckling after considerable yielding in the patch corroded area. In comparison, Specimen P4-C2 (614 kips) showed a 10% increase in ultimate load capacity after the previously buckled portion was removed.

6.3 Test Results

6.3.1 General

This section discusses the results obtained from the four patch-corroded specimens, P1-C1, P2-C1, P3-C1 and P4-C2. Three of the specimens, P1-C1, P2-C1 and P3-C1, had their ultimate strength limited by local buckling. Specimen P4-C2 failed as a column, indicating that patch corrosion did not reduce the thickness sufficiently to initiate local buckling before column-type failure.

Thickness measurements in the most-corroded areas were made by using ultrasound. These areas are marked 'A' through 'F' in Fig. 2-1 (Specimen P1-C1), 'A' through 'C' in Fig. 2-2 (Specimen P4-C2), and 'E' and 'F' in Figs. 2-1, 4-5a and 4-5b (Specimens P2-C1 and P3-C1, respectively). Results of the analysis of the thickness variation for these areas are presented in the form of tables, graphs and contour maps. In addition, out-of-straightness was examined for the long specimens P1-C1 and P4-C2.

In the later Chapters 14, 15 and 17, an idealized model of the variation of thickness around the circumference was used in the development of a simplified engineering method. This method allowed the calculation of the expected stress level and the determination of whether local buckling or first yielding would control the ultimate strength of a patch-corroded member. Currently available local buckling formulas for tubes with constant wall thickness were used to calculate the local buckling load.

6.3.2 Thickness Variation in Corrosion Patches

6.3.2.1 Specimen P1-C1

The overall view of Specimen P1-C1 in Fig. 2-1 and Photo 2-1(a), includes the location and extent of corrosion patches. To illustrate the effect of patch corrosion on the reduction of thickness around the circumference, Figs. 6-1 and 6-2 show the cross-sectional profiles of the thickness variation at the hole and where local buckling originally took place (Specimen C1 of Ref. 8), respectively. One hundred equally spaced values of thickness were used in each plot. The original, uncorroded thickness (0.385 inches) of the tube is shown in Figs. 6-1 and 6-2 by a solid horizontal line.

The area that had buckled previously during the testing of Specimen C1, is shown in Fig. 6-4. The extent of reduced thickness in this area was greater than in the vicinity of the hole as can be seen in Fig. 2-1. After repairing this buckled portion with an Epoxy sleeve (Sect. 4.3), the next weakest area was at the location of the hole. For Specimen P1-C1, local buckling occurred at this hole as shown in Photo 5-3. To more clearly illustrate the

variation of thickness in this area, a contour map and an isometric view are shown in Fig. 6-3.

6.3.2.2 Specimen P2-C1

The overall view of Specimen P2-C1 in Fig. 2-2 and Photo 2-1(b) shows the location and extent of the corrosion patches. Thickness measurements were taken before the test at End B and at what was formerly grid location 'E' for Specimen P1-C1 in Fig. 2-1 and Photo 5-1. These were the two areas where local buckling appeared to most likely occur. In fact, local buckles did develop at section 'E.' The extent of the buckles was almost entirely confined to this grid. A small amount of bulging extended above the grid, as shown in Photo 5-1. After the test, the grid was extended 5 inches above the original grid to include this bulging. Measurements were then taken over the entire extent of these buckles. The original 2.0×2.0 inch grid was subdivided into a finer 1.0×1.0 inch grid in order to produce a more accurate representation of the thickness variation in the buckled area. Figure 6-5 shows the thickness variation around the circumference 2 inches from End A, where no local buckles developed. The original uncorroded thickness is shown as a straight solid line.

Figures 6-6, 6-7 and 6-8 show the thickness variation around the circumference in the three areas that buckled 25, 23 and 22 inches from End A, respectively. The corrosion patch extended around the whole circumference. The reduction in thickness at the thinnest point (Buckle 2) was 67.18% with respect to the original, uncorroded thickness. Contour maps of the thickness variation in the area of local buckles are presented in Figs. 6-9, 6-10, 6-11 and 6-12. Figure 6-9 shows the contour map in the area of the specimen where local buckles did develop, with the location of these buckles shown. Comparison of Figs. 6-10, 6-11, and 6-12 with Fig. 6-5 more clearly shows this amount of thickness reduction in the areas with local buckles.

6.3.2.3 Specimen P3-C1

Figure 2-1 and Photo 2-1(c) show the overall view as well as the location and extent of patch corrosion. Thickness measurements were taken before the test at End A and at what was formerly section 'C' of the original Specimen P1-C1 as shown in Fig. 2-1 and Photo 5-2. These were the two areas where local buckling appeared to be most likely, and local buckles indeed developed at section 'C.' The extent of the buckles was entirely confined to the grid of measured thickness (2.0×2.0 inch squares) previously marked on Specimen P1-C1. To study the thickness reduction in this area more accurately, a more detailed 1.0×1.0 inch grid was generated by subdividing the original grid. For comparison purposes, thickness measurements were also taken around the circumference 67 inches from End A where no local buckles developed, and Fig. 6-13 shows the thickness variation there.

Figures 6-14 and 6-15 show the thickness variation in the two areas with buckles, 25 and 22 inches from End A, respectively. The original, uncorroded thickness is shown as a straight, solid line. The reduction in thickness at the thinnest point was 71.53% of the original, uncorroded thickness. Figure 6-16 shows the contour map in the area where local buckles did develop, with the location of these buckles shown. Contour maps of the thickness variation in the vicinity of the local buckles are shown in Figs. 6-17 and 6-18 together with the isometric views of the portions that buckled. In comparing Figs. 6-13, 6-14 and 6-15, it can be seen that the thickness reduction in the buckled areas was noticeably greater than in the unbuckled area.

6.3.2.4 Specimen P4-C2

Specimen P4-C2 had several patches of corrosion as can be seen in Fig. 2-2 and Photo 2-1(d). Utilizing the same procedure as for Specimen P1-C1, thickness measurements were taken in the areas marked 'A', 'B' and 'C', which were determined to be the areas most affected by corrosion. Since Specimen P4-C2 failed as a column, one can conclude that the thickness reduction was not severe enough or did not extend over a sufficient area to initiate failure by local buckling. Figure 6-19 shows the thickness variation for the thinnest

area. It appears to be more gradual and not as irregular as the thickness variations shown in Figs. 6-1, 6-2, 6-6, 6-7, 6-8, 6-14 and 6-15 for other specimens.

7. TESTS ON SPECIMENS WITH SIMULATED CORROSION DAMAGE (P5 TO P15)

7.1 Introduction

In addition to the four salvaged corroded Specimens P1-C1 to P4-C2, eleven specimens with corrosion damage simulated by grinding were tested. These specimens, Specimens P5 to P15, were all made from the long uncorroded Specimen P2PS and its companion stub-column P2PS-SC which were tested in a previous project and themselves were originally cut from one tube.[8] As a result, all these new specimens had the same geometrical and material properties.

The new specimens consisted of two groups, Specimens P5 to P9 which were 27 to 28 in. long and Specimens P10 to P15 which were 12.5 in. long. Specimens P5 to P9 were made from the undisturbed segments of Specimen P2PS and from Specimen P2PS-SC, and Specimens P10 to P15 from Specimens P5 to P7 after they themselves were tested. The layouts for the necessary cuts, specimen labeling and longitudinal reference lines are described next.

7.2 Layout of Specimens

Figure 7-1 shows the layout of the cuts made in Specimen P2PS which was tested in a previous project as a column with a dent at mid-length.[8] The saw cuts had to be made so that any inelastic distortions of the cross section near the dent were outside the new specimens. This consideration controlled the lengths of Specimens P5 to P8 to make them each 28 in. long. The distorted middle portion of 24 in. was not used. Also shown in the figure are the labels End A and End B which were used to differentiate between the bottom

and top ends of the specimen, respectively, during testing. These labels were transferred to the new specimens.

As shown in Fig. 7-2, Specimen P9 was cut from Specimen P2PS-SC which was originally tested as a stub-column.[8] This specimen had a buckled portion at one end, and again, the saw cut had to be made so that any inelastic distortions of the cross section would be outside Specimen P9. As a result, Specimen P9 was 27 in. long. The End A and End B labels of Specimen P2PS-SC were also transferred to Specimen P9.

Figures 7-3 to 7-5 show the location of the cuts made in Specimens P5 to P7, after testing, to make the second group of specimens, P10 to P15. Again, the saw cuts were made to remove the portion with the cross section distorted due to buckling of the corrosion patches. In the immediate vicinity of the buckle, the distortion was due to plastic deformations. However, in the areas further away from the buckle, the distortion was caused by elastic deformations, and the original geometry could be recovered upon removal of the plastically deformed buckle. As a result, Specimens P10 to P15 were made 12.5 in. long. The End A and End B labels of Specimens P5 to P8 were again transferred.

The original Specimens P2PS and P2PS-SC were cut from a manufactured tube which had been formed and then longitudinally welded during the manufacturing process. The weld seam was used as a starting location for the four longitudinal reference lines drawn along the length of the specimens.(Fig. 7-6) The line along the weld seam was labeled 'N' for north and the remaining lines, spaced at 90°, were labeled 'S' for south, 'W' for west, and 'E' for east. Four additional reference lines were used for Specimen P9 at 45 degrees from the other four lines. They were labeled 'SE', 'NE', 'NW' and 'SW', as shown with dashed lines in Fig. 7-6.

7.3 Preparation of Specimen Ends

Two methods were used to make the ends of the specimens planar for uniform load transmission: by grinding against a circular grinder (Specimens P5 to P9) and, an improved method, by milling in a lathe (Specimens P10 to P15). Although neither of these methods provided the ends perfectly perpendicular to the wall of the specimen, this was not a requirement since the end bearing fixtures readily accommodated minor deviations.

Before making the ends planar, the end plates of the original Specimen P2PS were removed by cutting through the tack welds and grinding off the remaining weld metal with a belt sander. Also, after the saw cuts were made, the roundness of the ends was restored, when necessary, by "pinching" the specimen end in a vice.

Grinding the ends of Specimens P5 to P9 involved pressing the end of the specimen against a circular grinding stone which had a slightly larger diameter. The specimen was supported so that it was perpendicular to the stone. Grinding continued until contact between the grinding stone and the specimen was all around the circumference. To check if the ends were planar, a flat, transparent plate with a slightly wetted surface was pressed against the specimen end. If contact was made, the water would be squeezed out and the variation of the end surface could be determined. Grinding was completed when the ends were acceptably planar.

The ends of Specimens P10 to P15 had to be milled since the specimens were much shorter than the others, and the ends were in close proximity to the corrosion patch. Any irregularities of the ends would cause stress concentrations which may not fully disappear in the short distance between the end and the corrosion patch. This consideration required the ends of the specimens to be more accurately flat than could be achieved through the grinding process described above. A lathe was used to mill the ends of the specimens. To support the free end of the specimen in the lathe, a cylindrical wooden block with a diameter

slightly smaller than the inside diameter of the tube was inserted into the specimen and held in place with wooden wedges at both ends as shown in Fig. 7-7. These wedges were inserted in a slow, even manner to minimize any irregular distortion of the tube. A 1/8 in. thick aluminum plate was nailed to the end of the cylindrical block as a bearing surface for the center lathe support. The other end of the specimen was clamped from the inside by the lathe chuck and the free end was centered using the procedure described later in Sect. 8.2.4. The lathe cutter was perpendicular to the specimen end, and material was removed until the cutter was in contact all around the end. The ends were checked using the same process as was used for Specimens P5 to P9.

8. INITIAL GEOMETRY OF SPECIMENS P5 TO P15

8.1 General

Specimens P5 to P15 had minor cross-sectional distortions which were present in the original tube. The surface of Specimen P9 had additional distortions since it was made from the stub column Specimen P2PS-SC.[8] Several methods were used to determine the extent of these distortions, primarily by measuring the diameter at various locations.

8.2 Diameter Measurements

The diameter of Specimens P5 to P7 was not measured, although the surface distortion of these specimens was determined by measuring the out-of-straightness (Sect. 8.4). The diameter of Specimens P8 to P15 was measured in four different ways:

1. 'Pedestal' method with depth micrometer
2. 'Pedestal' method with dial gage rig
3. Six-inch micrometer (5 to 6 in. range)
4. 'Lathe' method with dial gage rig

Whereas the first two methods could be used to measure the diameter only at the ends of the specimens, the other two methods were applicable for measuring the diameter at any location along the length of the specimens.

8.2.1 'Pedestal' Method Using Depth Micrometer

Figure 8-1 illustrates the use of a depth micrometer to measure the diameter at the end of a specimen. This method was used for Specimens P8 and P9 only. The first step was to center the specimen on the circular steel pedestal by approximately making the edge

distances equal on opposite sides at two or more locations around the circumference. A minimum of three readings were then taken 1/2 in. from the end at each reference line and then averaged. The measurements at opposite reference lines were then used to compute the diameter from

$$D_{N-S} = D_p - (m^N + m^S) \quad (8-1)$$

where

D_p is the diameter of the pedestal equal to 6.01 in.

m^N and m^S are the offset measurements at opposite reference lines (shown here as North and South)

D_{N-S} is the computed diameter of the specimen

As an example, the resultant diameters for Specimen P9 are shown in Col. C of Table 8-1.

8.2.2 'Pedestal' Method Using Dial Gage Rig

Figure 8-2 shows the use of the 0.0001-in. dial gage rig in conjunction with the circular pedestal to measure the diameter of the ends of the specimen. First, the specimen was centered on the pedestal and then at least three readings were taken 1/2 in. from the end at each reference line and then averaged. The dial gage readings were calibrated against the micrometer readings at some points, and the resultant adjustment parameter, δ_p from Eq. 8-2, was used for all other readings.

$$\delta_p = g - m \quad (8-2)$$

where g and m are, respectively, the dial gage and micrometer readings. The diameter was then calculated from Eq. 8-3

$$D_{N-S} = D_p - (g^N + g^S - 2\delta_p) \quad (8-3)$$

where

D_p is the diameter of the pedestal.

g^N , g^S are the dial gage readings on opposite sides of the specimen (here, North and South).

δ_P is the adjustment parameter computed from Eq. 8-2.

D_{N-S} is the computed diameter of the specimen.

The computed end diameters for Specimen P9 are shown in Col. D of Table 8-1.

8.2.3 Six-inch Micrometer

The third method used a micrometer with a range of 5 to 6 in. and an accuracy of 0.001 in. to measure the diameter of Specimens P8 to P15 along the specimen. These diameter measurements were used primarily in calculating the diameter from the 'Lathe' method. For Specimens P8 and P9, measurements were taken 1/2 in. from each end and at the strain gage cross sections (Sect. 10.3), and for Specimens P10 to P15, 1/2 in. from each end, at the 1/4 and 3/4-points of the specimen and at both edges of the corrosion patch just outside the ground region. The measured diameters are shown in Col. E of Table 8-1 for Specimen P9 and in Col. C of Table 8-2 for Specimen P13.

8.2.4 'Lathe' Method

For the 'Lathe' method, a lathe was used with the same dial gage rig as for the 'Pedestal' method to measure the diameter of Specimens P8 to P15 at the same locations as in the 6-inch micrometer readings. This method was ideal because, in addition to giving all the diameters, it gave the longitudinal profile and, thus, the topography of the whole specimen surface. First, End A of the specimen was clamped into the head of the lathe. The dial gage rig was attached to the movable support for the lathe cutter and positioned 1/2 in. from the free End B of the specimen. A general view of the setup is shown in Photo 8-1. The free end was centered by gently nudging the specimen until the dial gage readings for points on opposite sides of the specimen were within 0.01 to 0.02 inches of one another. Since the specimen could be rotated by turning the head of the lathe, it was possible to position the dial gage rig at any desired location around and along the specimen surface. To convert the dial gage readings to diameter values, an adjustment parameter, δ_L , was used.

$$\delta_L = \frac{1}{2} (D_m^{N-S} - (g^N + g^S)) \quad (8-4)$$

Diameter D_m^{N-S} was measured using the 6-inch micrometer at the same locations as for the dial gage readings, g^N and g^S . Parameter δ_L was computed at several locations, and then the average value was used in Eq. 8-5 to compute the diameter at other locations.

$$D_{N-S} = 2\delta_L + (g^N + g^S) \quad (8-5)$$

The resultant diameters are shown in Col. F of Table 8-1 for Specimen P9 and in Col. D of Table 8-2 for Specimen P13.

Similar readings were made on other specimens, and the resultant average values are summarized in Table 8-3 for all the remaining specimens. It can be seen there that, except for Specimens P9 and P13, the diameters are very little different among the specimens as well as from the originally measured diameter of 5.502 in.[8]

8.3 Out-of-Roundness (OOR)

Column G of Table 8-1 and Column E of Table 8-2 show the average relative out-of-roundness for Specimens P9 and P13, respectively, which were computed for each cross section from Eq. 8-6.

$$OOR = \frac{D_{max} - D_{min}}{D_{max} + D_{min}} \quad (8-6)$$

D_{max} and D_{min} are the maximum and minimum diameters computed from the 'Lathe' method, and, therefore, do not necessarily correspond to the maximum and minimum diameters of the specimen. The average relative OOR values were used to determine the extent of ovalization of the cross section.

8.4 Out-of-Straightness (OOS)

Tables 8-4 and 8-5 show the out-of-straightness (OOS) values computed using the dial gage readings from the 'Lathe' method for Specimens P9 and P13, respectively. These values represent the deviations of the centroid of the specimen from a straight line between the centroids 1/2 in. from each end of the specimen and were computed, for Specimen P9 for example, from Eq. 8-7

$$\text{OOS} = g_{0.5} + \frac{g_{26.5} - g_{0.5}}{26.5 - 0.5} (d_i - 0.5) - g_i \quad (8-7)$$

where

$g_{0.5}$ and $g_{26.5}$ are the dial gage readings in the 'Lathe' method at the ends of the specimen

g_i is the dial gage reading at a distance d_i from End A

The OOS values could have been used to determine the topography of the specimens, however, as shown in Tables 8-4 and 8-5, the deviations were too small to make this necessary.

For Specimens P5 to P7, the OOS was measured using a different procedure shown in Fig. 8-3. Here, a feeler gage was used to measure the gap between a straight edge and the specimen surface. The measurements obtained from this procedure indicated very minor distortion of the specimens.

8.5 Conclusions

It was decided, after studying the diameter, OOR and OOS measurements, that the OOR and OOS values were small enough that they could be neglected in the analysis of the specimens. To determine the effect of different diameters on the behavior, Specimen P13 was analyzed via a finite element program using both the original diameter of 5.502 in. and

the measured diameter of 5.394 in. Shown in Fig. 8-4 is a comparison of the load-displacement curves from these analyses where the difference in the ultimate load is approximately 3%. This difference was considered to be small enough to accept the results of the analysis performed with the original diameter before the diameter measurements were made, and not to repeat the calculations with the measured diameters for the remaining specimens.

9. CORROSION PATCHES ON TEST SPECIMENS P5 TO P15

9.1 General

Test Specimens P5 to P15 had corrosion patches which were simulated by manually grinding the specimen wall. In the following, the geometry of the corrosion patches, the methods for measuring thickness in the patch and the grinding procedure are described.

9.2 Geometry of Corrosion Patches

The corrosion patches on the specimens were centered 180° away from the seam weld as shown in Fig. 9-1. Thus, the effects of the surface unevenness and the residual stresses in the vicinity of the weld, were minimized. Figure 9-2 shows the geometry of the corrosion patches as defined by the following principal dimensions:

- a = length of the constant-thickness portion in the circumferential direction
- b = height of the constant-thickness portion in the longitudinal direction
- c = overall circumferential length
- h = overall longitudinal height
- t_p = wall thickness in the constant-thickness portion
- t = original wall thickness

These dimensions were varied from specimen to specimen in a certain pattern so that each specimen had a unique patch geometry as listed in Table 9-1. Specimens P5 and 5A, P6 and P7 had the same overall patch dimensions but different patch thicknesses. Specimens P8, P9 and P10 had larger patches than Specimens P5 to P7, but Specimens P8 and P9 had the same thickness as Specimens P6 and P7, respectively, and Specimen P10 had a smaller

thickness of 0.035 in. The corrosion patches of Specimens P11 and P12 were much larger in the circumferential direction, and they had the same thickness as Specimens P7 and P9. The patch of Specimen P12 also had the largest longitudinal dimension $b=1.5$ in. The patch of Specimen P13 had the same overall dimensions, a and c , as of Specimens P8, P9 and P10, but a smaller thickness. Specimens P14 and P15 had the largest sinusoidal transition dimensions, but the area reduction for these specimens was the same as for Specimens P9 and P13, respectively.

9.3 Methods for Measuring Patch Thickness

Three methods were used to measure the wall thickness in the patch during the grinding procedure: the angle method, the fork method, and the ultra-sound method.

9.3.1 Angle Method For Measuring Thickness

The angle method was used primarily to monitor the depth of the patch during grinding. The tool was constructed from a five-inch long equal-legged aluminum angle as shown in Fig. 9-3. The tip of a 0.001-inch dial gage protruded through a hole in the middle of the angle at the intersection of the legs. A dial gage fixture was used to attach the dial gage, via a C-clamp, to the smaller angle. This assembly was manipulated so that the gage bisected the angle and the circular arm of the C-clamp rested against the specimen surface keeping the gage perpendicular to the specimen. A sharply rounded tip on the dial gage stem minimized the effect of any rocking of the angle.

Before measurements were made, the dial gage was zeroed by placing the angle tool on an undisturbed portion of the specimen and setting the dial gage to a zero reading. Then, measurements of the patch depth were taken by positioning the angle over the corrosion patch with the angle parallel to the longitudinal axis of the specimen and with the dial gage tip at the desired location in the patch. The reading on the dial gage gave the depth of the

patch. The wall thickness was then the difference between the original wall thickness and the reading. For Specimen P9, however, a different procedure with two sets of readings was followed because of some unevenness of the surface of this specimen. The first set of readings (denoted g_1 in Eq. 9-1) was made prior to grinding, and the second (denoted g_2 in Eq. 9-1) after grinding. Then, the reduced wall thickness was given by the difference between the two readings subtracted from the original wall thickness:

$$t_r = t - |g_1 - g_2| \quad (9-1)$$

The angle method was also used to make the final thickness measurements. A minimum of three readings were taken at each grid point within the constant-thickness portion of the patch and then the average of these readings was the wall thickness at the given location. The angle method was the easiest and most convenient method and it could have been used for any size specimen and for corrosion patches of any size as long as the C-clamp was adjusted to fit the radius of the specimen and the angle was long enough to bridge the patch.

9.3.2 Fork Method for Measuring Thickness

The fork tool was made from three pieces of aluminum angle connected to each other with C-clamps as shown in Fig. 9-4. The fork tool can be seen in Photo 9-1 lying on top of the tested Specimens P5, P6 and P7. The cross-bar joined the inner and outer arms and was approximately 5 in. long. The inner and outer arms were both 17 in. long. A hole, large enough to accommodate the dial gage tip, was drilled through the outer leg of the fork. The dial gage was C-clamped to the outstanding leg of the fork with its stem and rounded tip protruding through the hole. A small nail with a rounded end was attached to the inner leg of the fork directly opposite the dial gage tip. The purpose for the rounded tips on the dial gage and the inside tip was to minimize the effects of small movements of the fork on the dial gage reading. A small block of wood (the pivot bar) was taped to the outer arm to be used as a pivot point during positioning of the tool.

In order to measure the wall thickness directly, the dial of the gage was set to zero when the dial gage tip and the inside tip were brought in contact. This was done while the

fork tool was held vertically by the cross-bar so that there would be no bending of the arms under their own weight during the zeroing process. As shown in Fig. 9-4, the fork tool was positioned from the top end of the specimen over the specimen wall, and the wall thickness was measured. The fork was supported by the cross-bar with one hand and at the bottom of the outer arm with the other hand. The pivot bar was placed against the outside surface of the specimen and the dial gage tip was positioned at the desired location. The fork was then lightly tilted about the pivot bar and the reading was taken as the inside tip lightly touched the inside surface of the specimen. (If the inside tip were pressed too hard against the specimen, the measurement would not be accurate.) At least three readings were taken at each grid point to obtain the averaged thickness. Periodically, the fork tool was removed from the specimen, and the zero setting checked and, if necessary, adjusted to assure the accuracy of the thickness measurements. This method was convenient for the short specimens of this series as the corrosion patches were located only a short distance from the open end.

9.3.3 Ultrasound Method for Measuring Thickness

Ultrasonic thickness measurements were taken with an Epoch Model 2002 Unit¹ which had an accuracy of ± 0.001 inches.(Fig. 9-5) The unit consisted of the transducer which transmitted and received the ultrasonic signals at the measured point and the monitor which displayed the ultrasonic wave variations and the thickness of the material. The monitor had various function keys which were used, among other things, to calibrate the equipment for the type of material being measured. The calibration was made at the ends of the specimen at the points where micrometer measurements were previously made. These locations were sanded prior to the micrometer measurements to remove the mill scale. Coupling gel was spread over the sanded points in order for the transducer to function properly. The sound-wave velocity in the material and the range of the sound-wave reflections were adjusted until the wall thickness measured ultrasonically correlated with the micrometer readings.

¹ Epoch Model 2002 Ultrasonic Thickness Gage by Panametrics

Within the corrosion patch, the final thickness measurements were conducted only in the constant-thickness portion since the cosine transition portions were too steep for the 1/4-inch diameter transducer tip. Because of the curved surface in the circumferential direction, the transducer had to be rocked back and forth at the measurement location and the minimum thickness value was recorded. Three thickness readings were taken at each grid point and the values averaged.

This method was very convenient because of the ease of use and the transportability of the equipment. As with the angle method, it can be used for specimens and corrosion patches of any size.

9.3.4 Comparison of Methods

Table 9-2 gives a sample of thickness readings for Specimen P5 which were determined from the depth measurements taken with the angle tool. The column listing the node locations refers to the numbering scheme used to map the grid points on the one-eighth inch grid (Sect. 9.4) to particular locations within the corrosion patch. The first number gives the row and the second the column on which the grid point is located. This table shows that there is very little variation, if any, between the three readings at each point. This was characteristic of all the thickness measurement methods.

Table 9-3 lists the average and standard deviation of all the thickness measurements taken in the constant-thickness portion with the three methods. The table also shows the average standard deviation for each method. The ultrasound method has the smallest average standard deviation, and thus, is the most accurate method. The difference between the ultrasonically measured thickness and the desired, or nominal, thickness, t_p , is small enough to warrant using the nominal thickness from this point on. The difference between the angle and fork methods and the ultrasound method is typically approximately 1.5%. Therefore, it can be concluded that any of the three methods could have been used to measure the patch thickness. However, because the angle method was very quick and easy to use, it is the more practical method for use during the grinding process. For salvaged specimens with

irregular patterns of corrosion, only the fork and ultrasound methods are practical. The ultrasound method is the best because of its accuracy, ease of operation and ability to access points at any distance from the ends of the tube. Its disadvantages, however, are that it requires a flat surface of 1/4 inch diameter at the point of measurement and that coupling gel must be used at the measurement points which would be very impractical during the grinding process.

9.4 Patch Grinding Procedure

As shown in Fig. 9-6, a 1x1-inch grid extending 2 in. in the longitudinal direction and 4 in. in the circumferential direction was laid out as a reference for defining the patch. Soapstone was used to draw the grid lines and the grid points were center punched so that the grid could be recreated if necessary. The patch layout lines were then drawn, initially with soapstone and then with ink.

Grinding the corrosion patches was a very time-consuming and repetitive process to achieve the required accuracy. The procedure was to repeatedly remove some material and check the remaining thickness with the angle tool until the thickness in the constant-thickness portion was within ± 0.002 in. of the desired thickness.

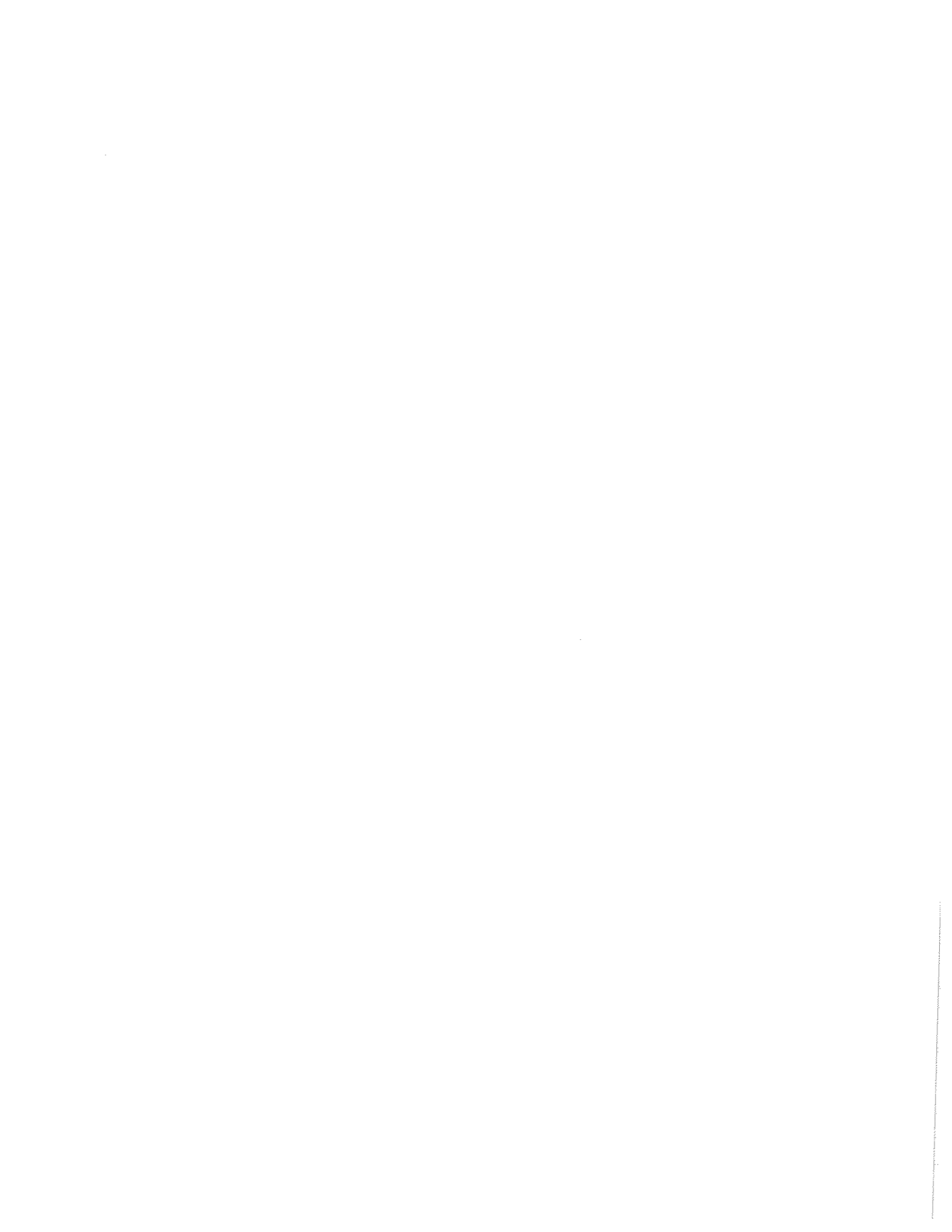
The first stage was the coarse grinding to remove the bulk of the material. The fastest way to accomplish this was to grind heavily in small areas, referred to as the initial grind zones (Fig. 9-7), and then remove the ridges between these areas. The initial grind zones adjacent to the circumferential limits were ground with the tip of the grinding stone, pictured in Fig. 9-7, overlapping the patch layout line. The initial grind zones along the circumferential layout lines were centered on the line. Placing the initial zones at these locations allowed for easier formation of the sinusoidal transitions simply by smoothening the ridge formed outside the constant-thickness portion. The transition zones were formed

by eye although later checked at the mid-point with the angle tool. All initial grind zones were ground to within 0.01 to 0.015 in. of the desired t_p .

The next stage of the grinding process was to refine the patch to achieve a smooth patch area and to have a remaining thickness within 0.001 to 0.002 in. of t_p . First, all the ridges created by coarse grinding were completely removed to make the patch smooth. Then material was removed in a much more controlled manner than before, with frequent checks of the thickness using the angle tool. Grinding continued until the thickness was within the acceptable limits.

The next step was to finish forming the transition zones by grinding them until they were smoothly looking sinusoidal curves with a mid-point depth equal to one-half the difference between t and t_p as measured with the angle tool.

In the final stage, a one-eighth inch grid was drawn over the entire patch, and thickness measurements were taken at each grid point so that grinding adjustments could be made where necessary. Photo 9-2 shows the grid for Specimen P9. All three methods for measuring thickness were used in the constant-thickness portion. In the transition portions, however, only the angle tool could be reliably used because the ultrasonic equipment works only on flat areas, and the fork tool was too awkward to use on the varying thickness. Specimens P8 and P9 with the corrosion patches completed are shown in Photo 9-3.



10. TEST SETUP AND INSTRUMENTATION (SPECIMENS P5 TO P15)

10.1 General

Three types of end bearing fixtures were used in the tests on Specimens P5 to P15 to simulate different end conditions; Specimens P5 to P9 were tested using spherical bearings which were intended to permit rotation of the ends of the specimens in any direction, Specimens P10 to P12 were tested using fixed-end bearing fixtures which prevented the ends from rotating at all, and Specimens P13 to P15 were tested using cylindrical bearings which allowed rotation of the ends in one direction only. Instrumentation consisted of dial and electric-resistance strain gages.

10.2 End Bearing Fixtures

10.2.1 Spherical Bearing Fixtures

Figure 10-1 shows a cross-sectional view of the type of spherical bearings used. The spherical contact surfaces shown in the figure were greased for easier sliding, but the first test (on Specimen P5) indicated that too much friction developed at the spherical interface, and the bearing tended to freeze under higher load. To improve the free rotation, a grinding and then a polishing compound were used to polish the contact surfaces. However, even after additional grinding and replacing the regular grease with graphite grease and, later, adding a teflon sheet in the interface, some binding still developed at higher loads, inhibiting the free rotation of the specimen ends. Figure 10-2 shows the wooden centering blocks used to aid in centering the specimen on the bearing fixture so that the load would be evenly distributed over the cross section. These blocks were used at both the top and bottom of the specimen. The wooden wedges shown in the figure secured the specimen once it was properly positioned.

The test setup with spherical bearings was started by attaching the top bearing to the machine head and placing the bottom bearing on the machine pedestal at its center. Then, the specimen was positioned with aluminum foil between the bearings and the ends of the specimen. The foil compensated for small burrs, cuts and other imperfections of the contact surfaces. The machine head was moved down until it almost touched the top end of the specimen. Centering of the specimen on the bearings was refined and the wooden wedges inserted. Then, the head was moved to make full contact with the specimen, and a 1-kip load was applied to keep the assembly securely in place.

10.2.2 Fixed-end Bearing Fixtures

The arrangement for the fixed-end bearings is shown in Fig. 10-3. A 2-inch thick circular plate with a diameter of 6 inches was used at the bottom of the specimen.(Fig. 10-3b) The thickness of 2 inches provided enough clearance for the stems of the dial gages attached near the bottom of the specimen to extend beyond the end of the specimen. A 1-inch thick 7-inch square plate was used at the top of the specimen where the only consideration was to have enough surface area to support the specimen.(Fig. 10-3a)

In the setup of the fixed-end bearings, the bottom bearing was positioned first. Figure 10-3b shows the arrangement. A sheet of plastic was placed on the machine base, then a small amount of Hydrostone, followed by another sheet of plastic. The plastic sheets prevented the hydrostone from bonding to the plate or to the testing machine surface. Then, the 6-inch diameter plate was centered on the machine base. The weight of the plate was enough to squeeze out the hydrostone, and contact between the plate and machine base was made at some three or more points. With a sheet of aluminum foil under it, the test specimen was then centered on the circular plate.

The assembly of the top bearing is shown in Fig. 10-3a. The 7-inch square plate was centered on top of the specimen which was covered with aluminum foil. Plastic sheets and hydrostone were located on top of the plate. Prior to placing the plastic and the hydrostone, the machine head was lowered to determine the location of the smallest gap between the

7-inch plate and the machine flat plate. The machine head was then raised, the plastic sheets and the hydrostone added, and the machine head lowered a second time until the smallest gap was approximately 1/16 of an inch. This was done to compensate for the possibility that the 7-inch plate and the machine flat plate were not parallel, and to insure that there would be no metal-to-metal contact. In the two hours allowed for hardening of the hydrostone, the instrumentation was connected and checked before the test was started.

10.2.3 Cylindrical Bearing Fixtures

The top and bottom fixtures of the cylindrical bearings are shown in Fig. 10-4 and Photos 10-1(a) and 10-1(b). In addition to the 6-inch diameter plate and the 7-inch square plate used for the fixed-end bearings, two more plates, another 7-inch plate and an 11-inch square plate with a 2-inch thickness, were used, as well as two half-circular 3-inch diameter cylindrical bars. Photo 10-2 gives a close-up of the cylindrical components attached with Epoxy to the end plates.

As shown in Fig. 10-4b, the 6-inch diameter plate and the 11-inch plate were used at the bottom. A 3/4-inch thick section of the 3-inch diameter steel bar was used for the cylindrical rocking surface and was attached with Epoxy to the round plate. This bar was placed precisely at the center of the round plate. The 11-inch plate served as a bearing surface for the cylindrical bearing bar. As shown in the figure, the centering blocks used with the spherical bearing fixtures were again used, but only on the bottom bearing fixture. The two 7-inch plates were used in a similar manner at the top of the specimen as shown in Fig. 10-4a. Another cylindrical bearing bar was centered on and attached with Epoxy to the lower plate, and the upper plate served as the bearing surface.

To set up the bottom cylindrical bearing fixture (Fig. 10-4b), the round plate was centered on the 11-inch plate and the end of the specimen was centered on the round plate which was covered with aluminum foil. This assembly was then centered on the machine base. No hydrostone was used at the bottom, but it was needed at the top to eliminate potential eccentricity of the load in the direction along the line of rotation. (Fig. 10-4a) The

hydrostone, plastic sheets and aluminum foil were located as shown in the figure, and the procedure used for placing the hydrostone was the same as was used for the top fixed-end bearing fixture. A specimen with cylindrical bearing fixtures and ready for completing instrumentation (Specimen P13) is shown in Photo 10-3.

10.3 Strain Gage Instrumentation

The electric-resistance strain gages used were from the Micro-Measurements Division of Measurements Group, Inc., and the procedure used to install the gages was in accordance with the directions of the manufacturer. Each specimen had 10 to 18 gages. All the strain gages were in the longitudinal direction of the specimens and were only on the outside surface. The basic arrangement of the strain gages and the gage numbering system are shown in Fig. 10-5. One row of four gages around the circumference was over the corrosion patch cross section with one gage directly at the center of the patch. These gages were intended to measure strains in the patch cross section. Another set of four gages was near the bottom end of the specimen (End A) at a distance of 5.5 inches (one diameter) for Specimens P5 to P9 and 1.25 inches for Specimens P10 to P15. The purpose of these gages was to verify the intended uniform distribution of stresses at the end of the specimen. To check the relaxation and redistribution of the stresses near the patch in the longitudinal direction, two gages were positioned one-half radius or less from the cross section with the patch. One of these gages was right below the patch and the other on the diametrically opposite side.

As shown in Figs. 10-6 and 10-7, Specimens P8 and P9 had, respectively, two and one additional cross sections with strain gages. These figures also show the gage numbering system used for Specimens P8 and P9. One of the justifications for these additional gages was to take advantage of some of the gages which were left from the parent test Specimen P2PS.[8]

10.4 Dial Gage Instrumentation

Four dial gages were used on Specimens P5 to P15. The location of these gages, shown in Fig. 10-8, was the same for all specimens. Two of the gages were attached to the specimen (specimen dials) and the other two to the testing machine (machine dials). The purpose of the specimen dials was to measure the axial shortening of the specimen and the relative end rotation. The purpose of the machine dials was to measure the downward displacement as well as the rotation of the machine head.

10.4.1 Specimen Dial Gages

The specimen dial gages were attached via screws approximately 3/8 in. from End A of the specimen to plastic brackets which were attached with Epoxy to the specimen surface. The brackets were located so that the line of action of the dial gage stems was parallel to the longitudinal axis of the specimen and in line with the South and North reference lines. Similar brackets were attached at End B, and a connecting wire was strung from them to the top of the dial gage stems.

10.4.2 Machine Dial Gages

The machine dial gages were attached to the machine base using magnets, approximately 6 in. from the surface of the specimen. Again, these gages were positioned so that the line of action of the dial gage stem was parallel to the axis of the specimen and in line with the South and North reference lines. A connecting wire connected the magnet on the machine head to the dial gage.

10.5 Test Setup

With the exception of the type of the bearing fixtures, the test setup for Specimens P5 to P15 was the same as shown in Figs. 10-9 to 10-11. Once the bearing fixtures were set up, a 1-kip load was applied, and then the specimen and machine dials were attached. The

connecting wire was stretched to yielding prior to attachment so that it would remain straight. If needed, either a weight was hung from the bottom of the dial gage stem (Fig. 10-9) or a rubber band was used to keep tension on the connecting wire.

The next step was to attach the wire leads from the strain gages to the switch box. The switch box, a Measurements Group SB-10 Switch and Balance Unit¹, was capable of maintaining ten strain gages and was used to balance each gage prior to testing, as well as, to switch from one gage to another. The switch box was then wired to the strain indicator, either a Vishay/Ellis-20 Digital Strain Indicator¹ (Specimens P5 to P9) or a P-3500 Digital Strain Indicator¹ (Specimens P10 to P15), which displayed the strain values.

As the final step in the test setup process, the outside surface of the specimen was whitewashed with the exception of the areas directly over the strain gages. Care was taken to insure that the corrosion patch was well coated. A 1/4 to 3/8 inch grid was drawn with pencil over the corrosion patch area in order to accentuate the development of buckling there. Whitewash also helped to see the buckles and the yielding outside the patch as it would crack and flake away in the areas of yielding. A view of a specimen ready for testing (Specimens P5) is given in Photo 10-4.

¹ Instruments Division, Measurements Group Inc., P.O. Box 27777, Raleigh, North Carolina 27511

11. TEST RESPONSE OF SPECIMENS

11.1 General

All Specimens P5 to P15 were tested under an axial compressive load in a displacement controlled, screw driven universal testing machine with a maximum load capacity of 120,000 pounds¹. The initial strain and dial gage readings were generally taken under a load of 1 kip. The specimens were loaded and unloaded using controlled increments of load or displacement. Dial and strain gage readings were taken at the end of each increment. The final load in all tests was 1 kip which was released after removing the dial gages and disconnecting the strain gages.

The results are presented by plots of load vs. deformation with deformation being the strain or axial shortening. A zero adjustment was made for each load vs. deformation plot by performing a linear regression analysis of the visually selected portion of the curve in the loading branch. The horizontal-axis intercept determined from this analysis was then subtracted from the deformation values for each data point. This adjusted the entire curve so that an extension of the linear portion would pass through the point corresponding to zero load and zero deformation. This adjustment may for some specimens cause the initial portion of the load-deformation curves to be to the left of the zero deformation point. The load-deformation curves were plotted with shortening treated as positive and to the right.

11.2 Static and Dynamic Ultimate Loads

Static and dynamic ultimate loads, as defined below, were recorded for each specimen because, as the machine head was very gradually moved during the test, the load increased to a predetermined value. However, near the ultimate load, deformation increased, as

¹ Tinius-Olsen Co.

observed from the motion of the needle on the dial gages and/or by the change of strain on the strain indicator, without a change in the load. This indicated that the ultimate capacity was reached, and the machine would be stopped, and the strain and dial gage readings taken. The load recorded at this point is referred to as the dynamic ultimate load (P_D). Invariably, the load gradually decreased and eventually stabilized without any observable changes of the strain or dial gage readings. This load is referred to as the static ultimate load (P_{us}).

The cause of this reduction in the load is apparently a mixture of material and machine responses. Since essentially all specimens started yielding before the static load level due to the curvature of the local buckles in the corrosion patch and elsewhere, the effect of the strain rate led to some reduction in the load even for the slow rate used in these tests. Another, albeit minor, contribution to the load reduction was made by the slow, viscous squeezing out of the grease in the threads of the machine screws after they were stopped.

11.3 Spherical Bearing Tests

Specimens P5 to P9 were tested using the spherical bearings. Loading increments were 3 to 5 kips corresponding to approximately 4% to 6% of P_y , the full plastification ("squash") load

$$P_y = AF_y = 86.8 \text{ kips} \quad (11-1)$$

where

$A = \pi(D - t)t$ is the undamaged cross-sectional area of the specimen.

The unloading increments were approximately 5 to 10 kips (6% to 12% of P_y). To limit the distortion of these specimens so that later they could be cut for reuse as additional shorter specimens, the post-ultimate axial shortening was limited to only one or two additional deformation increments beyond the ultimate load.

11.3.1 Specimen P5

The strain indicator used during the test of Specimen P5 malfunctioned and was giving incorrect readings. This was noticed from the strains since they did not correlate with the strains anticipated for the load increments. Since at the time it was impossible to take any corrective measures, the test was continued in the hope that the data could still be salvaged. Later, the source of the error was found and the readings corrected. (See Sect. 11.3.2) Specimen P5 before the test is shown in Photo 10-4.

The load-deformation curve for Specimen P5 ($t_p = 0.07$ inches) is shown in Fig. 11-2. For Specimen P5, inward motion of the constant-thickness portion of the corrosion patch was observed during the range from 57 to 62 kips, as indicated by the deviation of the strain curve from linearity toward compression in Fig. 11-1. Outward buckling of the corrosion patch started at approximately 80 kips as indicated by the sudden strain reversal into the region of tension of the curve in Fig. 11-1. Yielding outside the corrosion patch was also observed at a load of approximately 80.0 kips. The loading was continued up to the dynamic ultimate load of 84.5 kips. This ultimate load stabilized to the static ultimate load of $P_{us} = 81.5$ kips with an axial shortening of 0.063 in.

11.3.2 Specimen P5a

This was a retest of Specimen P5 with a new strain indicator. The slopes of the strain gage curves for Gages 1 to 4 of Specimens P5 and P5a were compared and a multiplier of 2.8 was determined to be used for correcting the strain readings recorded during the test on Specimen P5. Photo 11-1 shows the local buckle in the pre-test condition of Specimen P5a. The local buckle grew in the testing of P5a, and areas of yielding developed on the sides of the patch. This can be seen in Photo 11-2.

The load was applied in increments up to the dynamic ultimate load of 73.0 kips [$P_{us} = 60.5$ kips]. The curves for this test are shown in Figs. 11-1 and 11-2 together with the curves for Specimen P5.

11.3.3 Specimen P6

Photo 11-3 shows Specimen P6 before the test. Specimen P6 ($t_p = 0.05$ inches) was loaded in increments, and local buckling was observed during the range from 60 to 64 kips as indicated in the strain curve shown in Fig. 11-3. Yielding outside the corrosion patch was noticed at approximately 68 kips. A dynamic ultimate load of 76.3 kips was attained with an axial shortening of approximately 0.053 in. This value was approximated because the dial and strain gage readings were taken at the static ultimate load [$P_{us} = 73.0$ kips] and not at the dynamic ultimate load. Figure 11-4 shows the load-deformation curve for Specimen P6. The local buckle in the patch after the test is shown in Photo 11-4.

11.3.4 Specimen P7

Specimen P7 ($t_p = 0.04$ inches) was loaded in increments, and local buckling was observed during the range from 64 to 69 kips as indicated in Fig. 11-5. The specimen at the start of the test and the final view of the local buckles are shown in Photos 11-5 and 11-6, respectively. Yielding outside the corrosion patch was noticed at a load of approximately 69.0 kips. Load increments were continued to the ultimate load of 76.5 kips [$P_{us} = 73.4$ kips], and the axial shortening at the ultimate load was approximated to be 0.078 in. The load-deformation curve for Specimen P7 is shown in Fig. 11-6.

11.3.5 Specimen P8

The corrosion patch for Specimen P8 ($t_p = 0.05$ inches) was larger than for the previous specimens. However, the wall thickness in the constant-thickness portion of the corrosion patch was the same as for Specimen P6. Specimen P8 was loaded in increments, and local buckling was observed during the range from 48 to 54 kips as indicated in Fig. 11-7. Photo 11-7 shows Specimen P8 during the test. Yielding outside the corrosion patch was noticed at a load of approximately 60.0 kips. The loading increments were continued to the dynamic ultimate load of 68.6 kips [$P_{us} = 63.8$ kips] at an axial shortening of 0.087 in. Figure 11-8 shows the load-deformation curve for Specimen P8.

11.3.6 Specimen P9

The corrosion patch of Specimen P9 ($t_p = 0.04$ inches) was of the same size as the patch of Specimen P8. However, the thickness in the constant-thickness portion of the patch was the same as for Specimen P7. Specimen P9 is shown in Photo 11-8 before the test.

During the test of Specimen P9, the load indicator on the testing machine malfunctioned, and, before this was realized, a load of 54 kips was already reached. At this load, a slight buckle was already visible in the corrosion patch. The first strain and dial gage readings taken for this specimen were therefore at the load of 54 kips, and the readings for the loading path before this were lost. The specimen was unloaded in increments to a load of 10 kips and then reloaded to a dynamic ultimate load of 66.0 kips [$P_{us} = 63.0$ kips] with a 0.031 in. axial shortening. For this specimen, yielding outside the corrosion patch was observed at a load of approximately 64.0 kips. In order to avoid confusion in the presentation of the strain and deformation readings in Figs. 11-9 and 11-10, the unloading branch from 54 kips to 10 kips is shown offset by approximately 1500 microstrains (Fig. 11-9) and by approximately 0.015 in. (Fig. 11-10) from the reloading branch and the remainder of the test.

11.4 Fixed Bearing Tests

Specimens P10 to P12 were tested using the fixed bearings. These specimens were loaded, for the most part, in increments of 5 kips (6% of P_y). Smaller increments were used as the ultimate load was approached. The post-ultimate deformation range for these specimens was made much larger than for Specimens P5 to P9 using displacement controlled increments of 0.02 to 0.04 inches until the deformation was approximately three times the deformation at the ultimate load. Unloading was done using load-controlled steps of approximately 15 kips (18% of P_y).

11.4.1 Specimen P10

For Specimen P10 ($t_p = 0.035$ inches), local buckling started at approximately 40 kips as indicated by the strain readings in Fig. 11-11. However, the strain readings indicate that the corrosion patch stiffened after the initial buckling because the curve reversed at approximately 55 kips, and then the buckle continued to bulge outward at approximately 65 kips. The cause of this behavior is not clear. Yielding outside the corrosion patch was observed at approximately 65.0 kips. Loading was continued until a dynamic ultimate load of 76.0 kips [$P_{us} = 74.9$ kips] was reached with a shortening of 0.034 in. Loading continued using displacement increments to a final shortening of 0.202 in. at a load of 57.5 kips. Figure 11-12 shows the load-deformation curve for this specimen, and Photo 11-9 the final configuration of the buckled cross section.

11.4.2 Specimen P11

Specimen P11 ($t_p = 0.04$ inches) buckled locally in the patch during the range from 35 to 37 kips as indicated in Fig. 11-13. Yielding outside the corrosion patch was noticed at a load of approximately 55.0 kips. The dynamic ultimate load for this specimen was 67.1 kips [$P_{us} = 63.9$ kips] with an axial shortening of 0.031 in. Post-ultimate loading continued to a final shortening of 0.123 in. at a load of 53.7 kips. Figure 11-14 shows the load-deformation curve for this specimen, and Photo 11-10 the buckled corrosion patch.

11.4.3 Specimen P12

Specimen P12 ($t_p = 0.04$ inches) had the largest corrosion patch in the longitudinal direction (the b dimension). The local buckle developed during the range from 42 to 45 kips as indicated in Fig. 11-15. Yielding outside the corrosion patch for Specimen P12 was noticed at a load of approximately 55.0 kips. The dynamic ultimate load was 65.0 kips [$P_{us} = 61.8$ kips] with an axial shortening of 0.03 in. Loading continued using displacement increments to a final shortening of 0.139 in. at a load of 53.1 kips. The load-deformation curve for the specimen is shown in Fig. 11-16, and the final shape of the local buckle in Photo 11-11.

11.5 Cylindrical Bearing Tests

Specimens P13 to P15 were tested using cylindrical bearing fixtures, but otherwise in a similar manner as the fixed-end specimens. Loading was in increments of 5 kips (6% of P_y). Post-ultimate loading was done in displacement increments of 0.02 to 0.04 in. until the total axial displacement was approximately three times the axial displacement at the ultimate load. The specimens were unloaded in 10 kip (12% of P_y) steps down to the final load of 1 kip.

11.5.1 Specimen P13

Specimen P13 is shown in Photo 11-12 in the process of testing. The local buckle for Specimen P13 ($t_p = 0.03$ inches) developed during the range from 43 to 45 kips as shown by the strain in Fig. 11-17. The buckle was not clearly visible until one or two increments before the ultimate load was reached. The dynamic ultimate load was 60.6 kips [$P_{us} = 57.8$ kips] with an axial shortening of 0.024 in. No yielding outside the corrosion patch was observed until after the ultimate load had been reached. This behavior is different from the specimens with spherical or fixed-end bearing fixtures which experienced yielding in these areas as described above prior to the ultimate load. Loading was continued to a final shortening of 0.148 in. at a load of 44.6 kips. Figure 11-18 shows the load-deformation curve for Specimen P13, and Photo 11-13 the locally buckled cross section.

11.5.2 Specimen P14

Local buckling for Specimen P14 ($t_p = 0.04$ inches) started during the range from 45 to 50 kips as shown in Fig. 11-19. For this specimen, yielding outside the corrosion patch was noticed at approximately 60.0 kips, just before the ultimate load. Similarly to Specimen P13, the buckle was not clearly visible until just prior to the dynamic ultimate load of 63.9 kips [$P_{us} = 61.1$ kips] with an axial shortening of 0.018 in. The total axial shortening before unloading was 0.102 in. at a load of 49.5 kips. The load-deformation plot

for Specimen P14 is shown in Fig. 11-20. Photo 11-14 gives the view of the specimen after testing, and Photo 11-15 a closer view of the local buckle.

11.5.3 Specimen P15

Specimen P15 ($t_p = 0.03$ inches) had a corrosion patch of the same overall dimensions as Specimen P14, but a smaller patch thickness. The local buckle initiated during the range from 40 to 45 kips as indicated by the strain plot in Fig. 11-21. Specimen P15 yielded outside the corrosion patch at a load of approximately 55.0 kips which was, again, just before the ultimate load. The dynamic ultimate load was 60.0 kips [$P_{us} = 57.4$ kips] with an axial shortening of 0.018 in. The total axial shortening prior to unloading was 0.133 in. at a load of 45 kips. Figure 11-22 shows the load-deformation curve for this specimen. A view of the specimen before the test is given in Photo 11-16. The local buckle for this specimen, as shown in Photo 11-17, is much more "pinched" than for Specimen P14 (Photo 11-15) since it had a smaller patch thickness.

12. BEHAVIOR OF TEST SPECIMENS P5 TO P15

Since the behavior of the specimens in each group was very similar, it is described in detail for only one representative specimen from each group. The specimens described are: Specimen P6 for the specimens with spherical bearings (Specimens P5 to P9); Specimen P10 for the specimens with fixed-end bearings (Specimens P10 to P12); and Specimen P13 for the specimens with cylindrical bearings (Specimens P13 to P15).

12.1 Behavior of Specimens with Spherical Bearings

12.1.1 Load-deformation Behavior

Typical load-deformation behavior of the specimens with spherical bearings can be described by using the dial gage readings for Specimen P6 shown in Fig. 12-1¹. To clarify the plots, the curves are shifted by an amount large enough so that the curves would not interfere with one another. One characteristic of the dial gage curves for these specimens is the non-linear portion at the beginning of loading. The slope of this initial portion of the curves is typically steeper for the specimen dials (SS and SN) than for the machine dials (MS and MN), thus, indicating a smaller rate of shortening of the specimen than the displacement of the machine head. For the specimen dials, this behavior is due to a slight binding in the dials, and for the machine dials, due to the seating of the bearings, that is, crushing of the aluminum foil and other adjustments in the end fixtures. The slopes of the straight-line portions of the curves for the specimen dials are also steeper than those of the curves for the machine dials. This typical behavior can be attributed to the squeezing out of the grease on the loading screws and the longer overall distance between the machine head and base compared to the length of the specimen.

¹ Positive values represent shortening for all dial gage plots discussed in this chapter.

After the straight-line portions, the curves indicate non-linear behavior of the specimen which is due to local buckling or yielding in the corrosion patch. For Specimen P6, this non-linear response starts at approximately 60 kips, the same load at which the strains at Gages 1 to 4 show yielding (Fig. 12-2) and at which the strain in the patch (Gage 7 in Fig. 12-4) reverses from the increasing compressive values (compression corresponds to positive strain values) to the increasing tensile values (tension corresponds to negative strain values) indicating that the local buckle is bulging outward. As the ultimate load is approached, the dial gage curves, particularly the specimen and machine South curves (SS and MS), show accelerated non-linear behavior. After the ultimate load, the continued shortening of the specimen effects a decrease in the load. As expected, the slope of the unloading portion of the curves is the same as the slope of the loading portion. Near the end of the test, the curves show non-linear behavior. For the machine dials, this is due to the rotation of the machine head, and for the specimen dials, due to a sudden rotation of the spherical bearings. The cause of these rotations is described in Sect. 12.2.

12.1.2 Specimen Behavior from Strain Data

Strains for Gages 1 to 4 of Specimen P6 are shown sequentially in Fig. 12-2. For clearer presentation, the curves in this figure are shifted with respect to each other. The slopes of the loading portions (indicated by the directional arrows) are very close to each other for these four gages. This indicates that the specimen was loaded concentrically. At 60 kips, yielding occurs (curves become non-linear) with Gages 2 to 4 showing accelerated compressive strains and Gage 1 showing an accelerated decrease in compressive strain which is attributed either to the relaxation due to local buckling or the lessening of strain due to the end moments (Sect. 12.2). Again, as expected, the unloading branch of the curves has the same slope as the loading branch.

The strain plots for Gages 5 and 6 are shown in Fig. 12-3. The curve for Gage 5 becomes non-linear at approximately 40 kips, the same load at which the strain in the corrosion patch becomes non-linear (Gage 7 in Fig. 12-4). Thus, the non-linear response at Gage 5 at this load level can be attributed to the relaxation of the South side of the

specimen. At Gage 6, the strain becomes non-linear at 60 kips, the same load at which Gages 1 to 4 and the dial gages indicated a non-linear response and at which local buckling initiated (Sect. 11.3.3).

The strain plots for Gages 7 to 10 (cross section with the patch) are shown in Fig. 12-4. The gage in the corrosion patch (Gage 7) indicates elastic behavior up to 40 kips although, due to the reduced area on the patch side, the slope of the curve is shallower than that of the curves for Gages 8, 9 and 10. At 40 kips, the slope of the curve becomes much steeper and then it flattens out again up to 60 kips when the slope becomes negative due to the onset of local buckling. This type of behavior is due to the wall moving inward before it buckles outward, and this is the expected elastic response. At local buckling, the wall in the patch moves out with a rapid increase of tensile strain.

Another typical response of the patch cross section is the yielding on the sides of the patch shown in the curves for Gages 8 and 10 in Fig. 12-4. At 68 kips, both curves show accelerated non-linear behavior up to the ultimate load. One important observation is that this yielding occurred well before the ultimate load was reached. This indicates that local buckling of the corrosion patch was not enough to cause failure of this specimen, but that yielding of a significant portion of the cross section was needed in order to reach the ultimate load. The plot for Gage 9 is linear up to the ultimate load. This shows that there was no yielding on the back side of the specimen.

As the specimen is unloaded, the curves for Gages 8, 9 and 10 follow the same slope as the loading branches. The unloading branch for Gage 7 has a negative slope which is opposite to the slope of the loading branch. This is due to the strain reversal in the patch from tension during loading after local buckling, to compression as the buckle was straightening out during unloading. Thus, during unloading, the strain decreases from a larger tensile value to a smaller tensile value causing the negatively sloping curve.

12.2 Problems with Spherical Bearings

The test data for Specimen P6 indicate that moments developed at the ends. This means that the spherical bearings did not allow free rotation. As can be seen in Fig. 12-1, the data for the machine dials (MS and MN) show a larger head displacement on the South side of the specimen. The explanation for this appears to be as follows. As the corrosion patch buckled and the mid-point of the specimen displaced horizontally in the North direction, the ends of the specimen attempted to rotate, but the bearings restrained them thereby creating end moments on the specimen ends which shortened the North side of the specimen. The machine reacted to these moments in the opposite direction, and this rotated the South side of the machine head downward. The result was the difference in displacements between the North and South sides. At 20 kips on the unloading branch, the machine curve on the South side (MS) has a shallower slope. This is the result of the end moments decreasing under the smaller load and of the South side of the machine head displacing upward in larger increments. At 10 kips on the unloading branch of the specimen South curve (SS), the slope is steeper. This indicates that the bearings suddenly rotated under the smaller load, shortening the South side of the specimen.

Attempts to remedy this binding (friction) of the spherical bearings by changing the type of grease, polishing the contact surfaces and placing teflon sheets in the interface, as the specimens were tested one after another, proved to be not fully successful.

The topic of end restraints in the spherical bearings is addressed again in Chapter 15 where the relative end rotations of Specimens P5 to P9 are compared with the end rotations of the finite element models of these specimens.

12.3 Behavior of Specimens with Fixed-End Bearings

12.3.1 Load-deformation Behavior

Unlike the spherical bearings, the fixed bearings used to test Specimens P10, P11, and P12 did not allow the ends of the specimen to rotate, thus, the end moments were expected. The dial gage curves for a typical specimen, for example, Specimen P10 shown in Fig. 12-5, indicate development of the end moments. At approximately 50 kips on the loading branch, the slope of the curves for the South side dials (SS and MS) becomes smaller and the slope of the North side dials (SN and MN) becomes steeper. This can be seen to be due to the rotation of the machine head under the influence of the end moments. The larger displacement for the South side dials and the non-linear portions of the unloading branches of the curves at approximately 10 kips are also due to the head rotation. This indicates that even when the specimen is oriented so that it would have rotations at the ends in the plane of the machine head and screws, there was some rotation of the machine head, probably caused by the squeezing of the grease in the screw threads and the flexural deformation of the cross-head.

12.3.2 Specimen Behavior from Strain Data

Figure 12-6 shows the strain plots for Gages 1 to 4 for Specimen P10. The slope of the straight-line portions of the loading branches up to approximately 50 kips is the same for all four gages indicating a uniform loading of the specimen. At 50 kips, the curves become non-linear, but the slope of Gage 1 reverses, the slope of Gage 3 becomes steeper, and the slope of Gages 2 and 4 become shallower. After the ultimate load, the specimen at Gage 3 yields significantly in comparison with the other gages. The reversal of the slope of the Gage 1 curve and the increased yielding at Gage 3 are due to the end moments. The non-linearities in the unloading branches of the curves are due to the decreasing end moments.

The plot for Gage 5 in Fig. 12-7 becomes non-linear at approximately 40 kips which is the same load at which local buckling was observed in the corrosion patch

(Gage 7 in Fig. 12-8). This indicates relaxation of the South side of the specimen after local buckling. The curve for Gage 6 becomes non-linear at approximately 60 kips due to the load redistribution caused by local buckling. The unloading slope of the curve for Gage 5 is opposite to the loading slope because of the reversal of strain rate.

The strain data for Gages 7 to 10 are shown in Fig. 12-8. Again, the slope of the curve for Gage 7 is slightly shallower due to the reduced area and it is linear up to 40 kips. As for specimens with the spherical bearings, the corrosion patch moved inward (from 55 to 65 kips in the figure) before it bulged outward. Yielding on the sides of the patch (Gages 8 and 10) started at approximately 65 kips and the yielding in the vicinity of Gage 9 around 70 kips, but it was not significant until after the ultimate load. Therefore, as with Specimens P5 to P9, yielding of a significant portion of the cross section with the patch was needed in order to reach the ultimate load. Gages 8, 9 and 10 all show a large increase in compressive strain near the ultimate load and then a sudden decrease. The strain increased dramatically because the patch side of the specimen could not carry as much load as the opposite side. The sudden decrease in strain was due to the bulging outside of the corrosion patch which relieved the strain.

12.4 Behavior of Specimens with Cylindrical Bearings

12.4.1 Load-deformation Behavior

Specimens P13 to P15 were tested using cylindrical bearings which allowed essentially uninhibited rotation of the ends of the specimens as the specimens would deflect with the patch on the concave side. The dial gage curves for Specimen P13, shown in Fig. 12-9, illustrate the behavior of these specimens. Here, the South and North machine dial curves (MS and MN) are practically identical. This indicates that there was no rotation of the machine head and no end moments. The specimen South curve (SS) shows a larger degree of shortening compared to the specimen North curve (SN) which even shows a decrease in shortening near the ultimate load. This indicates the lengthening of the North

side of the specimen. These observations indicate that the specimen ends rotated without restraint. The slopes of the unloading branches of the machine dial curves are the same as the loading branch slopes. However, the unloading slopes of the specimen dials are slightly different, particularly near the end of the test where the curves become slightly non-linear. This behavior is apparently due to some minor deformation of the top bearing plate at the point of contact with the circular bearing bar (Sect. 10.2.3). This slight deformation was visually observed after the tests of all specimens with cylindrical bearings (Specimens P13, P14 and P15). As the load increased, the cylindrical bearings rotated and, at some point near the ultimate load, a slight depression in the top bearing plate was formed. Then, when the specimen was unloaded and the cylindrical bearings began to rotate back, the circular bearing bar had to rotate out of the depression, causing the specimen to shorten as indicated by the increase in the shortening for the specimen dials.

12.4.2 Specimen Behavior from Strain Data

Figure 12-10 shows the strain data for Gages 1 to 4 of Specimen P13. The initial slopes of the loading curves are the same indicating a uniform loading of the specimen. However, at approximately 40 kips, all the curves become non-linear with Gages 1 and 3 showing a decrease in compressive strain and Gages 2 and 4 showing an increase in compressive strain. After the ultimate load, the specimen yielded significantly in the vicinity of Gages 2 and 4 which were directly above the cylindrical bearing bar and the strain reversed to tensile increments in the vicinity of Gages 1 and 3. The large amount of yielding at Gages 2 and 4 indicates a stress concentration due to the cylindrical bearing bar and the strain reversal for Gages 1 and 3 indicates bending of the plate between the specimen and the bearing bar at either or both ends of the specimen. The unloading branches for Gages 2 and 4 are slightly non-linear near the end of the test due to the decrease in the stress concentration under the smaller load. Apparently, the end plates between the cylindrical bearing bars and the specimen ends were not sufficiently thick to provide more uniform distribution of the load to the specimens.

The strain plots for Gages 5 and 6 of Specimen P13 are shown in Fig. 12-11. The Gage 5 curve resembles the Gage 5 curve for the spherical and fixed-end specimens. However, the Gage 6 curve shows a strain reversal which did not occur for the other specimens. The Gage 5 curve becomes non-linear at approximately 50 kips, and local buckling initiated between 43 and 45 kips. (Gage 7 in Fig. 12-12) Thus, for the specimens with cylindrical bearings, the South side of the specimen does not relax with local buckling as was the case for the specimens with spherical and fixed-end bearings. Non-linear behavior at Gage 6 begins at approximately 55 kips, which is approximately 5 kips before the ultimate load for Specimen P13. The strain reversal at this load is due to the rotation of the specimen ends causing tensile strains on the North side of the specimen. The difference in slope of the unloading branch for each gage is due to the strain reversal, and the non-linear portion near the end of the test for Gage 6 is due to the elastic rebound of the specimen as the ends rotate back under the reducing load.

The Gage 7 to Gage 10 strain data are shown in Fig. 12-12. The Gage 7 curve (on the patch) reveals different behavior in the corrosion patch for the specimens with cylindrical bearings than for the specimens with other type bearings. The stiffening after the initial buckling experienced by the specimens with spherical and fixed-end bearings did not occur for the specimens with cylindrical bearings. Once the initial buckling took place, between 43 and 45 kips, the buckle continued to move outward. The strain readings for Gages 8 and 10 show that yielding did develop, but not until just prior to the ultimate load. Then, in the post-ultimate range, high compressive strain was followed by a sudden decrease in strain. This was due to the bulging of the specimen outside the corrosion patch as was observed during the test. At Gage 9 (opposite the patch), the specimen remained elastic (curve remained linear) until the ultimate load and then became non-linear during the post-ultimate loading. For these specimens, there was no sudden decrease in the strain on the North side of the specimen. The tensile strains exhibited by Gage 9 are due to the rotation of the specimen ends. The fact that there was no yielding outside the corrosion patch until just before the ultimate load indicates that, for the specimens with cylindrical bearings, local

buckling controlled the ultimate capacity of the specimens much more closely than for specimens with spherical or fixed bearings.

13. FINITE ELEMENT ANALYSIS

13.1 Introduction

Results of the tests on Specimens P5 to P15 were used to verify the accuracy of finite element (FE) method and the modeling techniques so that, if the method were found to be accurate, additional ranges of patch geometries could be studied by using computer rather than tests. The salvaged test specimens (P1 to P4) were not analyzed because of the complexity of the patch geometries and the uniqueness of each case which would have required a tremendous expenditure of time for modeling and would be taxing the computer resources.

The principal objectives of the FE analysis were to determine the following for comparison with the test results:

- a) Ultimate axial load.
- b) Axial load-deformation relationship in the pre- and post-ultimate ranges.
- c) Effect of the end conditions, pinned vs. fixed.
- d) Load at the initiation of local buckling in the corrosion patch.

Finite element analysis was performed by using the finite element program 'ABAQUS' which has the capability of considering material and geometric nonlinearities necessary in analyzing the full-range behavior.[1] The program was run on the following platforms:

- a. SUN workstations under UNIX operating system.
- b. IBM RS-6000 workstations also under UNIX operating system.

13.2 General Description of FE Models

Two types of FE models were used in the analysis. In one type, the whole tubular member was discretized with shell elements, and in the other, the damaged tubular portion, discretized with shell elements, was supplemented with beam-column elements to increase the length of the member.

Due to the doubly-symmetric geometry of the specimens, only one-quarter of the specimen was modeled. Proper boundary conditions were imposed to simulate the behavior of the whole specimen. Several discretization models were used to account for the variety of corrosion patch sizes and specimen lengths and to keep the aspect ratio of the elements to reasonably low values.

13.2.1 Description of Shell and Beam Elements

Figures 13-1 and 13-2 show the typical FE models for Specimens P5 to P9 and for Specimens P10 to P15, respectively. Only shell elements were used for these specimens. The shell elements, shown as surface elements in the figures, were nine-node, isoparametric shell elements with six degrees-of-freedom (DOF) per node. However, the rotational DOF perpendicular to the surface of the shell elements was, with a few exceptions, restrained by the program because these elements lack stiffness in that direction. This DOF was not restrained for the nodes located on a line where shell elements with different surface normals came together, or where the node was shared with an element which used six DOF per node. The thickness of each shell element was constant. The nodes were located at mid-thickness, and, through the thickness, there were five integration points at which stress and strain could be calculated. The load point (central node) was analytically (in ABAQUS) connected to the end nodes of the shell elements to provide pinned or fixed end conditions.

Figure 13-3 shows a typical combination model in which shell elements of Specimens P10 to P15 were used over the tubular damaged portion, and beam-column

elements were used to increase the length to the length of Specimens P5 to P9. The beam-column elements, shown as line elements in Fig. 13-3, were two-node general beam elements with six DOF per node. They were limited to the elastic range since no plastic deformations were expected outside the tubular portion which contained the corrosion patch. No particular cross-sectional shape was specified for these elements, except that the area, moments of inertia, and polar moment of inertia were given with values corresponding to one-half of the full cross section of the specimen. The load point node had the required pinned or fixed end conditions, and the central node at the bottom end of the beam-column elements was analytically constrained to have the same rotation and vertical displacement as a plane passing through the end nodes of the shell elements.

13.2.2 Modeling of the Corrosion Patch

Figure 13-4 shows the discretization of the corrosion patch and of the region between the patch and the remainder of the specimen. The scheme for modeling the sinusoidal transition region is shown in Fig. 13-5.[5]

As shown in Fig. 13-4, four rows of elements were used for both the longitudinal and circumferential sinusoidal transitions so that a constant thickness could be used for each row. This simplified the modeling of the region where the two transition regions overlap. Modeled in this way, the edge nodes of each row of elements were located directly on the sinusoidally curved line as shown in Fig. 13-5, and the nodes between the edges fell on a straight line connecting the edge nodes. Thus, the elements formed straight-line approximations to the curved segments. The thickness of each row of elements was specified to be the average of the actual thicknesses at the nodes along the edges of the row.

Figure 13-4 also shows that only two rows of elements were used in the constant-thickness portion of the corrosion patch. An analysis was also performed on one specimen using four rows of elements in this region, and the difference in the local buckling and ultimate loads between the two models was extremely small. Also, the computer time required to analyze the model with the additional elements was much greater. For these

reasons, it was decided that two rows of elements in the constant-thickness portion of the corrosion patch were sufficient.

13.2.3 Solution Process

The load was applied to the FE model by introducing a displacement of the node at the center of the end opposite the corrosion patch.(Figs. 13-1 and 13-2) For the pinned-end models, the displacement of the nodes around this end of the specimen were all in the plane controlled by the displacement and the free rotation of the central node. For the fixed-end models, all the nodes around the end were constrained to displace the same amount as the central node thereby simulating the fixed-end condition. The loading point was subjected to incremental displacements. The program produced the load-shortening curve as shown in Fig. 13-6. Figures 13-7 and 13-8 show the final deformations for a typical pinned-end and fixed-end model, respectively. The extent of bulging of the specimen outside the corrosion patch is evident in these two figures. Figure 13-9 shows the final deformations for a combined specimen.

13.2.4 Material Properties

The material was the same for all specimens, and the following material properties were used:

Modulus of Elasticity,	$E = 29,500$ ksi
Poisson's ratio,	$\nu = 0.3$
Yield Stress,	$F_y = 42.11$ ksi

The stress-strain relationship was assumed to be bi-linear elastic-plastic without strain hardening. The value of the modulus of elasticity (E) was based on the test results for Specimens P6, P7 and P8. Table 13-1 lists the loading and unloading E values for Gages 1 to 4 for each of the three specimens. These values were determined by first performing a linear regression analysis using the strain and load data for the visually linearly varying portions of the loading and unloading branches, and then using the slope output from the regression analysis to determine the modulus of elasticity. Gages 1 to 4 were used because they were located in the region on the specimen where the strains were expected to maintain

a planar distribution and to stay in the elastic range. The total average E was determined to be 29,619 ksi. However, since the calculated E values depended on the range of values used in the regression analysis which were visually selected, it was concluded that 29,500 ksi was the appropriate value.

13.3 Finite Element (FE) Models

13.3.1 FE Models for Specimens P5 to P9

Specimens P5 to P9 were modeled as pin-ended specimens. The model for these specimens contained 348 elements and 1484 nodes. Thus, there were approximately 7470 global degrees-of-freedom. Although the corrosion patches for Specimens P8 and P9 were larger than for Specimens P5 to P7, they were not too large to warrant revising the model.

13.3.2 FE Models for Specimens P10 to P12

Specimens P10 to P12 were tested under fixed-end conditions which prevented the ends of the specimens from rotating. The model for these specimens was the model of Specimens P5 to P9 adjusted to account for the shorter length. A different model was required for Specimens P11 and P12 because of the larger circumferential dimension of the corrosion patch. The model for Specimen P10 had 216 elements and 844 nodes and the model for Specimens P11 and P12 had 288 elements and 1246 nodes which resulted in approximately 4720 and 6230 global DOF, respectively.

13.3.3 FE Models for Specimens P13 to P15

Specimens P13 to P15 were tested under pin-ended conditions using cylindrical bearings. Modeling this condition was done the same way as for Specimens P5 to P9. Specimen P13 had a corrosion patch of the same dimensions as Specimen P10, and, thus, the discretization and number of DOF were the same. The model for Specimens P14 and P15 had to be slightly modified from the model for Specimen P13 to incorporate the larger

sinusoidal transitions and keep the elements not too slender. The model for these two specimens had 188 elements and 862 nodes with 4310 global DOF.

13.3.4 Combined FE Models

The technique of using beam-column elements to model the portions of a long member that remain elastic is a common approach for simplifying finite element analysis.[8] Initially, five beam-column elements were used to construct the 'beam-stem' attached at the central node of the specimen portion modeled with shell elements, as described in Sect. 13.2.3. Later, the number of beam-column elements was extended to fifteen. Previously, the central node was the reaction point, and it was not permitted to displace horizontally. Now, for the combined models, the reaction point was at the end of the 'beam-stem', and, consequently, the boundary conditions at the central node were modified to allow horizontal displacement. The nodes around the end of the tubular portion were, at first, prevented from displacing radially, but later the radial displacement was allowed. The load was applied to these models by introducing a displacement of the node at the end of the beam-column stem.(Fig. 13-3)

The purpose of the combined models was to determine if the capacity of the specimens was dependent on the length of the specimens. From this comparison, which is discussed in Sect. 13.4.6, it was concluded that for the short lengths of specimens in this series, the capacity was not dependent on the length. Thus, a direct comparison of the effect of a corrosion patch on the ultimate loads of the specimens with the range of lengths in this series may be made.

13.4 Comparison of Test Results with FE Analysis

13.4.1 General

This section compares the load-deformation behavior of Specimens P5 to P15 with the load-deformation behavior of the corresponding FE models. A load-deformation

comparison is also made between the combined FE model of Specimen P10 and the FE model of Specimen P9. The load-deformation curves for the test specimens were computed by averaging the specimen dial gage readings, and then, in order to make a comparison with the FE solutions, these values were adjusted to account for the fact that the gage length, the distance between the dial gage and the bracket at the top of the specimen (Sect. 10.4.1), was shorter than the length of the specimen. Equation 13-1 was used to make this adjustment.

$$\delta_{\text{adj}} = \delta + \frac{P}{AE}(L_s - L_g) \quad (13-1)$$

where

δ_{adj} = adjusted axial shortening

δ = axial shortening from the dial gages

$L_s - L_g$ = (specimen length) - (gage length) = 1.25 in. for all specimens

13.4.2 Specimens P5 to P9 (Spherical Bearings)

Due to the uncertain behavior of the spherical end bearings for Specimens P5 to P9, the FE analysis was performed for both pinned and fixed end conditions. A comparison of the ultimate loads is shown in Table 13-2. Also listed are the FE ultimate loads nondimensionalized with respect to the dynamic and static ultimate loads from the tests, as well as the average and the standard deviation of the nondimensionalized ultimate loads. Figures 13-10 to 13-14 show the load-deformation curves for Specimens P5 to P9 from the tests and from the FE analysis using pinned and fixed-end conditions. It is evident from the figures and from the data in the table, that the ultimate test loads for Specimens P5 to P7 are closer to the ultimate load from FE analysis for the fixed ends, but for Specimens P8 and P9, which were tested after additional polishing of the bearing surfaces and using graphite grease and teflon (Specimen P9), the test ultimate load is between the pinned and fixed FE ultimate loads. This indicates that the spherical bearings did not allow full rotation of the specimen ends, but the rotation did improve with more polishing of the bearings and with the use of teflon.

Figures 13-10 to 13-14 illustrate that, with the exception of Specimens P5 and P9, the stiffness of the FE models is very close to that of the test specimens. However, the axial shortening at the ultimate load for all the specimens, except Specimen P9, is significantly larger than for the FE models.

13.4.3 Rotation of Spherical Bearings

The rotation of the spherical bearings was studied by comparing the end rotation of Specimens P5 to P9 from the tests with the end rotation of the FE models analyzed as pin-ended. (Figs. 13-15 to 13-19) The end rotation of the test specimens was determined from Eq. 13-2.

$$\theta = \frac{\Delta_S - \Delta_N}{2L_g} \quad (13-2)$$

where

Δ_S and Δ_N = readings of the dials on the specimen on the South and North sides
 L_g = distance between the North and South dial gages on the specimen (= 8 in.)

The curves representing the rotation of the FE models have a relatively steep straight-line portion up to approximately two-thirds of the maximum load, meaning that the ends started rotating at the very beginning of the test. This is expected for the ideal pinned-end condition. Then, the rotation rapidly increases indicating the effects of local buckling and yielding in the patch area. The curves for the rotation of the test specimens typically show some initial disturbance (probably, due to "seating" of the fixtures) and, then, a straight line portion, which, as the load increases, becomes steeper or even reverses direction indicating, respectively, decreased rotation or rotation in the opposite direction. These observations reveal that the spherical bearings did not allow full rotation of the specimen ends, and there was significant friction in the bearings used in these tests. An earlier study of spherical bearings used for larger columns showed only very insignificant friction.[8]

13.4.4 Specimens P10 to P12 (Fixed Ends)

The ultimate loads for Specimens P10 to P12 from tests and FE analysis are listed in Table 13-2. The ultimate loads from the FE analysis are conservative, and they are closer to the static than to the dynamic ultimate test loads as indicated by the averages listed in line 5 at the bottom of the table being closer to 1.0.

The load-deformation curves from tests and FE analysis are given in Figs. 13-20 to 13-22. The stiffnesses exhibited by the FE models compare very well with the test specimens as indicated by the similarity in the slopes of the linear portions of the curves. The axial shortening at the ultimate load is smaller for the FE models than for the tests. However, compared to Specimens P5 to P9, it is much closer to the axial shortening of the test specimens. In the post-ultimate range, the FE prediction is generally conservative as the slope of the curve after the ultimate load is steeper.

13.4.5 Specimens P13 to P15 (Cylindrical Bearings)

The ultimate loads for Specimens P13 to P15 are listed in Table 13-2. The averages in line 7 at the bottom of the table indicate a conservative prediction by FE and a better correlation with the static ultimate test loads, thus, indicating a better correlation of the end conditions between the test specimens and FE analysis. The load-deformation plots for these specimens are shown in Figs. 13-23 to 13-25. These figures show a much smaller stiffness for the FE models, but a good prediction of the axial shortening at the ultimate load, and a conservative prediction of the post-ultimate behavior. The cause for the difference in stiffness and ultimate load is described next.

Figures 13-26 to 13-28 compare the end rotation of the FE models and the test Specimens P13 to P15. For the test specimens, the end rotation was computed using Eq. 13-2. The figures show that the FE models started rotating at the beginning and then the rotation accelerated after local buckling started. The curves representing the rotation of the test specimens, however, typically have a straight-line portion followed by a slightly curving portion and then accelerated rotation. This observation indicates that there was some

restraining of the rotation due to the indentation of the bearing plate (Sect. 12.4.1). This restraining stiffens the specimen, and this explains the difference in the stiffness and the higher ultimate load exhibited by the test specimens.

13.4.6 Combined FE Specimens

Figure 13-29 gives a comparison of the load-deformation curves between the FE model for Specimen P10 analyzed as pin-ended and the combined FE model P10C also analyzed as pin-ended. The ultimate load for the short Specimen P10 was 55.0 kips and the ultimate load for the combined Specimen P10C was 54.9 kips, that is, the difference was only 0.2%. Thus, it can be concluded that for the short specimens tested, the length did not affect the capacity of the specimens, and, therefore, the comparison of the ultimate loads of test specimens with different lengths can be accepted as valid.

14. APPROXIMATION OF CORRODED SECTIONS

14.1 Previous Work

As shown in Chapter 6, the thickness variation in patch-corroded members of actual structures is very irregular. Although such thickness variation of a particular case can be smoothed out and discretized for non-linear finite element analysis, this approach is not practical for routine analysis. What is needed is a simplified idealization of typical thickness variation patterns in terms of a small number of parameters, yet sufficient to be able to predict the load capacity of the damaged segment (or cross section) with adequate accuracy. Two idealization models of the corrosion patch have been previously introduced, and two more are considered in this study.

14.1.1 "Shifted Circles" Model

Ostapenko used an approximation of the variation of the reduced thickness by "shifted circles." [8] Figure 14-1 shows this idealization of the thickness variation around the circumference. In this model the cross section is defined by the circle of the inside surface (assumed not to be corroded) and an outside circle which touches the outside point of minimum thickness and the outside point of the maximum thickness, if necessary moved to be directly opposite the point of minimum thickness. The original outside surface is shown by the dashed circle with diameter D . As can be seen in Ref. 8, the approximation of the actual thickness pattern may be very crude, and the stresses computed for the idealized cross section may be quite different from the stresses in the actual section. Local buckling analysis was then performed by using an average weighted thickness for a rectangular area with dimensions of one radius (R) circumferentially and one-quarter radius ($R/4$) longitudinally, centered at the location of the smallest thickness in the corrosion patch. (These dimensions have been found from test observations as sufficient to accommodate a local buckle at the lower stress level for the average thickness.) However, the results were not very promising since the stresses in the idealized cross section may significantly differ from the actual stresses.

14.1.2 "Cosine Patch" Model

Ricles and Hebor idealized the thickness reduction by a cosine curve over a portion of the circumference and similarly in the longitudinal direction ("cosine patch") as shown in Fig.14-2.[5,10] Compared to the previous method, this pattern allows consideration of corrosion patches extending over a small portion of the circumference. If the patch extends over the whole circumference ($c = \pi D$), the thickness variation is essentially identical to that from the "shifted circles". The two main drawbacks of this model are that the reduction of the thickness outside the patch is not considered, and that, similarly to "shifted circles", the *variation* of thickness in the area of minimum thickness is totally controlled only by the overall dimensions of the patch.

Hebor tested seven specimens with this corrosion patch model prepared by grinding. Using three more specimens without damage and 30 cases analyzed by a finite element method, an approximate formula was proposed for predicting the ultimate strength.[5,10] This formula is discussed in Sect. 15.1.2. However, this approximation was not checked against sections with actual irregular corrosion damage patterns, and no indication was given how to approximate such patterns.

14.2 "Constant-Thickness Patch" Model

14.2.1 Definition of Patch

A more general model of thickness variation in the corrosion patch is shown in Figs. 14-3 and 14-4. In comparison with the "cosine patch" model, a greater flexibility in modeling the circumferential thickness variation is achieved by introducing a constant-thickness portion "a" with minimum thickness t_p in the patch and a reduced thickness t_d outside the main patch. The following parameters describe this model:

- D Outside diameter.
- t Uncorroded wall thickness.

- t_p Minimum wall thickness in patch.
- t_d Wall thickness around the circumference reduced (decreased) by corrosion outside the main corrosion patch.
- c Circumferential width of the main corrosion patch.
- a Circumferential width of the constant minimum thickness in the patch (t_p).
- w ($w/2$) = circumferential width of cosine variation of wall thickness within the main patch.
- h Longitudinal height (length) of the corrosion band which is assumed to be of the same length around the circumference.
- b Longitudinal height of the constant minimum thickness in the patch (t_p).
- v ($v/2$) = longitudinal height of cosine variation of wall thickness within the main patch.

Note that the two previous models are only special cases of this new model. The model of "shifted circles" results from the new model if $a = 0.0$, $c = w = \pi D$, $t_p = t_{\min}$ and $t_d = t_{\max} \leq t$, and the "cosine patch" model if $a = 0.0$, $c = w$, $t_p = t_{\min}$ and $t_d = t$. Although more sophisticated, this model still has the disadvantage of creating a symmetrical section as an approximation of generally unsymmetrical actual patterns.

14.2.2 Geometrical Properties of Constant-Thickness Patch Model

As shown in Fig. 14-3, the thickness in the middle of the corrosion patch is assumed to have a constant value of t_p over length "a" circumferentially and length "b" longitudinally. The reduced thickness, circumferentially outside the main patch, is labeled t_d . The transition of the thickness from t_p to t_d in the circumferential direction is idealized as a cosine curve and has length $w/2$ on each side. With the origin of the variable x at the edge of the constant-thickness portion (t_p), the thickness is given by Eq. 14-1.

$$t(x) = \frac{1}{2}(t_d + t_p) - \frac{1}{2}(t_d - t_p) \cos\left(\frac{2\pi}{w}x\right) \quad (14-1)$$

A special case is when the thickness outside the main patch is the uncorroded thickness t . Then, Eq. 14-1 becomes Eq. 14-2.

$$t(x) = \frac{1}{2}(t + t_p) - \frac{1}{2}(t - t_p) \cos\left(\frac{2\pi}{w}x\right) \quad (14-2)$$

Analogously, the thickness variation in the longitudinal direction, with the origin of y at the edge of the constant-thickness portion is given by Eq. 14-3.

$$t(y) = \frac{1}{2}(t + t_p) - \frac{1}{2}(t - t_p) \cos\left(\frac{2\pi}{v}y\right) \quad (14-3)$$

For the portion of reduced thickness around the circumference outside the main patch, the longitudinal variation of the thickness is defined by Eq. 14-4.

$$t(y) = \frac{1}{2}(t + t_d) - \frac{1}{2}(t - t_d) \cos\left(\frac{2\pi}{v}y\right) \quad (14-4)$$

Equations 14-1 (or 14-2) and 14-3 give the thickness variation in the main patch (shown dashed in Fig. 14-3) within the limits of the constant-thickness portion (a-circumferentially and b-longitudinally). Outside this portion, a product function would properly describe the transitional variation of thickness.

Figure 14-4 presents a cross-sectional view of the thickness variation around the circumference. Three cross-sectional properties are needed to quantify the effect of patch corrosion on the stress distribution, local buckling and strength. These are the effective area A_p , the effective moment of inertia I_p , and the centroidal shift c_y .

The effective area of the resultant cross section A_p is given by the following equation (Eq. 14-5) using the notation of Figs. 14-3 and 14-4.

$$A_p = \pi t t_d \left[\frac{D}{t} + \frac{t_d}{t} - 2 \right] - \frac{t^2}{16} \left[\frac{t_d}{t} - \frac{t_p}{t} \right] \left[\frac{a}{R} - \frac{c}{R} \right] \left[4 \frac{D}{t} + 3 \left(\frac{t_p}{t} \right) \right] + 2 \left[\frac{a t_p}{R t} + \frac{c t_d}{R t} \right] \quad (14-5)$$

where t is the original uncorroded thickness. And the effective moment of inertia about the horizontal axis x through the centroid (c.g.) is given by

$$I_x = I_d - I_a - I_w - A_p c_y^2 \quad (14-6)$$

where:

- I_d Moment of inertia of the tube with a reduced thickness of t_d and a diameter of $D_d = D - 2(t - t_d)$.
- I_a Moment of inertia of the shaded portion extending over angle α_a with thickness $t_a = t_d - t_p$.
- I_w Moment of inertia of the transition region with length $w/2$ and the thickness variation modeled with a cosine function.

All these moments of inertia are taken about the center of the circle, and $A_p c_y^2$ is the parallel-axis adjustment to compute the moment of inertia with respect to the centroid.

The shift of the centroid from the center C of the original, uncorroded cross section is found from Eq. 14-7

$$c_y = \frac{Q}{A_p} = \frac{\int y dA}{A_p} \quad (14-7)$$

where Q is the static moment of inertia about the center C .

Finally, the ratio of the maximum stress in the corroded cross section to the average stress, the **stress amplification factor k** , is given by Eq. 14-8.

$$k = 1 + \frac{A_p c_y}{I_p} \left[\frac{D}{2} - t \left(1 - \frac{t_p}{t} \right) + c_y \right] \quad (14-8)$$

Then, the maximum stress in the *patch*, as a function of the axial load P applied at C , becomes

$$f_{\max} = \frac{P}{A_p} k \quad (14-9)$$

The maximum stress due to the ultimate experimental load P_u , non-dimensionalized with respect to the yield stress F_y , is given by Eq. 14-10.

$$\frac{f_{\exp}}{F_y} = \frac{\left(\frac{P_u}{P_y} \right)}{\left(\frac{A_p}{A} \right)} k \quad (14-10)$$

where A is the uncorroded cross-sectional area, and P_y is from Eq. 6-1. The stress ratio from Eq. 14-10 gives an indication of the mode of failure at the ultimate load. If the ratio is less than 1.0, failure was caused by local buckling before yielding. If the ratio is very slightly above 1.0, and local buckles were observed at the ultimate load during the test, then the cross section started yielding and local buckles developed later and affected the post-ultimate deformation. A computed value from Eq. 14-10 larger than 1.0 by approximately 20% or more indicates that the cross section had significant yielding before reaching the ultimate load. Often, the member in such a case fails as a column, and local buckles, if any, develop only after considerable deformation in the post-ultimate range.

14.2.3 Input Parameters and Modeling Considerations

Figure 14-5 shows a typical corroded cross section with a very irregular thickness variation. To apply the Constant-Thickness model to this cross section, four input parameters are required: t_p , t_d , a and c . As can be seen in Fig. 14-6 where the measured

thickness and a tentative outline of the model are superimposed, considerable insight and intuitive judgment must be exercised to make a suitable approximation. The following are the principal considerations to be kept in mind during modeling:

- a) Dimension a , the width of constant thickness t_p , should not be less than radius R . This is the circumferential length of typical local buckles observed in tests.
- b) The area of the actual (measured) cross section and the approximation should be the same. Thus, the areas above and below the dashed line defining the model should approximately balance.
- c) The moments of inertia of the actual corroded area and approximated (modeled) cross sections should also be as close as possible. As can be seen in Fig. 14-6, this may be more difficult to achieve since not just the areas, but areas multiplied by the squared distance to the centroid must be balanced.

Once the free-hand approximation is made, the values of a , c , t_p and t_d are scaled off, and the values of A_p , I_x , c_y and k can be computed. Comparison of these properties with the properties computed from the actual measured thickness readings would indicate how the next trial model should be modified to obtain better accuracy. Figure 14-7 shows the model after several trials that gave a good agreement for the moment of inertia (within +3%). As expected, after practicing with several sections, one's intuitive feel had developed to the point that the properties for the last section analyzed were quite accurate even after the first trial.

Referring to Fig. 14-7, there are some common characteristics associated with each cross section. First, there is a "valley" region in the area of greatest corrosion, the patch. The patch thickness, t_p , is assumed to be the constant thickness in this valley. The extent of the valley, width a , should be approximately equal to the radius R or more. To model the areas outside the patch, an averaging of the areas above and below the

choice for t_d is attempted. The transition region, or "slope", from t_d to t_p on each side of the main patch is modeled as a cosine curve of length $w/2$. If the thickness variation is very irregular, such as for Specimen P1-C1 (Fig. 6-1), the slopes can be modeled as being very steep and short. On the other hand, if the thickness variation is more gradual, such as for Specimen P4-C2 (Fig. 6-19), the slopes will be flatter and longer. The width, $w/2$, of the slopes is assumed to extend from where the thickness reduction begins to climb uphill ($a/2$ from the middle point of the main patch) to where the thickness begins to level off at t_d .

14.2.4 Comparison of Cross-Sectional Properties: Thickness from "Constant-Thickness Patch" Model vs. Measured Thickness

Analysis by using the thickness values around the circumference from the "constant-thickness" model and from the measurements was performed on the test Specimens P1-C1, P2-C1, P3-C1 and P4-C2. Table 14-1 lists the deviation of the cross-sectional properties, that is, area, moments of inertia, centroidal shift, and the stress amplification factor computed with the model from the values based on the actual thickness variation. Corroded specimens from Ref. 8 and from this study are evaluated together.

In general, the model gave reasonably good results in comparison with the actual thickness measurements. For example, Figure 14-8 compares the stress variation around the circumference calculated from the thickness idealization model and thickness measurements for Specimen P2 at the location of Buckle 2. It can be seen that there is a redistribution of stress in the cross section resulting in an increase of the stresses in the areas where the wall is thinnest and that the idealized stress distribution is reasonably close to the measured. The worst error was 12.26% for I_x of Specimen P2-C1. Table 14-1 indicates that as one progresses through the table listing from Specimen P2-C1, the error becomes smaller. This is due to the fact that Specimen P2-C1 was analyzed first. As one became more familiar with the procedure

of choosing the parameters t_p/t , t_d/t , a/R and c/R , the computed properties became closer to the actual values.

Although good correlation between the estimated and actual properties and stresses can be achieved as shown above, the drawbacks of the "Constant-Thickness Patch" model are

- 1) Replacement of a generally unsymmetrical cross section with a symmetrical one, thus, the effect of potential bi-axial bending is neglected.
- 2) As brought out with the examples shown above, the model is not easy to apply since it requires not only an approximation of the thickness profile, but also the intuitive consideration of equal areas, moments of inertia and centroidal shift. As demonstrated, it is possible to develop this intuition, but this is very subjective and not very consistent, as the outcome depends on practice.

One of the convenient advantages of this model is that once the geometrical parameters (a , c , t_p , t_d) are defined, the cross-sectional properties can be readily computed.

14.3 "Linear Segments" Model

14.3.1 Definition of Model

The disadvantages of the "Constant-Thickness Patch" model (Sect. 14.2) have led to another model, "Linear Segments", in which the irregular thickness variation is approximated with a series of segments with the thickness assumed to vary linearly in each segment. Figure 14-9 illustrates the concept by showing an idealization of a corroded section by five thickness values at five angle locations around the circumference. For clarity, the thickness is greatly exaggerated. The thickness variation is also shown on the unfolded circumference (to a different scale). Here, the corroded surface becomes a series of straight lines.

The overwhelming advantage of this model over the others is that the subjective approximation is limited to matching the areas in each segment which is easily done by inspection and requires very little intuition. Normally, five to twelve segments are sufficient to approximate a typical irregular cross section. Although the application is still subjective, the variation of the final cross-sectional properties (A_p , I_x , I_y , I_{xy} , c_x , c_y) from one trial to another has been found to be very minimal.

14.3.2 Procedure for Modeling

The procedure for determining the actual thickness variation of a corroded section had the following steps:

- 1) Measurement of the thickness in a fine mesh (two-inch, one-inch or smaller spacing).
- 2) Analytically passing an approximation surface through these points.
- 3) Reading the thickness values from this surface at 100 or 136 equally spaced points (depending on the diameter) around the circumference in the cross section of interest.

The resultant thickness values were then plotted against the unfolded circumference, and the approximation with linear segments was made by using visual judgment. Although this time-consuming process was found to be productive under laboratory research conditions, it is hardly suitable for field applications.

The approach for obtaining the circumferential profile of the actual thickness variation that appears to be quite convenient for practical field application is the following:

- a) Measure thickness at at least fifteen to twenty locations around the circumference at convenient points.
- b) Obtain the profile of the outside surface by "scribbling" as described in Ref. 8 or by using special templates with the points of measured thickness marked and the "scribed" portions overlapping the circumference.

- c) Overlapping of the "scribed" portions will produce an outline of the outside surface in a circular form. After the thickness values at the points of measurement are marked to scale, a circle with the inside radius adjusted for the scale can then be drawn to pass through the marked points.
- d) Then, the thickness at any intermediate points can be scaled off as the distance between the profile line and the inside circle.

A plot of the scaled thickness values on the unfolded circumference can then be used for laying out the approximation with straight-line segments.

14.3.3 Cross-Sectional Properties

The thickness for a particular segment $[i, (i+1)]$ as a function of angle α is given by Eq. 14-11.

$$t(\alpha) = t_i + \frac{t_{i+1} - t_i}{\alpha_{i+1} - \alpha_i} (\alpha - \alpha_i) = \frac{t_i \alpha_{i+1} - t_{i+1} \alpha_i}{\alpha_{i+1} - \alpha_i} + \frac{t_{i+1} - t_i}{\alpha_{i+1} - \alpha_i} \alpha \quad (14-11)$$

With the thickness defined, the cross-sectional properties with respect to the center C of the circle are computed from Eqs. 14-12 to 14-17.

Net area:

$$A_n = \sum_{i=1}^{i=n} \int_{\alpha_i}^{\alpha_{i+1}} \left[R + \frac{t(\alpha)}{2} \right] t(\alpha) d\alpha \quad (14-12)$$

Static moments:

$$Q_x = \sum_{i=1}^{i=n} \int_{\alpha_i}^{\alpha_{i+1}} \left[R + \frac{t(\alpha)}{2} \right]^2 \cos \alpha t(\alpha) d\alpha \quad (14-13)$$

$$Q_y = \sum_{i=1}^{i=n} \int_{\alpha_i}^{\alpha_{i+1}} \left[R + \frac{t(\alpha)}{2} \right]^2 \sin \alpha \, t(\alpha) \, d\alpha \quad (14-14)$$

Moments of inertia:

$$I_x = \sum_{i=1}^{i=n} \int_{\alpha_i}^{\alpha_{i+1}} \left[R + \frac{t(\alpha)}{2} \right]^3 \cos^2 \alpha \, t(\alpha) \, d\alpha \quad (14-15)$$

$$I_y = \sum_{i=1}^{i=n} \int_{\alpha_i}^{\alpha_{i+1}} \left[R + \frac{t(\alpha)}{2} \right]^3 \sin^2 \alpha \, t(\alpha) \, d\alpha \quad (14-16)$$

$$I_{xy} = \sum_{i=1}^{i=n} \int_{\alpha_i}^{\alpha_{i+1}} \left[R + \frac{t(\alpha)}{2} \right]^3 \sin \alpha \cos \alpha \, t(\alpha) \, d\alpha \quad (14-17)$$

where R is the inside radius.

Location of the centroid is then computed from Eqs. 14-18 and 14-19.

$$c_x = \frac{Q_y}{A} \quad (14-18)$$

$$c_y = \frac{Q_x}{A} \quad (14-19)$$

and the other properties with respect to the centroidal axes by the parallel-axis theorem.

$$I_x = I_{x_c} - A c_y^2 \quad (14-20)$$

$$I_y = I_{y_c} - A c_x^2 \quad (14-21)$$

$$I_{xy} = I_{x_y c} - A c_x c_y \quad (14-22)$$

To perform all these computational operations, a FORTRAN-77 computer program was written, and it is described in Sect. 17.1 and Appendix A.

15. RESIDUAL STRENGTH OF MEMBERS WITH PATCH-CORROSION DAMAGE

15.1 Background and Research by Other Investigators

The objective of the project is to formulate an engineering procedure for evaluating the residual strength of patch-corrosion damaged members. The procedure should consist of simple formulas and require the least amount of information from the damaged member.

15.1.1 Research at Texas A&M

Compression tests were performed on twenty (20) tubular bracing members salvaged from old dismantled offshore platforms.[9] Some specimens were intact, some were dented, others had uniform and/or patch corrosion or a combination of dents and corrosion. In some cases, corrosion produced holes in the wall. The analytical approach to corroded members was to treat them as members with an equivalent reduced thickness and/or to compute the uniform yield capacity of sections with the greatest reduction of area. Seven specimens failed by local yielding and buckling. The loads predicted for these specimens on the basis of full yielding of the affected cross section deviated from the test loads by +12 to +34 % except for one specimen which apparently had large out-of-straightness and deviated by +57 %.

15.1.2 Research by Hebor and Ricles

Research by Hebor and Ricles was conducted concurrently with this project, and it was on short patch-corroded members with the damage assumed to be of the "Cosine Patch" type as described in Sect. 14.1.2. [5,10,11] Tests were conducted on ten specimens. Seven had corrosion patches produced by grinding, and three were undamaged control specimens. The test specimens developed local buckles, but only after initiation of yielding in the patch section. In order to expand the data base, nonlinear FE analysis was performed on 30

specimens including the test specimens. In all cases (tests and analysis), the ends of the specimens were assumed to be fixed. Parametric study and regression analysis of the obtained data resulted in three formulas for predicting the ultimate axial strength as a function of three parameters: D/t , t_p/t , and the angle subtending the circumferential extent of the patch θ (degrees).[5,10,11] All three formulas have essentially the same degree of accuracy¹ with respect to the data base used, and the simplest one (from Ref.10) is given here as Eq. 15-1.

$$p = \frac{P_u}{P_y} = 1.0 - 0.001 \left(\frac{D}{t} \right) + 0.052 \left(\frac{t_p}{t} \right) - 0.0026(\theta) + 0.0028 \left(\frac{t_p}{t} \right) (\theta) \quad (15-1)$$

The range of applicability is stated to be

$$34 \leq \frac{D}{t}; \quad 0 \leq \frac{t_p}{t} \leq 1.0; \quad 58^\circ \leq \theta \leq 311^\circ$$

Figure 15-1 shows a comparison of Eq. 15-1 with three groups of specimens analyzed via FE method and arranged in each group according to decreasing capacity. The first group labeled MFH-FEM represents the 30 specimens from Ref.5 used in the regression analysis for deriving the formulas. The second and third groups are for Specimens P5 to P27 of the current project analyzed with pinned and fixed ends, respectively. The x's mark the values from Eq. 15-1, and the empty squares give the values from the FE analysis performed in Ref.10 or in this project.

As can be seen in Fig. 15-1, the ultimate loads from FE analysis (hollow squares) in the first group agree well with the values from Eq. 15-1 (x's). This should be expected since Eq. 15-1 was derived to approximate the FE points. However, the x's in the second group are significantly above the FE points for the pin-ended Specimens P5 to P27 because

¹ After the formulas in Refs.5 and 10 were corrected to make the last term positive rather than negative.

Eq. 15-1 was derived for fixed-ended conditions. In the third group for which Specimens P5 to P27 were analyzed as fixed-ended, Eq. 15-1 tends to give somewhat higher values since the equation was derived for a "Cosine Patch" model, and Specimens P5 to P27 had "Constant-Thickness Patch" model with greater reduction of the area in the cross section. However, comparison of the loads for Specimens P24 and P26 points to a disturbing anomaly. Both specimens had the same reduction of area due to corrosion, but Specimen 26 had a much larger circumferential extent of the patch ($\Theta=265.2^\circ$) than Specimen 24 ($\Theta=170.2^\circ$). Whereas the loads from the FE analysis are essentially the same, Eq. 15-1 gives a dramatically lower load for Specimen P26 (larger Θ) than for Specimen P24. It can be concluded that consideration of angle Θ in Eq. 15-1 and in Refs. 5, 10 and 11 needs further study.

Unfortunately, no comparison of this formula (Eq. 15-1) was made in the references with any tests on field-corroded (salvaged) members, nor any suggestions were made on how to model the irregular field-corroded tubes for applying the formula, that is, how to define the angle Θ and t_p/t parameters for damaged sections. Furthermore, Eq. 15-1 was developed to apply only to fixed-ended members and, thus, would overpredict the capacity of actual members. Also, as pointed out above, consideration of Θ needs revision if the formula were to be used for other than "Cosine Patch" damage patterns.

15.2 Study of Damage Parameters and of Their Effect on Strength

15.2.1 Selection of Parameters

Since the salvaged specimens P1-C1 to P4-C2 had very irregular thickness variation which could not be readily defined in terms of a small number of parameters, the "Constant-Thickness Patch" model was used as the basis for the strength study. Note that, as discussed in Sect. 14.2, a section of a salvaged specimen can be approximated with this model. Table 15-1 lists the basic data of the test Specimens P5 to P15, as well as of the additional Specimens P16 to P27 and Specimen P10C that were analyzed via the finite element (FE) program to supplement the ranges of the parameters of the test specimens. The common

values of the diameter (D), the thickness (t), and the inside radius (R_i) are given at the top of the table. Table 15-2 gives the common yield stress (F_y) at the top and lists both ultimate test loads, the dynamic and static, and the FE solutions for the ultimate loads for pinned and fixed end conditions of the specimens.

The "Constant-Thickness Patch" model has the following parameters for the thickness variation around the circumference: a, c, t_d and t_p. Thus, there are two more parameters than in the "Cosine Patch" model of Sect. 15.1.2 which had only c (or θ) and t_p. But, even if t_d is taken out by treating it to be equal to t_{max} or t in the analysis of the damaged cross section, there remain six parameters (D, t, a, c, t_p, b). Previous test observations and some checks by Hebor [5] on "Cosine Patch" models showed that the longitudinal dimension of the reduced patch thickness should be approximately greater than R/4 to have essentially no effect on the local buckling stress. However, to clarify this limitation further, dimension b (the longitudinal dimension of the constant-thickness portion) was varied in the specimens with the "Constant-Thickness" model (Specimens P5 to P27).

A direct consideration of all these parameters in a multi-variable regression analysis would lead to an unduly long formula. Considering that Specimens P5 to P27 had the same D and t, a study of reducing the number of parameters by combining them into a fewer number led to the use of the following set:

"Width Reduction" WR which is the mean width of the corrosion patch

$$WR = \frac{a+c}{2} \tag{15-2}$$

"Area Reduction" AR

$$AR = \frac{a+c}{2} (t-t_p) = WR (t-t_p) \tag{15-3}$$

"Patch Slenderness" D/t_p

Longitudinal dimension of the constant-thickness portion b

Specimens P5 to P23 of Tables 15-1 and 15-2 were used in the initial study. As can be seen in Col. J of Table 15-1, except for a few matching pairs, the values of AR are different among the specimens. However, with some sacrifice of accuracy, they can be grouped into four separate sets of width reduction WR as shown in Table 15-3. The values of AR and WR, as well as of the "patch slenderness" D/t_p , are also listed for each specimen in Cols. J, H, and I of Table 15-1, respectively.

Patch corrosion damage can then be defined by parameters WR, D/t_p and b. The interrelation of Specimens P5 to P23 in terms of these parameters is shown graphically in Fig. 15-2. The lines connecting the three parameters are different for each specimen as shown at the bottom of the figure. For example, the line representing Specimen P14 starts at $D/t_p=138$ and connects to $WR=3.15$ and then to $b=0.75$ and, finally, back to $D/t_p=138$. Thus, a triangle is formed for each specimen. The specimens were designed so that there would be at least two specimens to show the variation of each parameter for most of the combinations of other parameters.

15.2.2 Effect on Strength

It can be observed in Table 15-2 that the FE analysis gives more consistent ultimate loads than the tests, in particular when compared with the specimens tested with spherical bearings which gave uncertain end conditions (Specimens P5 to P9). Comparison between FE analysis and tests is much better for Specimens P10 to P15, particularly for the static ultimate loads P_{us} . Then, it can be concluded that the FE analysis is adequately accurate.

The FE results for pinned-end conditions were used in studying the effect of the damage parameters. Initially only three parameters were studied, dimension b, D/t_p , and WR, the effects of which are described next.

15.2.2.1 Effect of Longitudinal Dimension of Constant-Thickness Portion b

Two groups of specimens, Specimens P11, P12 and P23 and Specimens P13 and P15, can be compared to study the effect of varying the 'b' dimension of the corrosion patch. As

shown in Table 15-1 and Fig. 15-2, the corrosion patches in each of these groups of specimens have the same values of WR and D/t_p , but different values of 'b' equal to 0.5 in. $\approx R/5$ for Specimens P15 and P23, 0.75 in. $\approx R/4$ for Specimens P11 and P13, and 1.5 in. $\approx R/2$ for Specimen P12. Thus, the effect of different values of 'b' on the ultimate (or local buckling) load can be directly compared. Referring to the FE ultimate loads for pinned-end conditions (P_{up}), it can be seen in Col. E of Table 15-2 that the ultimate load for Specimen P12 (35.74 kips) was only slightly higher than for Specimen P11 (34.84 kips) which, in turn, was only slightly higher than for Specimen P23 (34.48 kips). Also, the ultimate load for Specimen P15 (55.88 kips) was only slightly higher than for Specimen P13 (55.40 kips). These loads are plotted as a function of the 'b' dimension in Fig. 15-3. Because the difference in ultimate loads is so small among the specimens, it can be concluded that the variation of patch length with $b \geq R/5 \approx 0.5$ in. has essentially no effect on the ultimate load. Thus, $b \approx R/5$ may be considered to be larger than the critical value of the constant-thickness portion of the corrosion patch in the longitudinal direction.

15.2.2.2 Effect of Patch Slenderness D/t_p

Figure 15-4 shows the plots of the FE ultimate load for pinned-end conditions (P_{up}) for Specimens P5 to P23 as a function of the D/t_p ratio. Although the length differed among some of the specimens, the comparison in this figure is valid due to the conclusion made in Sect. 13.4.6 that the length had no effect on the ultimate load. The different data point symbols used for the three curves in the figure represent the different WR values which are listed at the top right corner of the graph. The curves show that there is a non-linear relationship between the ultimate load and D/t_p . It is not clear why the curve for $WR=3.15$ shows flattening out in the range of $D/t_p=138$ to 183. However, a general conclusion can be made that as the ratio D/t_p is increased, the ultimate load decreases, and that the relationship is of a hyperbolic (concave) type.

15.2.2.3 Effect of Effective Width of Reduction WR

Figure 15-5 shows the plots of the FE ultimate load for pinned-end conditions (P_{up}) versus the width reduction (WR) for Specimens P5 to P23. The different D/t_p ratios are

represented by different data point symbols as listed at the top right corner of the graph. The effect of b is neglected.

By comparing the plots for different values of D/t_p , one can conclude that the non-linearity of the relationship between the ultimate load and the "width of reduction" WR becomes less pronounced (smaller concave curvature) with the increasing value of D/t_p .

15.2.3 Effect of Area Reduction AR -- Initial Study

To study the effect of the area reduction parameter AR , two additional specimens, Specimens P24 and P25, were analyzed using the FE program. The relationship between the FE ultimate loads (P_{up} and P_{uf}) and AR (defined by Eq. 15-3 and listed in Table 15-1) is plotted in Fig. 15-6 for Specimens P5 to P25. The plots form two distinct sets: the lower one for the pinned-end specimens and the upper set for the fixed-end specimens. Different symbols are used to indicate specimens with the same values of D/t_p . These plots show that in each set an almost linear relationship exists between the ultimate load and AR with only a slight scatter introduced by the values of D/t_p . The two sets fall into relatively narrow bands which can be approximated by straight lines.

Similar curves are plotted in Fig. 15-7 for Specimens P5 to P25, however here the ultimate loads are non-dimensionalized with respect to the gross yield ("squash") load, $P_y = A_g F_y$, and the area reduction AR with respect to the gross area A_g .

$$p = \frac{P_{uFE}}{P_y} \quad (15-4)$$

$$a_r = \frac{AR}{A_g} \quad (15-5)$$

$$A_g = 2\pi(D - t_{max})t_{max} \quad (15-6)$$

Thus, Eq. 15-4 is used on the vertical axis in Fig. 15-7 and Eq. 15-5 is used on the horizontal axis. The straight-line approximations to these points are also shown in Fig. 15-7. The equations for these straight lines, found via regression analysis, are

for pinned ends

$$p_p = \frac{P_{uP}}{P_y} = 0.913 - 2.07(a_r) \quad (15-7)$$

and for fixed ends

$$p_f = \frac{P_{uF}}{P_y} = 0.97 - 1.08(a_r) \quad (15-8)$$

A comparison of these straight-line approximations with all available test loads is shown in Fig. 15-8. In addition to the test loads for Specimens P5 to P15 and the salvaged Specimens P1-C1 to P4-C2 and Specimens C1 and C2 from the previous project [8], the loads from the tests conducted by Ricles and Hebor [10] are included. Specimens P1-C1 to P4-C2 and C1 and C2 were salvaged field-corroded specimens which had corrosion damage all around the circumference. They were included in this comparison by using the net area as computed from the thickness measurements and the gross area based on the maximum thickness measured (t_{max}), not the original undamaged thickness. Thus,

$$a_r = 1 - \frac{A_n}{A_g} \quad (15-9)$$

was used as the relative area reduction for the field-corroded specimens. The gross area as a function of the inside radius, R_i , and the maximum thickness is given by Eq. 15-10

$$A_g = \pi(2R_i + t_{max})t_{max} \quad (15-10)$$

The test specimens with fixed-ends (Specimens P10 to P12) and the test specimens with cylindrical bearings (Specimens P13 to P15) of this study are closer to the respective straight-line approximations. However, the tests conducted by Ricles and Hebor (intended

to be fixed-end tests) and the tests with spherical bearings (Specimens P5 to P9) fall between the straight lines. For the salvaged specimens (all tested with spherical bearings) the test loads fall relatively close to the average between the lines. Only Specimens P4-C2 and C2 are significantly higher. This is because Specimen P4-C2 failed by overall column buckling with heavy yielding and no local buckling, whereas Specimen C2 of the previous project did develop local buckles but only after most of the reduced cross section had plastified.[8]

It appears that an average straight line between the lines for pinned and fixed end conditions would provide a good, slightly conservative approximation for estimating the ultimate load of tubular members damaged by patch corrosion. More conservatively, however, a straight line between the lines for the two extreme end conditions with one-third of the difference above the line for the pinned-end conditions can be accepted as a more suitable conservative estimate of the ultimate load for patch corroded tubular members. The equation for this line is given by Eq. 15-11

$$p = 0.932 - 1.74a_r \quad (15-11)$$

and it is labeled as **Design Approximation** in Fig. 15-8. As can be seen in the figure, Eq. 15-11 is only applicable for the range of the relative area reduction

$$0.05 < a_r = \frac{AR}{A_g} < 0.35 \quad (15-12)$$

studied here, that is, from 5% to 35% of area reduction. The transition from $p = 1.0$ for $a_r = 0.0$ to the formula given in Eq. 15-11 can be made either by a short straight line or by using one curve, either straight, parabolic, or cubic, over the full range of a_r from 0.0 to 0.35. In formulating the parabolic or cubic equation, the curve should be constrained to pass through the point $p = 1.0$ and $a_r = 0.0$. This is performed in the next section.

An alternative presentation of Eq. 15-11 is to use the remaining net area A_n rather than the area reduction a_r as the damage parameter. With the relative net area a_n defined by Eq. 15-13,

$$a_n = \frac{A_n}{A_g} \quad (15-13)$$

and a_r by Eqs. 15-9 and 15-14,

$$a_r = \frac{A_g - A_n}{A_g} = 1 - \frac{A_n}{A_g} = 1 - a_n \quad (15-14)$$

Equation 15-11 is readily transformed into Eq. 15-15.

$$p = 1.74a_n - 0.708 \quad (15-15)$$

The limits of applicability, Eq. 15-12, become

$$0.65 < a_n = \frac{A_n}{A_g} < 0.95 \quad (15-16)$$

15.3 Effect of Relative Area Reduction a_r -- Cubic Formula

After extending the data base by inclusion of Specimens P26 and P27 in order to broaden the range of damage parameters, the analysis discussed in Sect. 15.2.3 was repeated over the whole range and using a 3-term cubic equation (Eq. 15-17) to accommodate the slight upswings of the data points near the end points of $a_r = 0.0$ and $a_r = 0.35$.

$$p = 1.0 + a_1 a_r + a_2 a_r^3 \quad (15-17)$$

Again the limiting lines for the pinned and fixed end conditions were obtained from the FE solutions of Specimens P5 to P27 as shown in Fig. 15-9. The curve for pinned ends is defined by Eq. 15-18.

$$p = 1.0 - 2.8876a_r + 6.1095a_r^3 \quad (15-18)$$

and the curve for fixed ends by Eq. 15-19.

$$p = 1.0 - 1.3186a_r + 1.1277a_r^3 \quad (15-19)$$

Figure 15-9 shows all the ultimate load results available from tests and FE analysis plotted together with the limiting curves. Only the long salvaged specimens C2 and P4-C2 which failed in column mode without local buckling are excluded in order to make a cleaner emphasis on the effect of local buckling. Similarly to the straight-line solution of Sect. 15.2.3, the line lying one-third of the difference between the two limiting lines above the line for pinned ends is suggested as a reasonably conservative relationship for engineering applications.

$$p = 1.0 - 2.3646a_r + 4.4489a_r^3 \quad (15-20)$$

It is marked as **Design Recommendation** in Fig. 15-9.

An alternative presentation is by using the relative net area, a_n , rather than the relative reduction of area, a_r , as the argument. Since

$$a_r = 1 - a_n \quad (15-21)$$

Equation 15-20 becomes

$$p = 1 + a_1(1 - a_n) + a_2(1 - a_n)^3 = (1 + a_1 + a_2) - (a_1 + 3a_2)a_n + 3a_2a_n^2 + a_2a_n^3 \quad (15-22a)$$

Substitution of the numerical values of a_1 and a_2 from Eq. 15-20 results in a 4-term expression given by Eq. 15-22b.

$$p(a_n) = p = 3.0843 + 10.9821a_n + 13.3467a_n^2 + 4.4489a_n^3 \quad (15-22b)$$

Regression analysis was performed of p as a 3-term cubic function of a_n for the FE solutions of Specimens P5 to P27 with pinned and fixed ends. The following are the resultant curves constrained to pass through the point for zero damage ($a_n = 1.0$, $p = 1.0$):

Pinned ends

$$p(a_n) = 0.01614 - 0.14437a_n + 1.12823a_n^3 \quad (15-23a)$$

Fixed ends

$$p(a_n) = 0.07645 + 0.68191 a_n + 0.24164 a_n^3 \quad (15-23b)$$

The curve one-third of the difference above the pinned-end line can be recommended for design. It is given by Eq. 15-23c.

$$p(a_n) = 0.036 + 0.131 a_n + 0.833 a_n^3 \quad (15-23c)$$

Figure 15-10 shows the same data points as in Fig. 15-9, but plotted against a_n rather than a_r . The 4-term and 3-term formulas show hardly any difference.

A judicious manipulation of the constants in Eq. 15-23c led to the 2-term formulation of Eq. 15-24.

$$p(a_n) = 0.18 a_n + 0.82 a_n^3 \quad (15-24)$$

As illustrated in Fig. 15-11, the 4, 3 and 2-term approximations are hardly distinguishable from each other, and the simplest 2-term Eq. 15-24 seems to be the most suitable for practical use.

Although Eq. 15-24 smoothly extends to $a_n = 0.0$, it should be limited at present to

$$a_n \geq 0.65 \quad (15-25)$$

since no work has been done on sections with smaller net areas, that is, with larger area reduction than 35%.

15.4 Summary and Recommendations

1) The parametric study described in the previous sections indicates that the dominant simple parameter for evaluating the ultimate capacity of sections damaged by one-sided patch corrosion is the relative reduction of area $a_r = AR / A_g$ (or the relative net area $a_n = A_n / A_g$).

2) The wall slenderness parameter in the patch D/t_p was found to have rather small influence in the range of parameter a_r studied ($a_r \leq 0.35$ or $a_n \geq 0.65$). This can be seen from the narrow band of the curves for different values of D/t_p in Fig. 15-6 (P vs. AR) for the pin-ended and fixed-ended conditions.

3) The effect of end conditions becomes more and more significant with the increase in corrosion damage, of the relative reduction of area a_r (or the reduction of the relative net area a_n), as can be observed in Figs. 15-9 and 15-10. For example in Fig. 15-9, for $a_r = 0.3$, $(P/P_y)_{pinned} = 0.42$ and $(P/P_y)_{fixed} = 0.76$ indicate a reduction in the ultimate strength by $(0.76 - 0.42)/0.76 = 0.45$ (45%), or in terms of $P_{u, pinned}$, an increase of $(0.76 - 0.42)/0.42 = 0.81$ (81%).

4) Since the end conditions in an actual bracing member lie somewhere between the extremes of pinned and fixed, an increase by one-third of the difference above the strength for pinned end conditions was selected as a realistically conservative approximation. This approximation is shown in Fig. 15-8 as a linear function of a_r (Eq. 15-11, $0.05 \leq a_r \leq 0.35$), in Fig. 15-9 as a cubic function of a_r (Eq. 15-20, $a_r \leq 0.35$), and in Fig. 15-11 as a 2-term cubic function of a_n (Eq. 15-24, $a_n \geq 0.65$).

For convenience, the four relevant equations are repeated below with their limits of applicability.

Straight-Line Formulas:

$$p = 0.932 - 1.74 a_r \quad (15-11)$$

for $0.05 < a_r = \frac{AR}{A_g} < 0.35$

or $p = 1.74 a_n - 0.708 \quad (15-15)$

for
$$0.65 < a_n = \frac{A_n}{A_g} < 0.95$$

Cubic Formulas:

$$p(a_r) = 1.0 - 2.3646a_r + 4.4489a_r^3 \quad (15-20)$$

for
$$a_r \leq 0.35$$

or
$$p(a_n) = 0.18a_n + 0.82a_n^3 \quad (15-24)$$

for
$$a_n \geq 0.65$$

The first two formulas (Eqs. 15-11 and 15-15, straight-line) may be more convenient in some special applications, and the latter two (Eqs. 15-20 and 15-24, cubic) in general computations.

16. LOCAL BUCKLING

16.1 General

Although local buckling was found to have not very pronounced influence on the ultimate strength for the degree of patch corrosion damage studied here, it was observed visually and electronically (strain gages) in tests and in FE analysis. The odd figures of Chapter 11 [Figs. 11-1, 11-3, 11-5, 11-7, 11-9, 11-11, 11-13, 11-15, 11-17, 11-19, 11-21] show a sudden reversal of the strain in the outside surface of the patch at the load level of local buckling below the ultimate load for the tested Specimens P5 to P15. Further increase of the load was needed to plastify the cross section sufficiently in order to reach the maximum (ultimate) capacity. Chapter 12 discusses the phenomenon in greater detail. What is important at this point is that the load at local buckling was below the ultimate load, but it would have been closer had the circumferential extent of the reduced thickness been larger. In other words, the use of local buckling as a criterion for ultimate load may be too conservative, but it would be less so for larger extents of the corrosion patch. Specimens P26 and P27 were designed to illustrate this. Although they had the same reduction of area, the circumferential dimension 'a' (constant thickness portion) was 2.75 in. for P26 and 7.2 in. for P27.[Table 15-1] The ultimate load from FE analysis for Specimen P26 for pin-ended condition was $P_{26} = 24.58$ kips [Col. E in Table 15-2] which is higher than $P_{27} = 22.24$ kips. (It is not clear why there was hardly any difference in the ultimate loads, 52.0 kips vs. 52.06 kips [Col. F of Table 15-2] for fixed-end conditions.)

16.2 Effective Area for Local Buckles

The complex phenomenon of local buckling in tube walls with irregular thickness is idealized here by local buckling of a tube with constant wall-thickness that corresponds to an average thickness over a certain area in the irregular tube.

Initial observations of the local buckles formed during tests on salvaged specimens led to the use of the thickness averaged over a rectangular area with the dimensions of 1.0 R circumferentially and 0.25 R longitudinally. This approach is discussed in Ref. 8. However, the results obtained from the tests on specimens with simulated corrosion damage and from FE analysis (Sect. 15.2.2.1) indicate that a more realistic approach is to use a rectangular area with somewhat smaller dimensions of 0.8 R circumferentially and 0.2 R longitudinally.

16.3 Equivalent (Modified) Thickness in Patch

A simplified procedure for obtaining the "averaged" constant thickness t_a ¹ for irregular thickness variation is described next. In this description, the effective area is assumed to be 1.0 R circumferentially and 0.25 R longitudinally. The procedure, however, applies equally well to the refined limits of 0.8 R by 0.2 R.

A cross section with an irregular thickness variation cannot be analyzed for local buckling by any available tools except by the often cumbersome and expensive finite element method. However, methods are available for estimating the local buckling stress for tubes with uniform wall thickness. This section presents a procedure for estimating an equivalent average thickness t_a in the area of smallest thickness so that the available formulas can be used for computing the buckling stress.

The area with the most severe thickness reduction is the location where local buckles are most likely to develop. The cross section for this corroded portion should be idealized to select values for t_p , a , c and t_a in the circumferential direction (and, correspondingly, b and h in the longitudinal direction.) From these values, the cross-sectional properties, A_p , I_p , e and k can be calculated.

¹ Some Tables and figures use an earlier description of t_m ("modified") for t_a .

Figure 16-1 shows a reduced area where a local buckle developed during testing (Specimen P3-C1, Buckle 1). From test observations, the circumferential dimension 'a' should be approximately equal to the radius R¹ and the longitudinal dimension 'b' equal to R/4¹. Within this reduced portion, t_{p,circ} should be selected and the areas above and below this constant value should approximately visually balance each other. The same should be done in the longitudinal direction to obtain t_{p,long}, which is analogous to t_{p,circ}. The minimum thickness in the patch, t_{min}, can be found by either scribing, ultrasonic measurements or any other appropriate method. Then, from Fig. 16-1, the equivalent average thickness over the affected area can be estimated from the following proportional relationship

$$t_a = \frac{t_{a,circ} t_{a,long}}{t_{min}} \quad (16-1)$$

For example, t_a was estimated to be 1.2 t_p for Specimen C1 of Ref. 8. Using Eq. 16-2 (API), the uniform wall thickness corresponding to the critical stress at the ultimate condition was found to be ≈ 1.25.[8] Table 16-1 shows that for all specimens which developed local buckles, the choice of t_a was reasonable. The exception was Specimen P1-C1, which had local buckles around a hole.

16.4 Local Buckling Formulas

Analysis of local buckling in the portions of reduced thickness is a complex problem. A simplification can be made by comparing the stress in the reduced thickness area with local buckling stresses from engineering formulas for local buckling stress of tubular members with constant wall thickness and subjected to concentric loads. These formulas are also acceptable for axial loads with small eccentricity. Five formulas are given next. They have been modified to a uniform format and notation from the formats in the source references.

¹ These values are later revised to 0.8R and 0.2R.

1) API (American Petroleum Institute, RP2A) [3]

$$\frac{F_{cr}}{F_y} = \left(1.64 - 0.23 \sqrt[4]{\frac{D}{t}} \right) \quad \text{for } \frac{D}{t} > 60 \quad (16-2a)$$

$$\frac{F_{cr}}{F_y} = 1 \quad \text{for } \frac{D}{t} \leq 60 \quad (16-2b)$$

2) DnV (Det norske Veritas) [4,7]¹

$$\frac{F_{cr}}{F_y} = \left[1 - \frac{1}{3} \left(\frac{1.5 + 0.001 \left(\frac{D}{t} \right)^2}{\alpha} \right)^2 \right] \quad (16-3)$$

3) AISI (American Iron and Steel Institute) [2,8]

$$\frac{F_{cr}}{F_y} = 0.667 + 0.037 \alpha \quad \text{for } F_{cr} \leq F_y \quad (16-4)$$

4) SSRC (Structural Stability Research Council) [8]

$$\frac{F_{cr}}{F_y} = 0.61 + 0.043 \alpha \quad \text{for } 2.57 \leq \alpha < 9.1 \quad (16-5)$$

5) AO (A. Ostapenko) [7,8]

$$\frac{F_{cr}}{F_y} = 38 \xi - 480 \xi^2 + 2020 \xi^3 \quad (16-6a)$$

$$\frac{F_{cr}}{F_y} = 1.0 \quad (16-6b)$$

¹ This DnV formula represents a simplification of a rather complex semi-graphical procedure of the DnV specification. [4,7]

where

D is the outside diameter.

D_m is the mid-thickness diameter = $D - t$.

α , ξ are the slenderness parameters defined by Eqs. 16-7.

$$\alpha = \frac{1}{\left(\frac{D}{t}\right)} \frac{E}{F_y} \quad \text{and} \quad \xi = \frac{1}{\left(\frac{D_m}{t}\right)} \sqrt[3]{\frac{E}{F_y}} \quad (16-7)$$

An illustration of the (F_{cr}/F_y) values according to these five recommendations is shown in Fig. 16-2. The curves are functions of wall slenderness (D/t) for material properties $F_y = 42.11$ ksi and $E = 29,500$ ksi. (The specific values of F_y and E are needed since they are treated differently by some of the formulas.)

Since the API and DnV methods are commonly used in designing offshore structures, these were selected for application in the current study, the API as the more conservative and the DnV as the more optimistic.

After calculating the equivalent average thickness t_a , the stress and the corresponding load at which local buckles develop can be found by using any one of the formulas presented in this section. The local buckling analysis to estimate this axial load according to the API and DnV specifications (Eqs. 16-2 and 16-3) was carried out for each specimen and compared with the experimental ultimate load, and the results are shown in Table 16-1. It can be seen that the model was fairly accurate in predicting the ultimate load for each specimen that developed local buckles based on an estimated value of t_a . The error ranged from approximately 1% to 16%. The best case, Specimen P3-C1 had an error of less than 1% and the worst error was for the ultimate load for Specimen C2 from Ref. 8 which developed local buckles near one end after considerable yielding.

16.5 Local Buckling Loads for Specimens P5 to P27 (Specimens with Patch Corrosion)

The logic of Sections 16.3 and 16.4 was incorporated into the FORTRAN-77 computer program CXS.for to calculate the axial loads that would cause local buckling according to the API and DnV specifications. (The program is described in Chapter 17 and Appendix A.) Local buckling loads obtained for Specimens P5 to P15 from strain gage readings in the patches are listed in Col. B of Table 16-1. In addition, the local buckling loads found via FE analysis for all specimens of the P-series, P5 to P27, are shown in Col. C of Table 16-1. The results from the computer program CXS.for, based on the API and DnV specifications are shown in Cols. D and E of Table 16-1, respectively.

17. FORTRAN PROGRAM CXS AND COMPARISON OF METHODS

17.1 FORTRAN Program CXS.for

FORTRAN-77 program CXS.for was written specifically to perform the calculations needed in analyzing patch-corroded sections with thickness defined by linear segments (Sect. 14.3). Particular attention was put into orienting the program for application by individuals not necessarily intimately familiar with the details of the process. Once the geometrical and material parameters are input, the program computes all cross-sectional properties. In addition, the program considers the bi-axial eccentricity of the load and computes the stress amplification factor for the point with the smallest thickness which is the area of potential local buckling and for the point of the maximum stress in the cross section which is the point of first yielding. At this time, the spread of plastification, as usually occurs in sections with relatively small areas of significantly reduced thickness, is not considered. Consequently, the limiting loads predicted by the computer program for such sections are on the conservative side, that is, they tend to be lower than the test loads or the loads computed by using non-linear FE programs (which is a very labor and time-intensive procedure and requires expert knowledge). The details of the FORTRAN program and the steps in application are described in Appendix A. Below are given only the basic features of the program.

INPUT:

The data input can be made from the keyboard or from an external file prepared in advance, and it consists of the following items:

- a) Section Name, inside radius (It is assumed that all corrosion is on the outside surface.), counter for the smallest thickness, total number of segments.

- b) Sequential listing of the values of the angles at the segment ends (in radians or degrees; the program detects automatically which).
- c) Sequential listing of the thickness values corresponding to the angles.
- d) Load eccentricity (x and y components) with respect to the center of the circle, the test or FEM or an assumed reference load, yield stress, the ratio of the averaged (modified) t_a to minimum thickness t_p , an indicator of the type of units used (Customary-U.S. or Metric-S.I.).

OUTPUT:

The output of the computed results can be made to an external file for later processing and/or to the screen for immediate display. The principal items of the output are the following:

- a) Section name.
- b) Cross-sectional properties: Net area, moments of inertia with respect to the centroidal x and y axes and with respect to the principal axes. The formulas of Sect. 14.3.3 are utilized in the process in addition to other relationships.
- c) The load limited by first yielding in the cross section and the loads to cause local buckling according to the API and DnV specifications using the formulas listed in Sect. 16.4 (Eqs. 16-2 and 16-3). Loads computed from Eq. 15-24 and for pin-ended condition.

The net area A_n computed by the program can be conveniently utilized for applying the proposed approximate formulas, such as Eq. 16-24, in computing the ultimate load. The gross area A_g needed for computing the relative net area a_n is taken either as the original uncorroded area or, if corrosion is all around the circumference, by Eq. 17.1

$$A_g = \pi (2R_i + t_{\max}) t_{\max} \quad (17-1)$$

where R_i is the inside radius and t_{\max} is the largest value of thickness in the analyzed cross section. Then,

$$a_n = \frac{A_n}{A_g} \quad (17-2)$$

[Note: The program with the final version of the project report will have the computation of the approximate ultimate load incorporated.]

17.2 Comparison of Methods

Ultimate loads from tests and finite element analysis are graphically compared with the proposed formula(s) (Eqs. 15-11, 15-20, 15-24) in the course of deriving the formula and are shown in Figs. 15-8 to 15-10. Included there are the test results from the following groups:

- a) Salvaged Specimens C1 and C2 from the previous project.[8]
- b) Salvaged Specimens (P1-C1 to P4-C2) and specimens with simulated corrosion damage (P5 to P15) from the current project.
- c) Ten specimens with simulated corrosion damage from the concurrent research by Hebor and Ricles.[5]

Shown in the figures are also the ultimate loads computed by using a FE program for Specimens P5 to P27 of the current research program using pinned and fixed ends and for 30 specimens from Ref. 5 for fixed ends. The results are plotted with respect to the relative area reduction.

17.3 Comparison with Tests Conducted at Texas A&M

Seven of the twenty salvaged specimens tested at Texas A&M developed local buckles in the patch corroded areas.[9] Utilizing the limited information available in the reference for these sections, analysis was performed using program CXS.for and the proposed formula

(Eq. 15-24). The results are compared in Table 17-1 with the ultimate test loads P_{test} and the loads computed in the reference P_{comp} .

The errors (in percent) with respect to the test loads are listed in the five rows at the bottom of the table. The average errors and standard deviations are also given for each method. Specimen 14 failed at a significantly lower load than predicted by all the methods with the resultant error varying from +26.1 % to +56.6 %. The plausible reason for this is apparently a large, but not accounted for and unknown, load eccentricity in the damaged cross section. The average errors, including this specimen, vary from +2.54 % for Eq. 15-24 to +26.12 % for P_{comp} of the method in the reference. With Specimen 14 excluded, the range of errors drops to -1.4 % for Eq. 15-24 to +21.1 % for P_{comp} . The range of errors from Eq. 15-24 for this case (without Specimen 14) is from -15.4% to +14.1 % which is **surprisingly very small** for the few measurements given in the reference and the uncertainty of end conditions.

The loads from program CXS for [the first-yield load ($P_{fst-yld}$) and the loads according to API (P_{api}) and DnV (P_{dnv})] are relatively close to each other and are on the optimistic side with the error for all seven specimens halfway between those for Eq. 15-24 and P_{comp} , that is, approximately +16 %. If Specimen 14 is excluded, then the average error drops to approximately +9.4 % with the spread from -2.8 % to +20.4 %.

18. SUMMARY AND RECOMMENDATIONS

18.1 Summary

Ultimate strength of a tube segment with an irregular corrosion patch is a very complex three-dimensional phenomenon involving large deformations, non-linear material response (including strain reversal) and residual stresses. Conceptually, an analysis of this problem can be carried out by using modern finite element (FE) programs once all the information on the initial geometry, material properties and residual stresses is available and an optimum discretization scheme is determined. FE analysis of some segments with simplified idealizations of corrosion patches has been performed in this project and by others [5,10], and a reasonably good correlation with test results verified that the FE method may be used in lieu of testing. However, the FE method, requiring specialized knowledge and a trial-and-error procedure in the determination of suitable discretization patterns even for simplified damage idealizations, is hardly suitable for the irregular corrosion patch patterns of corrosion damage in actual structures.

Fortunately, it was found that the ultimate axial strength of segments with patch corrosion damage could be determined with sufficient engineering accuracy by assuming a planar distribution of strains¹ in the cross section having the greatest reduction of the cross-sectional area in the tube. Then, the basic simplified modes of section failure at the ultimate load are the following:

- Local buckling before yielding with a sudden reduction of wall strength over a sufficiently large portion of the circumference to cause collapse of the section. Thus, the member strength is directly limited by local buckling.

¹ Regular strength-of-materials analysis in the elastic range.

- Local buckling before yielding but over a smaller portion of the circumference. The ultimate load is reached only after yielding in the wall adjoining the buckled area and, thus, is higher than the load that caused initial local buckling.
- Yielding starts in the patch area, but, before it spreads to reach the maximum load, local buckles develop and reduce the capacity of the buckled area, so that the maximum (ultimate) load on the cross section is reached only after more yielding but at a lower load than it would have been without local buckling.
- Yielding starts in the patch area or at some other point and continues spreading over the cross section until the ultimate capacity is reached. Local buckles develop but only at essentially the ultimate load or somewhat later and cause the drop-off of the load.

Since neither local buckling nor the spread of yielding (plastification) needed to reach the ultimate load can be easily determined, only the initiation of yielding ("first yield") can be readily computed. However, the "first yield" load, although a lower bound in a general case, may be precipitated by local buckling as described above.

The research described in this report was performed with the principal objective of finding a simplified "engineering" method for computing the ultimate axial capacity of tubular columns damaged by patch corrosion. The work performed consisted of experimental and analytical studies and eventually resulted in a simple approximate formula which can be recommended for practical use.

In all, fifteen (15) specimens were tested to determine the effects of patch corrosion and local buckling on the strength of tubular members. Four specimens were field-corroded tubular members salvaged from decommissioned platforms. Two of these were long columns and two shorter columns. The remaining eleven specimens were short tubular specimens with patch corrosion of a simple pattern simulated by grinding.

Three of the four salvaged specimens failed by local buckling in combination with yielding of the cross section while the fourth specimen (a long specimen) failed as a column. All of the eleven specimens with simulated corrosion developed local buckling.

A simplified model of the thickness variation around the circumference was developed as an idealization of the irregular patch corrosion in field-corroded tubular members. In this model, the following four parameters were defined: patch thickness t_p , reduced thickness outside the patch t_d , the circumferential width of the constant thickness portion of the patch a , and the circumferential width of the main patch c . Analogous parameters t_p , b and h were defined for the longitudinal direction of the main patch except that t_d became the undamaged thickness t .

The eleven test specimens with corrosion damage simulated by grinding had this "constant-thickness patch" model pattern. However, the thickness outside the main patch (dimension c) was not reduced, that is, $t_d = t$. The advantage of studying specimens in which the dimensions of the corrosion patch are well defined rather than irregular is that they can be discretized for finite element analysis much more easily.

Although the "constant-thickness patch" model met with some success in idealizing the cross sections in the salvaged specimens and computing their cross-sectional properties and the strength for local buckling or first yielding, the model was found to be very demanding on intuitive judgement and, thus, subjective. Therefore, another model, a "linear-segments" model, was introduced which needed much less intuition. In this model, the irregular thickness pattern is replaced with a sequence of segments with linear thickness variation with respect to the distance around the circumference (or central angle). This model required computations which were much more inconvenient for manual work than for the "constant-thickness patch" model, and a special FORTRAN-77 program was written for this purpose.

Since local buckling of the areas with irregular thickness variations cannot be properly analyzed using available tools, the method proposed in the previous project was used. [8] In this method, the formulas for computing the local buckling stress of tubular members with uniform wall thicknesses according to the API and DnV specifications [3,4,8] were assumed to be applicable to the corrosion damaged wall by replacing the irregular thickness with thickness t_a averaged over an area in the patch sufficient to accommodate a single buckle at the lowest stress level. Initial test observations and later studies showed that this (rectangular) area should be taken $0.8R$ circumferentially and $0.2R$ longitudinally. For field-corroded and simulated patches, the averaged thickness t_a was defined by its ratio to the minimum thickness in the patch t_p , that is, t_a/t_p .

The primary purpose for the tests conducted on the eleven specimens with corrosion patches simulated by grinding was to provide benchmarks for the accuracy and reliability of using a finite element (FE) computer program in analyzing tubular members with patch corrosion. The patch geometry was defined by the parameters of the "constant-thickness patch" simplification pattern with the values selected to cover the ranges expected to clarify the various types of ultimate strength behavior as discussed above. Specifically, the circumferential width of the constant-thickness portion "a" and the thickness in the patch were to clarify the assumptions of the optimum dimensions for local buckles and the extent of yielding at the ultimate load. Due to the uncertainty of the end restraints for some of the test specimens, the FE analysis was performed with both pinned and fixed end conditions. A good correlation was established between the experimental and analytical results, and twelve additional specimens were analyzed. The initial parametric study of the information from these analytical data applied mainly to the following parameters: b, the longitudinal dimension of the constant-thickness portion of the corrosion patch which ranged from $R/5$ to $R/2$; D/t_p , the ratio of the outside diameter to patch thickness which ranged from 79 to 183; WR , the average circumferential width of the corrosion patch which ranged from $0.8R$ to $2.2R$; and a_r , the relative area reduction due to the corrosion patch which varied from 0.05 to 0.35. The observations drawn from this initial parametric study were as follows:

- 1) Although the strain and stress at local buckling may approximately be the same in patches with the same D/t_p but different overall dimensions, reaching the ultimate load required a considerable amount of yielding outside the patch and a significant increase of the load for smaller-sized patches ($a_r < 0.2$), whereas, for larger-sized patches ($a_r > 0.25$), the ultimate load was essentially precipitated by local buckling.
- 2) For values of $b \geq R/5$, the ultimate load was essentially the same. Therefore, $b \approx R/5$ can be considered to be above the critical value of the constant-thickness portion of the corrosion patch in the longitudinal direction.
- 3) As the D/t_p ratio was increased, the ultimate load decreased, and the relationship between the two is of hyperbolic concave type.
- 4) The relationship between the ultimate load and WR was non-linear, and the relationship was similar to that for D/t_p .
- 5) The non-dimensionalized relative area reduction $a_r = AR / A_g$ (or the relative net area $a_n = 1 - a_r$) was found to be the dominant parameter for the ultimate load, with the other parameters, particularly D/t_p , introducing relatively minor scatter.

A regression analysis of the 15 experimental and 46 FE loads of this project supplemented with 12 test loads from Refs. 8 and 10 led to a straight-line formula for relating the ultimate load to the relative area reduction $a_r = AR / A_g$ or, equivalently, to the relative net area, $a_n = A_n / A_g = 1 - a_r$. (Eqs. 15-11 and 15-15) However, the range of this formula was limited to $0.05 \leq a_r \leq 0.35$ (or $0.65 \leq a_n \leq 0.95$).

Then, the data base was further expanded with seven test loads from Ref. 9 and 30 FE loads from Ref. 5, and a new regression analysis performed to give a cubic

approximation for computing the ultimate load as a function of a_r or a_n over the whole range of $0 \leq a_r \leq 0.35$ (or $a_n \geq 0.65$). (Eqs. 15-20 and 15-24)

These straight-line and cubic formulas were set to fall between the regression curves for the pinned and fixed end conditions (up from the pinned conditions by one-third of the difference between the two) and give a slightly conservative match for the experimental results.

18.2 Recommendations

Two sets of recommendations are made here on the basis of the research completed in this project. One set is for the application of the information that was developed, and the other is for future research that is considered to be necessary in order to improve, generalize and expand the research completed in order to make it more valuable to industry.

18.2.1 Recommendations for Application of Completed Research

- 1) Idealization of a patch corroded section by using a series of segments with linearly varying thickness around the circumference is recommended for analyzing the cross section.
- 2) Analysis of the idealized cross section to compute the loads which can be used as limits of the member capacity: the loads to produce first yielding or local buckling. This can be conveniently done by using FORTRAN-77 program CXS.for developed in the project.
- 3) Ultimate load of a patch corroded section can be approximately computed from the formulas developed in the project, specifically, Eq. 15-24 repeated here as Eq. 18-1.

$$p = \frac{P_u}{P_{yld}} = 0.18 a_n + 0.82 a_n^3 \quad (18-1)$$

for $a_n \geq 0.65$

where

$$a_n = \frac{A_n}{A_g} \quad (18-2)$$

a_n is the relative net area with A_n being the net area of the reduced corroded section and A_g being the gross area defined by Eq. 18-3 .

$$A_g = \pi (2 R_i + t_{\max}) t_{\max} \quad (18-3)$$

where

R_i = inside radius

t_{\max} = maximum thickness in the corroded section.

In Eq. 18-1, $P_{\text{yld}} \neq (P_y = A_{\text{orig}} F_y)$ but $P_{\text{yld}} = A_g F_y$ where $A_g < A_{\text{orig}}$. When corrosion is not all around the circumference, $t_{\max} = t_{\text{orig}}$, and A_g is equal to the area of the original uncorroded section. [In the Final Report, these computations will be incorporated into program CXS.for.]

4) Repair of patch corroded segments can be accomplished by using epoxied or grouted split sleeves to compensate for the material lost to corrosion and to prevent local buckling. Repair with sleeves is also suitable for walls with local buckles already developed (as was done for Specimen P1-C1), or dents. When the loss of the cross section or the depth of dents is moderate (less than 25-30%), internal grouting can also be used for repairing the damage.

18.2.2 Recommendations for Future Research

The following studies are recommended for future work on the basis of the research described in this report:

1) Experimental and analytical studies in order to extend the simplified formula Eq. 18-1 (Eq. 15-24) to sections with net areas smaller than the $a_n = 0.65$ of Eq. 18-1, that is, for reduction of area a_r larger than 35%.

- 2) Refinement of the proposed ultimate strength formula to include the effect of patch thickness slenderness parameter D/t_{\min} (or D/t_p). This parameter is indicative of the initiation of local buckling, and Figs. 15-6 and 15-7 show that it introduces a consistent scatter, although rather narrow in the ultimate strength (p) relationship vs. the reduction of the area (a_p) within the range of the completed study. The effect should become more pronounced for sections with greater thickness reduction over larger area around the circumference.

- 3) Investigation of the effect of closely spaced interacting corrosion patches, such as were observed on the salvaged Specimens P2-C1 and P3-C1 in which local buckles formed an interlocking chain over longitudinally staggered patches as can be seen in Figs. 6-9 and 6-16 (contour plots showing the overlapping buckles) for Specimens P2-C1 and P3-C1, respectively. Testing of field-corroded salvaged specimens and of specimens with corrosion damage simulated by grinding should be accompanied and enhanced by FE analysis. Survey of the patterns of patch corrosion on members in existing or salvaged structures is very desirable in order to define geometrical patterns for developing a simplified engineering procedure and/or formulas.

- 4) Study of the effect of end conditions and member length on the ultimate strength. Figures, such as Figs. 15-8 and 15-9, show a growth of the effect on the strength with greater reduction of the cross-sectional area due to corrosion. Only a few test specimens had clearly defined pinned or fixed ends and they supported the limits obtained from FE analysis. Most of the test specimens fall between the limits for the specimens with pinned and fixed ends. With a few exceptions, the tested specimens were of short length, and no consistent pattern could be detected for the longer specimens.

- 5) Development of design guidelines for repairing corrosion damaged members by using epoxied or grouted sleeves. This method was used in this project (Specimen P1-C1) and in concurrent work by Hebor and Ricles [5], but the design approach was very elementary and over conservative.

19. ACKNOWLEDGMENTS

This report describes the work performed in Area One of the project "Residual Strength and Repair of Damaged and Deteriorated Offshore Structures" at Lehigh University, Department of Civil Engineering (Le-Wu Lu, Chairman). The project was within the managerial structure of ATLSS (Advanced Technology for Large Structural Systems, John W. Fisher, Director). Area One entitled "Corrosion Damage -- Effect on Strength" was directed by Dr. Alexis Ostapenko and was one of three areas, with Area Two directed by Dr. Stephen P. Pessiki and Area Three by Dr. James M. Ricles. The tests of Area One were all conducted in Fritz Engineering Laboratory.

The project was sponsored as a Joint Industry Project by the following: EXXON Production Research Company (Contract: PR-14257), Minerals Management Service (DOI) (Contract: 14-35-0001-30719), Mobil Technology Company (Contract: 055-20-017), and Shell Offshore, Inc. (Contract: ANE-090193-KAD). We are most grateful for the financial support provided by these organizations. We are also indebted for the advice and guidance of the following Representatives of these organizations: Jaime Buitrago (EXXON), Douglas R. Angevine (Mobil), Charles E. Smith (MMS/DOI), and Kris A. Digre (Shell).

Gratitude is extended to Mr. Stephen D. Long who was instrumental in the donation of several gallons of Epoxy cement by Protective Coating Co. of Allentown. This Epoxy was used in the sleeve repairs of damaged tubes and in test setups.

We are also thankful to undergraduate students Steven G. Kerr, Benjamin A. Graybeal and Huston M. Dawson who were helpful in testing and/or computations and reduction of the experimental data.

Thanks are also due to Frank E. Stokes, Charles F. Hittinger and Eugene P. Matlock, and others of the technical staff of the laboratory. Russell C. Longenbach ably helped with test instrumentation.

20. REFERENCES

[1] ABAQUS

"ABAQUS User's Manual" (Version 5.4) Copyright Hibbitt, Karlsson and Sorensen, Inc., 1080 Main St., Pawtucket, Rhode Island, 02860-4847, 1994.

[2] AISI

"Specification for the Design of Cold-Formed Steel Structural Members", American Iron and Steel Institute, Washington, D.C., pp. I-39, 1986.

[3] API

"Recommended Practice for Planning, Designing, and Constructing Fixed Offshore Platforms, API, RP2A", American Petroleum Institute, Washington, D.C., 1989.

[4] DnV

"Rules for the Design, Construction and Inspection of Fixed Offshore Structures", Det Norske Veritas (DnV), Oslo, 1974.

[5] Hebor, M.F., and Ricles, J.M.

"Residual Strength and Repair of Corrosion Damaged Steel Tubular Bracing", *Proceedings of the Structural Stability Research Council*, 1994, Annual Task Group Technical Session, June 20, 1994, Lehigh University, Bethlehem, PA, (ISBN 1-879749-57-2).

[6] Narayanan, R., ed.

"Axially Compressed Structures: Stability and Strength", Elsevier Science Publishing Co., New York, 1982.

- [7] Ostapenko, A.
"Local Buckling of Welded Tubular Columns", *Proceedings of the International Colloquium on Stability of Structures under Static and Dynamic Loads*, Washington, D.C., May, 1977, American Society of Civil Engineers, New York, 1977, pp. 367-374.
- [8] Ostapenko, A., Wood, B.A., Chowdury, A., and Hebor, M.F.
"Residual Strength of Damaged Tubular Members in Offshore Structures", Volume 1, Report 93-03, ATLSS-Lehigh University, Bethlehem, PA, 1993.
- [9] PMB/TX A&M
"Testing and Evaluation of Damaged Jacket Braces", PMB Engineering, Inc., and Texas A&M University, *Final Report*, PMB Engineering Inc., Houston, May 1990, (released December 1994).
- [10] Ricles, J.M., Bruin, W.M., Sooi, T.K., Hebor, M.F., and Schönwetter, P.C.
"Residual Strength Assessment and Repair of Damaged Offshore Tubulars", *Proceedings of the 27th Annual Offshore Technology Conference*, Houston, May, 1995, (OTC 7807), pp. 6-12.
- [11] Ricles, J.M., and Hebor, M.F.
"Residual Strength and Epoxy-Based Grout Repair of Corroded Offshore Tubulars", *Proceedings of the 7th International Conference on Behavior of Offshore Structures (BOSS'94)*, Volume 3: Structures, Pergamon Press, 1994, pp. 307-322.

21. NOMENCLATURE

a	Circumferential width of the constant minimum thickness in the patch. [in.]
a_n	Relative (non-dimensionalized) net area.
a_r	Relative (non-dimensionalized) area reduction.
a_1, a_2	Constants used in cubic approximation formulas.
A, A_{orig}	Uncorroded original cross-sectional area. [in. ²]
A_n	Calculated area of corroded tube cross section. [in. ²]
A_g	Gross cross-sectional area. [in. ²] ($A_g = A$ or $A_g = \pi (2 R_i + t_{max}) t_{max}$)
A_p	Calculated cross-sectional area of corroded tube cross section from idealized thickness model. [in. ²]
AR	Area reduction. [in. ²]
b	Longitudinal width of the constant-minimum thickness portion in the patch. [in.]
c	Circumferential width of the main corrosion patch. [in.]
c_x, c_y	Shift of centroid from center of undamaged cross section. [in.]
d_i	Distance from end 'A' to location 'i'. [in.]
D, D_o	Outside diameter. [in.]
D_d	Diameter of tube with reduced thickness t_d . [in.]
D_m	Mid-thickness diameter. [in.]

D_m^{N-S}	Outside diameter measured using 6-inch micrometer in North-South direction. [in.]
D_{max}	Maximum outside diameter used to compute out-of-roundness. [in.]
D_{min}	Minimum outside diameter used to compute out-of-roundness. [in.]
D_{N-S}	Computed outside diameter between North and South reference lines. [in.]
D_p	Pedestal diameter used in calculating specimen diameter. [in.]
e, e_x, e_y	End eccentricity from center of circle. [in.]
E	Modulus of elasticity. [ksi]
f_{exp}	Maximum stress due to the ultimate experimental load. [ksi]
f_{max}	Maximum stress in the <i>patch</i> which is a function of the axial load P . [ksi]
F_{cr}	Critical average column stress controlled by local buckling. [ksi]
F_y	Yield stress. [ksi]
g	Dial gage measurement used in calculating diameter adjustment parameter for 'pedestal' method. [in.]
g^N, g^S	Dial gage measurements at North and South reference lines. [in.]
g_i	Dial gage measurement at location 'i' from end 'A'. [in.]
$g_{0.5}$	Dial gage measurement at 0.5 in. from end 'A'. [in.]
$g_{26.5}$	Dial gage measurement at 26.5 in. from end 'A'. [in.]
g_1, g_2	Dial gage measurements using angle tool. [in.]
h	Longitudinal height (length) of corroded band. [in.]
I_a	Moment of inertia of minimum thickness portion of the corrosion patch. [in. ⁴]

I_d	Moment of inertia of the tube with a reduced thickness of t_d . [in. ⁴]
$I_p, I_x,$ I_y, I_{xy}	Effective moments of inertia taken from thickness measurements. [in. ⁴]
I_w	Moment of inertia of cosine transition portion of the corrosion patch. [in. ⁴]
k	Stress amplification factor. (Ratio of maximum to average stress)
L, L_s	Specimen length. [in., ft.]
L_g	Longitudinal gage length of specimen dial gages. [in.] or, Radial distance between specimen dial gages. [in.]
m	Depth micrometer measurement used in calculating diameter adjustment parameter for 'pedestal' method. [in.]
m^N, m^S	Depth micrometer measurements at North and South reference lines. [in.]
OOR	Specimen out-of-roundness.
OOS	Specimen out-of-straightness. [in.]
p	Non-dimensionalized axial load.
P_f, P_p	Straight-line approximation of fixed-end/pinned-end finite element ultimate loads. [kips]
P	Axial load acting on cross section either concentrically or eccentrically. [kips]
P_u	Ultimate (dynamic) experimental or computed load. [kips]
P_{uP}, P_{uF}	Finite element ultimate load for pinned/fixed-end conditions. [kips]
P_{uFE}	Ultimate load from finite element analysis. [kips]

P_{us}	Static ultimate test load. [kips]
P_y	Axial load causing yielding of undamaged cross section. ($P_y = AF_y$) [kips]
$Q, Q_x,$ Q_y	Static moments of inertia about the center of the tube. [in.^3]
R	Outside radius. [in.]
R_i	Inside radius. [in.]
t	Uncorroded tube thickness, actual. [in.]
t_a	Equivalent average thickness over the corroded area. [in.]
$t_{a, \text{circ}},$ $t_{a, \text{long}}$	Average thickness of $0.8R \times 0.2R$ (or $R \times R/4$) corrosion patch in circumferential, longitudinal direction. [in.]
t_d	Reduced thickness outside the corrosion patch. [in.]
t_m	Mean thickness of $R \times R/4$ corrosion patch used in local buckling formulas to estimate stress and load at which local buckles would develop. [in.]
t_{max}	Maximum thickness of corroded tube cross section. [in.]
t_{min}	Minimum thickness of $R \times R/4$ corrosion patch. [in.]
t_p	Wall thickness in constant-thickness portion of corrosion patch. [in.]
t_r	Reduced wall thickness. [in.]
v	($v/2$) = longitudinal width of cosine variation of wall thickness within the main patch. [in.]
w	($w/2$) = circumferential width of cosine variation of wall thickness within the main patch. [in.]

WR	Width reduction. [in.]
x	Distance in circumferential direction for unfolded cross section. [in.]
y	Distance in longitudinal direction. [in.]
α	Nondimensionalized parameter used in local buckling formulas.
δ	Initial out-of-straightness. [in.] or, Measured axial shortening of test specimens. [in.]
δ_{adj}	Adjusted axial shortening of test specimens. [in.]
δ_L, δ_P	Adjustment parameter used in 'lathe'/'pedestal' method. [in.]
Δ_S, Δ_N	Axial shortening from specimen South/North dial gage. [in.]
θ	End rotation of test specimens or angle encompassed by corrosion patch. [rad]
ν	Poisson's ratio.
ξ	Nondimensionalized parameter used in local buckling formulas.

TABLES

Table 1: Geometrical Data for all Specimens and Load Summary

Spec	L [ft.]	D [in.]	t [in.]	Fys [ksf]	Area		* Test	FEM			Load [kips]			Formulas		
					Ag gross [in. ^ 2]	An net [in. ^ 2]		Plep pin	Plef fix	Ply	CXS.for		Ppin (15-23a)	Pdes (15-24)		
											Pexp	Papi API			Dnv DnV	
1	2	3	4	5	6	7	8	9	10	11	12	13	14	15	16	
Salvaged																
P1-C1	24.50	10.70	0.385	40.89	11.495	7.964	S	232	---	---	228.7	NA	NA	136.9	186.8	
P2-C1	3.33	10.70	0.385	40.89	12.217	8.169	S	262	---	---	232.4	240.7	242.3	128.4	182.6	
P3-C1	6.00	10.70	0.385	40.89	11.612	9.018	S	275	---	---	271.4	271.3	270.7	205.3	248.7	
P4-C2	20.56	14.06	0.518	40.72			S	614	---	---						
Patch by Grinding																
P5	2.33	5.502	0.122	42.11	2.062	1.951	S	81.5	74.3	80.8	73.0	70.6	72.4	72.6	75.1	
P6	2.33	5.502	0.122	42.11	2.062	1.909	S	73.0	66.9	77.1	67.8	62.1	66.8	67.6	71.0	
P7	2.33	5.502	0.122	42.11	2.062	1.888	S	73.4	64.0	75.9	65.3	57.6	63.7	65.2	69.0	
P8	2.33	5.502	0.122	42.11	2.062	1.833	S	63.8	56.5	72.2	59.1	53.3	58.1	59.1	63.9	
P9	2.25	5.502	0.122	42.11	2.062	1.802	S	63.0	53.5	70.8	55.5	47.7	53.8	55.8	61.2	
P10	1.04	5.502	0.122	42.11	2.062	1.786	F	74.9	55.0	72.4	53.7	44.7	51.5	54.2	59.8	
P11	1.04	5.502	0.122	42.11	2.062	1.574	F	63.9	34.8	62.1	36.1	31.0	35.0	35.4	43.6	
P12	1.04	5.502	0.122	42.11	2.062	1.574	F	61.8	35.7	62.4	36.1	31.0	35.0	35.4	43.6	
P13	1.04	5.502	0.122	42.11	2.062	1.770	C	57.8	55.4	71.8	51.9	41.6	48.8	52.6	58.5	
P14	1.04	5.502	0.122	42.11	2.062	1.801	C	61.1	55.8	73.1	55.6	47.9	53.9	55.8	61.1	
P15	1.04	5.502	0.122	42.11	2.062	1.770	C	57.4	55.9	71.5	52.0	41.9	49.0	52.6	58.5	
P16	2.33	5.502	0.122	42.11	2.062	1.896			66.3	76.5	66.6	63.9	66.0	66.0	69.7	
P17	1.04	5.502	0.122	42.11	2.062	1.545			33.0	62.8	33.3	27.8	31.9	33.2	41.7	
P18	1.04	5.502	0.122	42.11	2.062	1.751			56.1	72.4	53.5	51.4	53.1	50.8	56.9	
P19	1.04	5.502	0.122	42.11	2.062	1.633			40.8	65.3	41.8	37.7	41.0	40.1	47.8	
P20	1.04	5.502	0.122	42.11	2.062	1.516			31.5	59.5	30.5	25.5	29.3	31.1	39.8	
P21	2.33	5.502	0.122	42.11	2.062	1.868			62.0	74.9	62.8	52.1	60.1	62.8	67.1	
P22	2.33	5.502	0.122	42.11	2.062	1.878			63.0	75.3	64.1	55.1	62.1	64.0	68.0	
P23	1.04	5.502	0.122	42.11	2.062	1.574			34.5	62.0	36.1	31.0	35.0	35.4	43.6	
P24	1.04	5.502	0.122	42.11	2.062	1.359			21.4	51.4	23.2	18.7	21.9	21.2	30.7	
P25	1.04	5.502	0.122	42.11	2.062	1.434			28.5	54.9	29.3	25.2	28.4	25.6	34.8	
P26	1.04	5.502	0.122	42.11	2.062	1.357			24.6	52.0	25.6	20.5	24.1	21.1	30.6	
P27	1.04	5.502	0.122	42.11	2.062	1.359			22.2	52.1	23.2	18.7	21.9	21.2	30.7	

Col. 6 Ag = Gross Area = 2 Pi (Ri + tmax) tmax [Eq. 18-3]
 Col. 7 An = Net Area, computed by CXS.for

*Col. 8 Type of end fixtures used in testing: f = fixed, s = spherical, c = cylindrical

Table 2-1: Material and Geometric Properties of Salvaged Test Specimens.

Specimen	D (in.)	t (in.)	L tube (ft)	D/t	D/tp	F _{y,static} (ksi)	F _{u,static} (ksi)	P _{exp} (kips)	Failure Mode
P1-C1	10.70	0.385	24.50	27.78	--	40.89	62.66	223 (232)	Loc. bckle at hole
P2-C1	10.70	0.385	3.33	27.78	59.42	40.89	62.66	268 (280)	Loc. bckle
P3-C1	10.70	0.385	6.00	27.78	54.69	40.89	62.66	275 (280)	Loc. bckle
P4-C2	14.06	0.518	20.56	27.14	43.08	40.72	69.72	614	As column

Note: Experimental ultimate loads, P_{exp}, are given as:

Static Loads, no parentheses
and Dynamic Loads, (in parentheses)

Table 2-2: Example Micrometer and Ultrasonic Calibration Data

Micrometer (in.)	Ultrasonic (in.)	% error
0.325	0.321	-1.23
0.773	0.773	0.00
0.998	0.994	-0.40
0.356	0.357	0.28
0.261	0.261	0.00
0.351	0.354	0.85
0.382	0.382	0.00
0.341	0.341	0.00
0.213	0.216	1.41
0.371	0.367	-1.08
0.417	0.419	0.48
0.375	0.375	0.00
0.960	0.960	0.00
0.120	0.120	0.00
0.488	0.485	-0.61

Table 8-1 Diameter and OOR Measurements for Specimen P9

Dist. from End 'A'	Diam. Dir.	Calculated and Measured Diameters				Ave. Rel. OOR
		Pedestal Micrometer	Pedestal Dial Gage	6-inch Micrometer	Lathe Method	
A	B	C	D	E	F	G
0.5	N-S	5.5047	5.5054	5.5113	5.5209	.0040
	E-W	5.5780	5.5749	5.5750	5.5657	
5.5	N-S	No Measurements Made		5.6143	5.6086	.0113
	E-W			5.4797	5.4837	
10.75	N-S			5.5800	5.5884	.0110
	E-W			5.4690	5.4666	
12.4375	N-S			5.5667	5.5686	.0056
	E-W			5.5090	5.5064	
13.5	N-S			5.4510	5.5310	.0003
	E-W			5.5360	5.5276	
15	N-S			5.5020	5.5001	.0067
	E-W			5.5660	5.5743	
21.5	N-S			5.4150	5.4048	.0216
	E-W			5.6490	5.6438	
26.5	N-S	5.5050	5.4982	5.4950	5.4865	.0078
	E-W	5.5897	5.5941	5.5810	5.5730	
* Average =		5.54433	5.54317	5.54058	5.5365	
* Std. Dev. =		0.03971	0.04196	0.03792	0.0351	
** Average =				5.53638	5.5343	
** Std. Dev. =				0.05740	0.0581	

* These values represent distances 0.5 and 26.5 only.

** These values include all readings

Table 8-2 Diameter and OOR Measurements for Specimen P13

Distance from End 'A'	Diameter Direction	Diameter Measurements		Average Relative OOR
		6-inch Micrometer	Lathe Method	
A	B	C	D	E
0.5	N-S	5.4300	5.4324	0.0002
	E-W	5.4300	5.4347	
3.125	N-S	5.4200	5.4267	0.0057
	E-W	5.3700	5.3657	
5.5	N-S	5.4100	5.4137	0.0006
	E-W	5.4200	5.4204	
7	N-S	5.3900	5.3907	0.0010
	E-W	5.4000	5.4017	
9.375	N-S	5.3700	5.3664	0.0054
	E-W	5.4200	5.4250	
12	N-S	5.2800	5.2637	0.0119
	E-W	5.3900	5.3907	
Average =		5.39417	5.39431	
Standard Deviation =		0.03989	0.04552	

Table 8-3 Average Diameter for Remaining Specimens

Spec.	P8	P10	P11	P12	P14	P15
Diam.	5.4985	5.4680	5.4680	5.4010	5.4930	5.4310

Table 8-4 OOS Measurements for Specimen P9

Dist. from 'A'	OOS Measurements	
	N-S (in.)	E-W (in.)
0.5	0.0	0.0
5.5	-0.0472	0.0417
10.75	-0.0405	0.0510
12.4375	-0.0318	0.0313
13.5	-0.0137	0.0209
15	0.0008	-0.0023
21.5	0.0442	-0.0361
26.5	0.0	0.0

Table 8-5 OOS Measurements for Specimen P13

Dist. from 'A'	OOS Measurements	
	N-S (in.)	E-W (in.)
0.5	0.0	0.0
3.125	-0.0043	0.0040
5.5	-0.0047	0.0013
7	-0.0044	0.0004
9.375	-0.0042	-0.0017
12	0.0	0.0

Table 9-1 Corrosion Patch Dimensions of Test Specimens [in inches]

Spec.	Principal Dimensions					Aux. Dimensions	
	a	c	b	h	t _p	w/2	v/2
P5	1.7	2.5	0.5	1.1	0.07	0.4	0.3
P5a	1.7	2.5	0.5	1.1	0.07	0.4	0.3
P6	1.7	2.5	0.5	1.1	0.05	0.4	0.3
P7	1.7	2.5	0.5	1.1	0.04	0.4	0.3
P8	2.75	3.55	0.75	1.35	0.05	0.4	0.3
P9	2.75	3.55	0.75	1.35	0.04	0.4	0.3
P10	2.75	3.55	0.75	1.35	0.035	0.4	0.3
P11	5.5	6.3	0.75	1.35	0.04	0.4	0.3
P12	5.5	6.3	1.5	2.1	0.04	0.4	0.3
P13	2.75	3.55	0.75	1.35	0.03	0.4	0.3
P14	1.7	4.6	0.5	1.3	0.04	1.45	0.4
P15	1.7	4.6	0.5	1.3	0.03	1.45	0.4

Table 9-2 Sample of Data for Patch Thickness Measurements
 Specimen P5 ($t_p = 0.07$ in.)

Node Location	Thickness 1	Thickness 2	Thickness 3	Average Thickness
5,5	0.070	0.070	0.070	0.0700
5,6	0.071	0.071	0.071	0.0710
5,7	0.071	0.071	0.071	0.0710
6,5	0.069	0.069	0.069	0.0690
6,6	0.069	0.069	0.068	0.0687
6,7	0.069	0.069	0.069	0.0690
7,5	0.069	0.069	0.069	0.0690
7,6	0.069	0.069	0.069	0.0690
7,7	0.069	0.069	0.069	0.0690
8,5	0.069	0.069	0.069	0.0690
8,6	0.069	0.068	0.068	0.0683
8,7	0.069	0.069	0.069	0.0690
9,5	0.069	0.069	0.069	0.0690
9,6	0.069	0.069	0.069	0.0690
9,7	0.069	0.069	0.069	0.0690
10,5	0.070	0.070	0.070	0.0700
10,6	0.070	0.070	0.070	0.0700
10,7	0.070	0.070	0.070	0.0700

Table 9-3 Comparison of Methods for Measuring t_p

Specimen	Desired t_p (in.)		Thickness Measurement Methods		
			Angle	Fork	UT
P5	0.07	Average	0.06968	0.07093	0.07001
		Std. Dev.	0.00070	0.00048	0.00016
P6	0.05	Average	0.04785	0.04907	0.05030
		Std. Dev.	0.00110	0.00094	0.00114
P7	0.04	Average	0.04069	0.04069	0.04016
		Std. Dev.	0.00069	0.00055	0.00031
P8	0.05	Average	0.05017	0.04927	0.05000
		Std. Dev.	0.00056	0.00060	0.00063
P9	0.04	Average	0.04042	0.04076	0.03998
		Std. Dev.	0.00076	0.00022	0.00068
P10	0.035	Average	0.03494	0.03489	0.03517
		Std. Dev.	0.00105	0.00104	0.00074
P11	0.04	Average	0.04017	0.03980	0.04001
		Std. Dev.	0.00131	0.00113	0.00058
P12	0.04	Average	0.03831	0.03898	0.03926
		Std. Dev.	0.00214	0.00143	0.00088
P13	0.03	Average	0.02920	0.02912	0.02895
		Std. Dev.	0.00175	0.00181	0.00140
P14	0.04	Average	0.03912	0.03921	0.03967
		Std. Dev.	0.00104	0.00105	0.00047
P15	0.03	Average	0.02950	0.02971	0.02973
		Std. Dev.	0.00149	0.00135	0.00112
Average Std. Dev. =			0.00114	0.00096	0.00074

Table 13-1 Modulus of Elasticity Calculations

Specimen	Gage Number	Loading Branch Modulus of Elasticity E (ksi)	Unloading Branch Modulus of Elasticity E (ksi)
P6	1	30,042	34,132
	2	31,261	29,100
	3	28,938	27,771
	4	27,272	28,299
P7	1	29,321	37,020
	2	28,285	28,502
	3	28,158	28,213
	4	27,420	27,700
P8	1	27,549	37,683
	2	32,863	26,752
	3	26,114	30,139
	4	33,136	25,190
Average =		29,197	30,042
Total Average =		29,619	

Table 13-2 Ultimate Loads from Tests and FE Analysis

Specimen Name	End Conditions		Pu-test (kips)		FE Analysis		
	TEST	F.E.	Dynamic (P _w)	Static (P _{us})	P _{uFE} (kips)	$\frac{P_{uFE}}{P_u}$	$\frac{P_{uFE}}{P_{us}}$
P5	Pin	Pin	84.5	81.5	74.34	0.880	0.913
		Fixed			80.82	0.956	0.992
P6	Pin	Pin	76.3	73.0	66.92	0.877	0.917
		Fixed			77.06	1.010	1.056
P7	Pin	Pin	76.5	73.4	64.00	0.837	0.872
		Fixed			75.86	0.992	1.034
P8	Pin	Pin	68.6	63.8	56.46	0.823	0.885
		Fixed			72.20	1.052	1.132
P9	Pin	Pin	66.0	63.0	53.52	0.811	0.850
		Fixed			70.84	1.073	1.124
P10	Fixed	Fixed	76.0	74.9	72.40	0.953	0.967
P11	Fixed	Fixed	67.1	63.9	62.14	0.926	0.972
P12	Fixed	Fixed	65.0	61.8	62.42	0.960	1.01
P13	Pin	Pin	60.6	57.8	55.40	0.914	0.958
P14	Pin	Pin	63.9	61.1	55.78	0.873	0.913
P15	Pin	Pin	60.0	57.4	55.88	0.931	0.974
SPEC. P5 TO P9 ONLY -- PINNED ENDS			Line 1	Average		0.8460	0.887
			Line 2	Standard Dev.		0.028	0.025
SPEC. P5 TO P9 ONLY -- FIXED ENDS			Line 3	Average		1.017	1.068
			Line 4	Standard Dev.		0.042	0.053
SPECIMENS P10 TO P12			Line 5	Average		0.946	0.983
			Line 6	Standard Dev.		0.015	0.019
SPECIMENS P13 TO P15			Line 7	Average		0.906	0.948
			Line 8	Standard Dev.		0.024	0.028

Table 14-1: Comparison of Cross-Sectional Properties and Stress Amplification Factors from Thickness Reduction Model and Measurements. ("Constant-Thickness Patch" Model)

Specimen / Failure	% error	% error	% error	% error	
	Area	Moment of Inertia	Centroid Shift	Amplification Factor, k	
C1 At buckle	7.11	-4.59	0.48	5.23	
C2 At buckle	0.30	-6.65	0.10	7.41	
P1-C1 At hole	5.59	-3.25	0.79	2.87	
P2-C1	Buckle 1	11.51	-1.88	2.60	11.11
	Buckle 2	12.26	2.21	1.37	11.15
	Buckle 3	6.47	-3.15	-0.46	8.93
	No buckle	0.89	-1.42	-0.90	2.45
P3-C1	Buckle 1	2.51	1.28	-0.60	3.95
	Buckle 2	1.09	-1.86	-1.21	4.55
	No buckle	1.01	-0.80	2.80	0.92
P4-C2 Column	0.47	-0.27	0.46	-3.52	

Note:

Amplification Factor, k = $\frac{\text{Maximum Stress in Cross Section}}{\text{Average Stress in Cross Section}}$

Table 15-1 Geometrical Parameters of Damaged Specimens

Common Dimensions D=5.502 in., t=0.122 in., Ri=2.629 in.									
Spec	L (in.)	t _p (in.)	Circumf		Longit		WR (in.)	D/t _p	AR (in. ²)
			a (in.)	c (in.)	b (in.)	h (in.)			
A	B	C	D	E	F	G	H	I	J
P5	28	0.07	1.7	2.5	0.5	1.1	2.1	79	0.105
P6	28	0.05	1.7	2.5	0.5	1.1	2.1	110	0.151
P7	28	0.04	1.7	2.5	0.5	1.1	2.1	138	0.172
P8	28	0.05	2.75	3.55	0.75	1.35	3.15	110	0.227
P9	27	0.04	2.75	3.55	0.75	1.35	3.15	138	0.258
P10	12.5	0.035	2.75	3.55	0.75	1.35	3.15	157	0.274
P11	12.5	0.04	5.5	6.3	0.75	1.35	5.9	138	0.484
P12	12.5	0.04	5.5	6.3	1.5	2.1	5.9	138	0.484
P13	12.5	0.03	2.75	3.55	0.75	1.35	3.15	183	0.290
P14	12.5	0.04	1.7	4.6	0.5	1.3	3.15	138	0.258
P15	12.5	0.03	1.7	4.6	0.5	1.3	3.15	183	0.290
P16	28	0.07	2.75	3.55	0.75	1.35	3.15	79	0.164
P17	12.5	0.035	5.5	6.3	0.75	1.35	5.9	157	0.520
P18	12.5	0.07	5.5	6.3	0.75	1.35	5.9	79	0.307
P19	12.5	0.05	5.5	6.3	0.75	1.35	5.9	110	0.425
P20	12.5	0.03	5.5	6.3	0.75	1.35	5.9	183	0.543
P21	28	0.03	1.7	2.5	0.5	1.1	2.1	183	0.193
P22	28	0.035	1.7	2.5	0.5	1.1	2.1	157	0.183
P23	12.5	0.04	5.5	6.3	0.5	1.1	5.9	138	0.484
P24	12.5	0.03	7.2	8.0	0.75	1.35	7.6	183	0.699
P25	12.5	0.04	7.2	8.0	0.75	1.35	7.6	138	0.623
P26	12.5	0.03	2.75	12.45	0.75	1.35	7.6	183	0.699
P27	12.5	0.03	7.2	8.0	0.3	0.9	7.6	183	0.699
P10C	27	0.035	2.75	3.55	0.75	1.35	3.15	157	0.274

$$WR = \frac{a+c}{2}$$

"Width Reduction" due to corrosion patch

$$AR = \frac{a+c}{2}(t-t_p)$$

"Area Reduction" due to corrosion patch

Table 15-2 Ultimate Loads from Tests and FE Analysis

F _y = 42.11 ksi		Ultimate Loads			
		Test		FE	
Spec	Brg Fixtr	Dynamic	Static	Pinned	Fixed
		P _u (kips)	P _u (kips)	P _{uF} (kips)	P _{uF} (kips)
A	B	C	D	E	F
P5	Sph	84.5	81.5	74.34	80.82
P6	Sph	76.3	73.0	66.92	77.06
P7	Sph	76.5	73.4	64.00	75.86
P8	Sph	68.6	63.8	56.46	72.20
P9	Sph	66.0	63.0	53.52	70.84
P10	Fixed	76.0	74.9	55.00	72.40
P11	Fixed	67.1	63.9	34.84	62.14
P12	Fixed	65.0	61.8	35.74	62.42
P13	Cyl	60.6	57.8	55.40	71.82
P14	Cyl	63.9	61.1	55.78	73.12
P15	Cyl	60.0	57.4	55.88	71.52
P16	--	No Test		66.34	76.48
P17	--	No Test		33.02	62.78
P18	--	No Test		56.14	72.38
P19	--	No Test		40.80	65.26
P20	--	No Test		31.50	59.48
P21	--	No Test		62.02	74.88
P22	--	No Test		62.96	75.34
P23	--	No Test		34.48	61.98
P24	--	No Test		21.38	51.40
P25	--	No Test		28.46	54.94
P26	--	No Test		24.58	52.00
P27	--	No Test		22.24	52.06
P10C	--	No Test		54.90	--

Table 15-3 Grouping of Specimens P5 to P15 according to WR and AR

WR [in.]	For AR [in. ²]	Specimens
2.1	0.105 - 0.193	P5,P6,P7,P21,P22
3.15	0.227 - 0.290	P8,P9,P10,P13,P14,P15, P16,P10C
5.9	0.307 - 0.543	P10,P12,P17,P18,P19, P20,P23
7.6	0.623 and 0.699	P24 and P25

Table 16-1 Local Buckling Loads from Tests, FE Analysis
and API and DnV Formulation

Specimen	Local Buckling Load (kips)			
	from Test	from FEM	from API	from DnV
A	B	C	D	E
P5	80	74	71.62	72.51
P6	60-64	59-64	64.05	67.10
P7	64-69	55-60	60.13	64.34
P8	48-54	51-53	53.33	58.07
P9	No Reading	47-51	47.84	53.94
P10	40, 65 (Fix)	47-52	44.74	51.46
P11	35-37 (Fix)	32-34	31.05	35.01
P12	42-45 (Fix)	35	31.05	35.01
P13	43-45	42-46	41.60	48.84
P14	45-50	47-50	48.36	54.09
P15	40-45	38-45	42.52	49.43
P16	No Test	67	63.94	66.05
P17	No Test	27-30	27.76	31.93
P18	No Test	47-52	51.44	53.13
P19	No Test	40	37.69	41.04
P20	No Test	25	24.49	28.74
P21	No Test	43-54	56.05	61.48
P22	No Test	52-58	58.11	62.93
P23	No Test	33	31.27	35.26
P24	No Test	21	18.66	21.90
P25	No Test	28	25.22	28.43
P26	No Test	24.5	20.54	24.11
P27	No Test	21.32	18.66	21.90

Table 17-1 Specimens of Ref. 5 which Developed Local Buckling
Comparison of Computed Loads with Test Loads

		Specimen								
		01	02	03	05	14	18	19		
Ptest [k]	1	424	601	436	465	198	262	614		
Fy [ksi]	1	35.7	43.6	36.6	35.9	36.0	34.5	59.7		
Pcomp [k]	1	516	683	488	612	310	297	823		
Agross	2	16.092	18.654	15.980	18.676	9.503	9.641	14.905		
Anet	3	14.573	15.550	13.568	16.907	8.420	8.421	13.601		
an=An/Ag		0.9056	0.8336	0.8491	0.9053	0.8860	0.8735	0.9125		
Papp [k]	4	443.55	508.36	382.97	517.17	249.70	234.06	700.54		
Pfst-yld [k]	3	489.35	602.30	469.88	558.75	295.33	272.37	753.51		
Papi [k]	3	468.295	584.087	438.308	544.842	297.044	273.120	724.677		
Pdrv [k]	3	486.658	597.482	467.143	556.546	296.614	272.505	739.430		
Error [%]	5								Avg.	S. Dev.
Papp	5	4.6	-15.4	-12.2	11.2	26.1	-10.7	14.1	2.542	14.548
Pfst-yld	5	15.4	0.2	7.8	20.2	49.2	4.0	22.7	17.057	15.195
Papi	5	10.4	-2.8	0.5	17.2	50.0	4.2	18.0	13.946	16.457
Pdrv	5	14.8	-0.6	7.1	19.7	49.8	4.0	20.4	16.467	15.461
P (Ref. 5)	5	21.7	13.6	11.9	31.6	56.6	13.4	34.0	26.121	14.925

1 From Table 3-15 of Ref. 9

2 $Agross = \pi(2R + T_{max})T_{max}$

3 Computed via program MXS.for

4 Computed using Eq. 15-24, Papp=function of an

5 [%]=100(P-Ptest)/Ptest

FIGURES

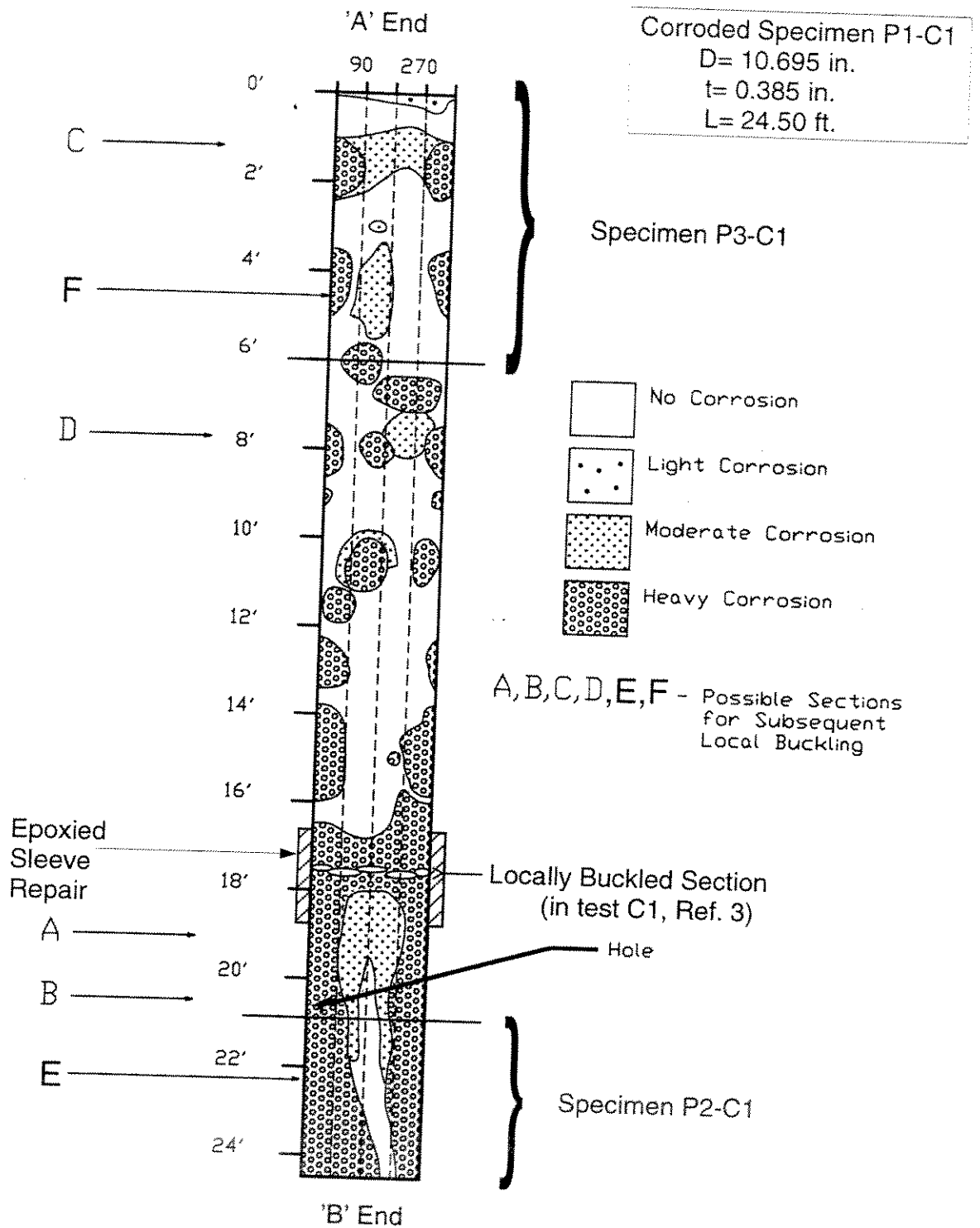


Figure 2-1: Specimen P1-C1 -- Map of Corrosion on Unfolded Surface of Tube.

Corroded Specimen P4-C2
 D= 14.06 in.
 t= 0.518 in.
 L= 20.56 ft.

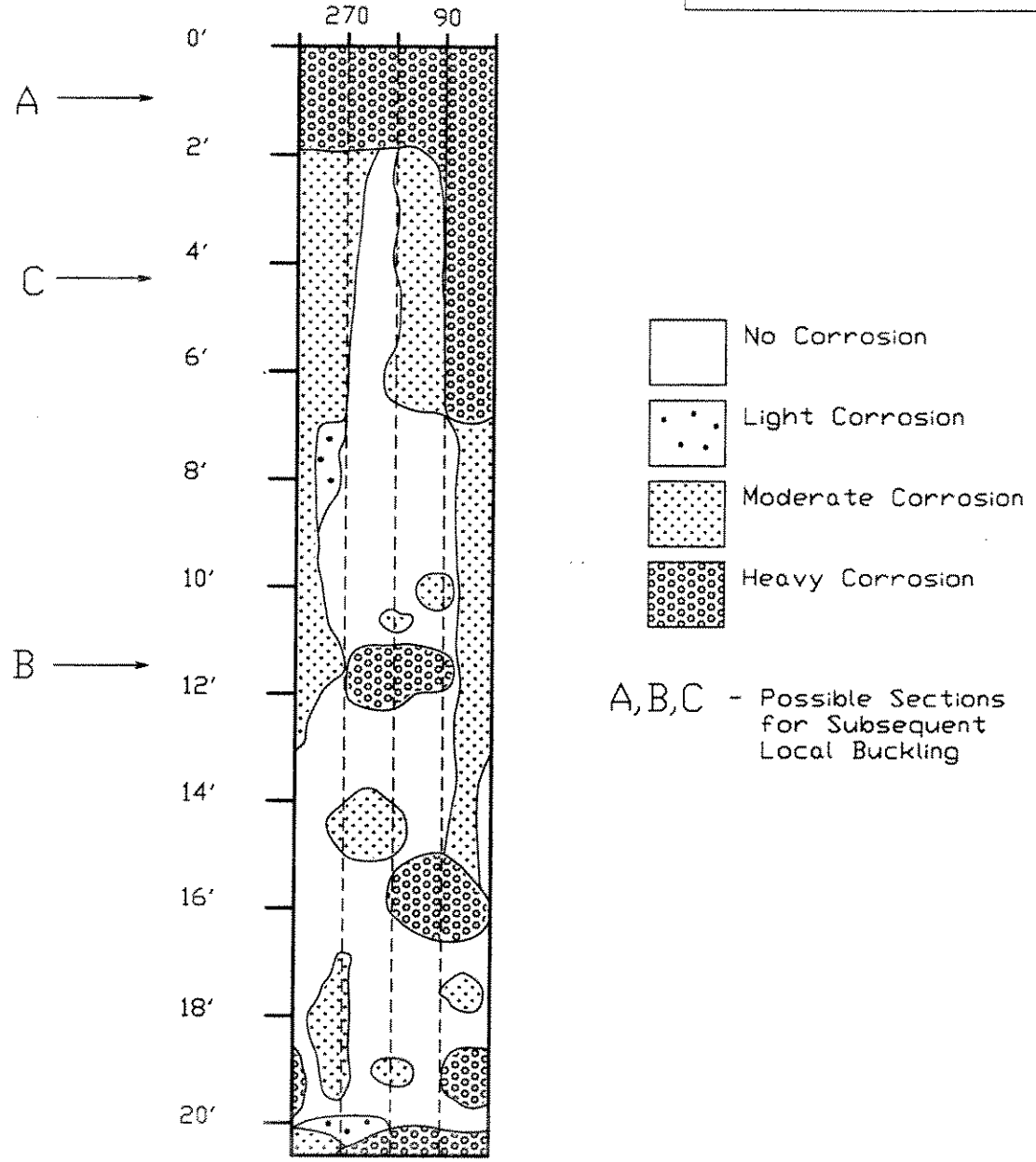


Figure 2-2: Specimen P4-C2 -- Map of Corrosion on Unfolded Surface of Tube.

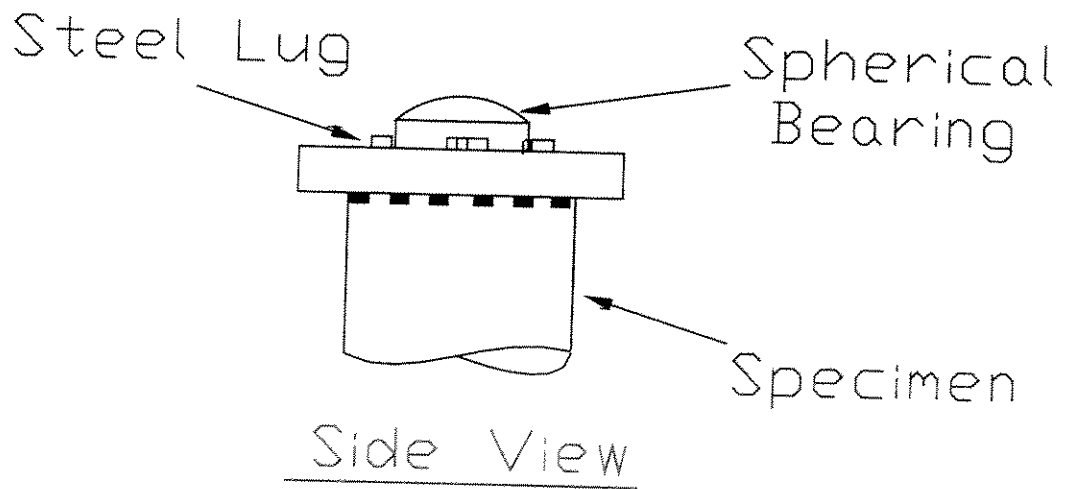
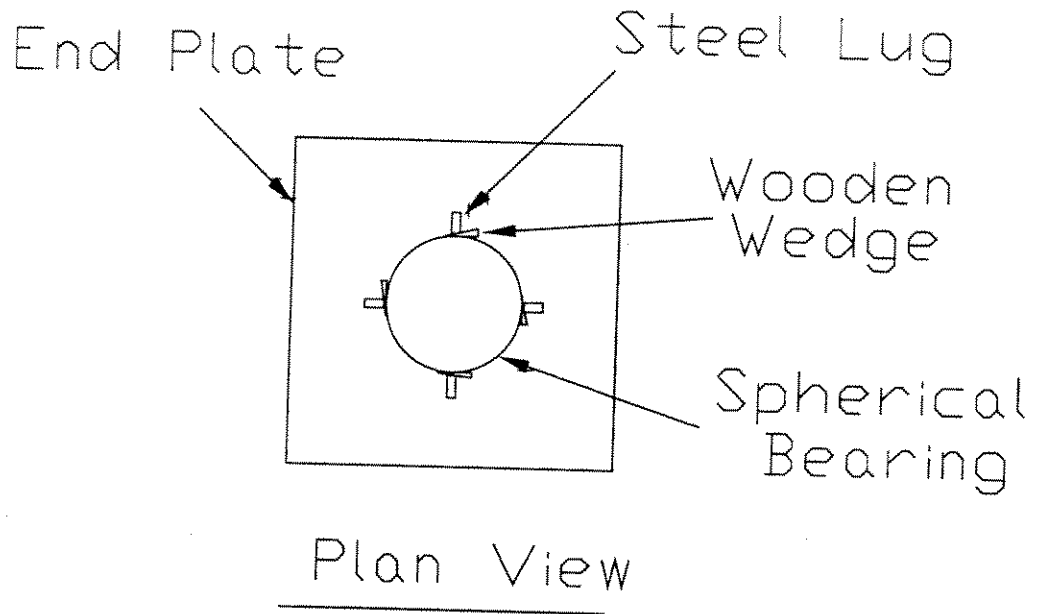


Figure 4-1: End Plates and Spherical Bearings of Long-Column Specimens

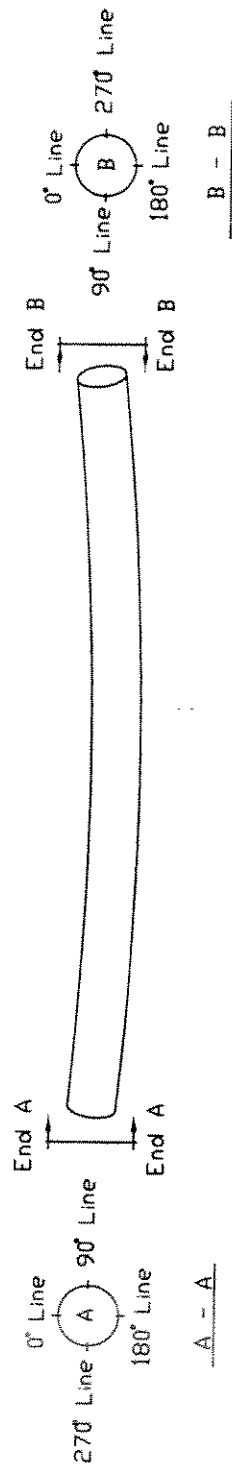


Figure 4-2: Scheme for Labelling Reference Lines.

SPECIMEN P1-C1

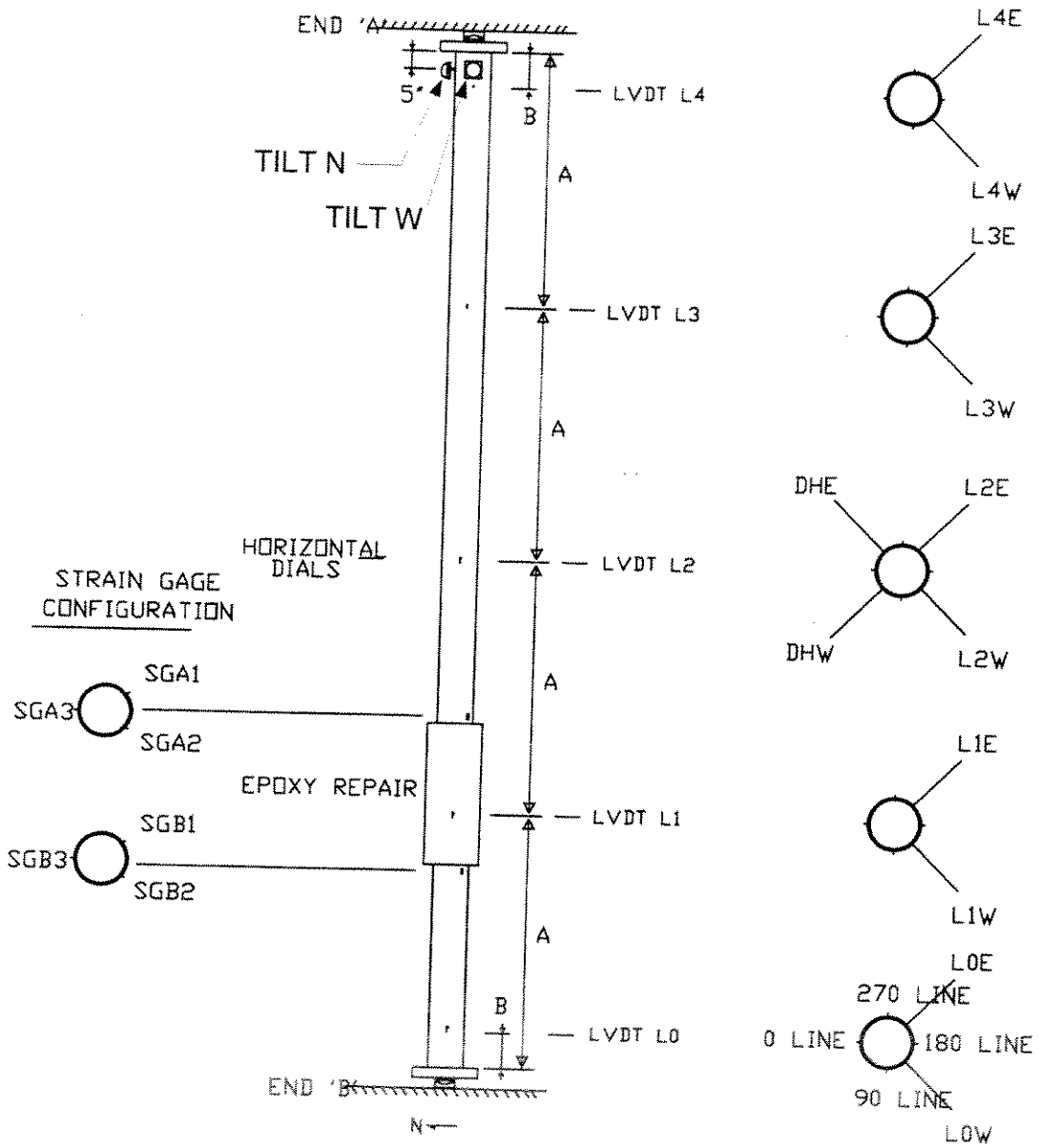


Figure 4-3: Instrumentation setup for Specimen P1-C1.

SPECIMEN P4-C2

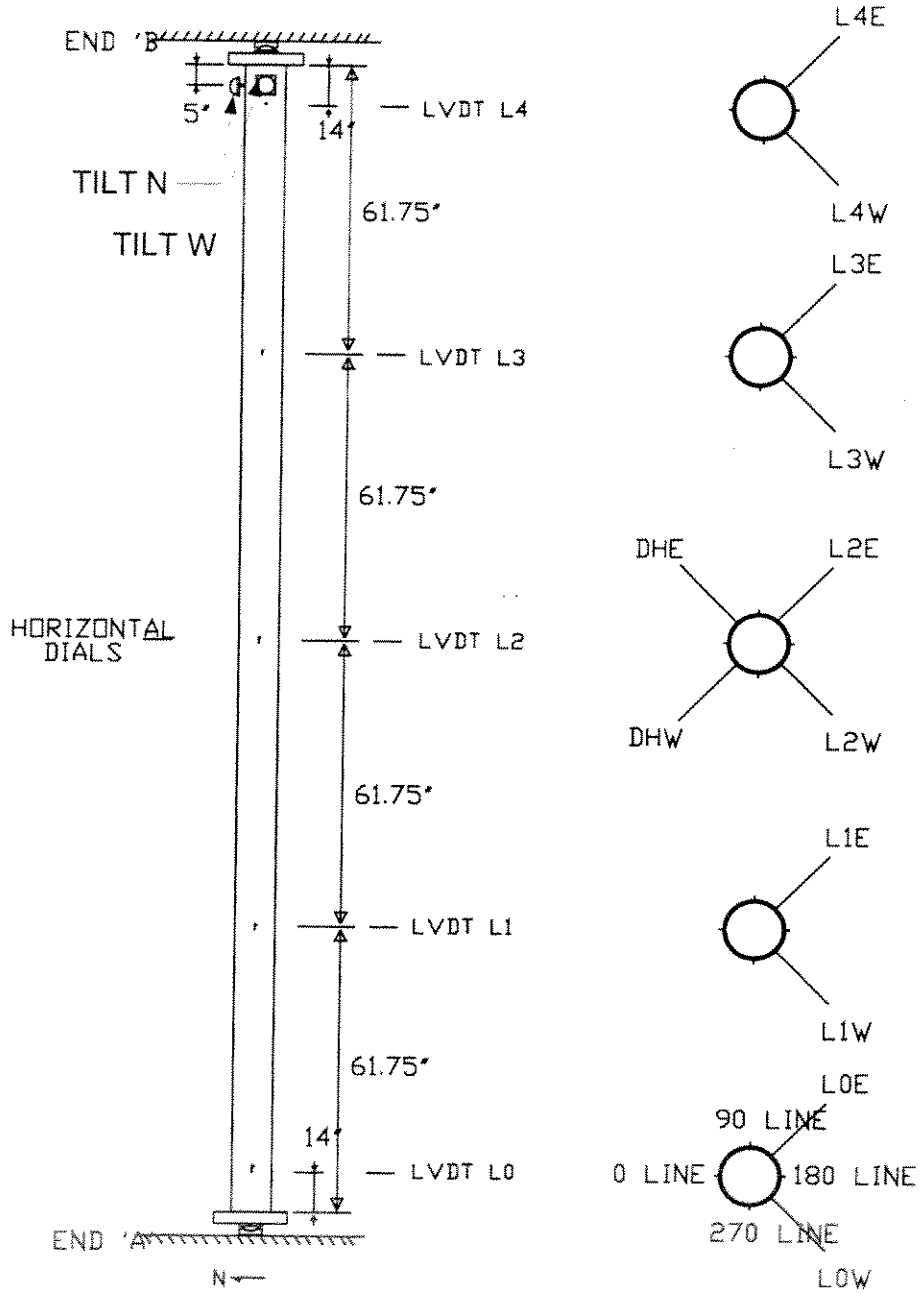


Figure 4-4: Instrumentation setup for Specimen P4-C2.

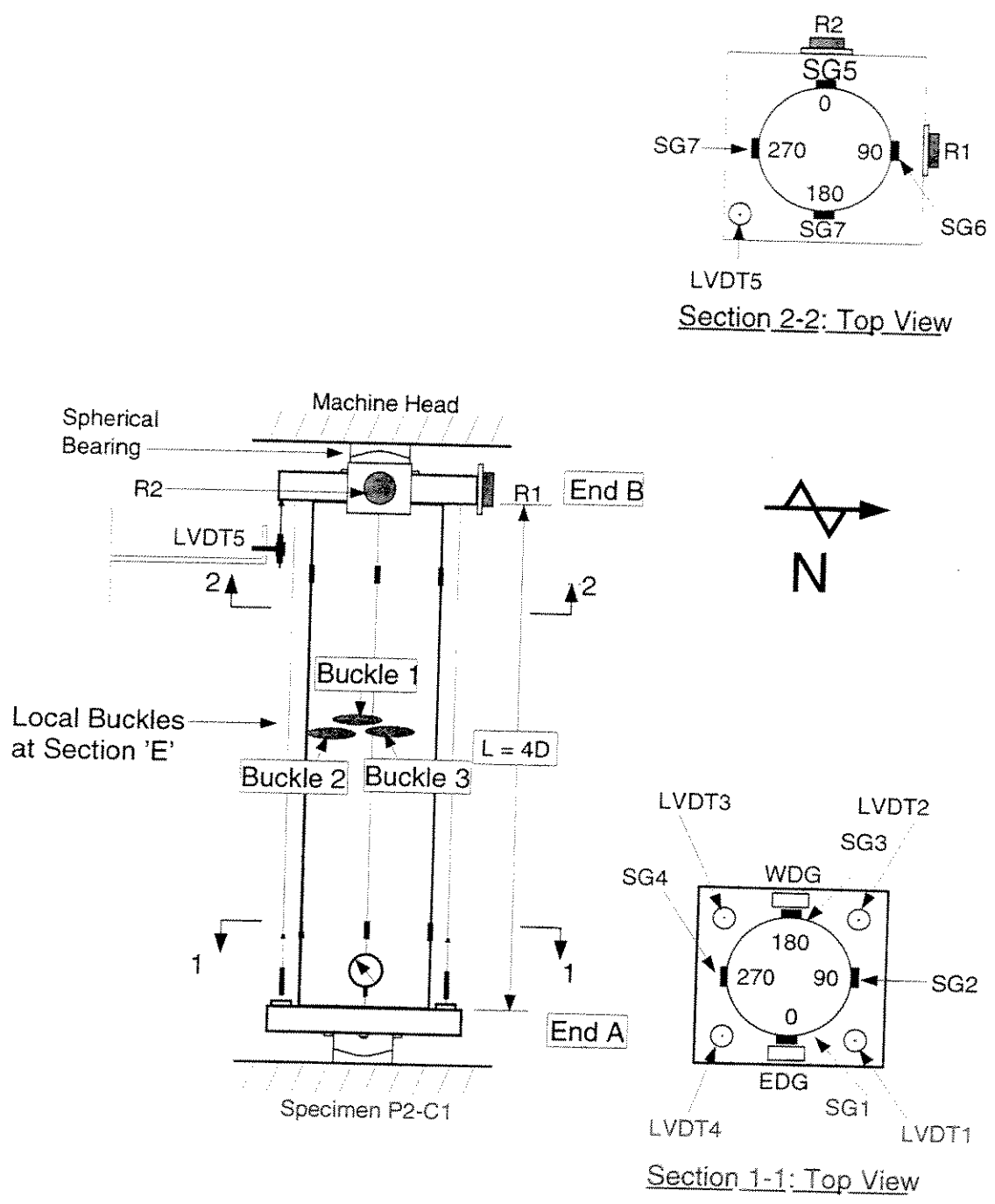


Figure 4-5a: Instrumentation Setup for Specimens P2-C1.

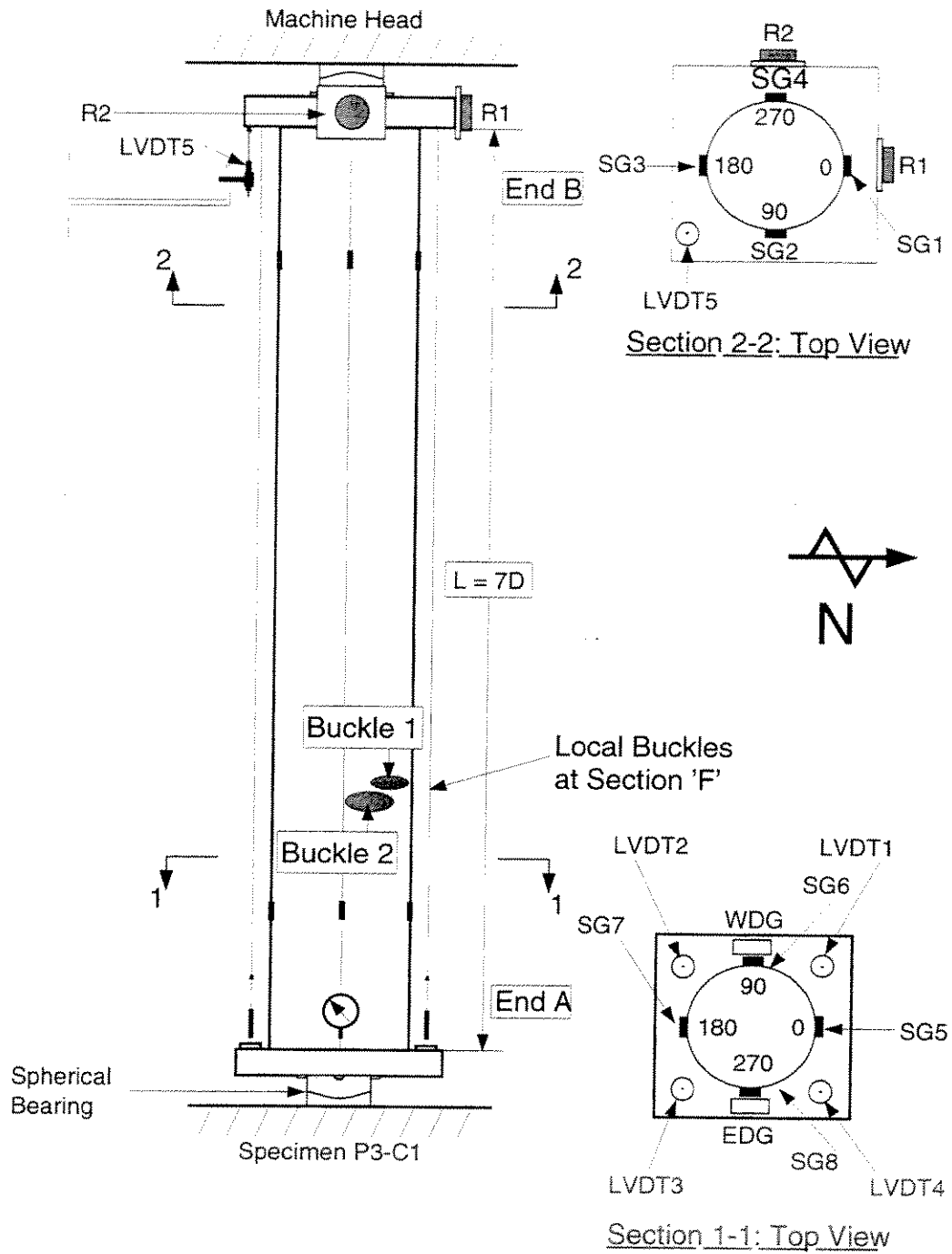


Figure 4-5b: Instrumentation Setup for Specimen P3-C1.

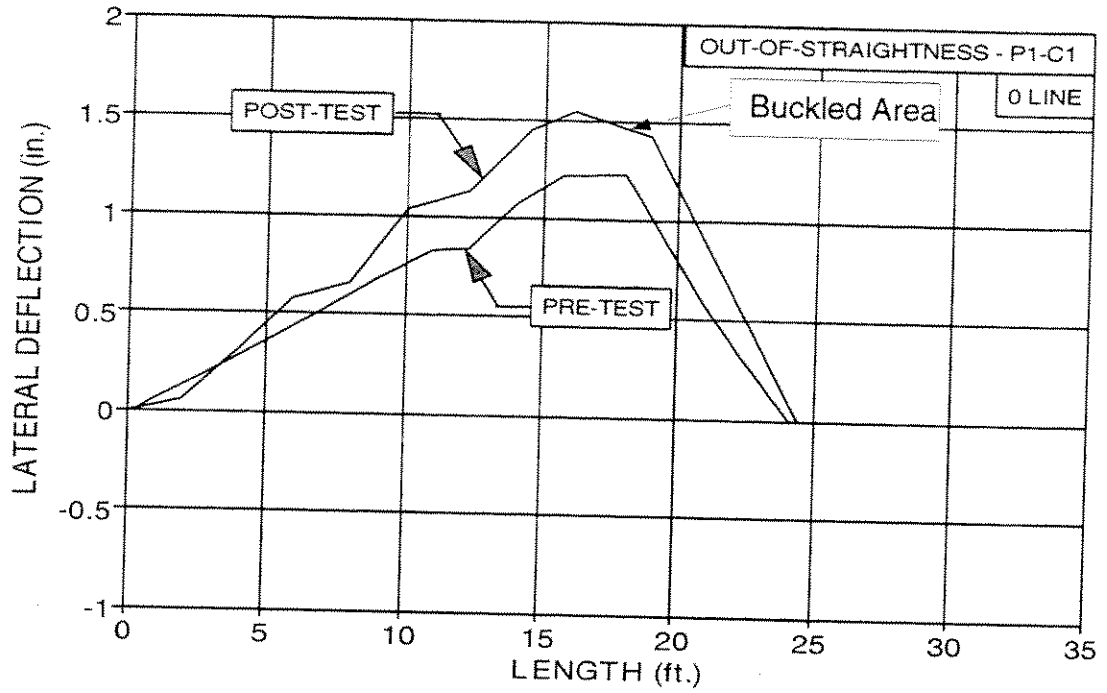


Figure 4-6: Pre and Post-Test Out-of-straightness Profiles for Specimen P1-C1, 0 degree longitudinal reference line.

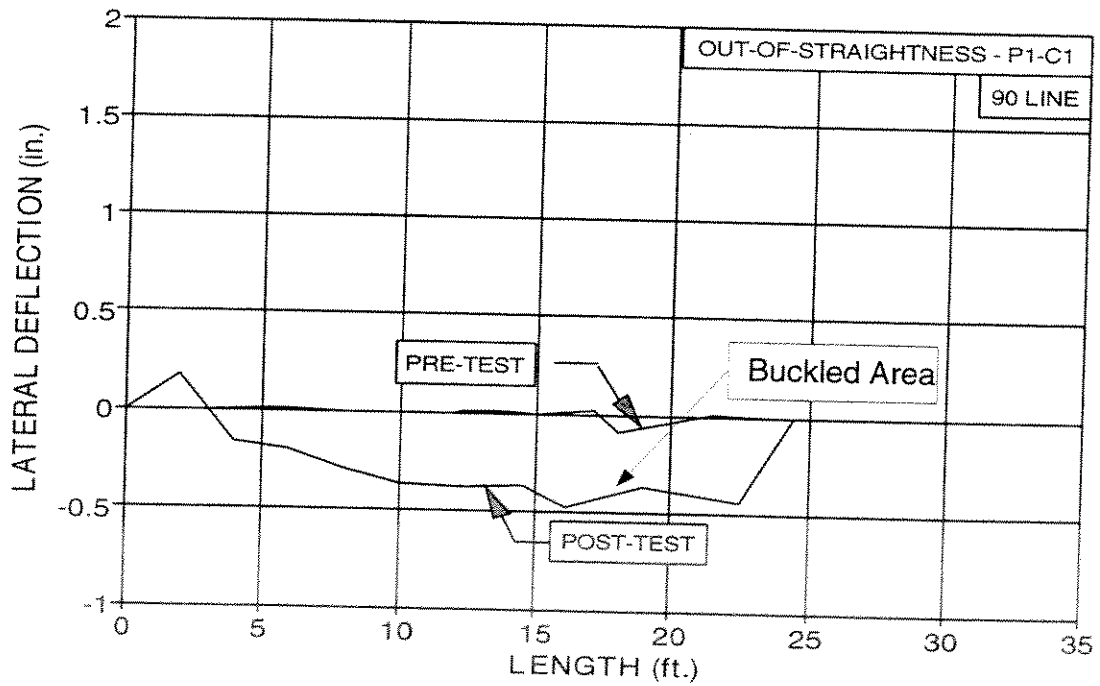


Figure 4-7: Pre and Post-Test Out-of-straightness Profiles for Specimen P1-C1, 90 degree longitudinal reference line.

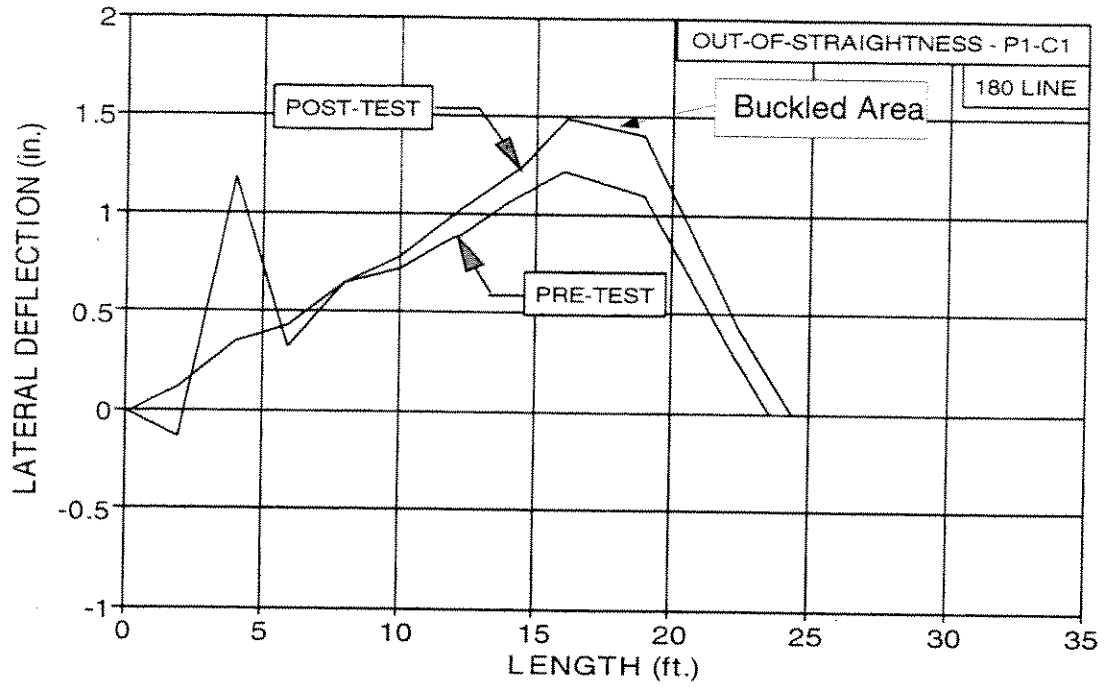


Figure 4-8: Pre and Post-Test Out-of-straightness Profiles for Specimen P1-C1, 180 degree longitudinal reference line.

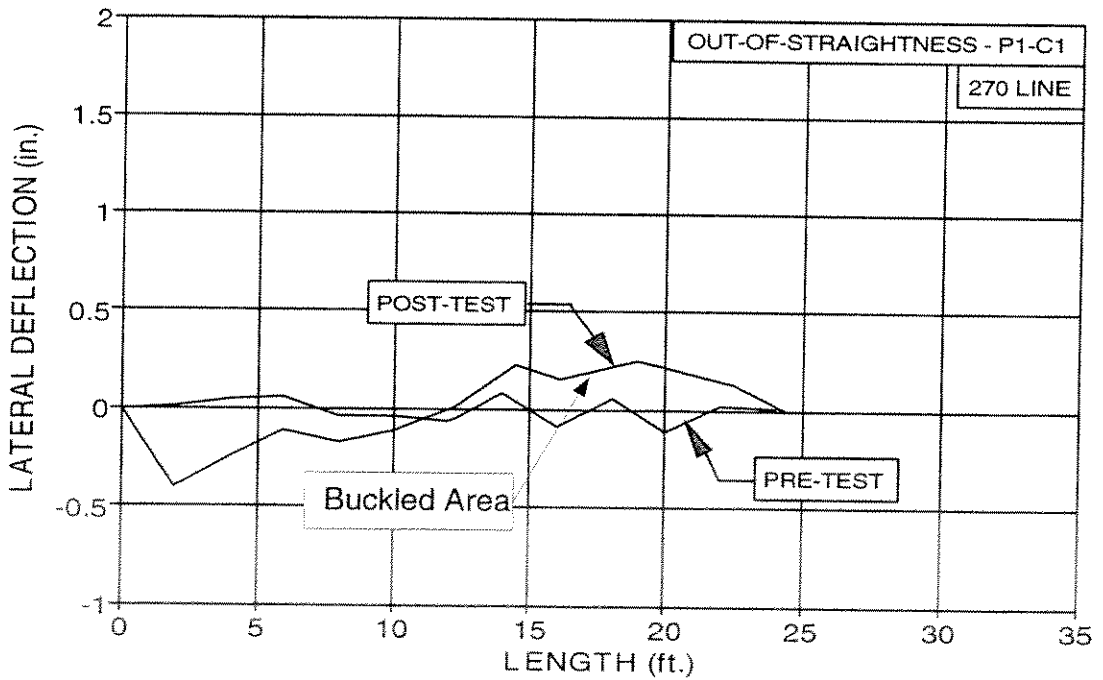


Figure 4-9: Pre and Post-Test Out-of-straightness Profiles for Specimen P1-C1, 270 degree longitudinal reference line.

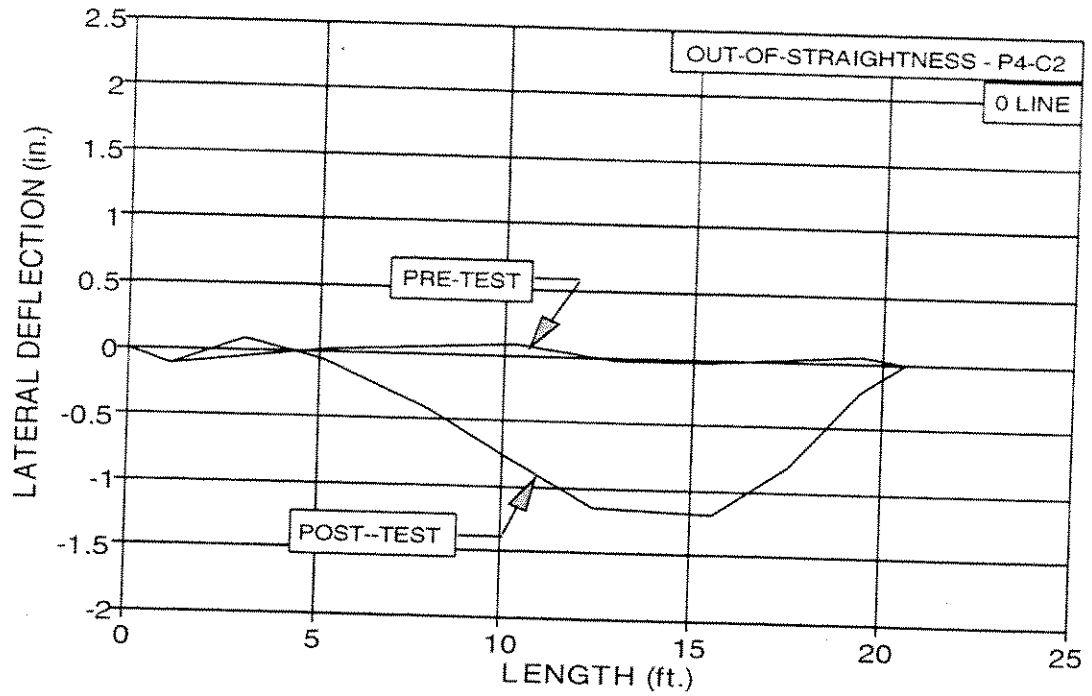


Figure 4-10: Pre and Post-Test Out-of-straightness Profiles for Specimen P4-C2, 0 degree longitudinal reference line.

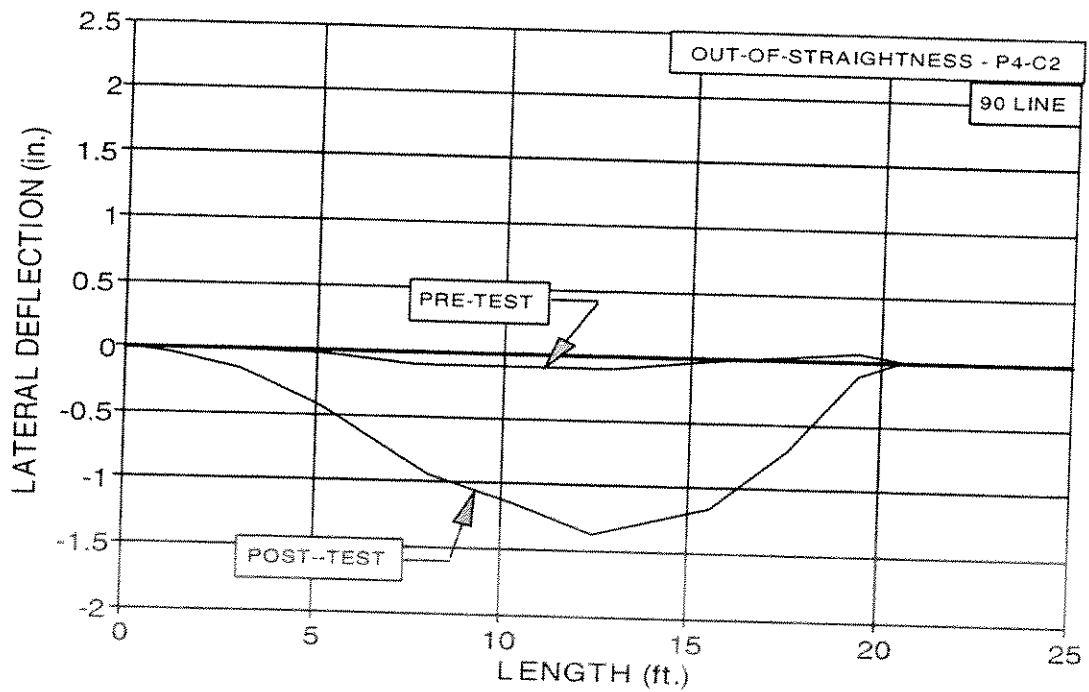


Figure 4-11: Pre and Post-Test Out-of-straightness Profiles for Specimen P4-C2, 90 degree longitudinal reference line.

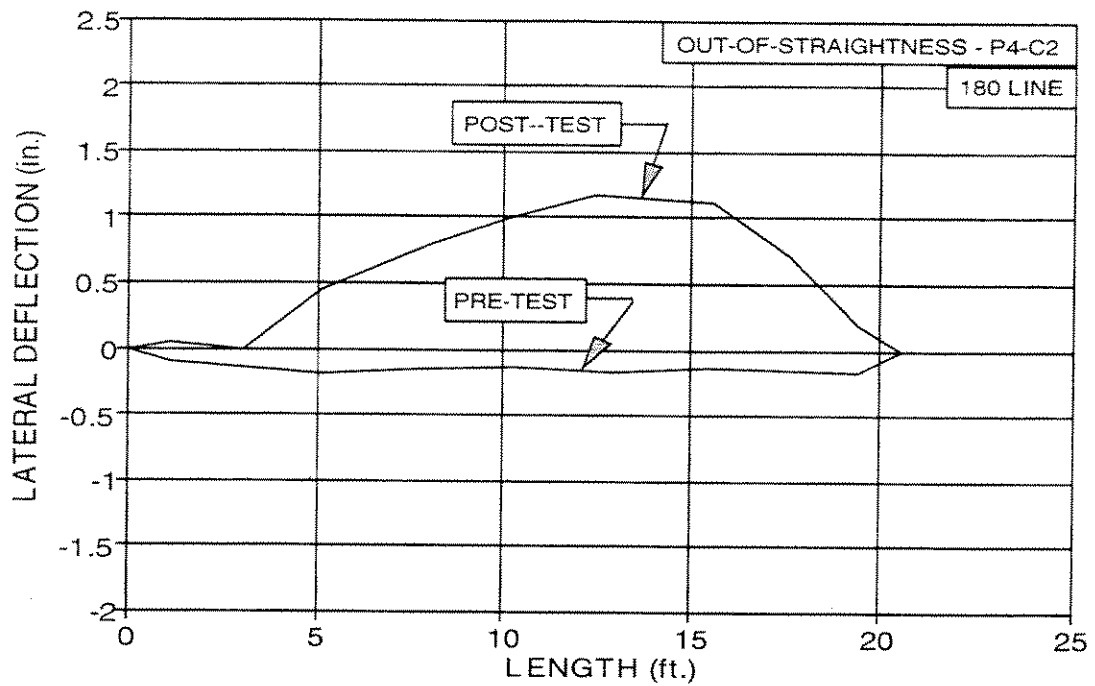


Figure 4-12: Pre and Post-Test Out-of-straightness Profiles for Specimen P4-C2, 180 degree longitudinal reference line.

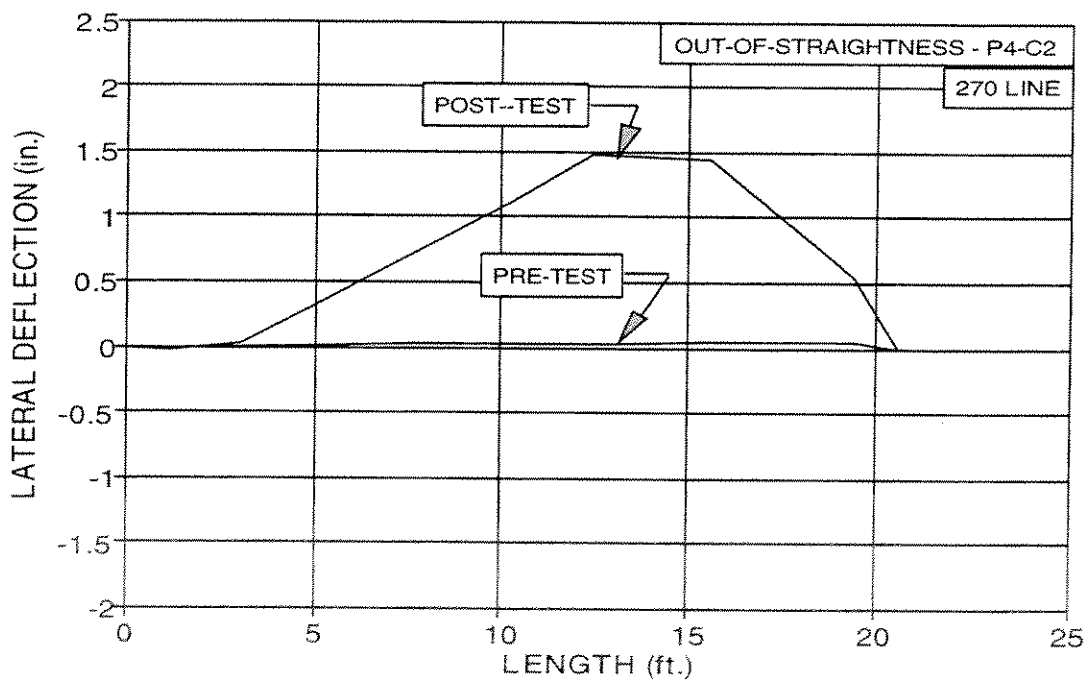


Figure 4-13: Pre and Post-Test Out-of-straightness Profiles for Specimen P4-C2, 270 degree longitudinal reference line.

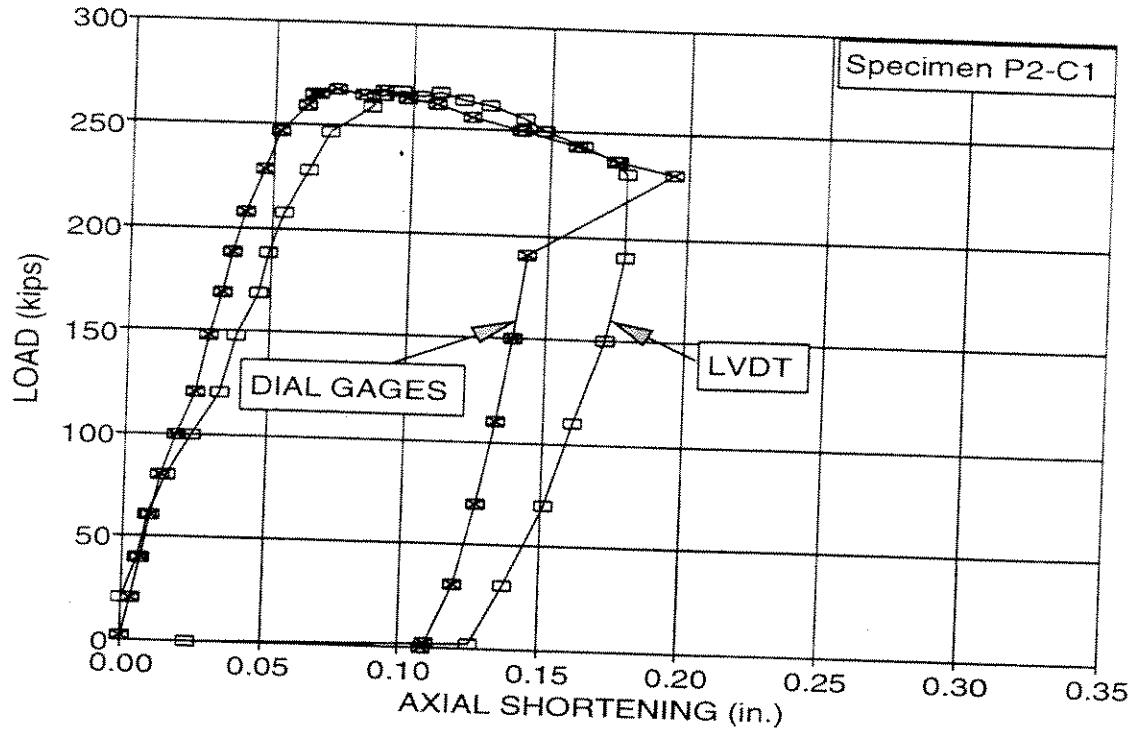


Figure 5-1: Specimen P2-C1 -- Average Axial Shortening.

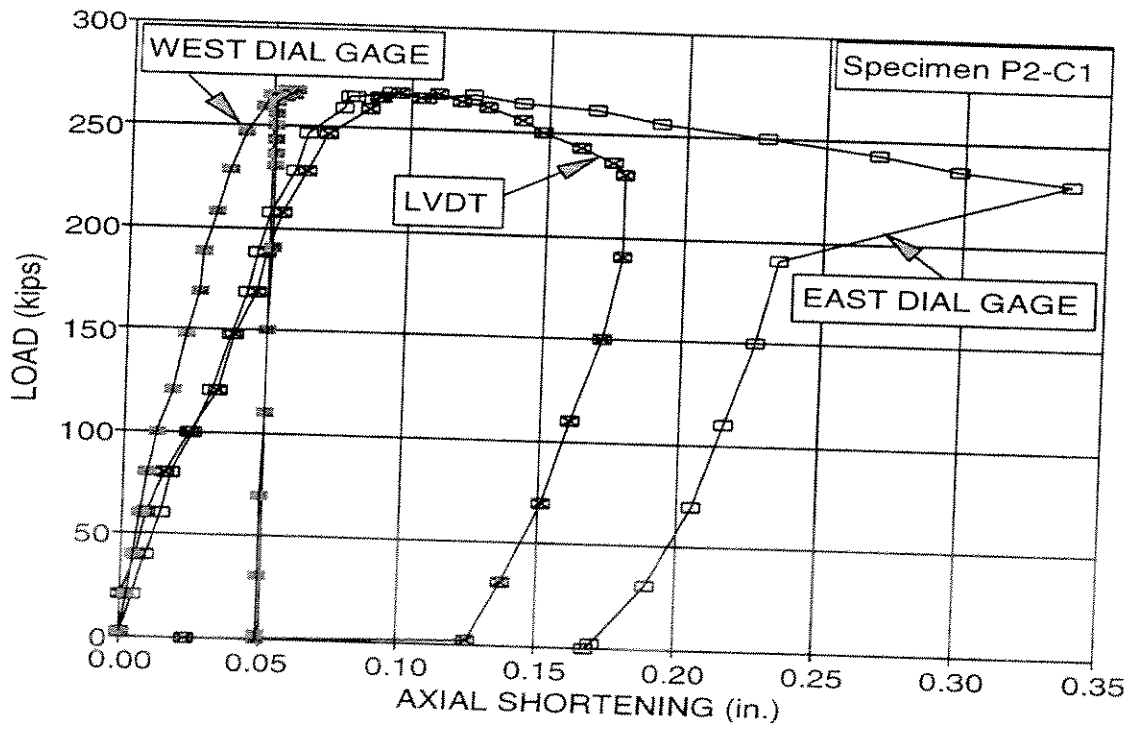


Figure 5-2: Specimen P2-C1 -- Axial Shortening from East and West Dial Gages.

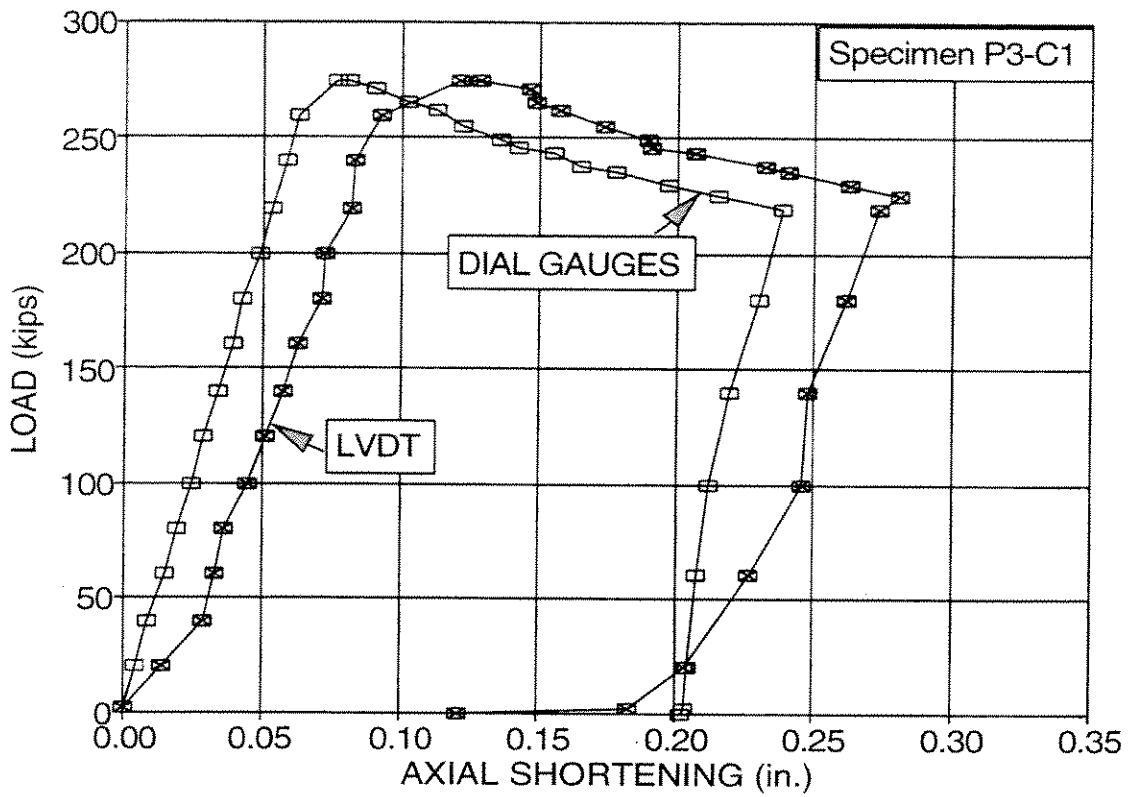


Figure 5-3: Specimen P3-C1 -- Average Axial Shortening.

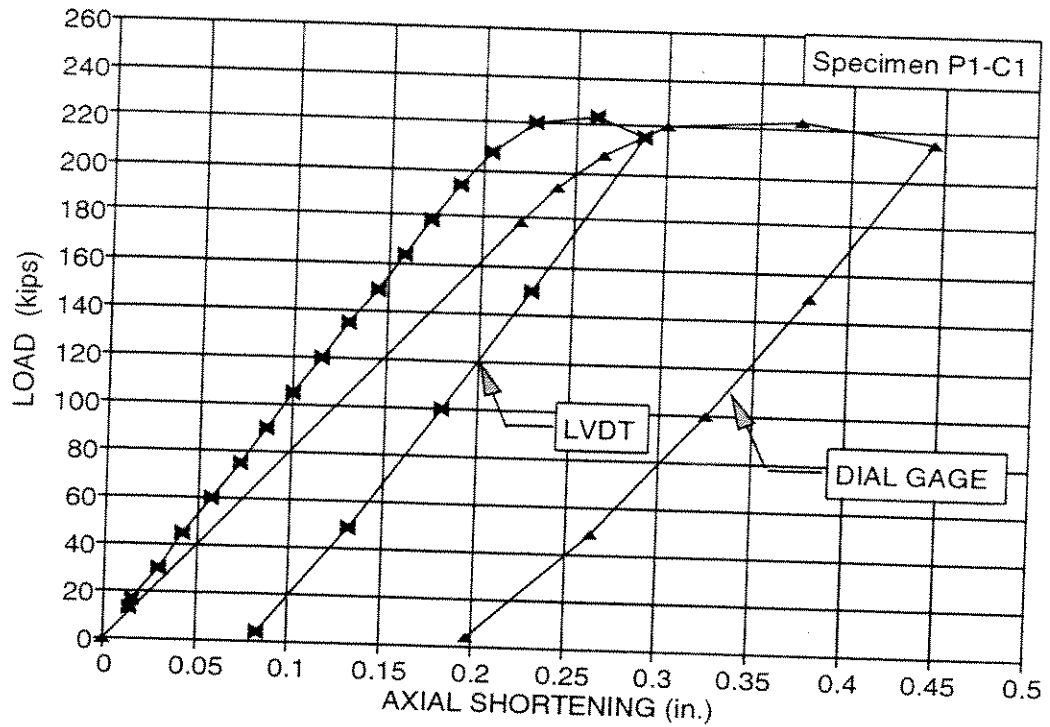


Figure 5-4: Specimen P1-C1 -- Axial Shortening.

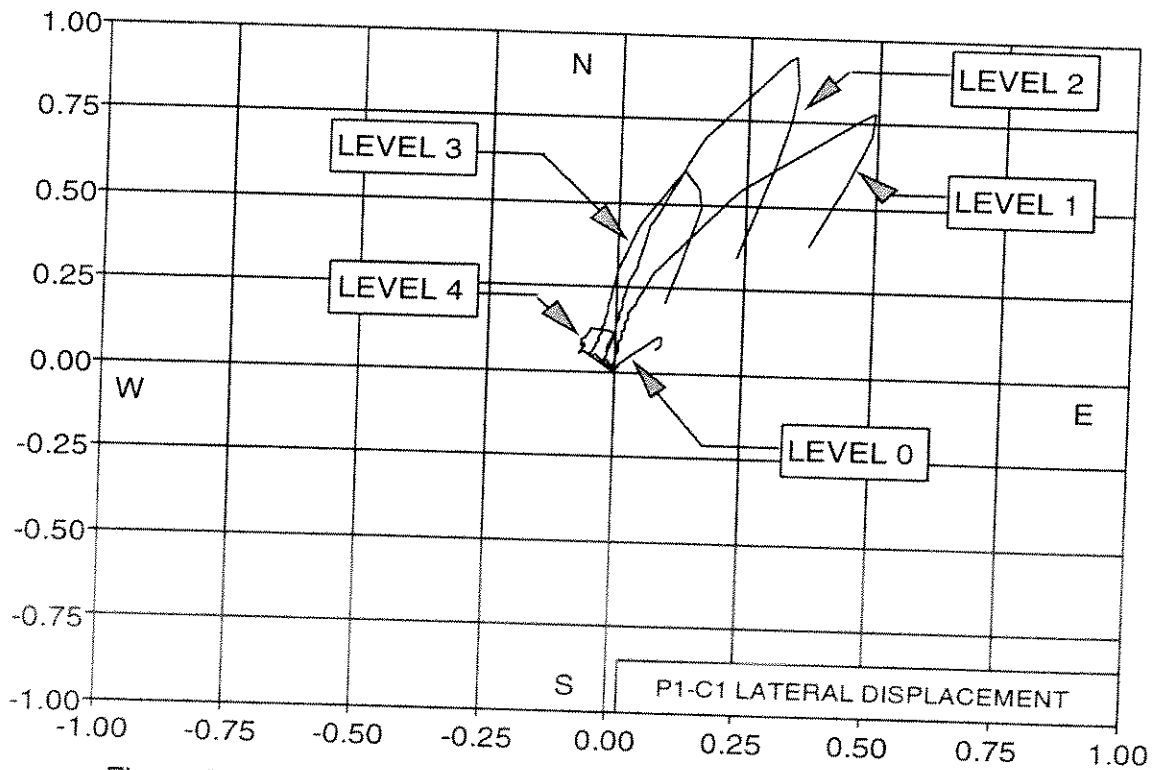


Figure 5-5: Lateral Displacement at Levels 0 through 4 - Specimen P1-C1.

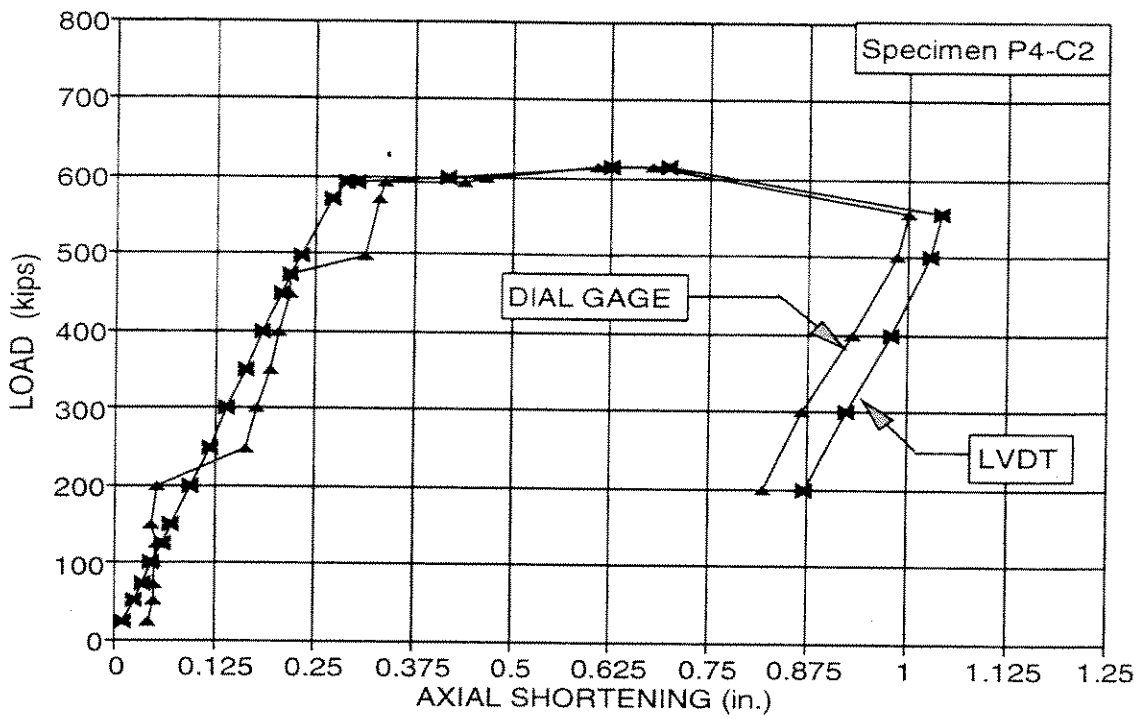


Figure 5-6: Specimen P4-C2 -- Axial Shortening.

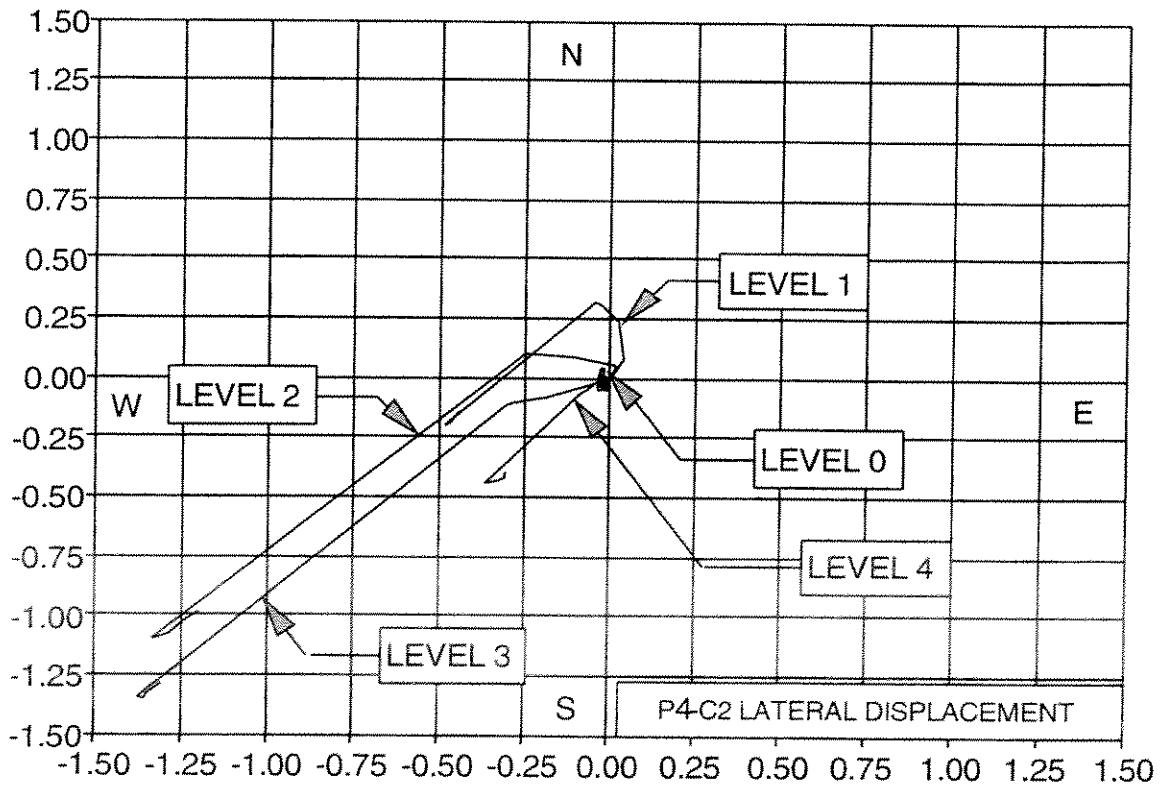


Figure 5-7: Lateral Displacement at Levels 0 through 4 - Specimen P4-C2.

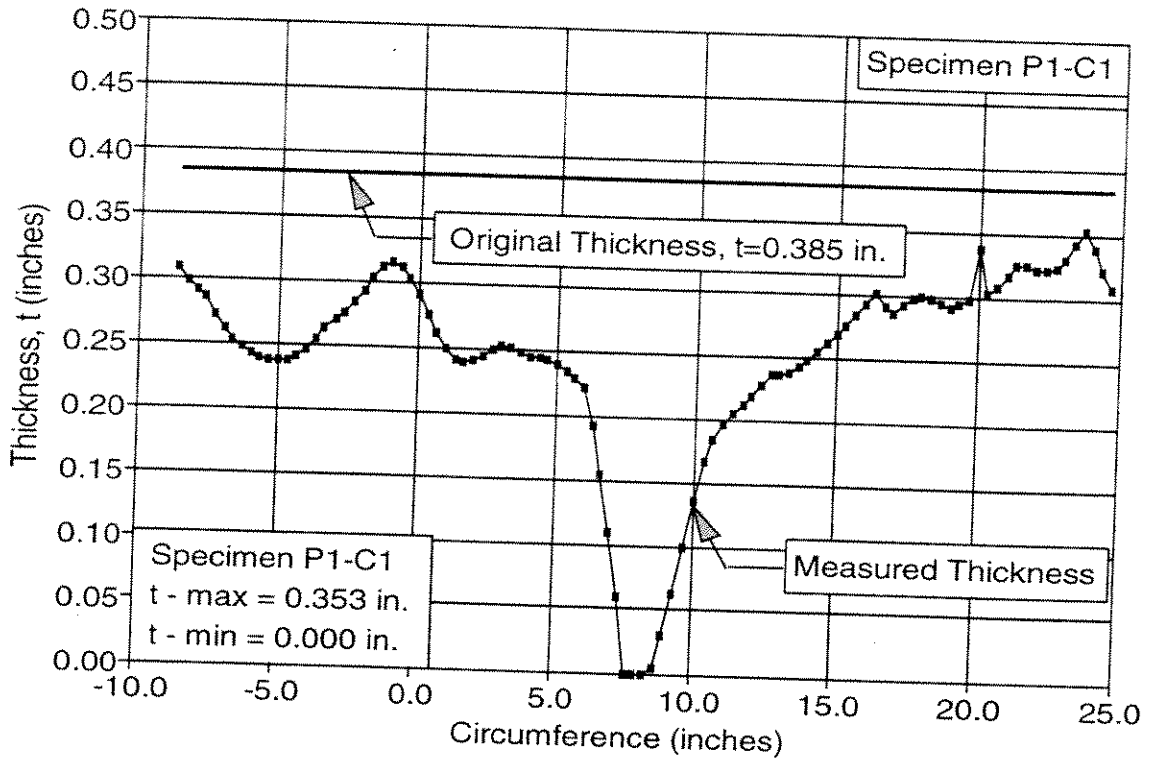


Figure 6-1: Thickness variation at hole for Specimen P1-C1.

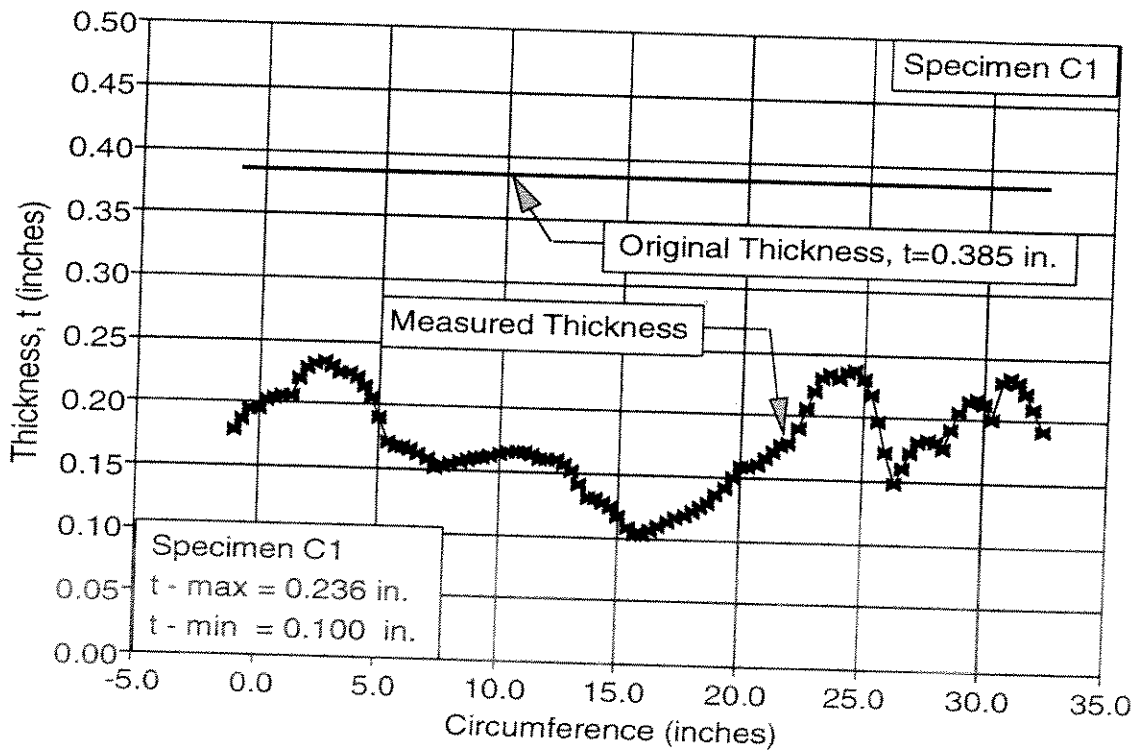


Figure 6-2: Thickness variation at Location of Local Buckling. Specimen C1. (Ref. 8)

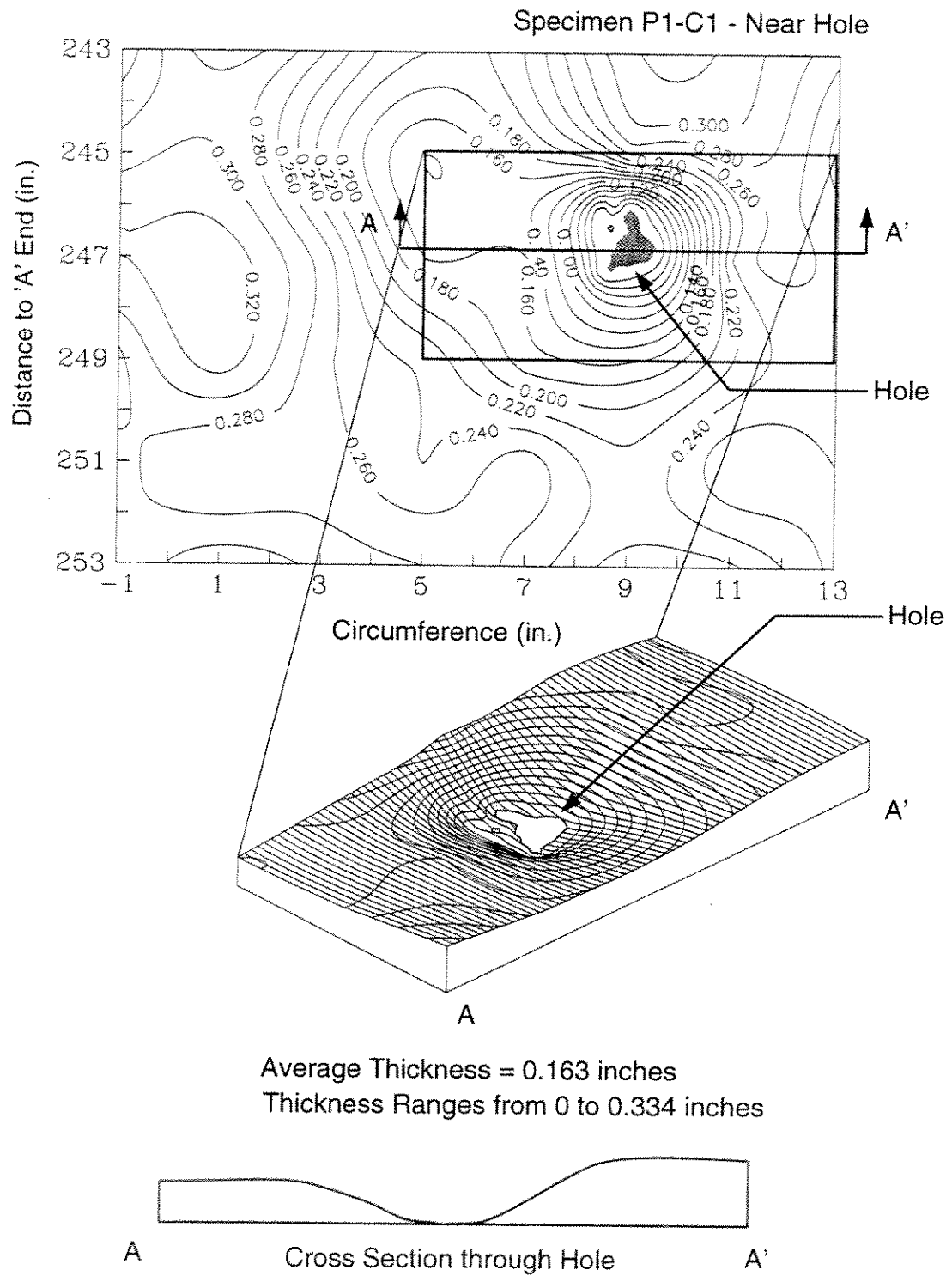


Figure 6-3: Specimen P1-C1 -- Contour Plot, Isometric View, and Cross Section of Thickness Variation at Location of Hole.

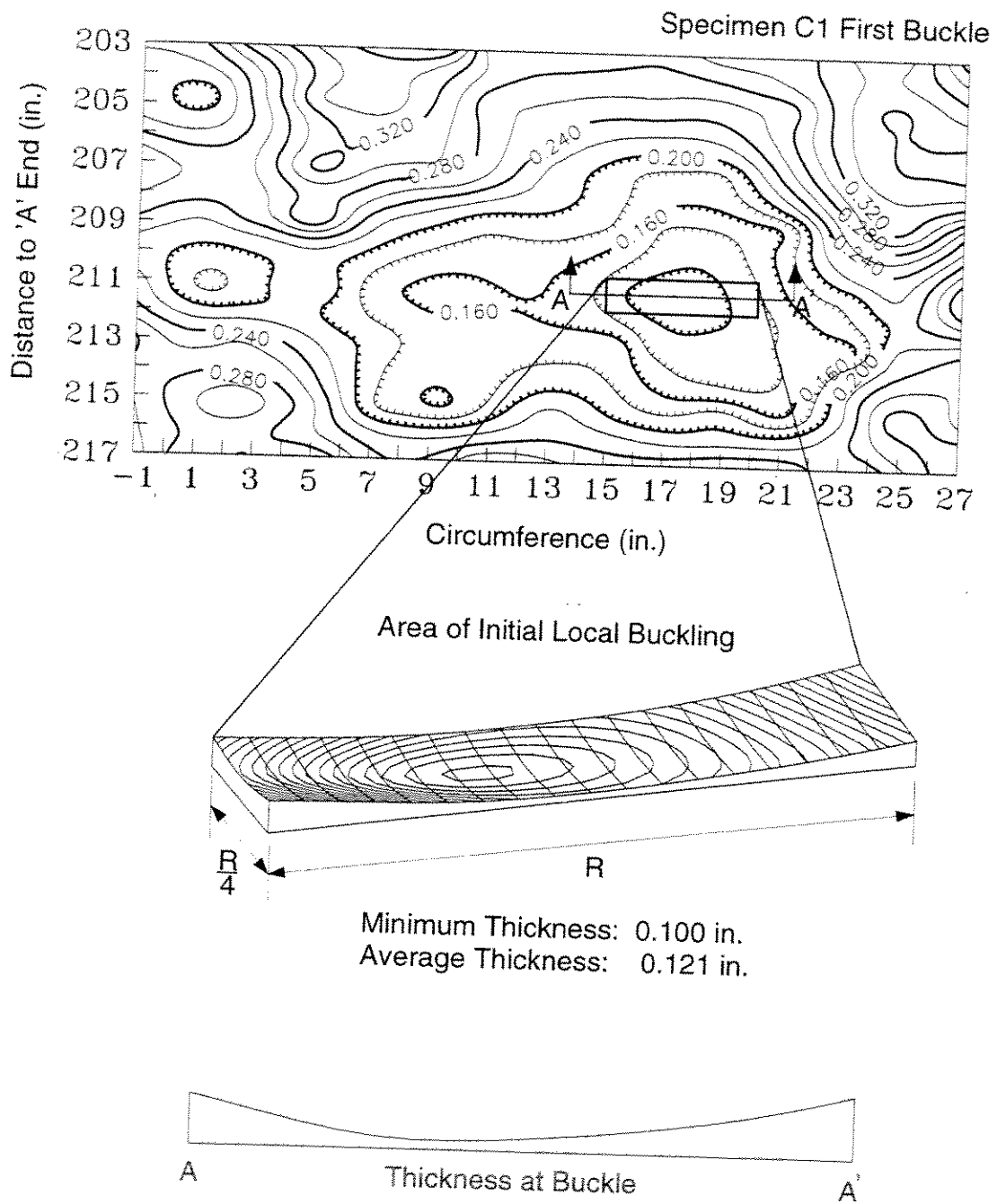


Figure 6-4: Specimen C1 -- Contour Plot, Isometric View, and Cross Section of Thickness Variation at Location of Local Buckles. (Ref. 8)

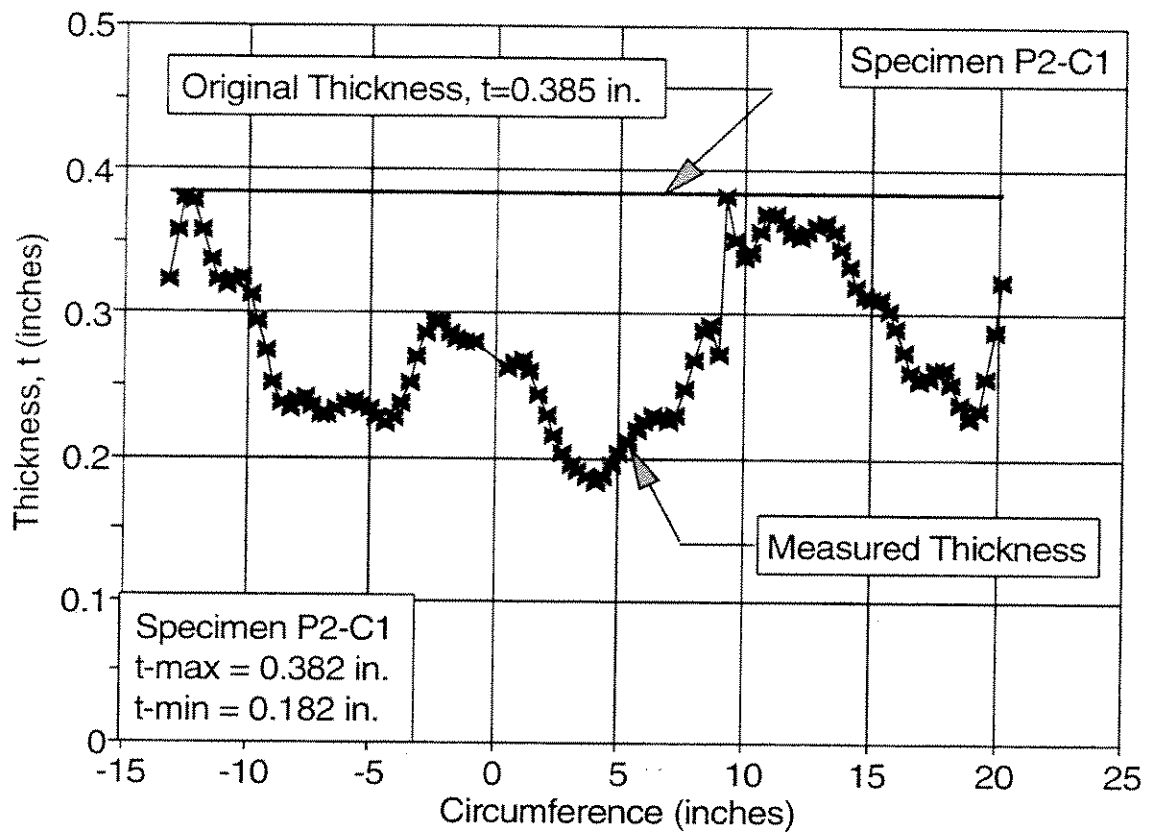


Figure 6-5: Thickness Variation at Section without Buckles Specimen P2-C1.

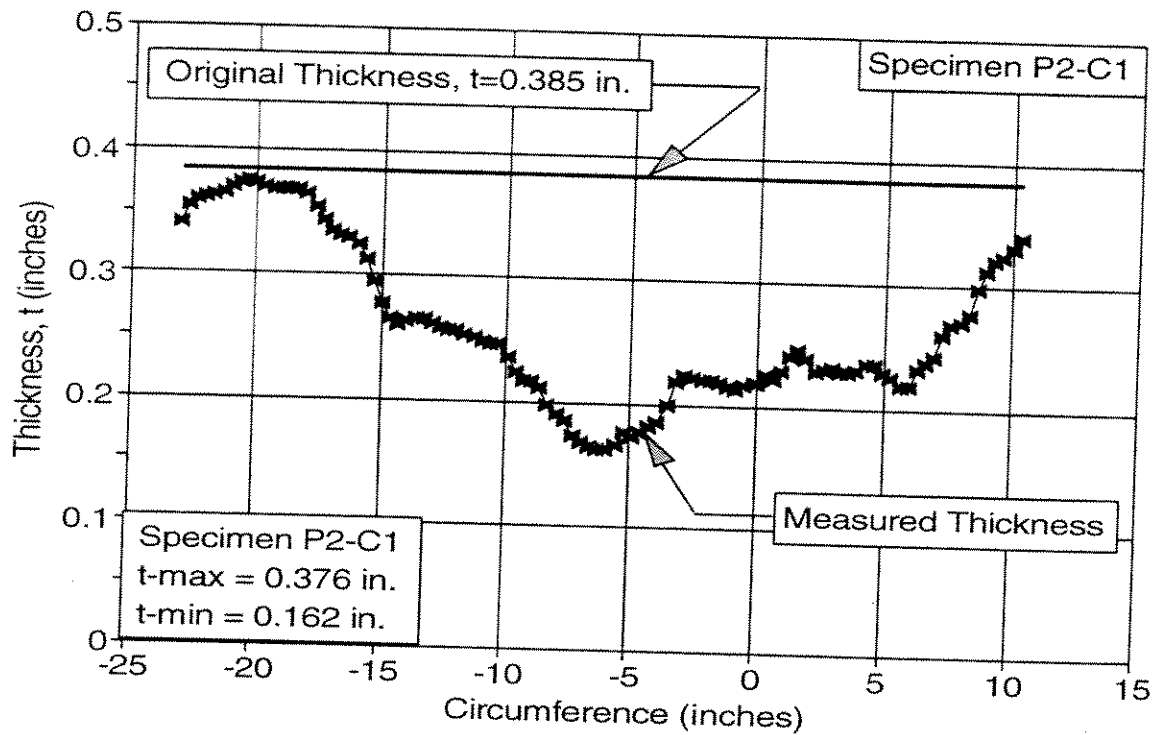


Figure 6-6: Thickness Variation at Location of Buckle 1 (25 in. from End 'A') -- Specimen P2-C1.

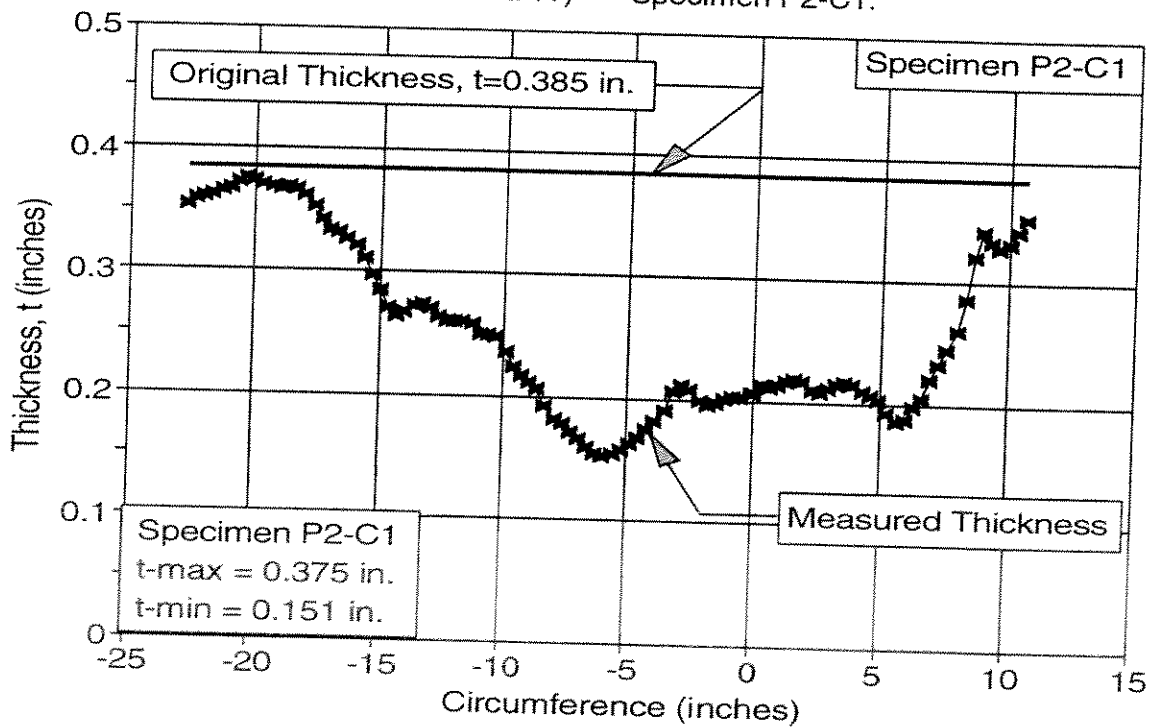


Figure 6-7: Thickness Variation at Location of Buckle 2 (24 in. from End 'A') -- Specimen P2-C1.

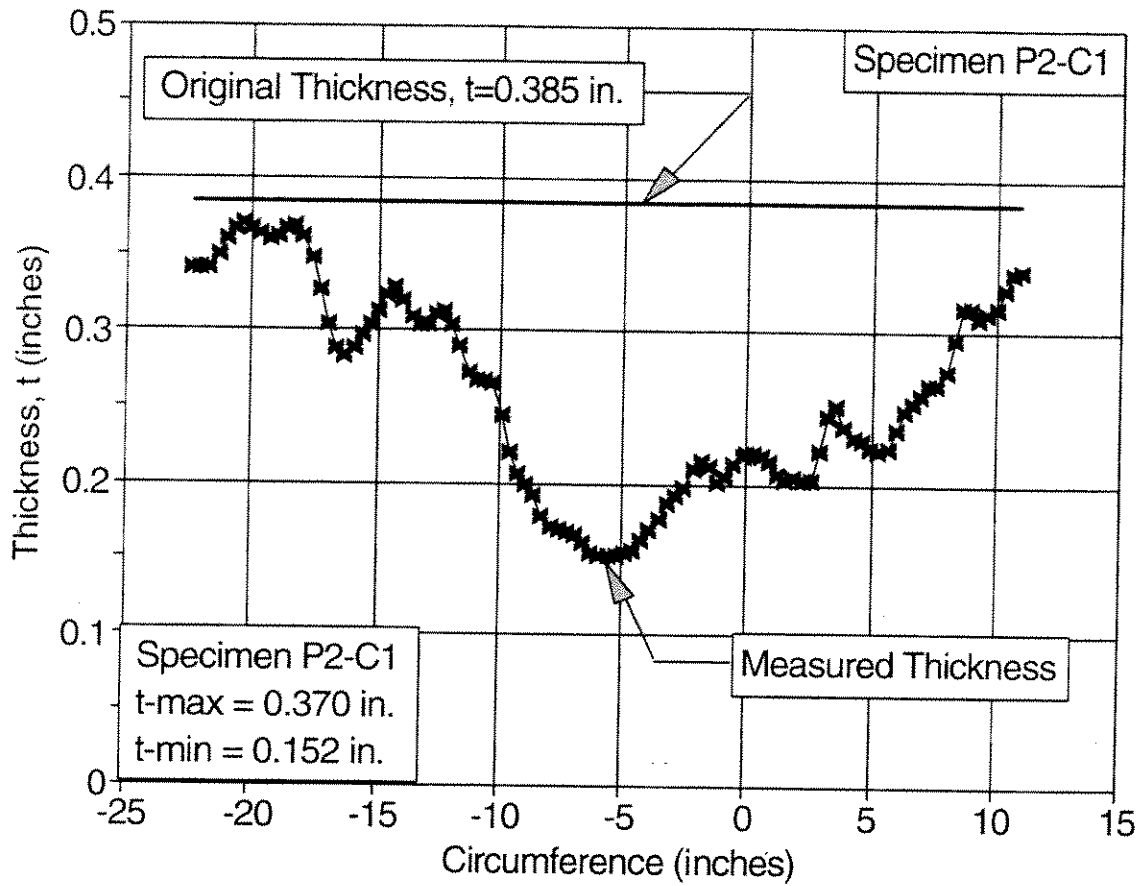


Figure 6-8: Thickness Variation at Location of Buckle 3 (22.5 in. from End 'A') -- Specimen P2-C1.

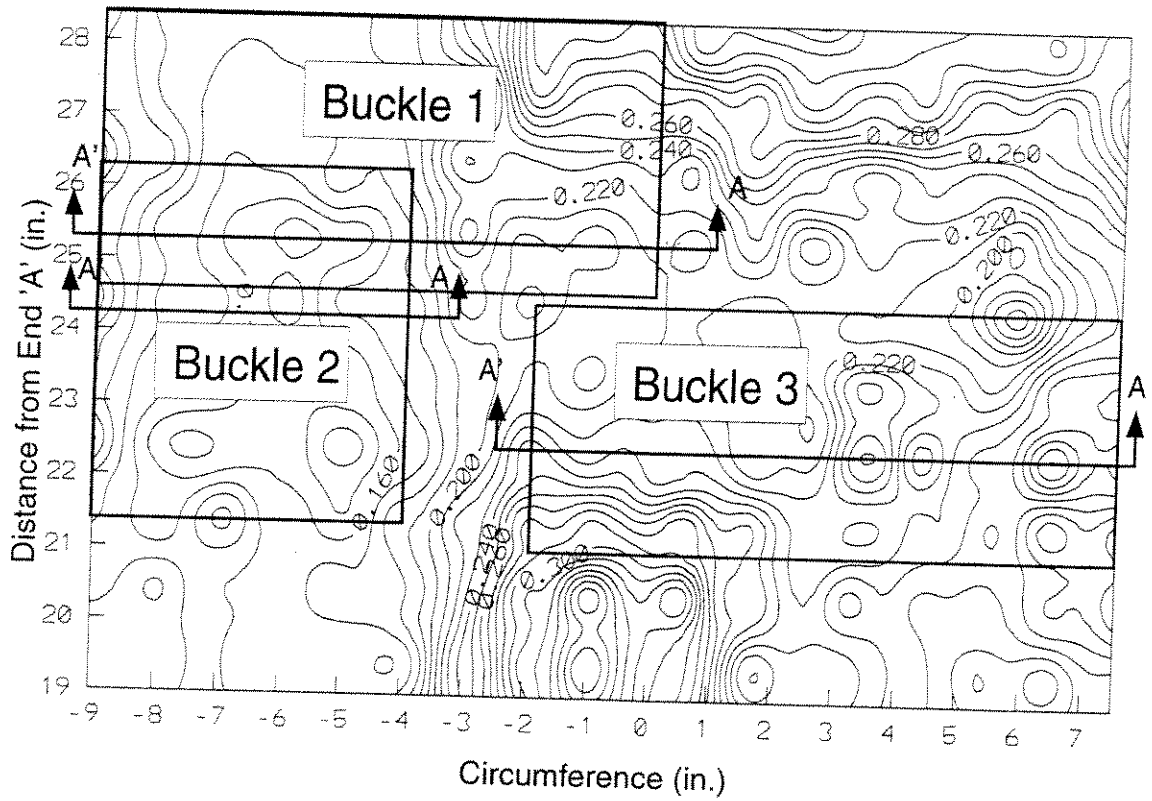
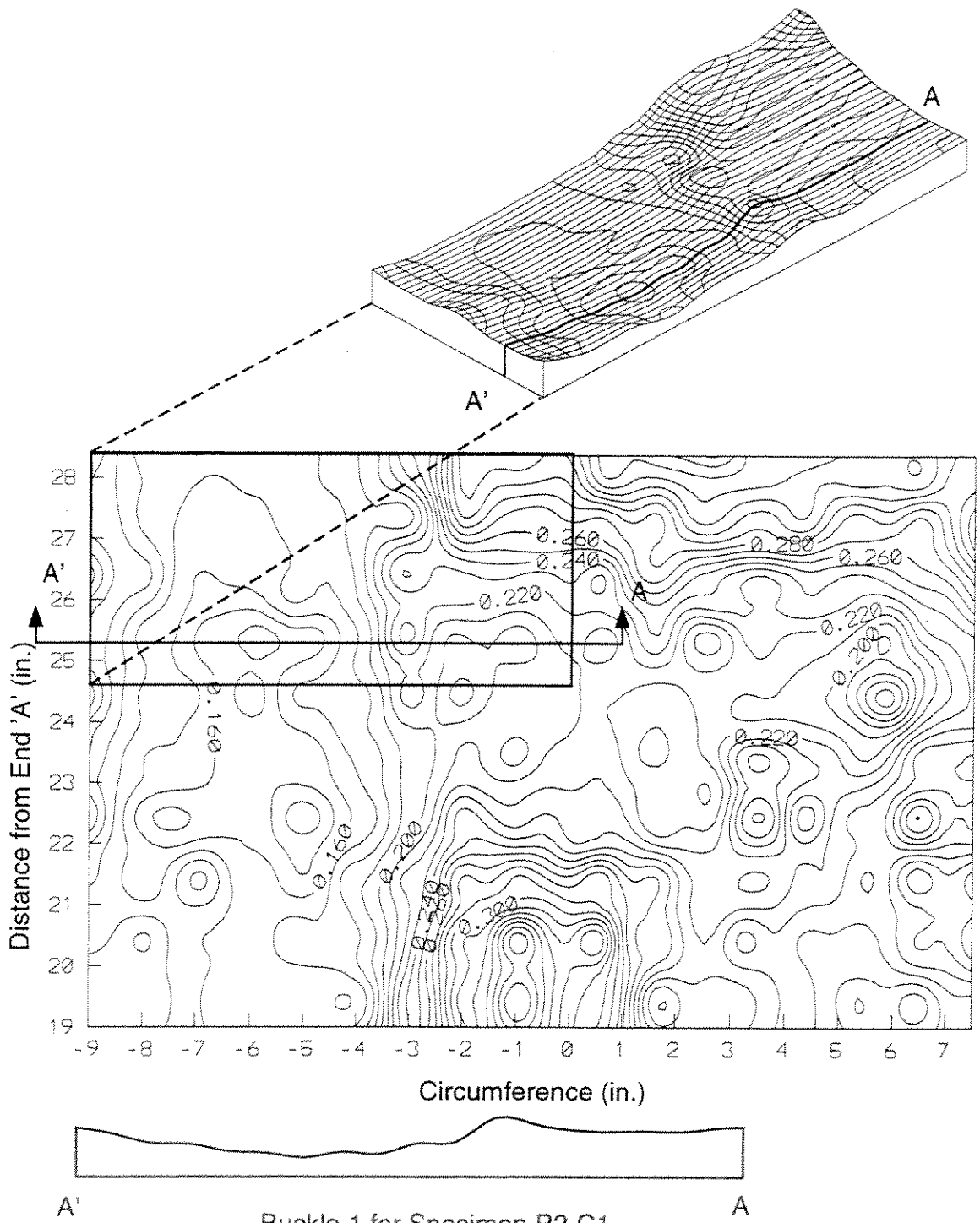


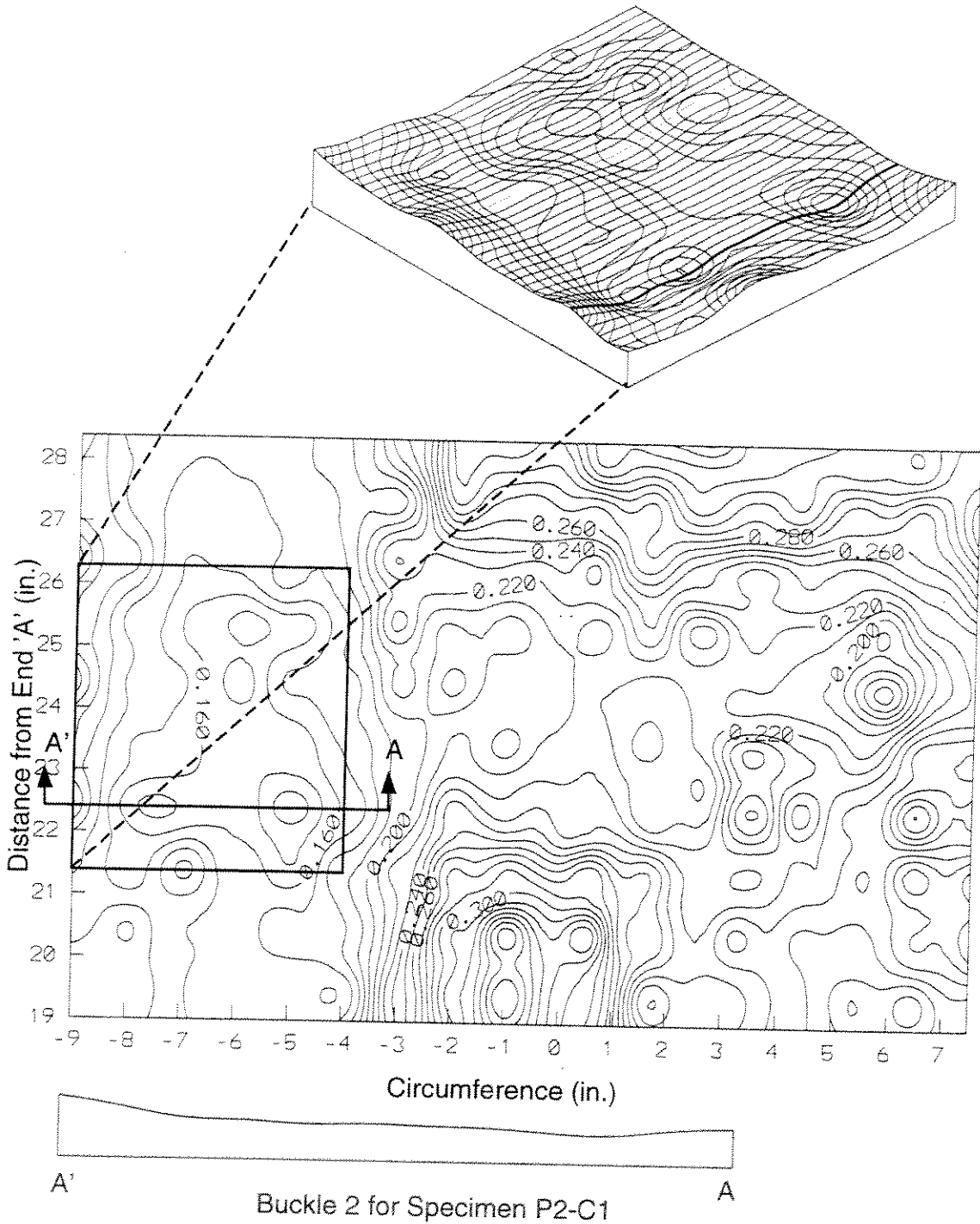
Figure 6-9: Location of Buckles 1, 2 and 3 for Specimen P2-C1.



Buckle 1 for Specimen P2-C1

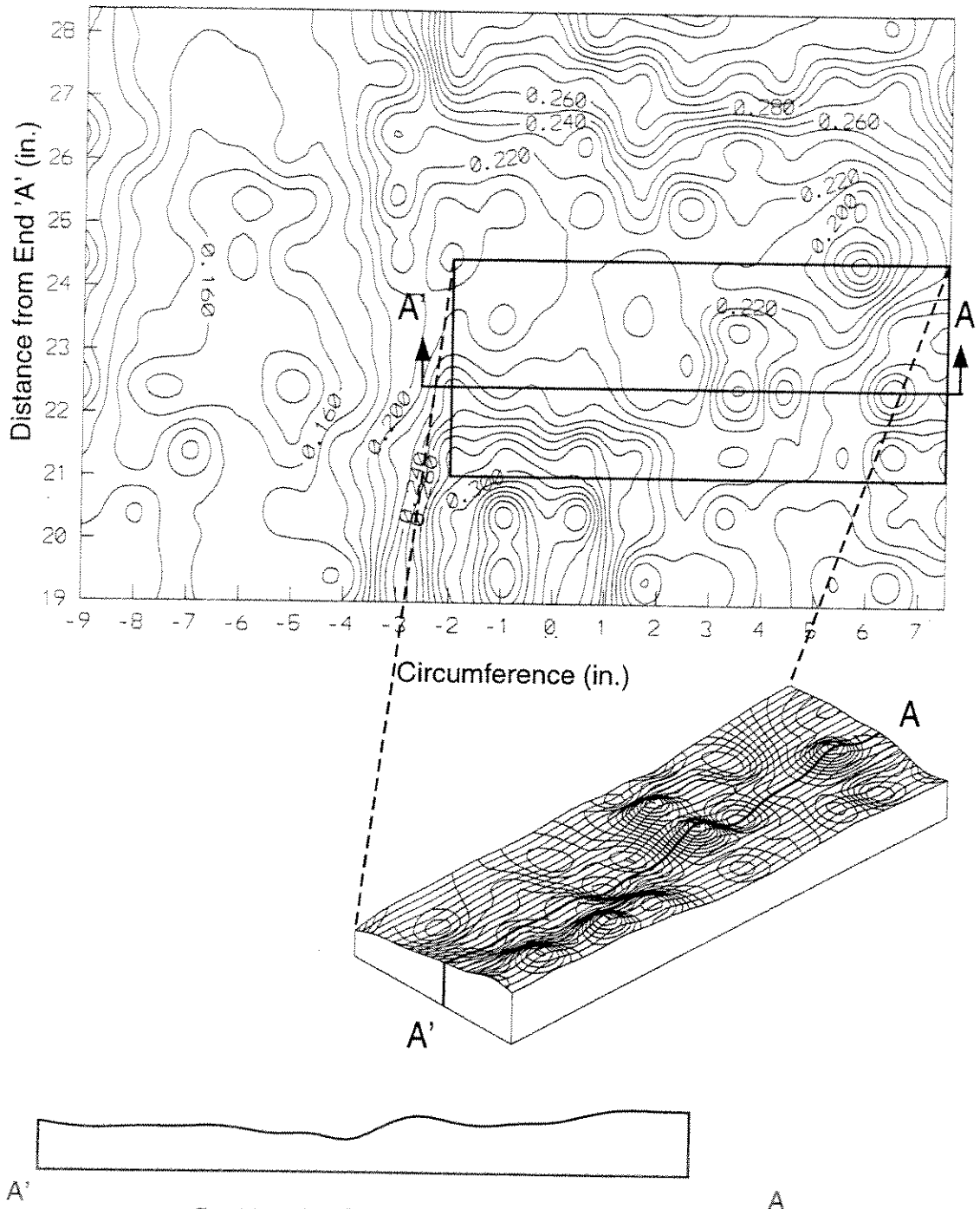
Average Thickness = 0.205 inches
 Thickness Ranges from 0.141 to 0.348 inches

Figure 6-10: Thickness Variation in the Area of Buckle 1 -- Specimen P2-C1.



Average Thickness = 0.167 inches
 Thickness Ranges from 0.126 to 0.235 inches

Figure 6-11: Thickness Variation in the Area of Buckle 2 -- Specimen P2-C1.



Buckle 3 for Specimen P2-C1

Average Thickness = 0.231 inches
 Thickness Ranges from 0.185 to 0.294 inches

Figure 6-12: Thickness Variation in the Area of Buckle 3 -- Specimen P2-C1.

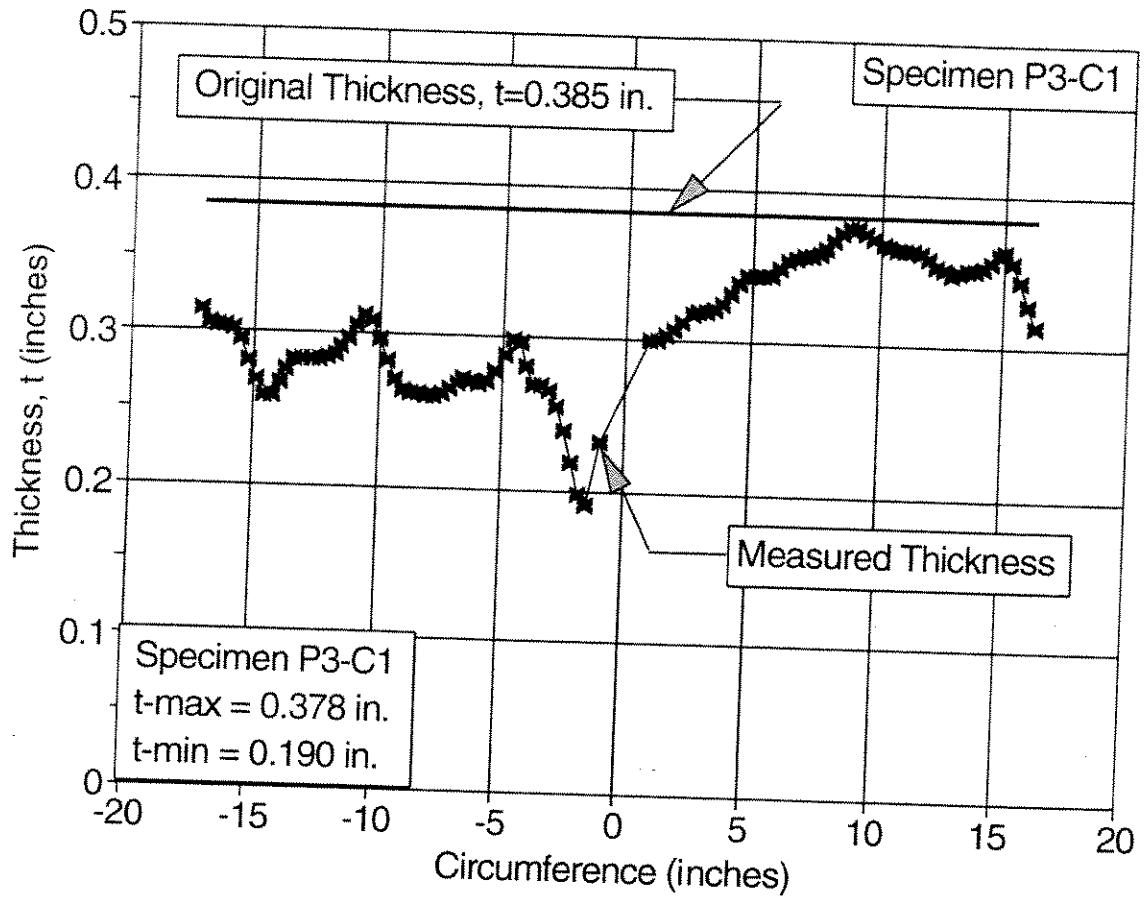


Figure 6-13: Thickness Variation at Location without Buckling (67 in. from End 'A') -- Specimen P3-C1.

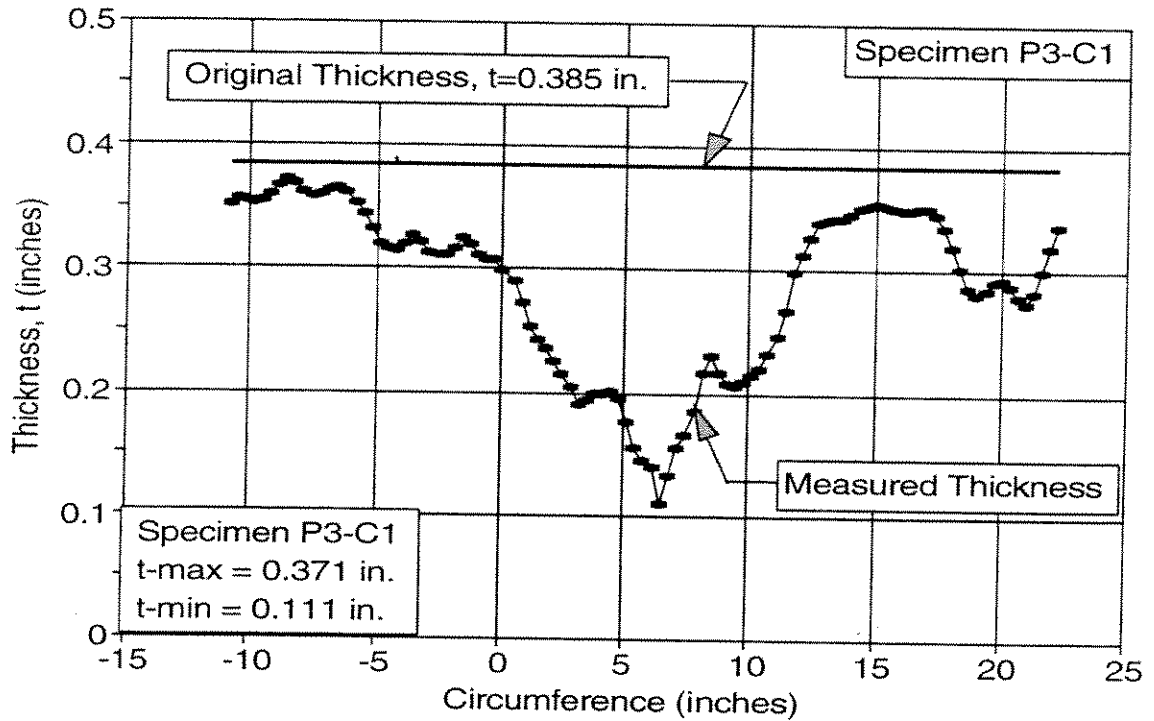


Figure 6-14: Thickness Variation at Location of Buckle 1 (25 in. from End 'A') -- Specimen P3-C1.

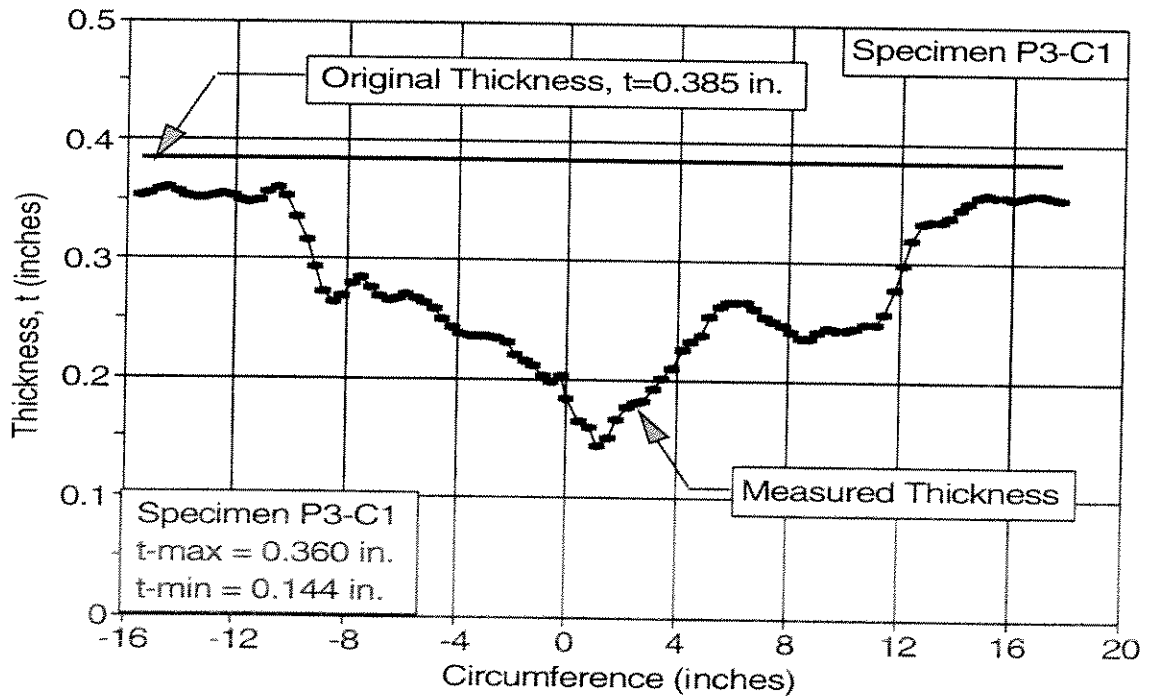


Figure 6-15: Thickness Variation at Location of Buckle 2 (22 in. from End 'A') -- Specimen P3-C1.

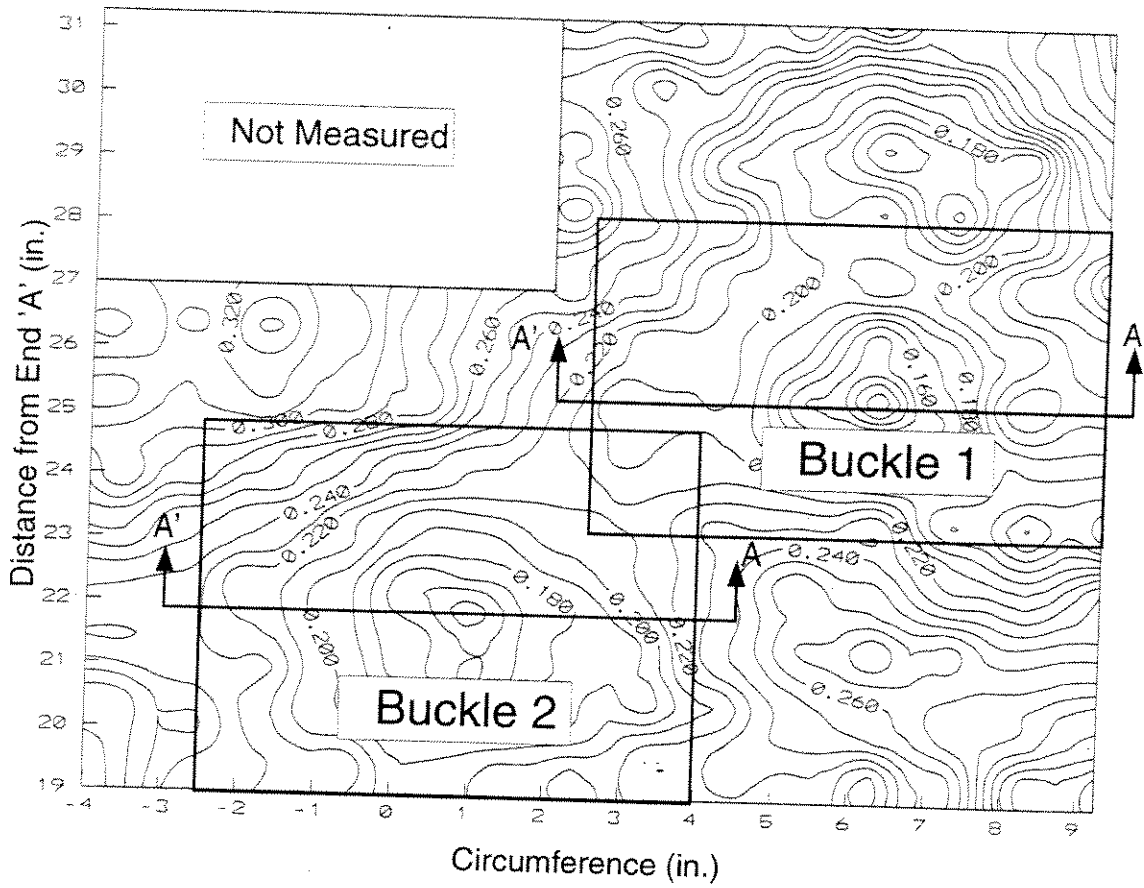
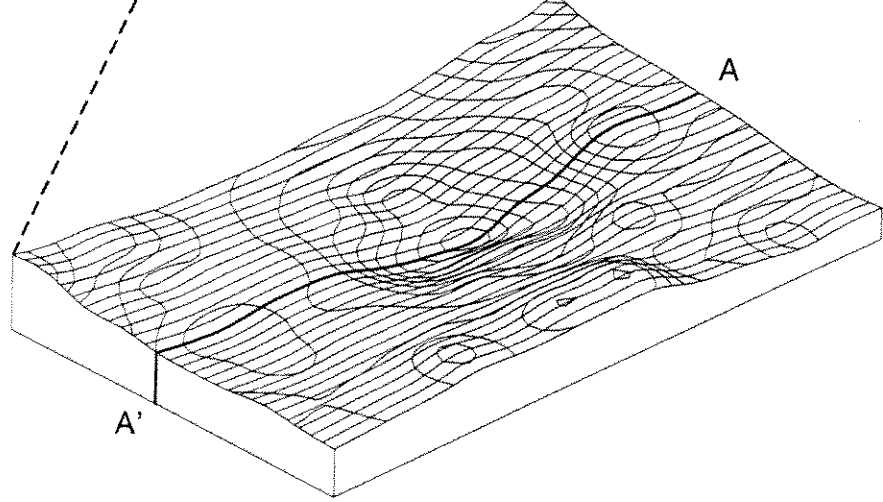
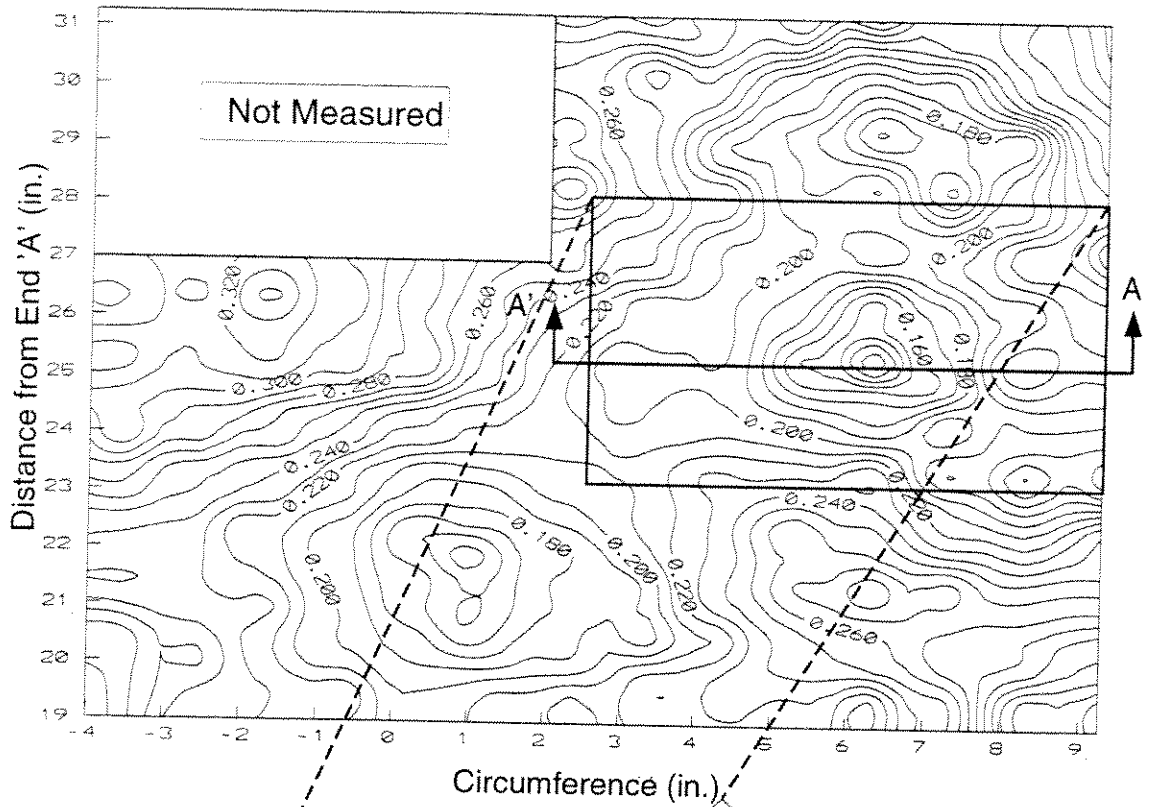


Figure 6-16: Location of Local Buckles 1 and 2 for Specimen P3-C1.



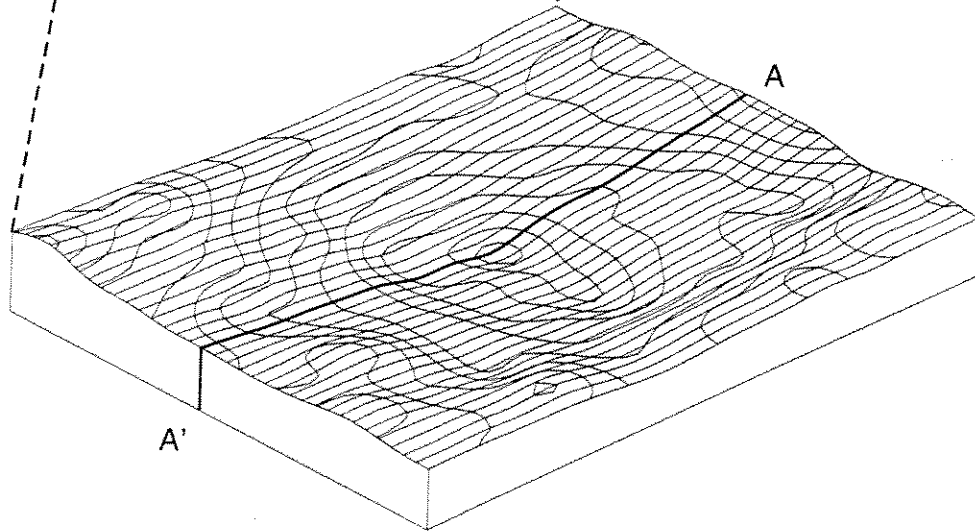
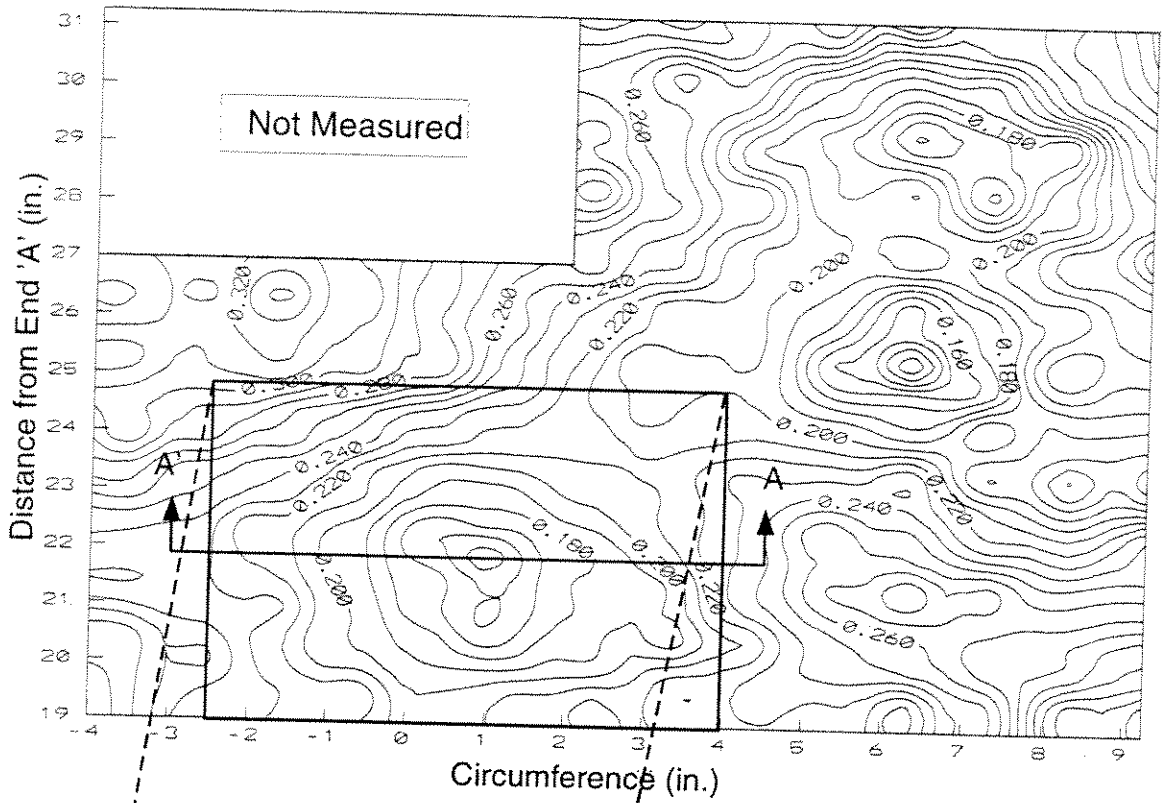
Specimen P3-C1 -- Buckle 1

Average Thickness = 0.197 inches

Thickness Ranges from 0.110 to 0.269 inches



Figure 6-17: Thickness Variation in the Area of Buckle 1 -- (Specimen P3-C1).



Specimen P3-C1 -- Buckle 2

Average Thickness = 0.208 inches

Thickness Ranges from 0.142 to 0.286 inches

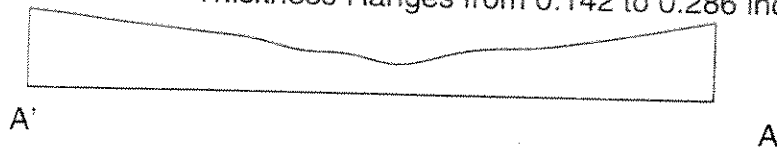


Figure 6-18: Thickness Variation in the Area of Buckle 2 -- (Specimen P3-C1)

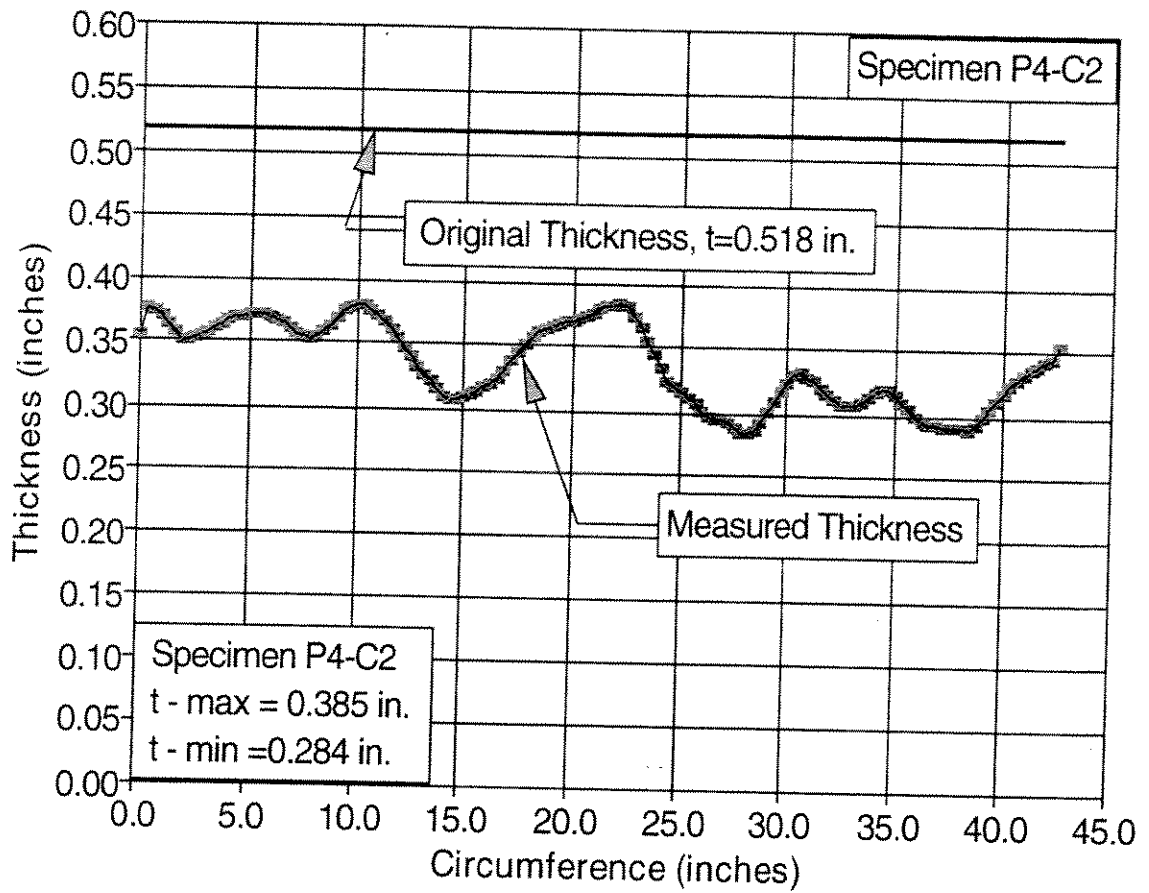


Figure 6-19: Uniform Thickness Variation Around Circumference (4 in. from End 'A') -- Specimen P4-C2.

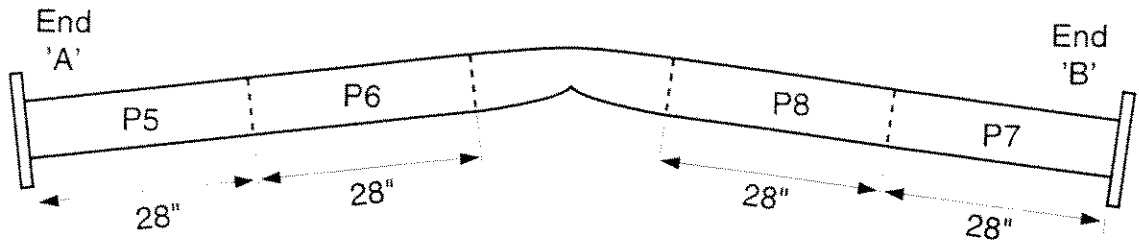


Fig. 7-1 Layout of Specimen P2PS [1] for Specimens P5 to P8

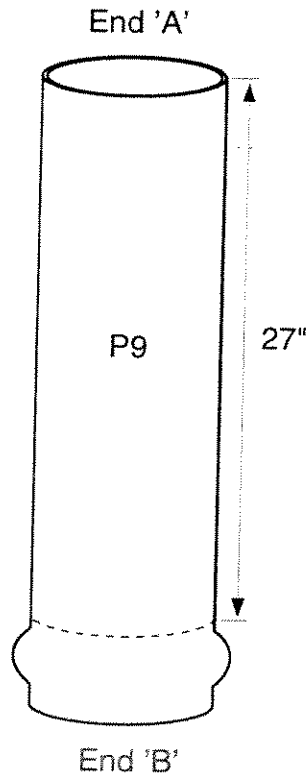


Fig. 7-2 Layout of Stub-Column P2PS-SC [1] for Specimen P9

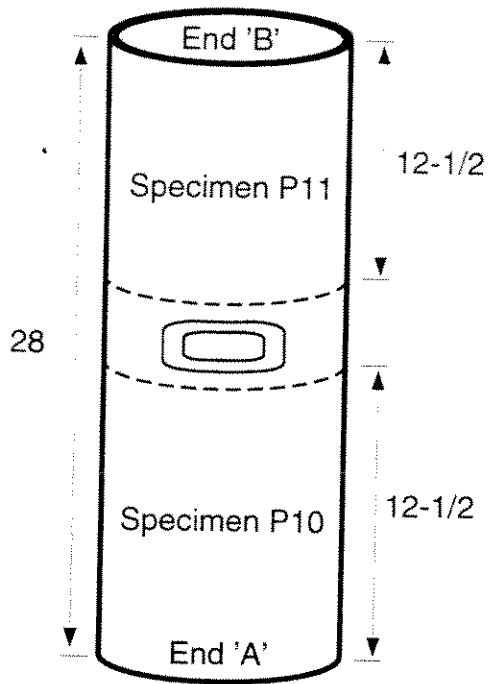


Fig. 7-3 Layout of Specimen P5 for Specimens P10 and P11

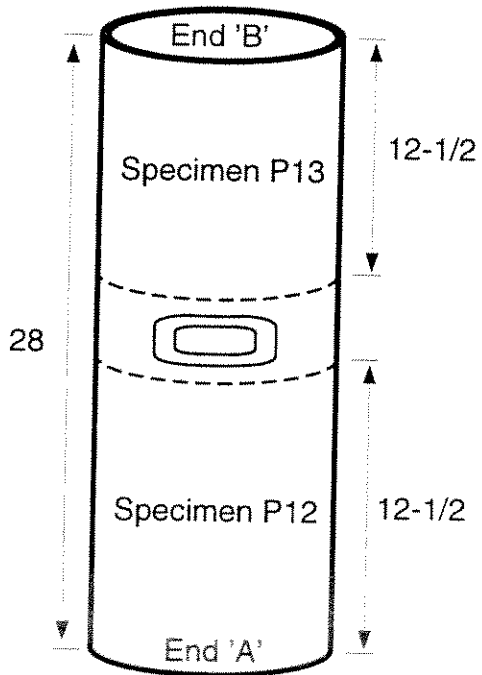


Fig. 7-4 Layout of Specimen P6 for Specimens P12 and P13

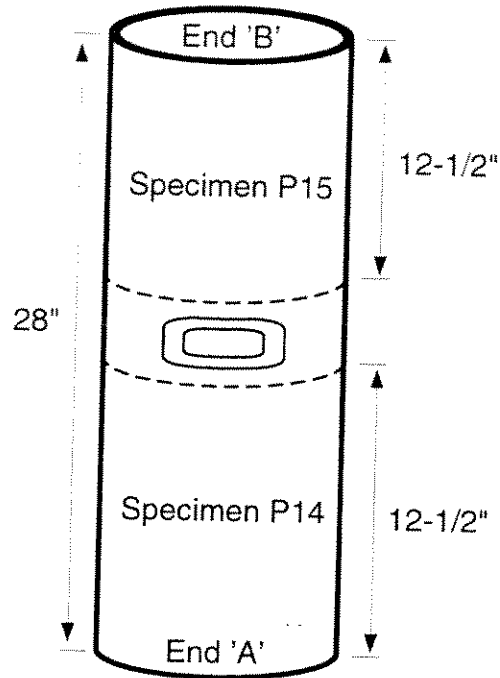
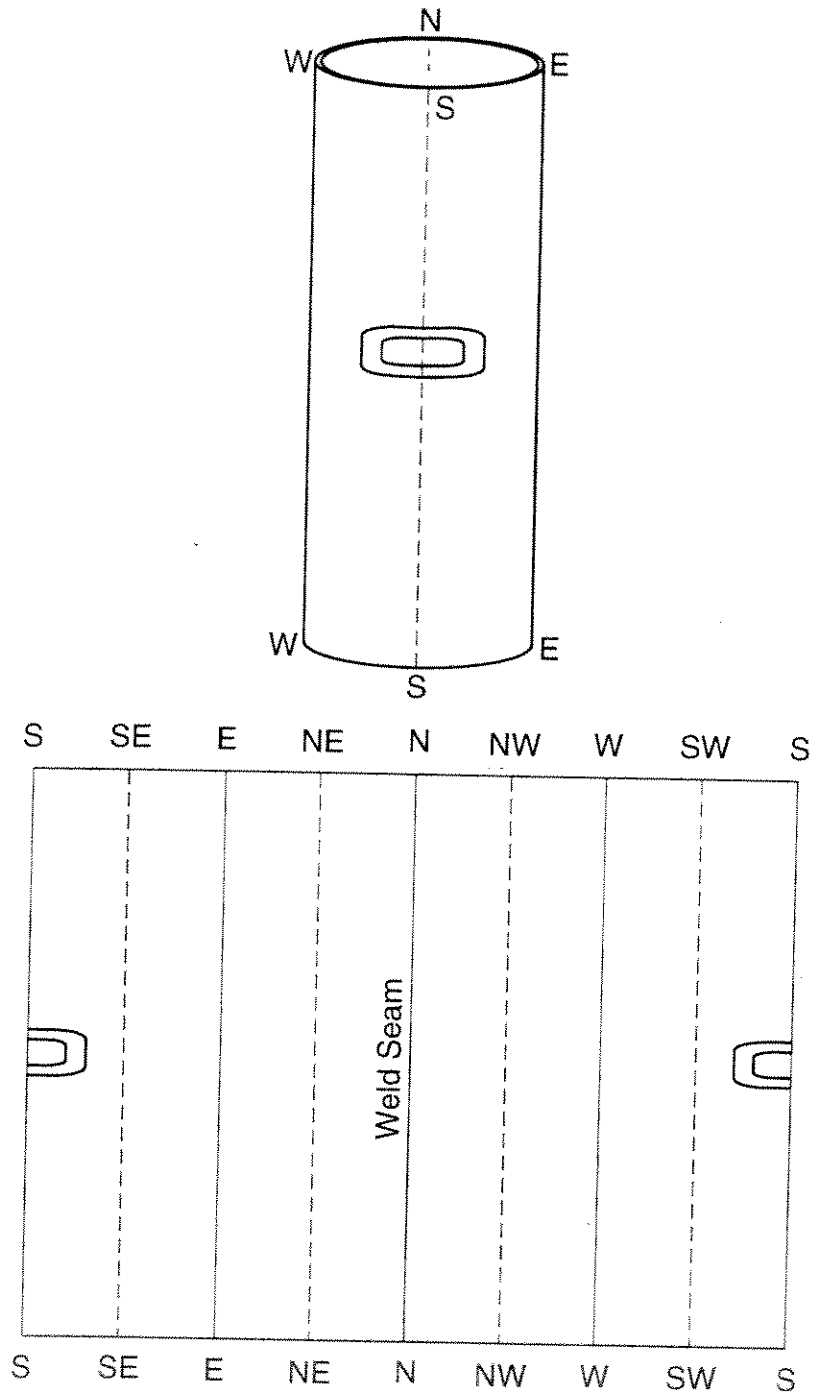


Fig. 7-5 Layout of Specimen P7 for Specimens P14 and P15



Note: SE, NE, NW, SW used for Specimen P9 only.

Fig. 7-6 Location of Longitudinal Reference Lines, Overall and Unfolded Views

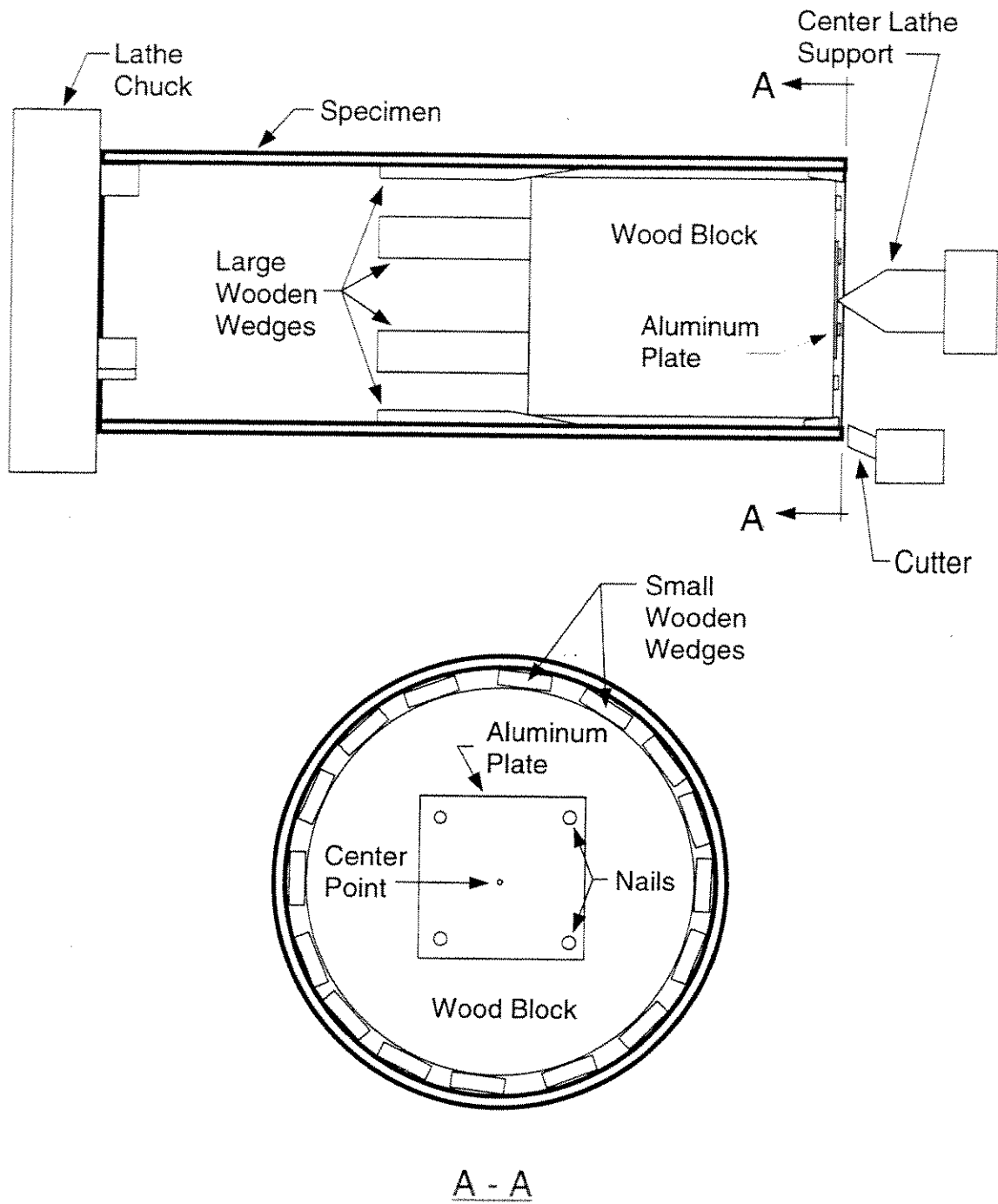


Fig. 7-7 Arrangement for Milling Specimen Ends

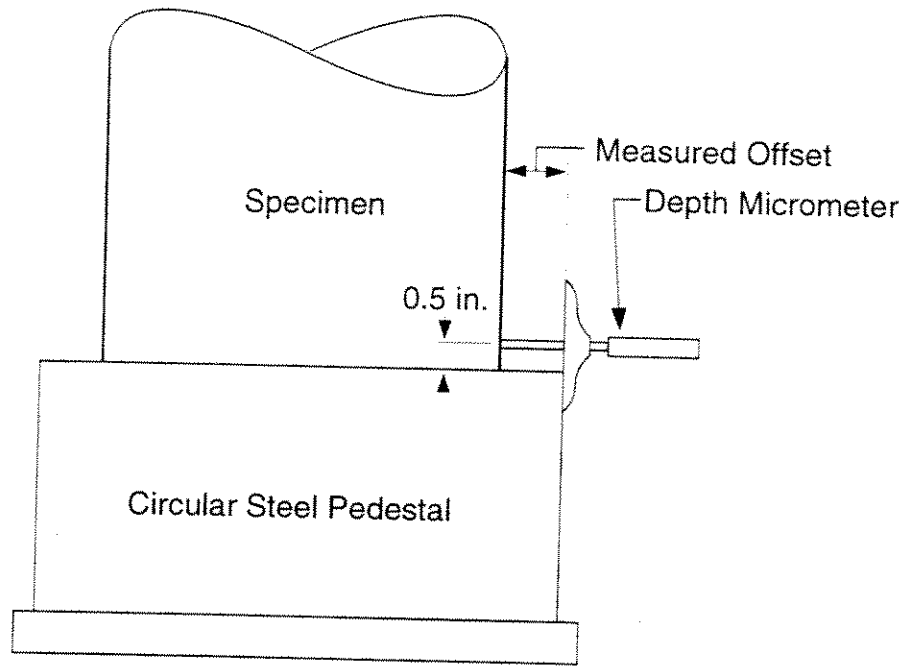


Fig. 8-1 Measurement of Diameter--
Pedestal Method Using Depth Micrometer

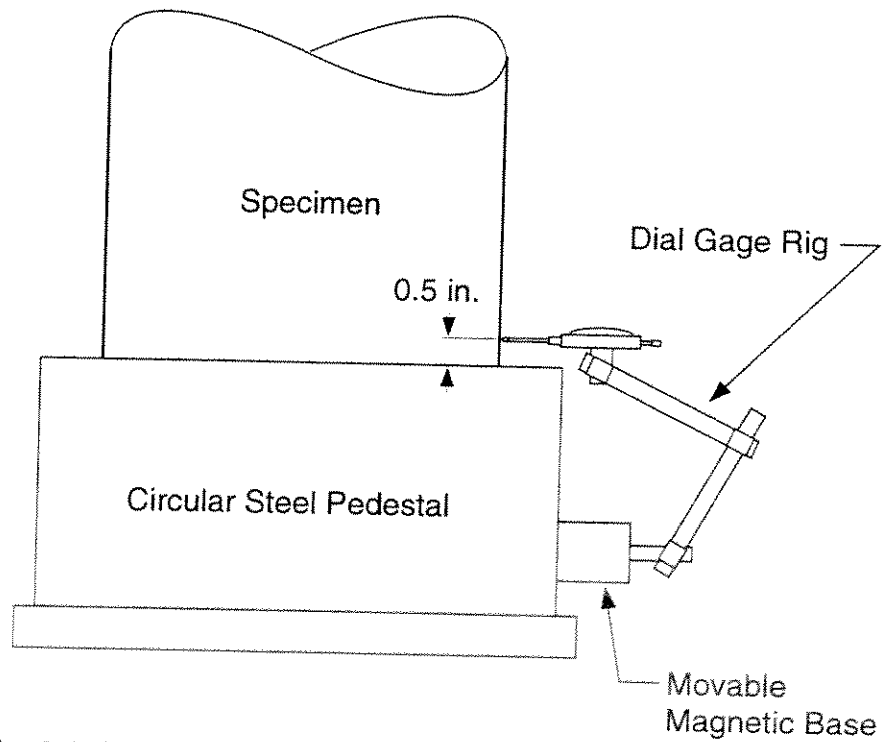


Fig. 8-2 Measurement of Diameter --
Pedestal Method Using the Dial Gage Rig

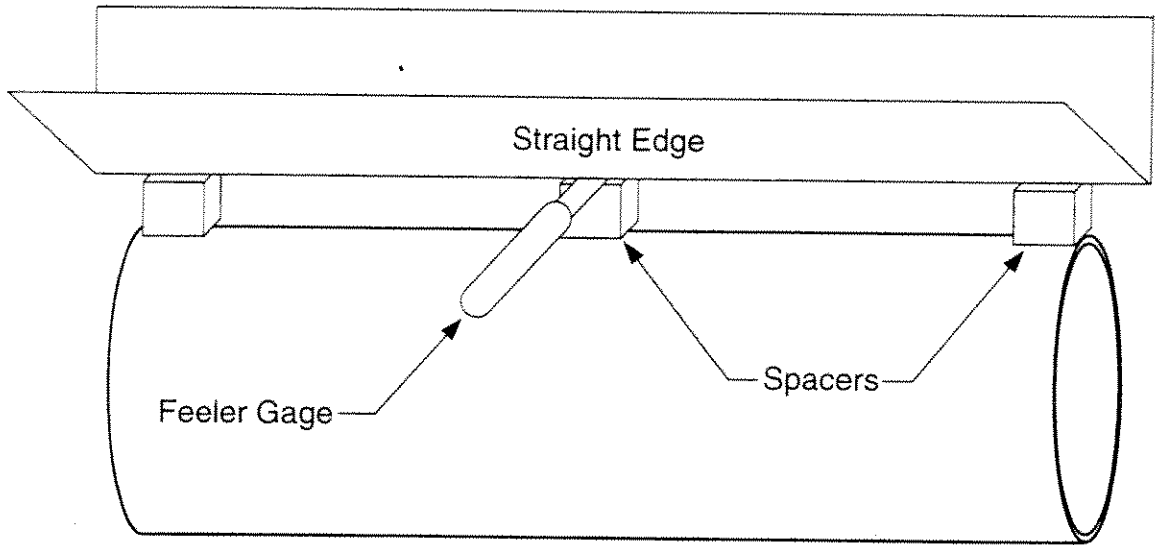


Fig. 8-3 Measurement of Out-of-Straightness Using Feeler Gage

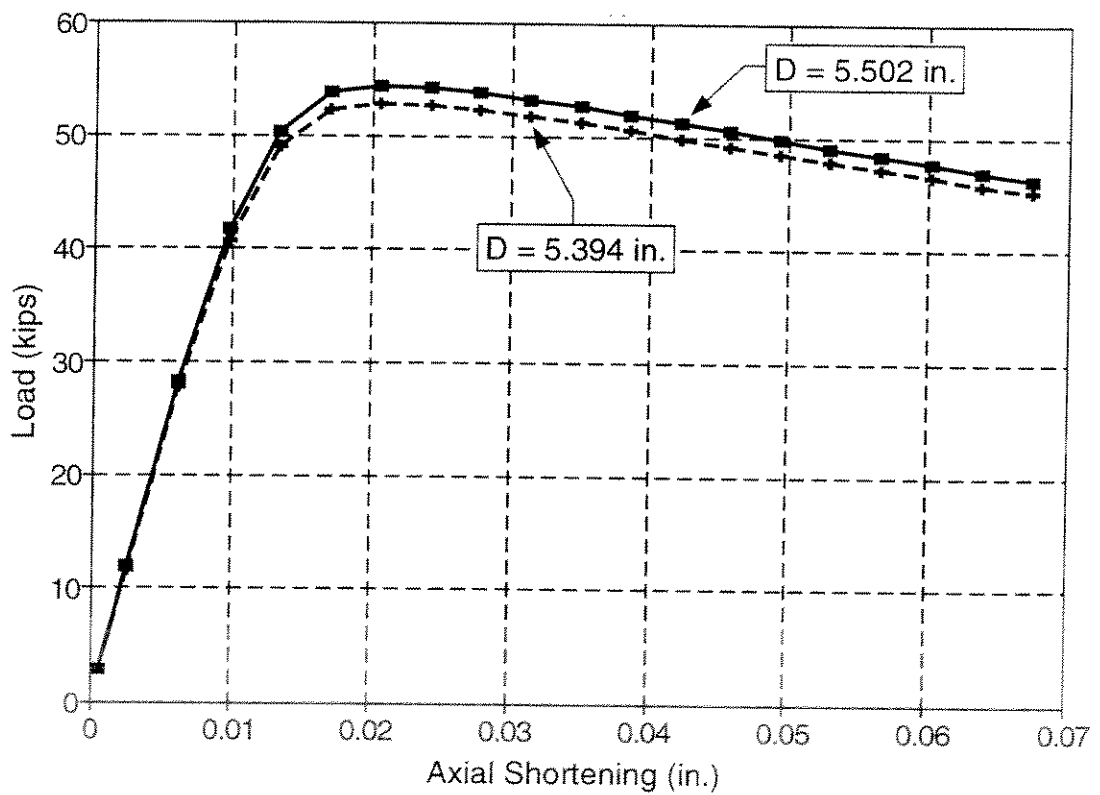


Fig. 8-4 Load-Displacement of Specimen P13 with Different Diameters

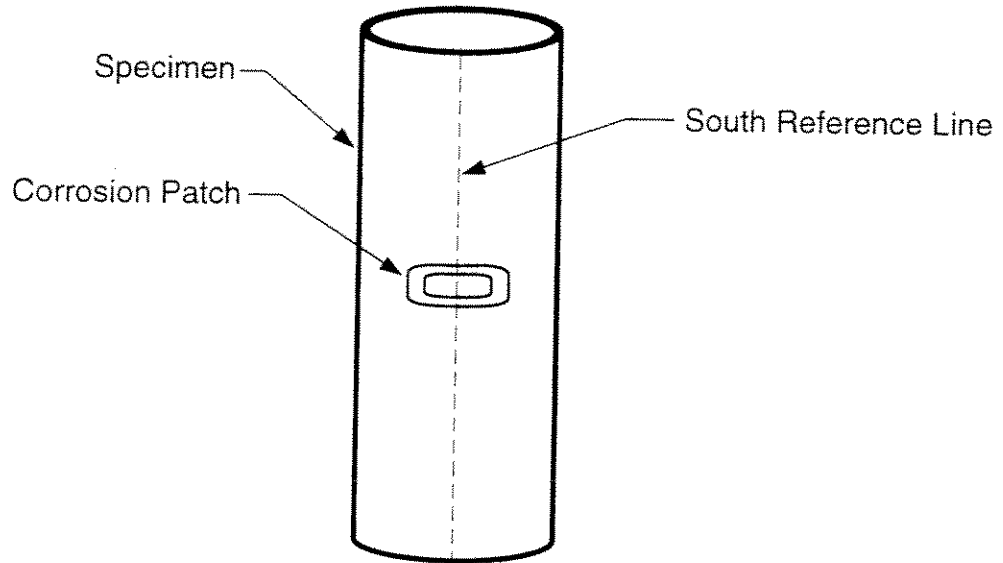


Fig. 9-1 Typical Specimen Showing Location of Corrosion Patch

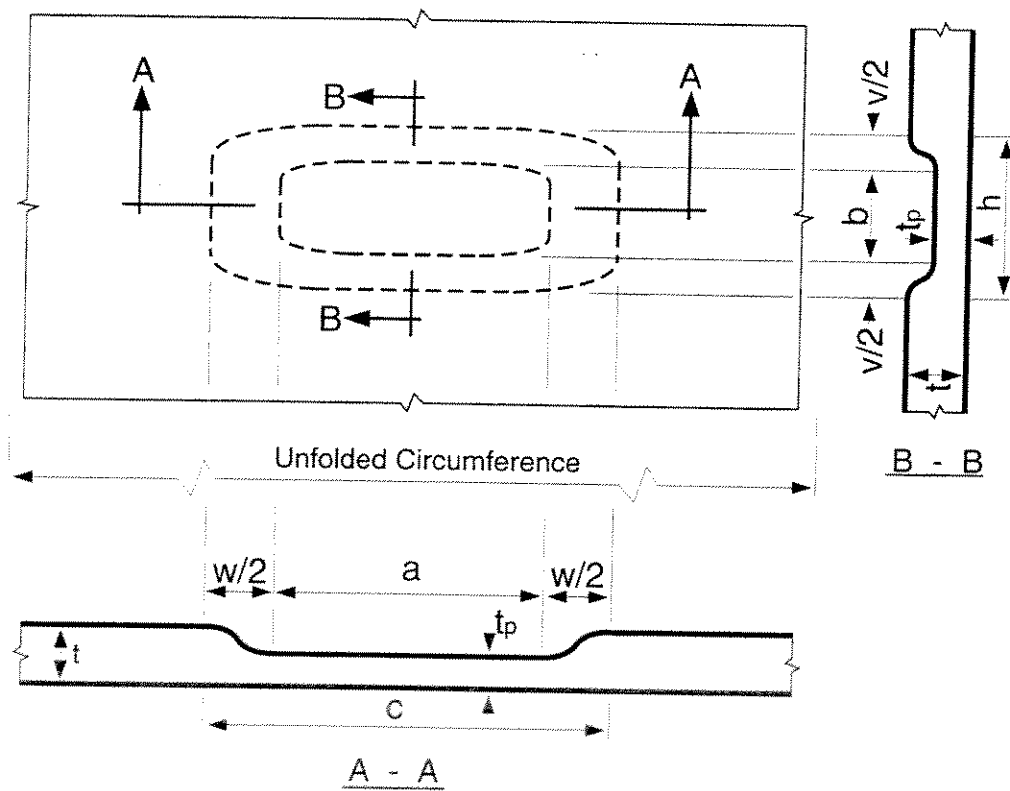


Fig. 9-2 Layout of Corrosion Patch Including Dimensional Parameters

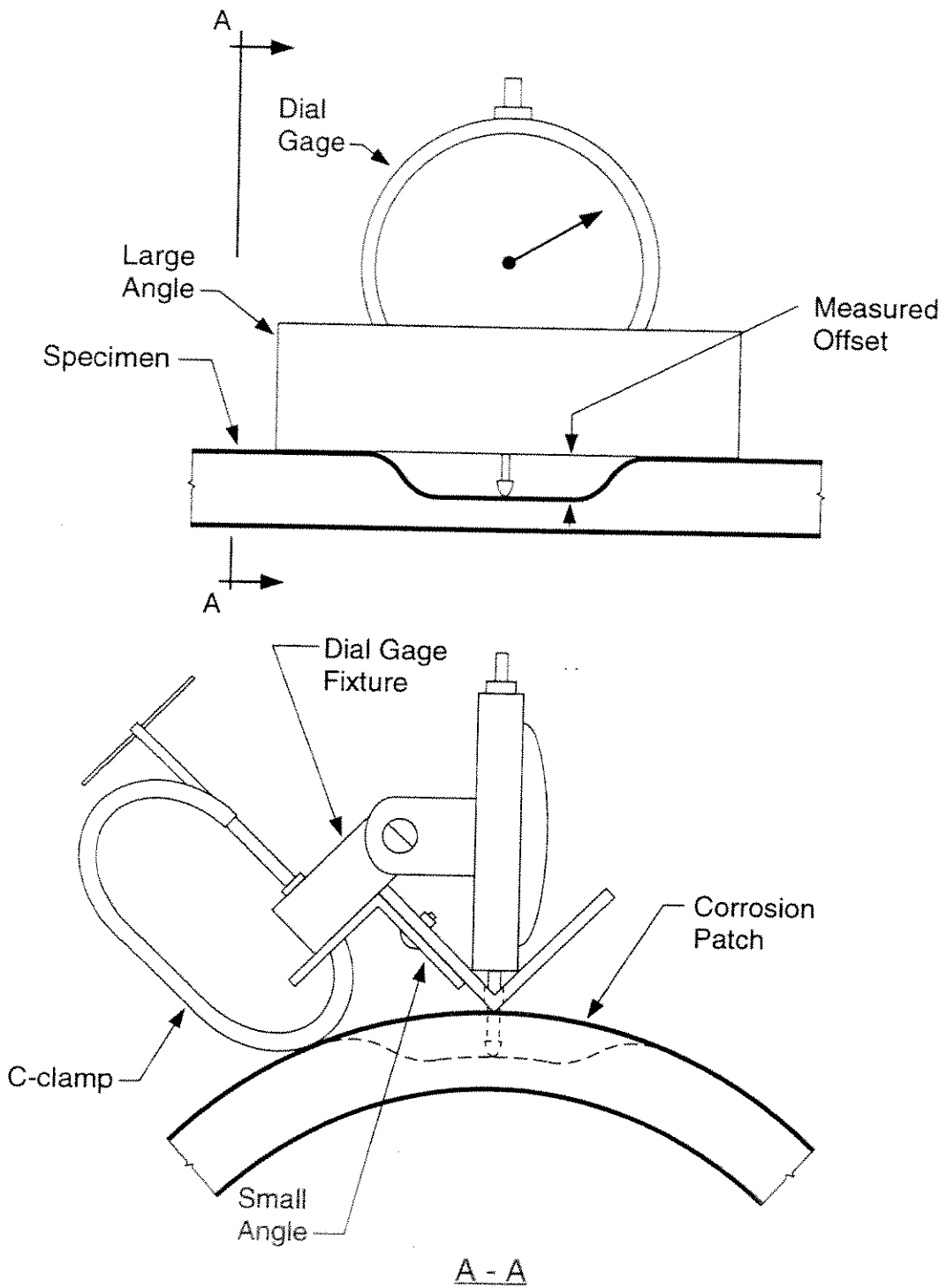


Fig. 9-3 Frontal and Cross-Sectional Views of the Angle Tool

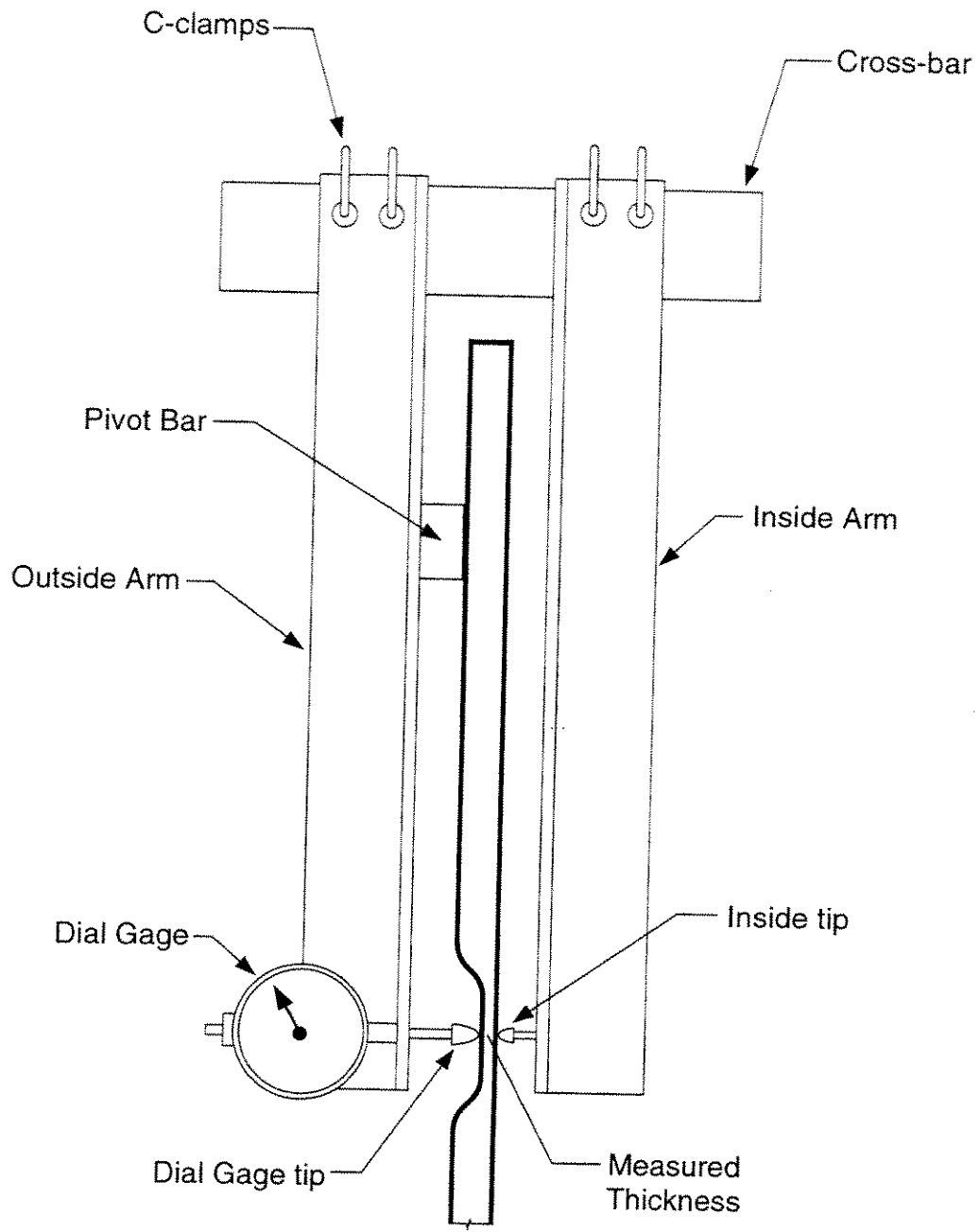


Fig. 9-4 The Fork Tool

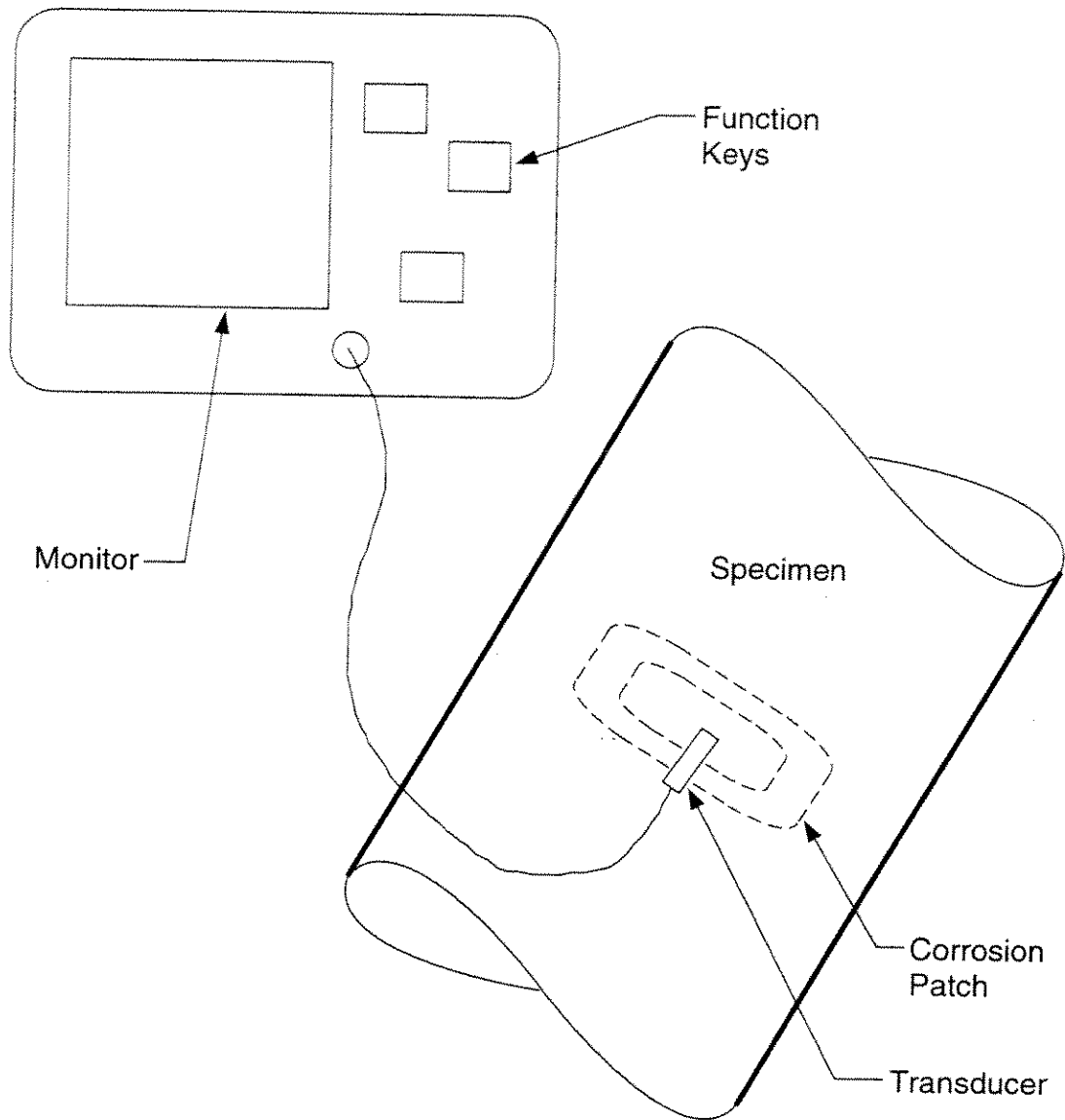


Fig. 9-5 Ultrasonic Equipment

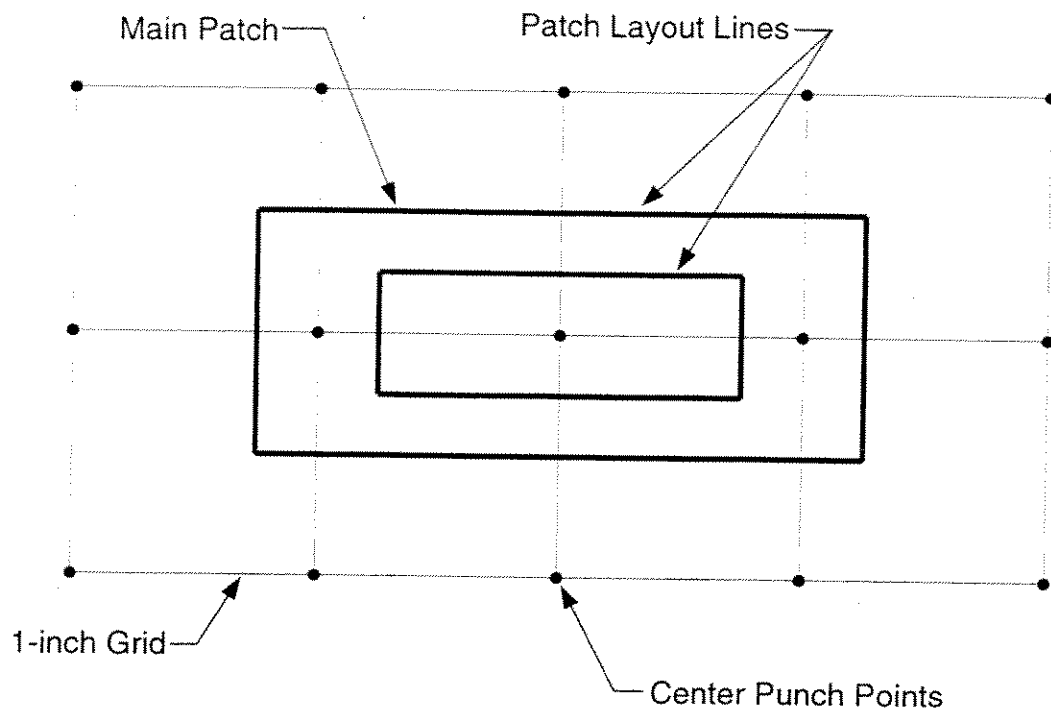


Fig. 9-6 Patch Layout Lines with 1-inch Grid and Center Punch Points

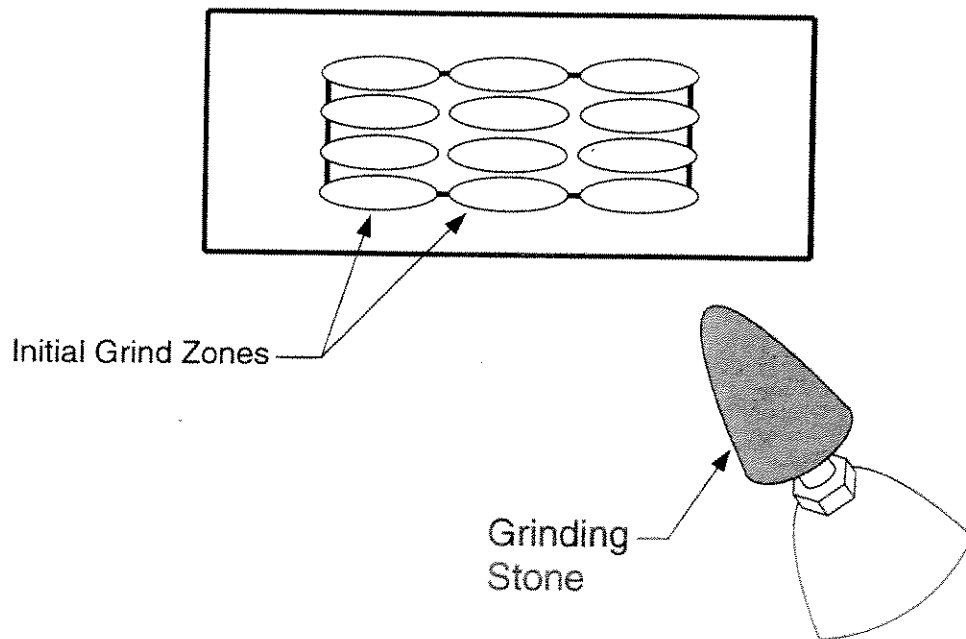


Fig. 9-7 Initial Grind Zones and Grinding Stone

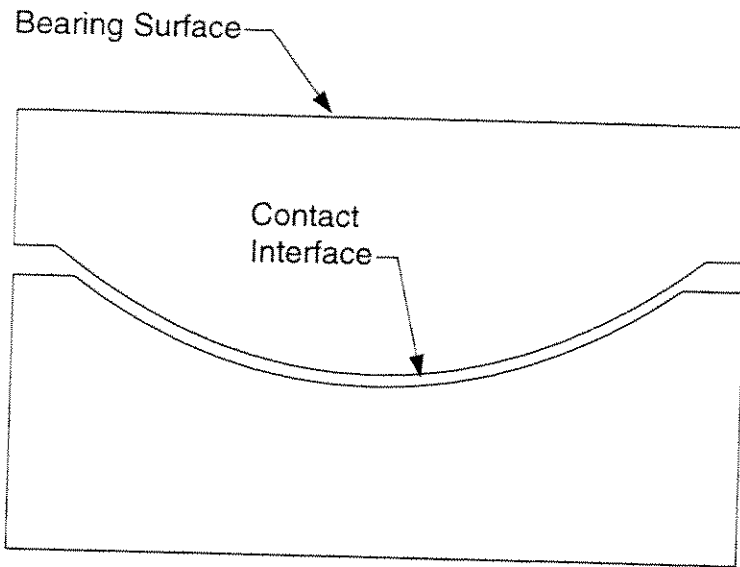


Fig. 10-1 Cross Section of Spherical Bearing Showing Spherical Contact Surfaces

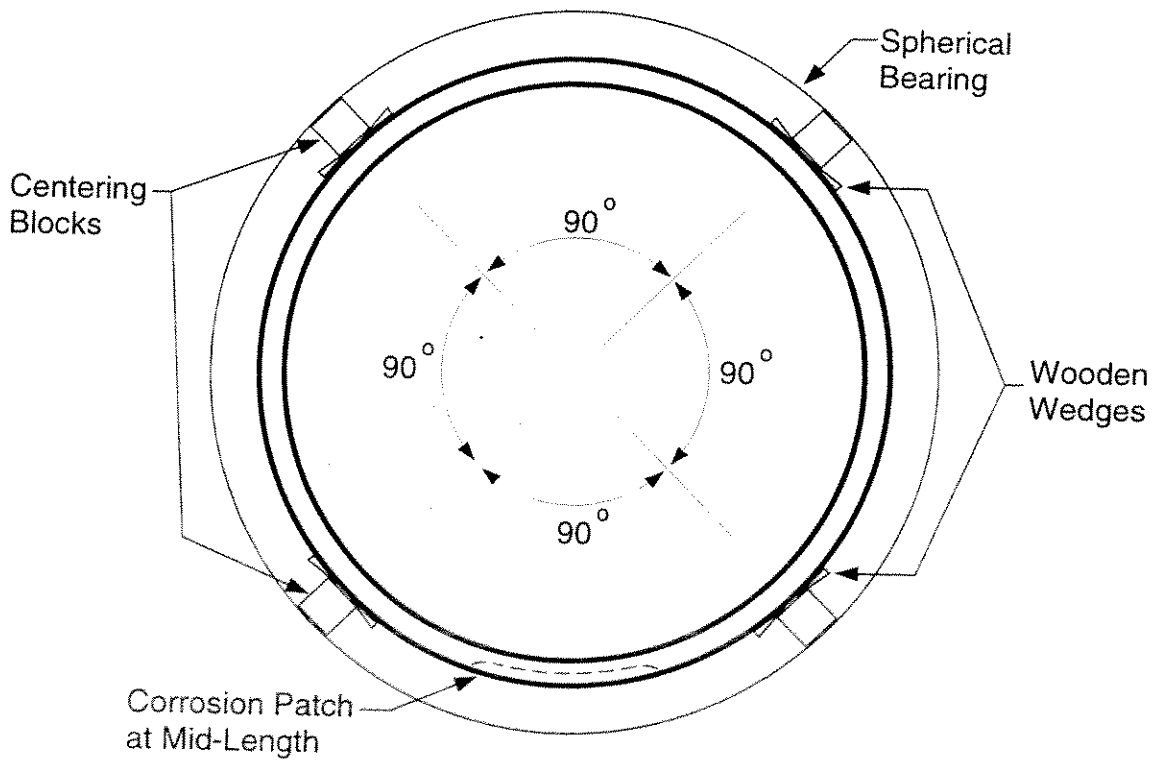
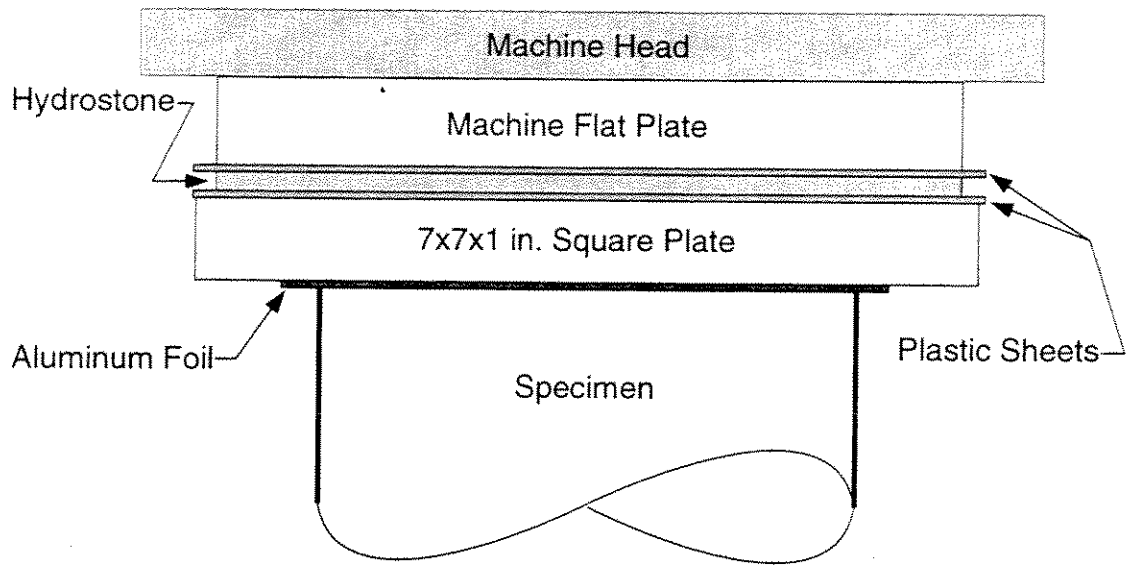
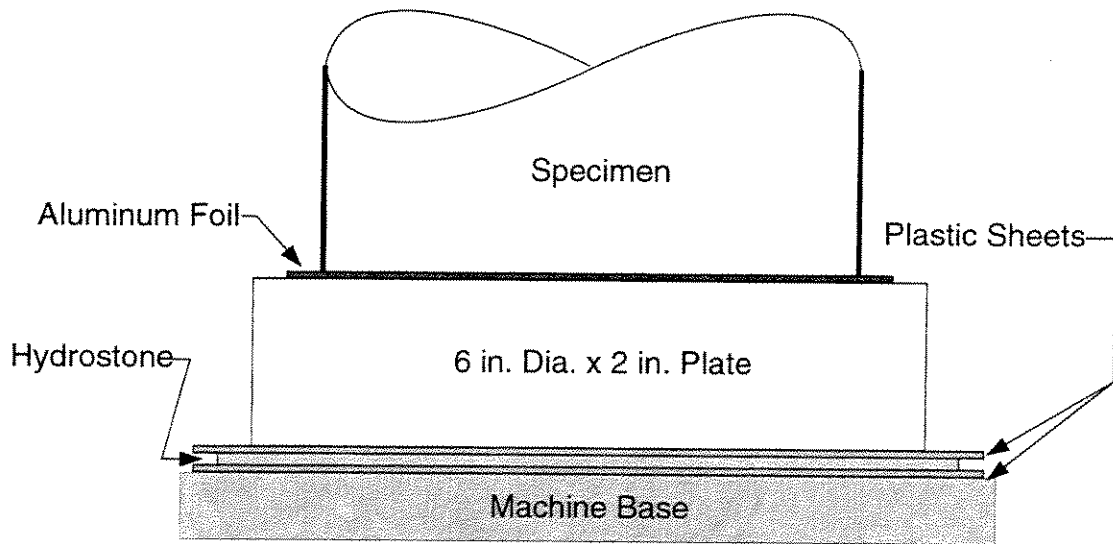


Fig. 10-2 Plan View of Spherical Bearing

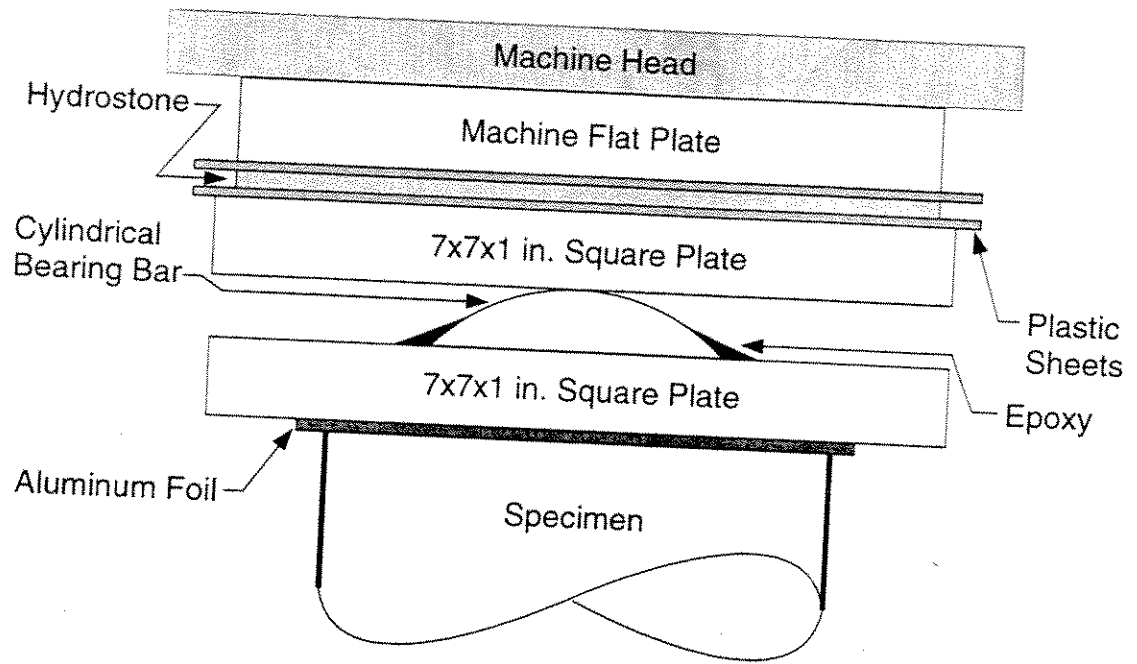


(a) Top Bearing for Fixed-End Tests

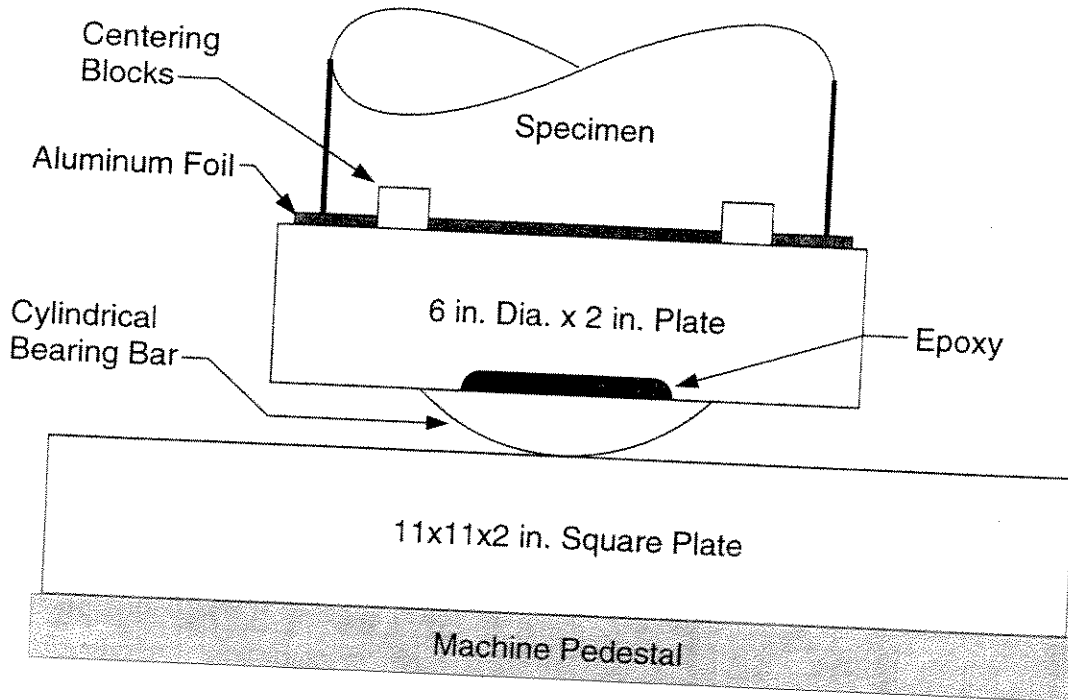


(b) Bottom Bearing for Fixed-End Tests

Fig. 10-3 Fixed-End Bearing Fixtures

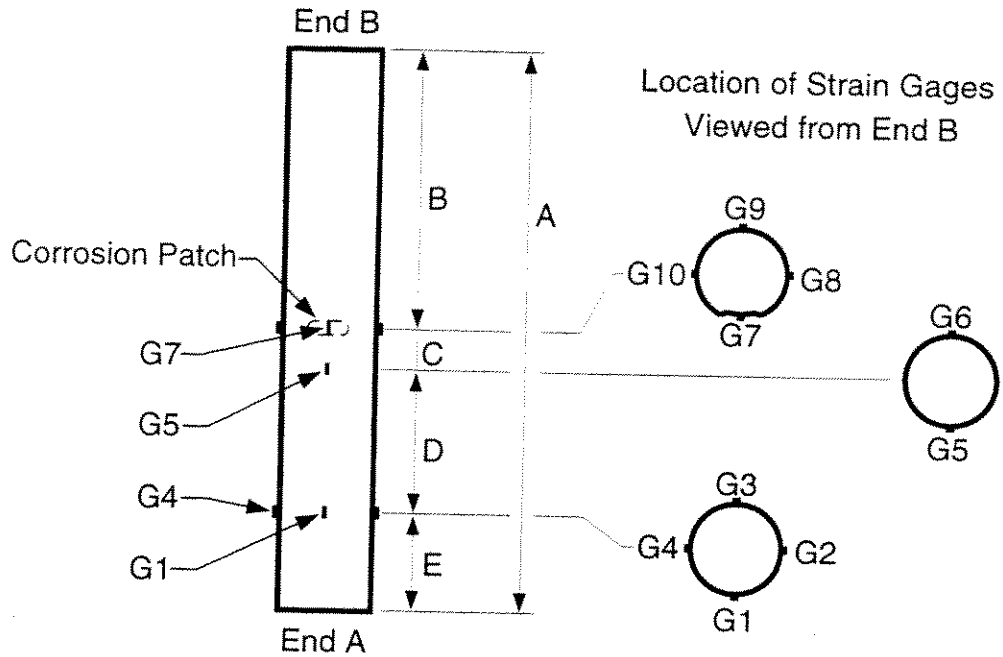


(a) Top Bearing for Cylindrical Bearing Tests



(b) Bottom Bearing for Cylindrical Bearing Tests

Fig. 10-4 Cylindrical Bearing Fixtures



Specimen	A	B	C	D	E
P5	28	14	2.75	5.75	5.5
P6	28	14	2.75	5.75	5.5
P7	28	14	2.75	5.75	5.5
P8	28	See Figure 10-6			
P9	27	See Figure 10-7			
P10	12.5	6.25	1.6875	3.3125	1.25
P11	12.5	6.25	1.6875	3.3125	1.25
P12	12.5	6.25	2.0625	2.9375	1.25
P13	12.5	6.25	1.6875	3.3125	1.25
P14	12.5	6.25	1.625	3.3750	1.25
P15	12.5	6.25	1.625	3.3750	1.25

Fig. 10-5 Strain Gage Layout for Specimens P5 to P7 and P10 to P15
(All Dimensions are in Inches)

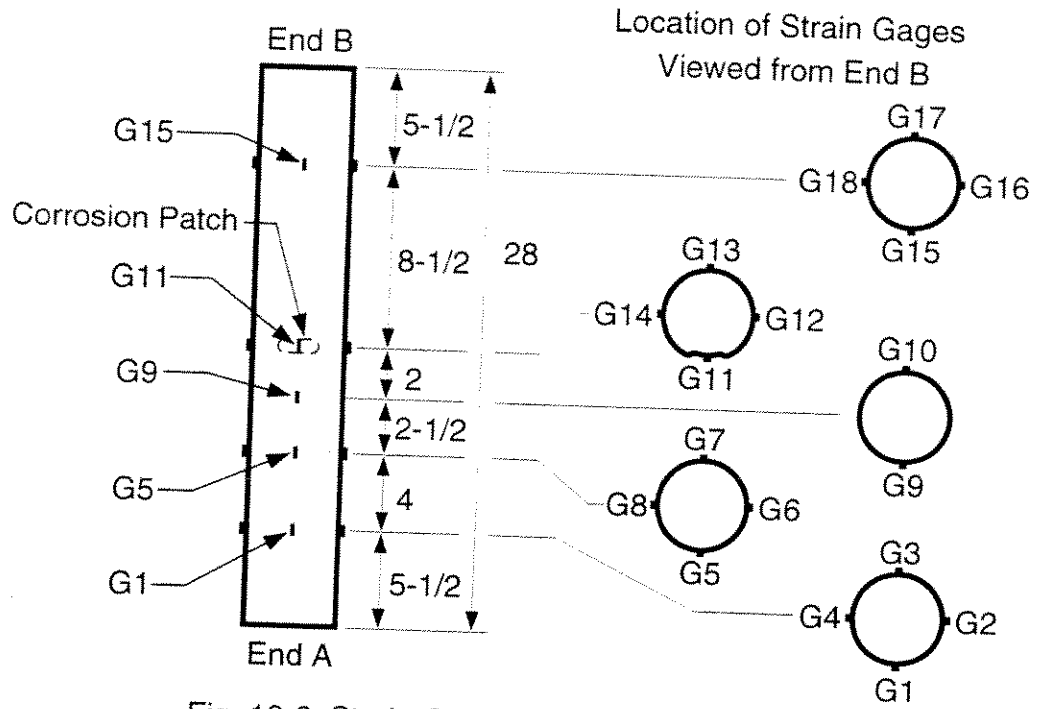


Fig. 10-6 Strain Gage Layout for Specimen P8

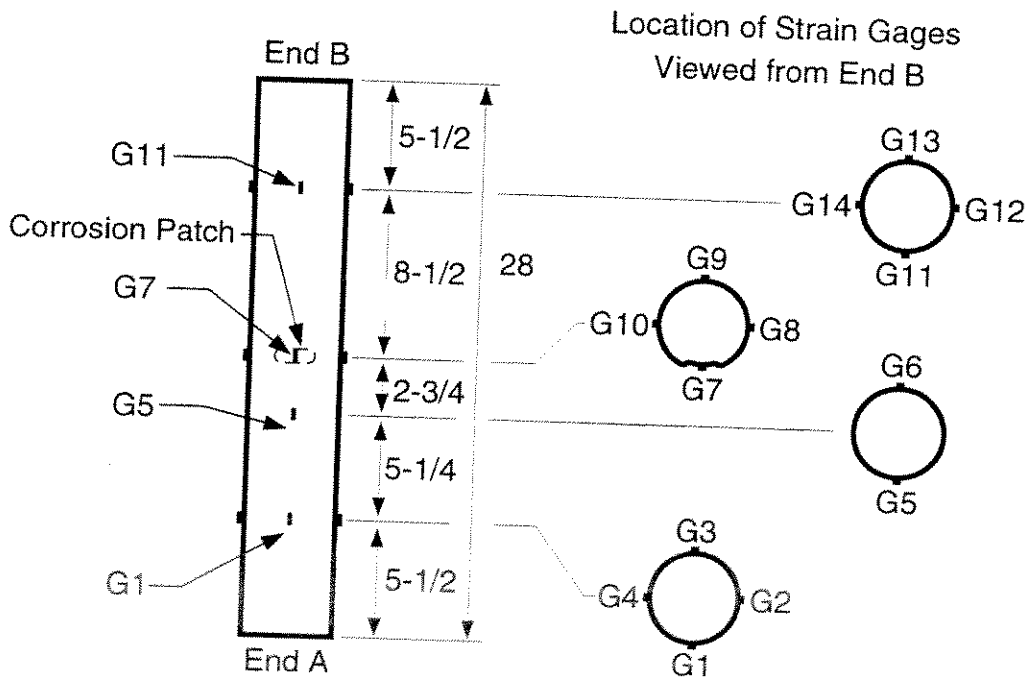


Fig. 10-7 Strain Gage Layout for Specimen P9

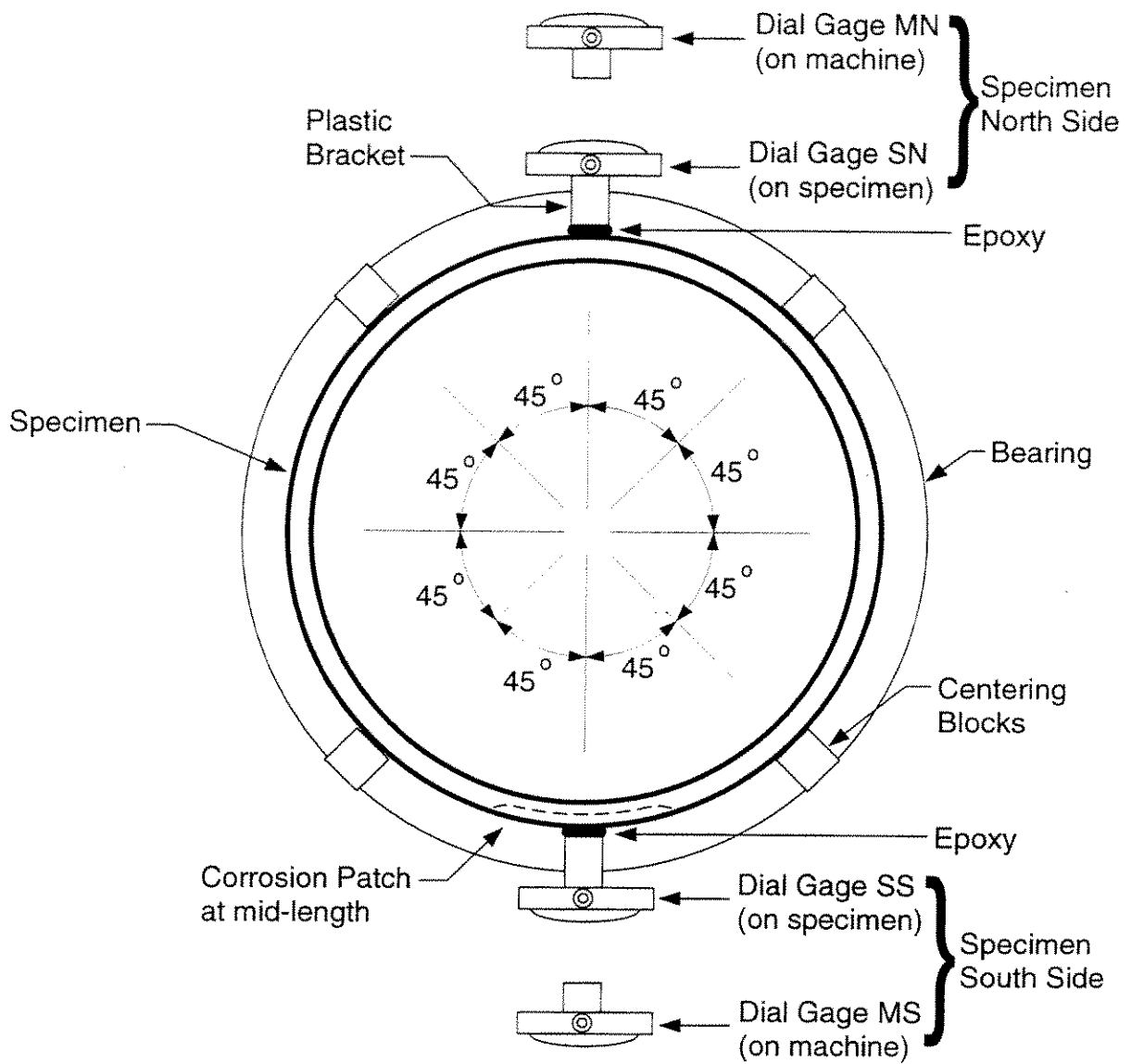


Fig. 10-8 Plan View of Test Setup Showing Dial Gage Locations

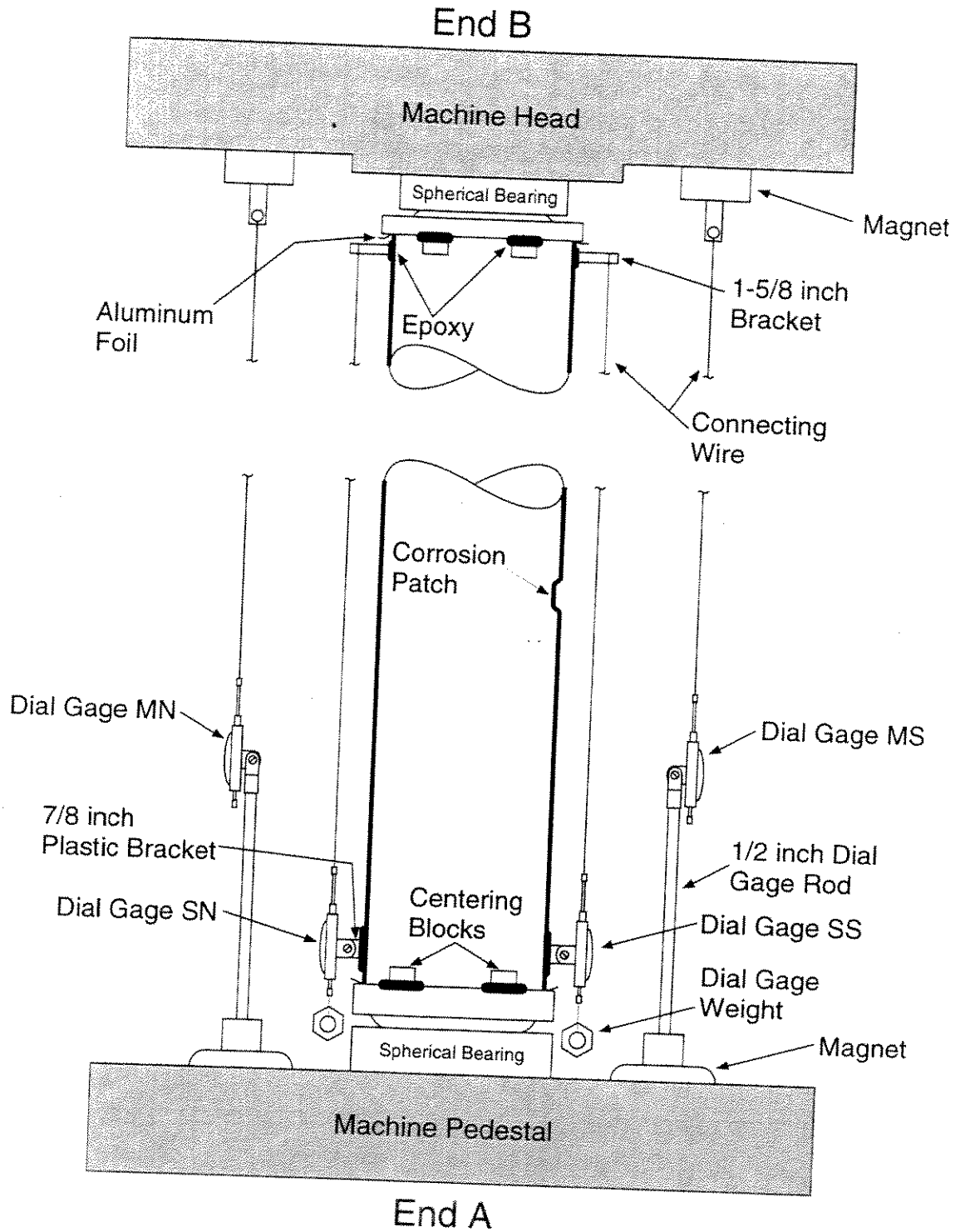


Fig. 10-9 Test Setup for Specimens P5 to P9
(Spherical Bearing Fixtures)

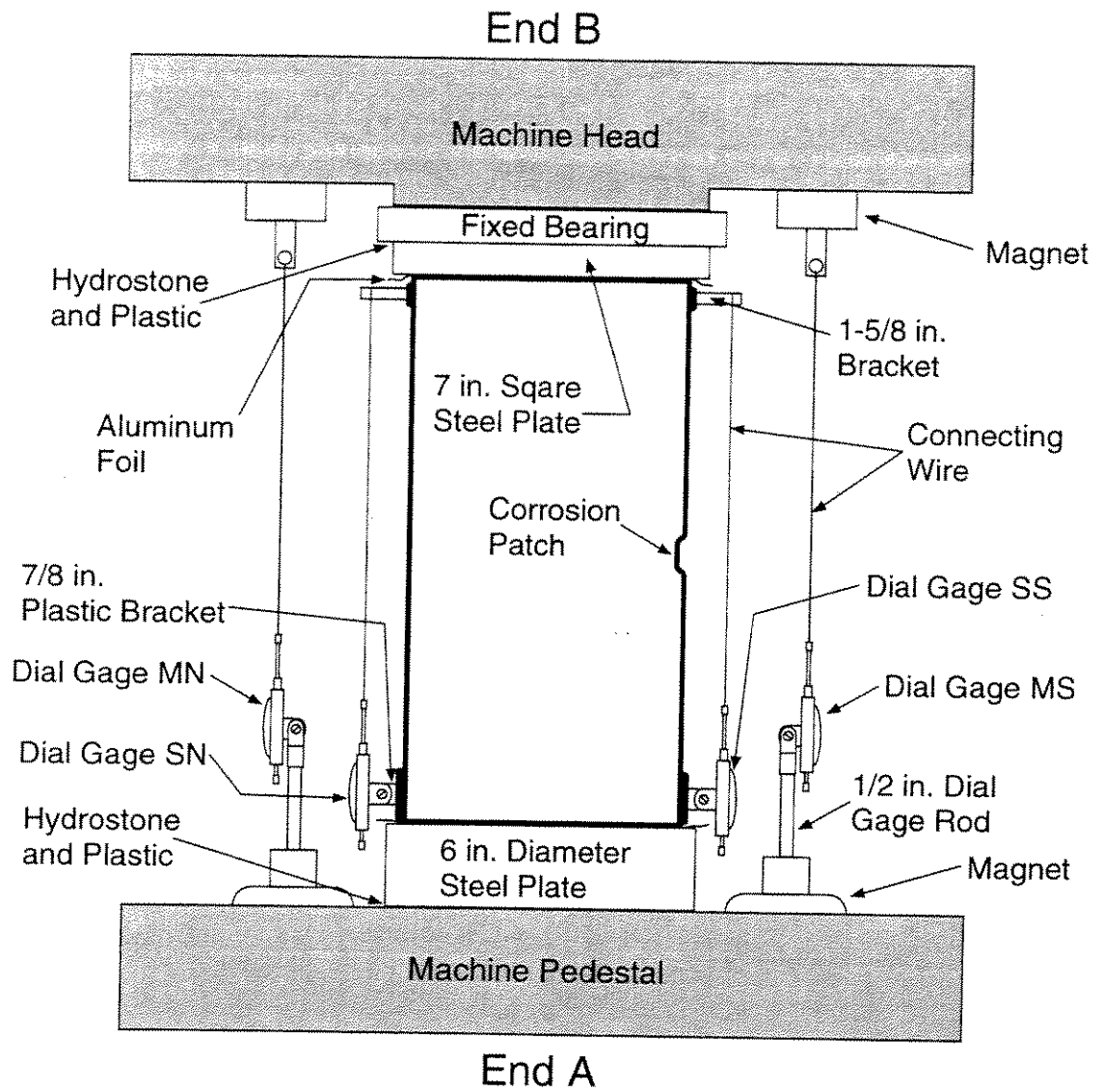


Fig. 10-10 Test Setup for Specimens P10 to P12
(Fixed-End Bearing Fixtures)

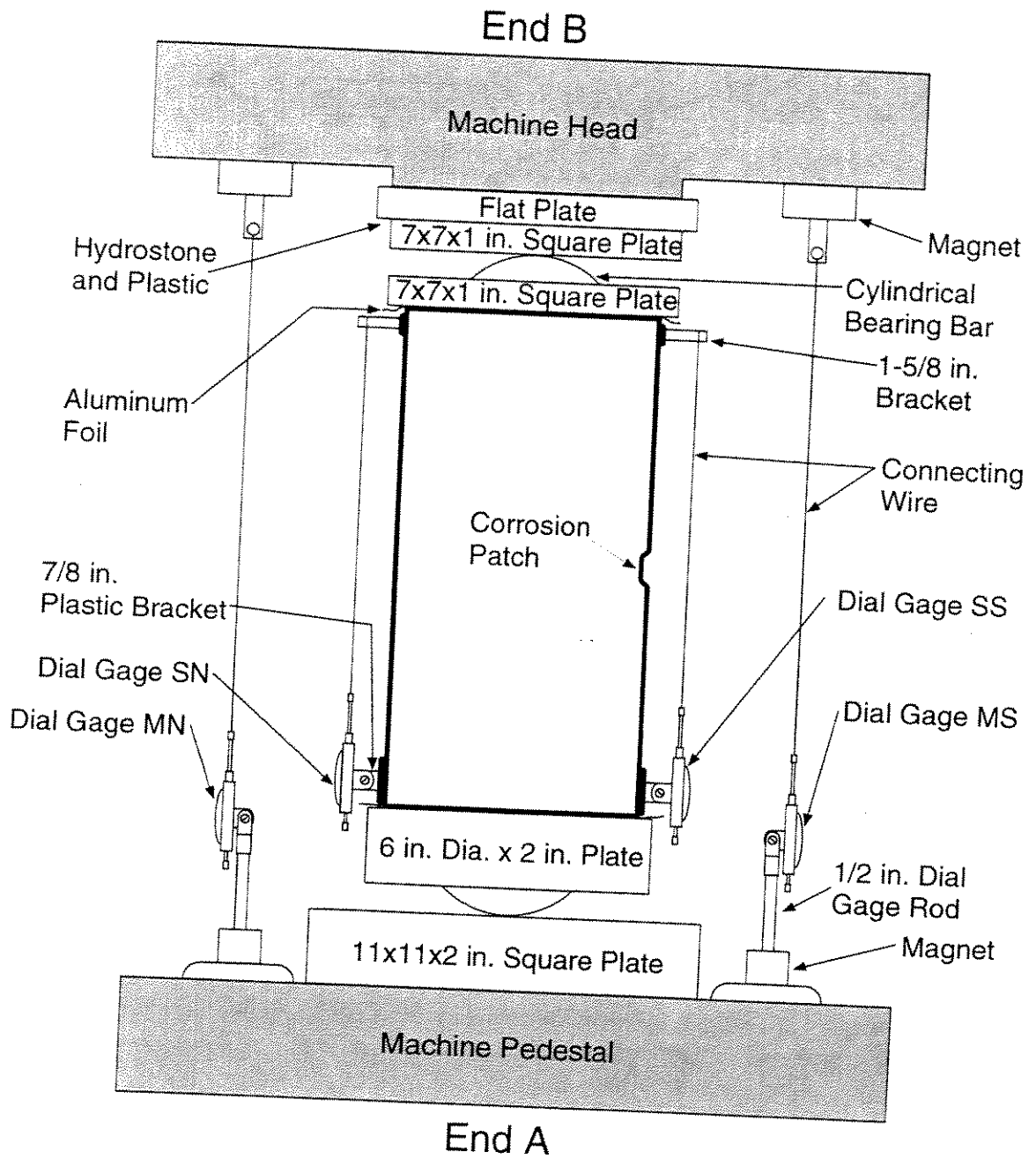


Fig. 10-11 Test Setup for Specimens P13 to P15
(Cylindrical Bearing Fixtures)

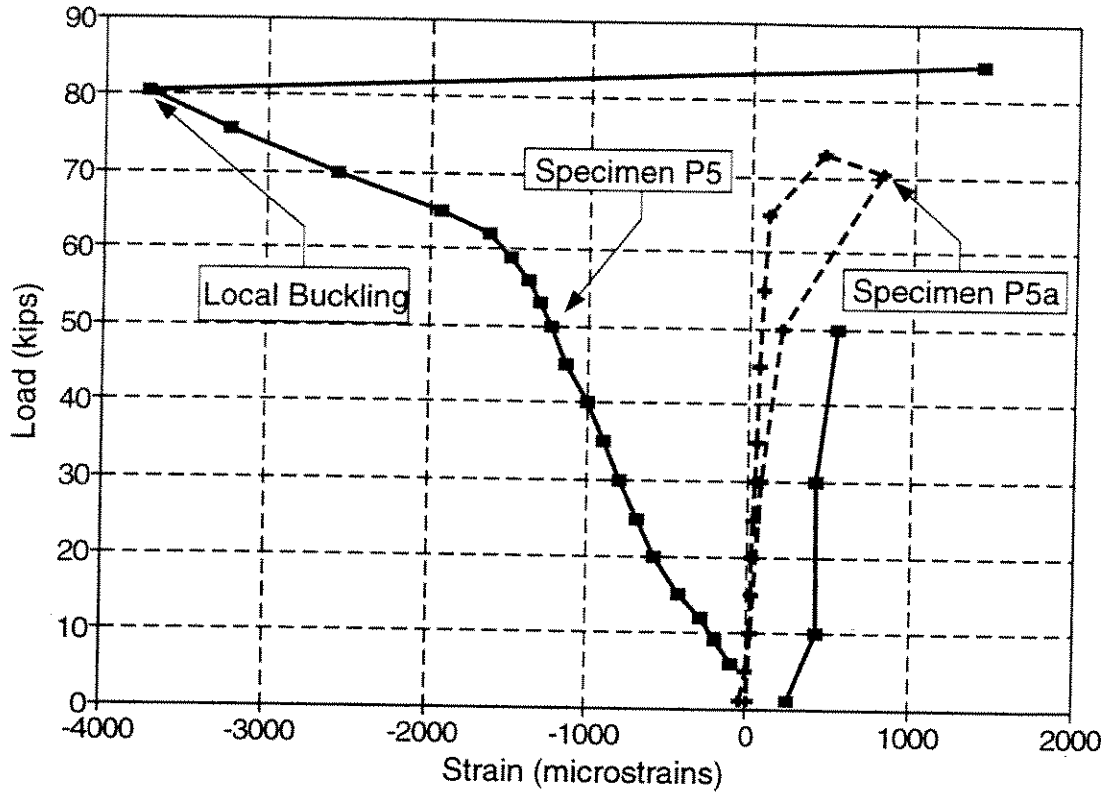


Figure 11-1 Strain in Corrosion Patch (Gage 7) for Specimens P5 and P5a

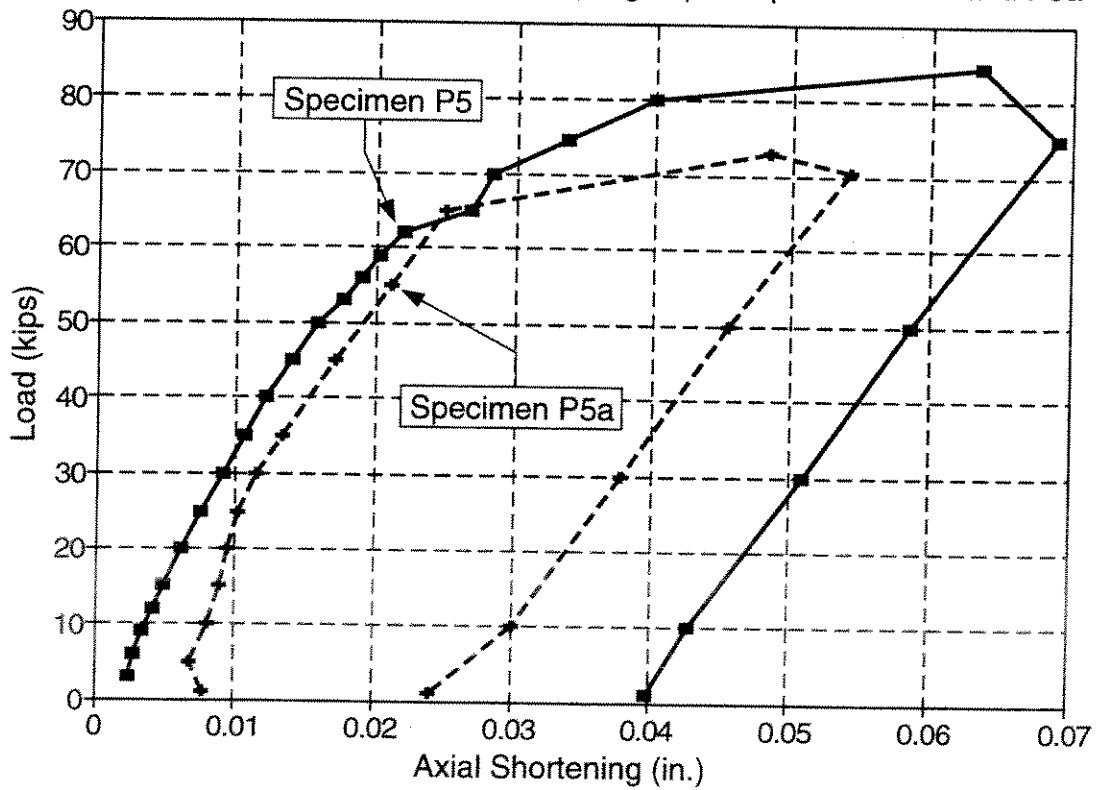


Figure 11-2 Load-Shortening for Specimens P5 and P5a

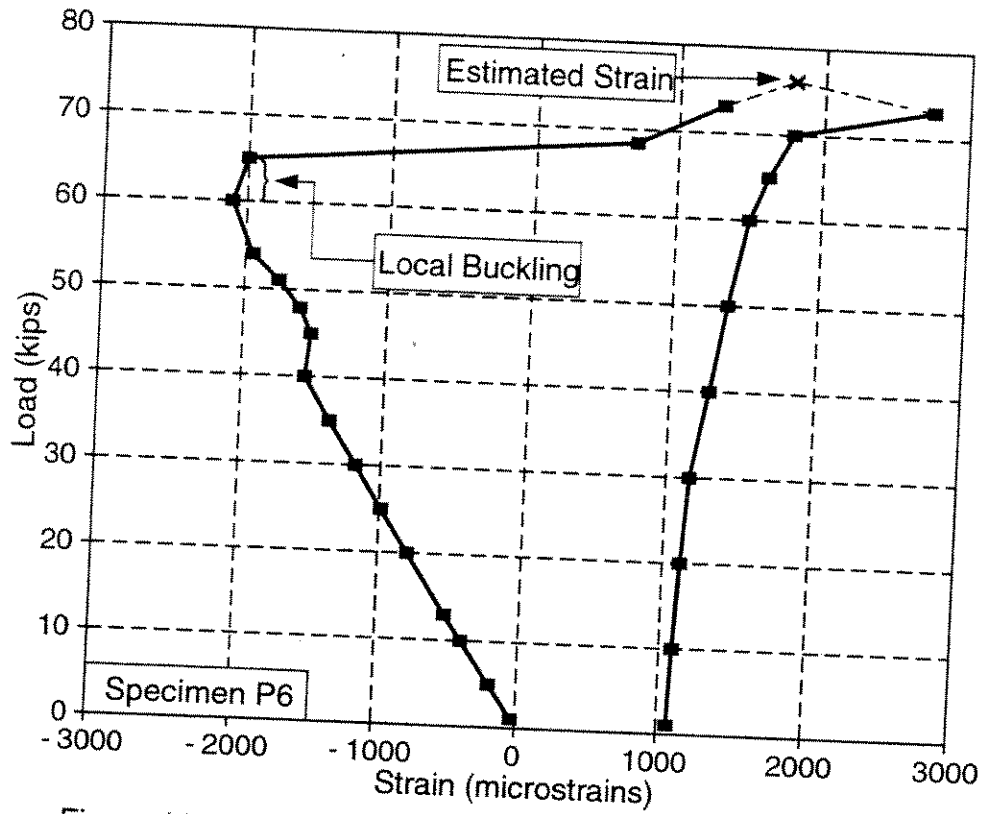


Figure 11-3 Strain in Corrosion Patch (Gage 7) for Specimen P6

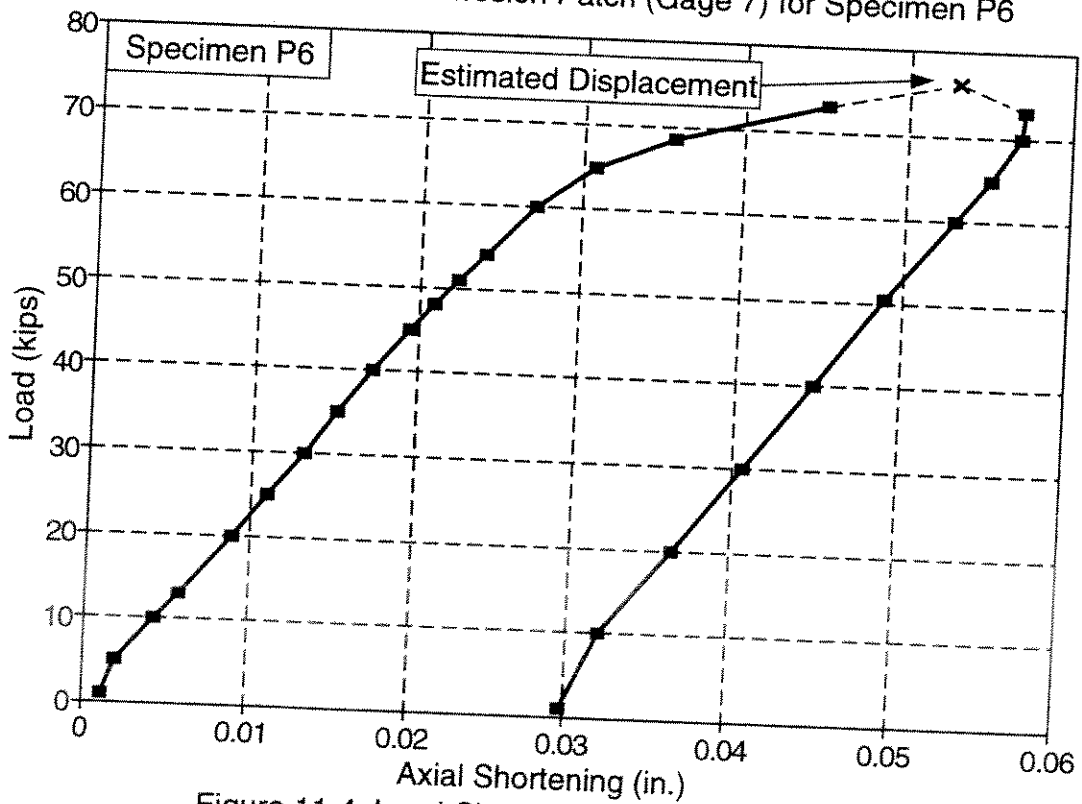


Figure 11-4 Load-Shortening for Specimen P6

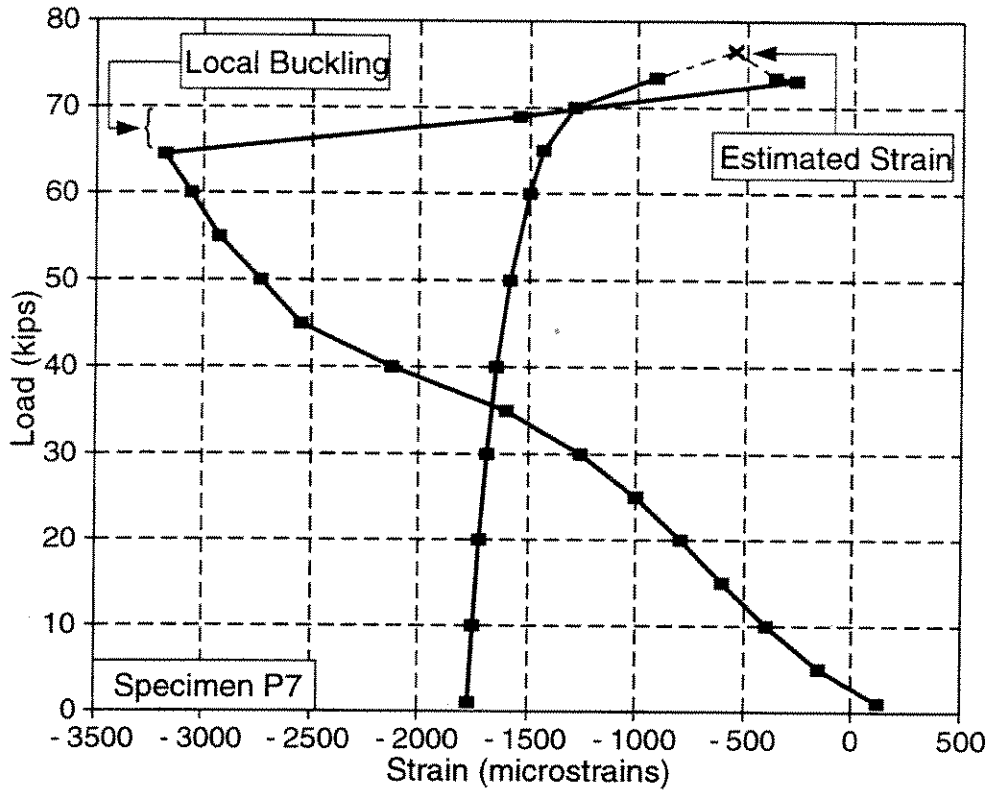


Figure 11-5 Strain in Corrosion Patch (Gage 7) for Specimen P7

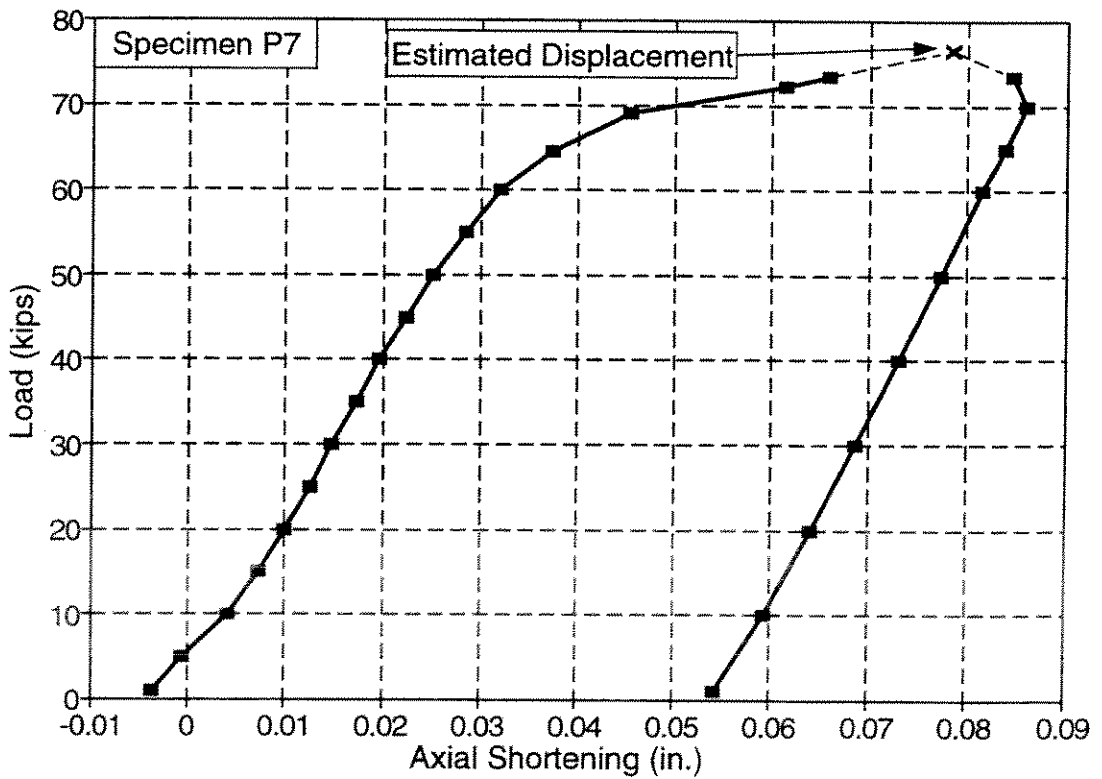


Figure 11-6 Load-Shortening for Specimen P7

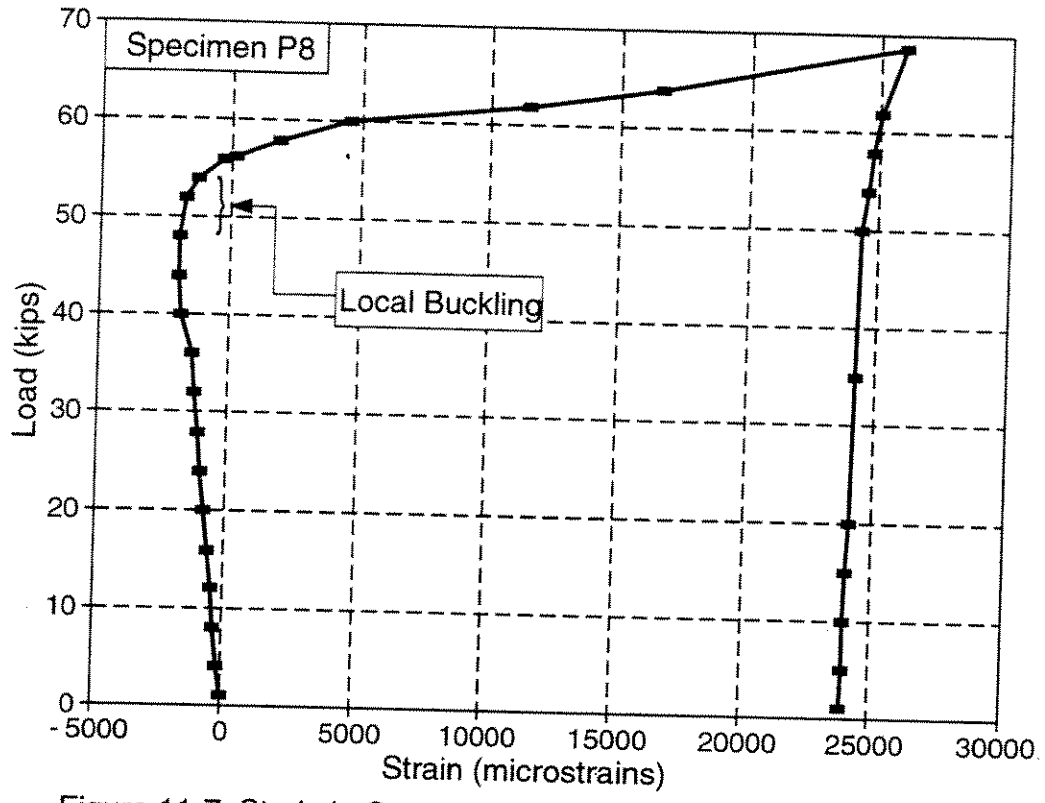


Figure 11-7 Strain in Corrosion Patch (Gage 11) for Specimen P8

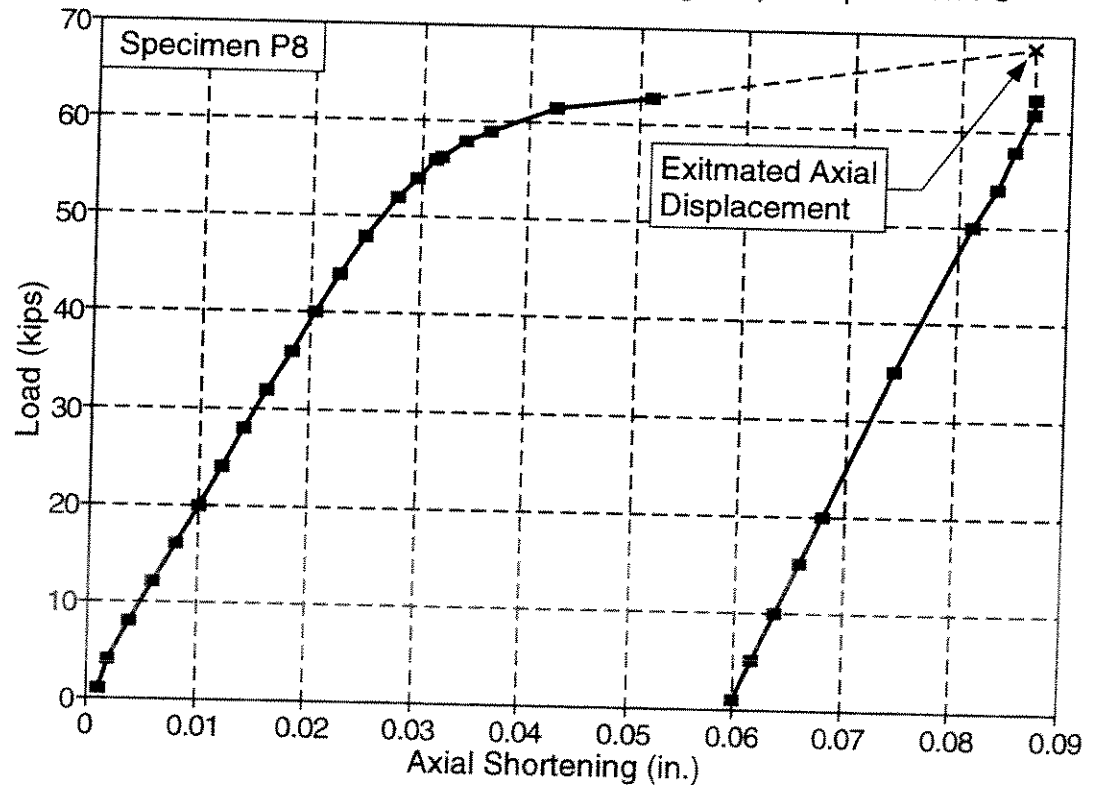


Figure 11-8 Load-Shortening for Specimen P8

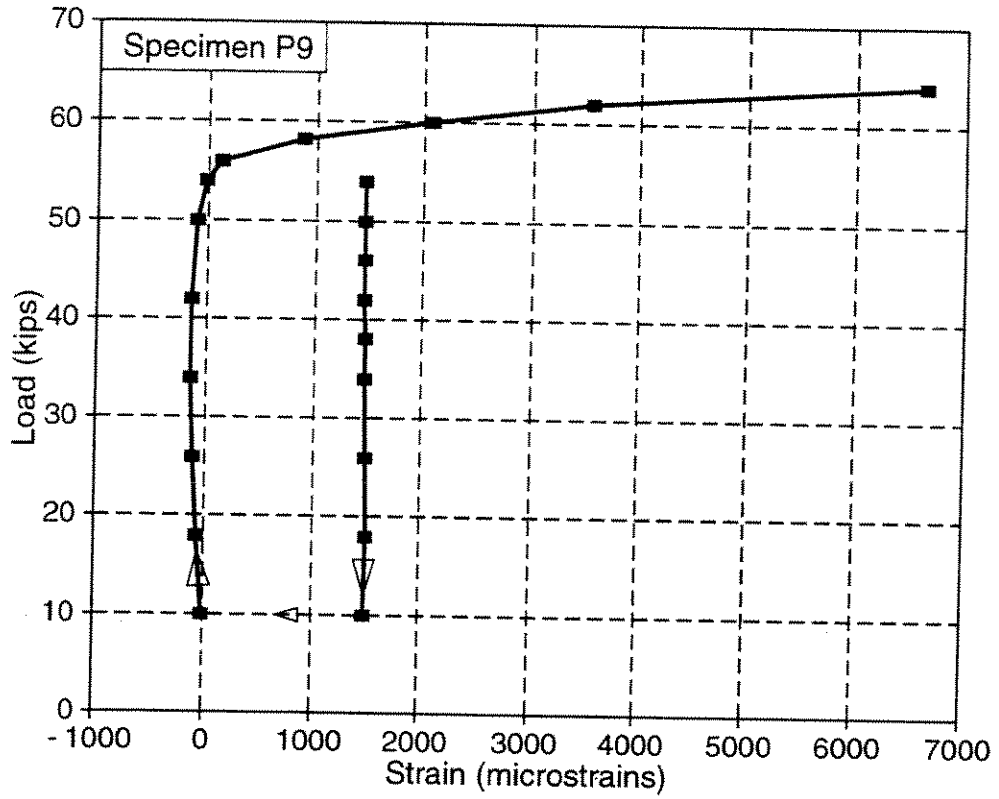


Figure 11-9 Strain in Corrosion Patch (Gage 7) for Specimen P9

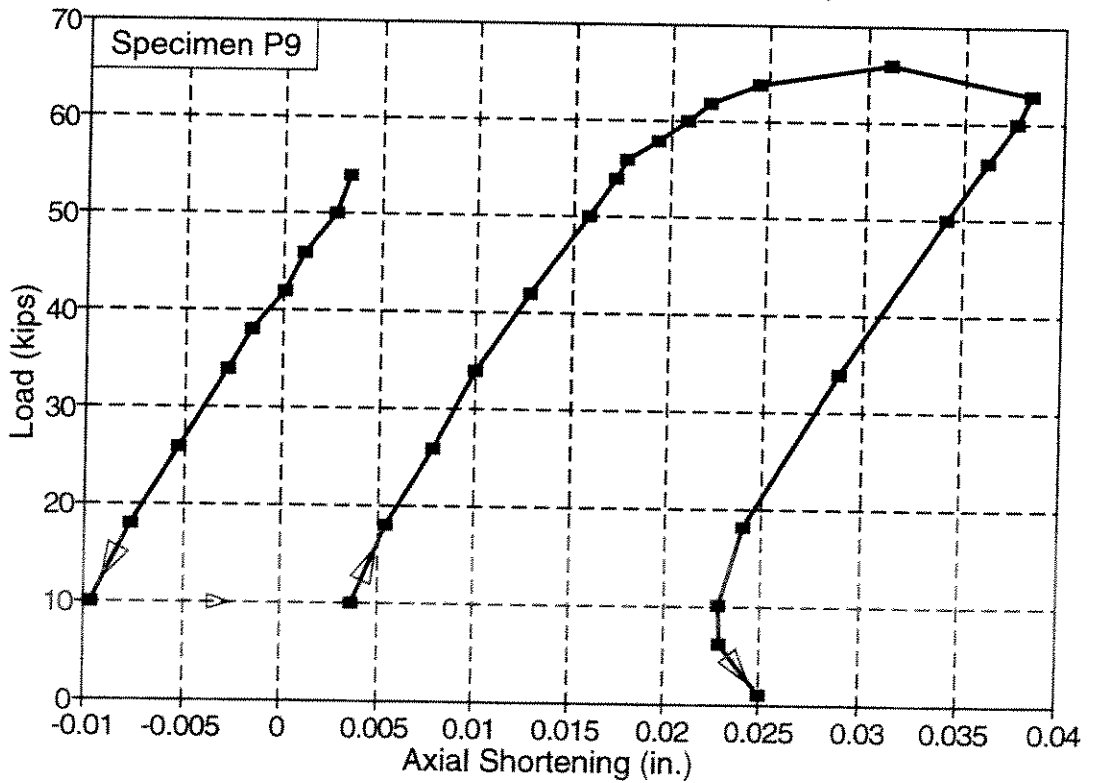


Figure 11-10 Load-Shortening for Specimen P9

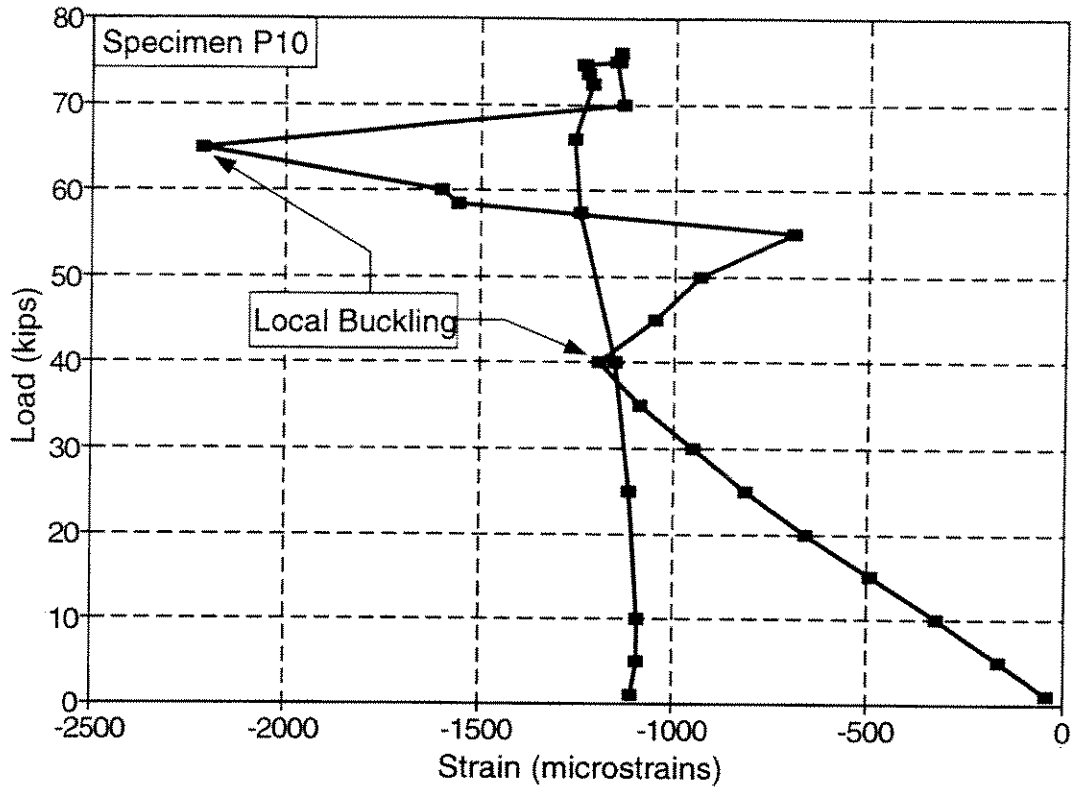


Figure 11-11 Strain in Corrosion Patch (Gage 7) for Specimen P10

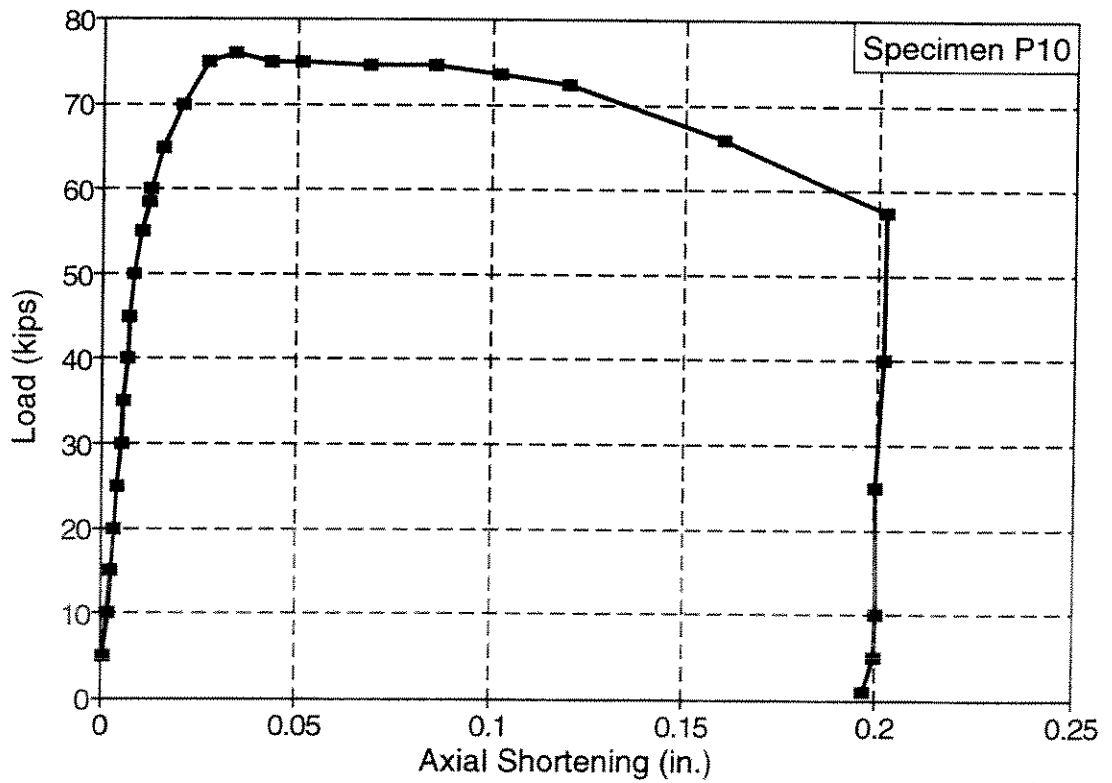


Figure 11-12 Load-Shortening for Specimen P10

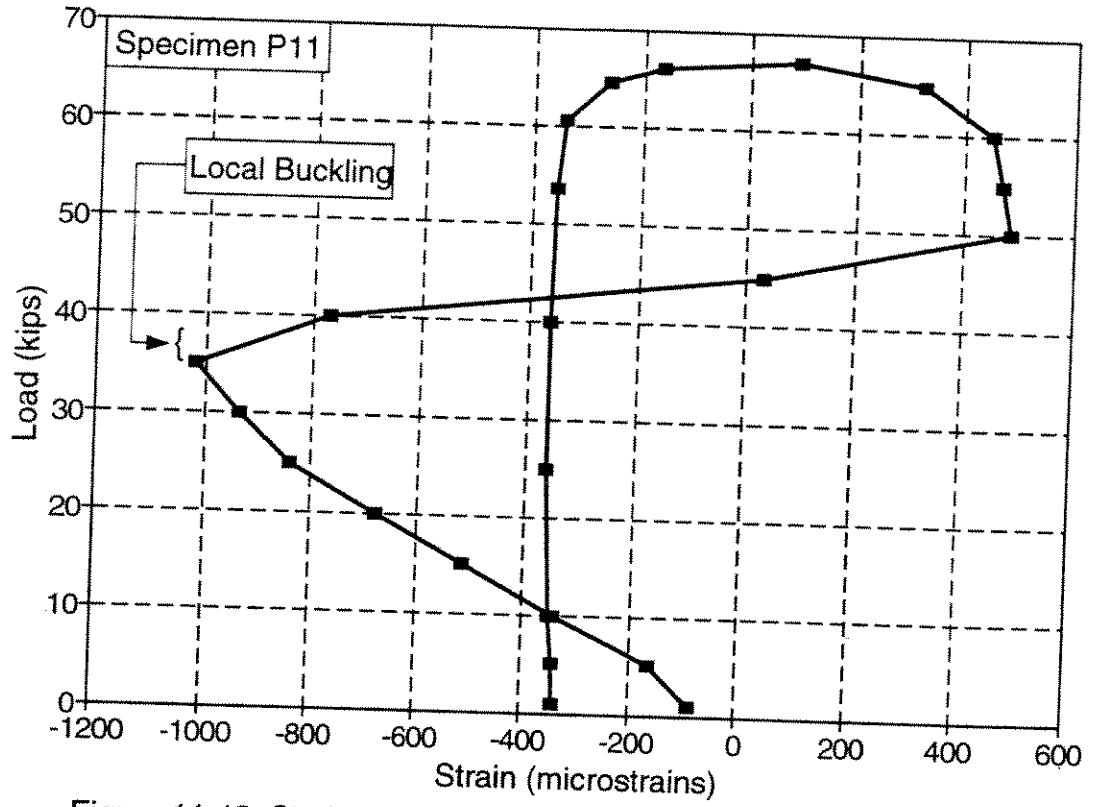


Figure 11-13 Strain in Corrosion Patch (Gage 7) for Specimen P11

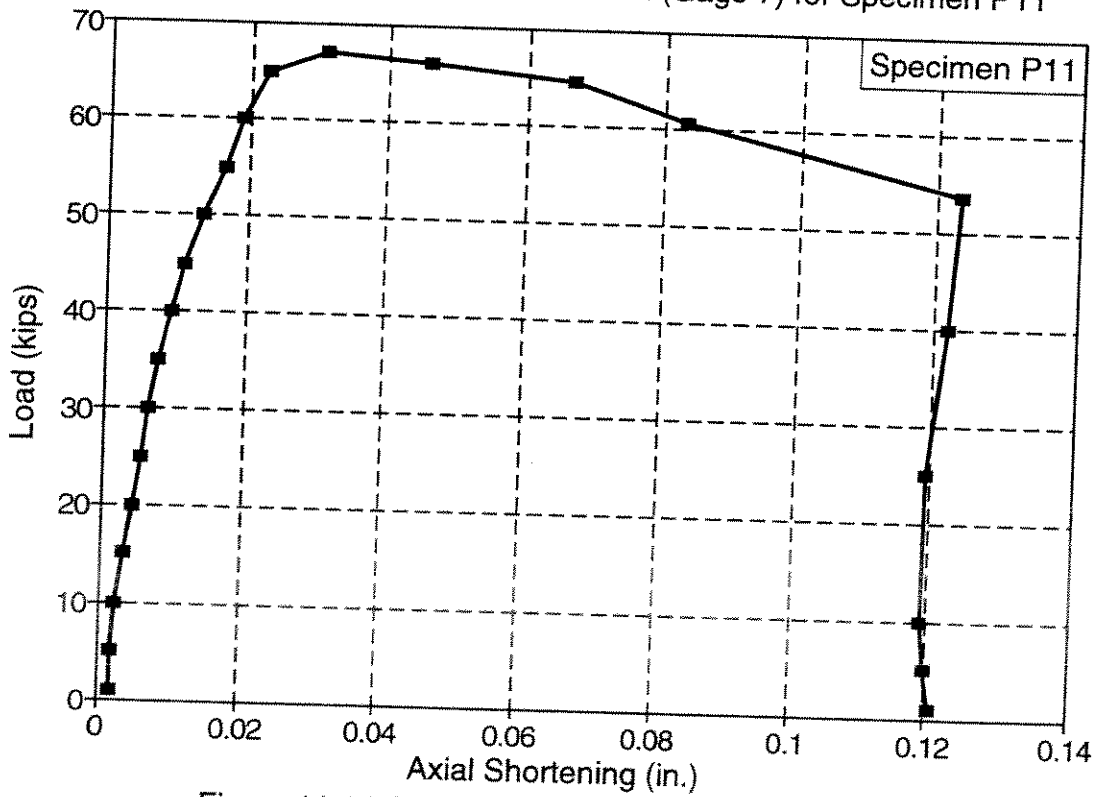


Figure 11-14 Load-Shortening for Specimen P11

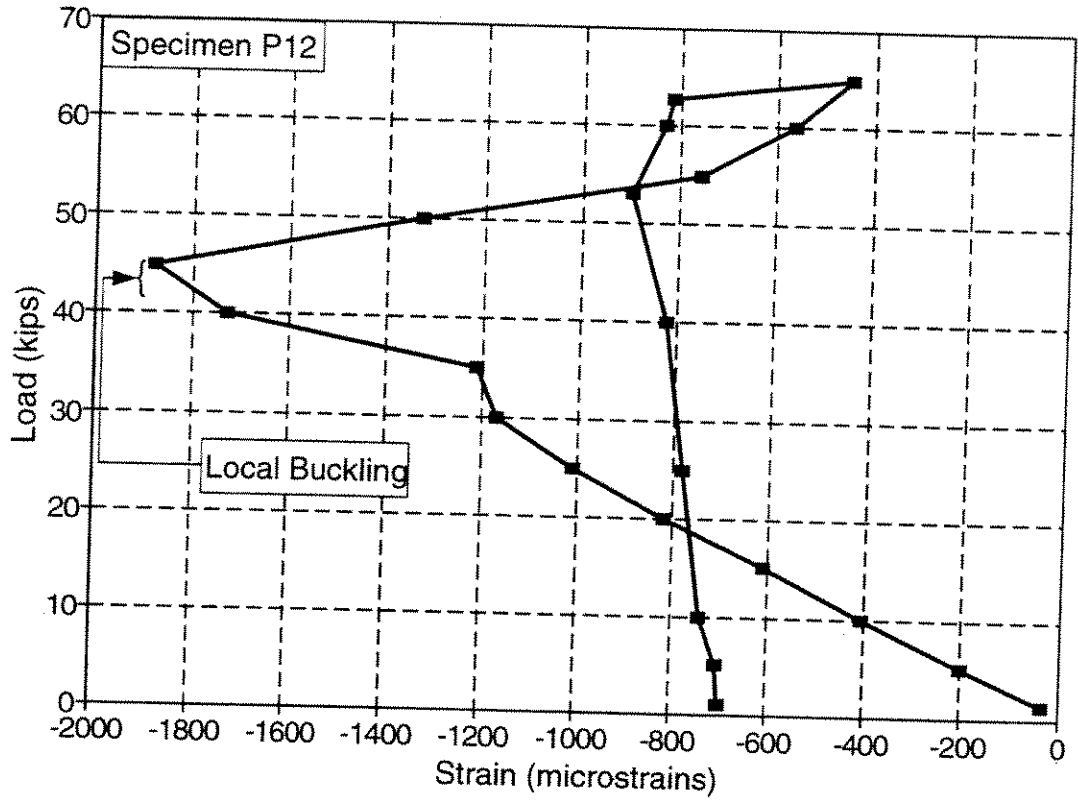


Figure 11-15 Strain in Corrosion Patch (Gage 7) for Specimen P12

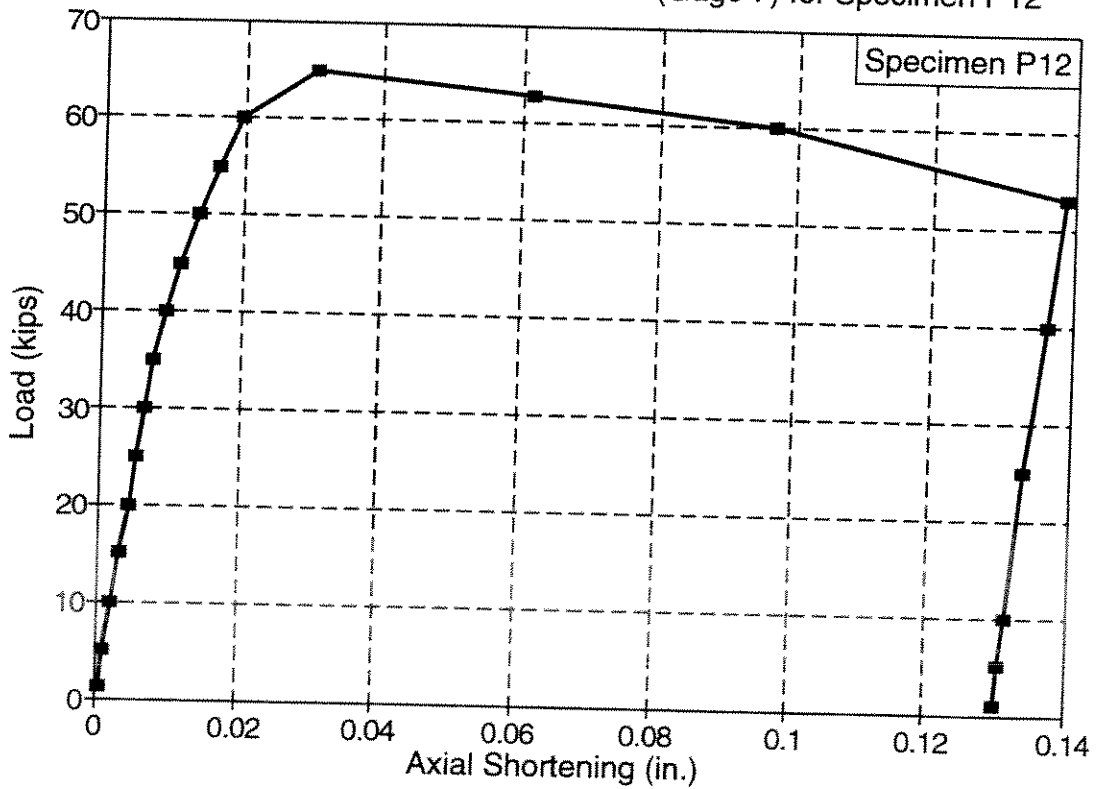


Figure 11-16 Load-Shortening for Specimen P12

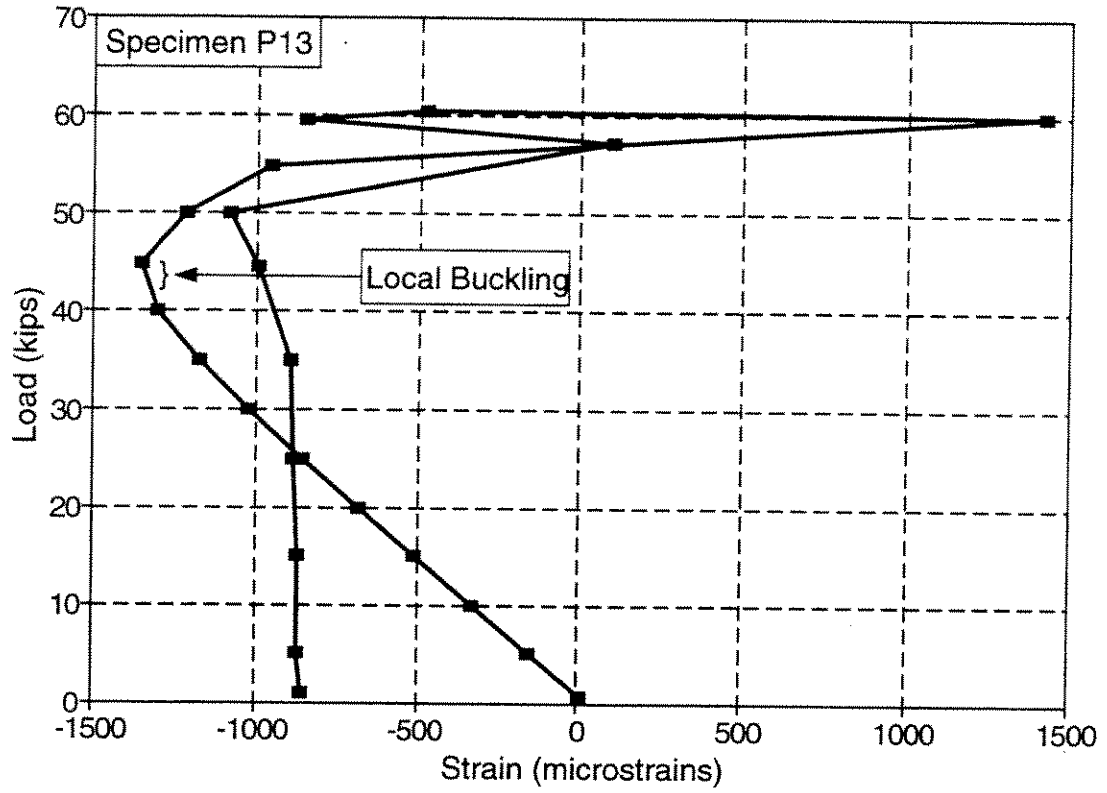


Figure 11-17 Strain in Corrosion Patch (Gage 7) for Specimen P13

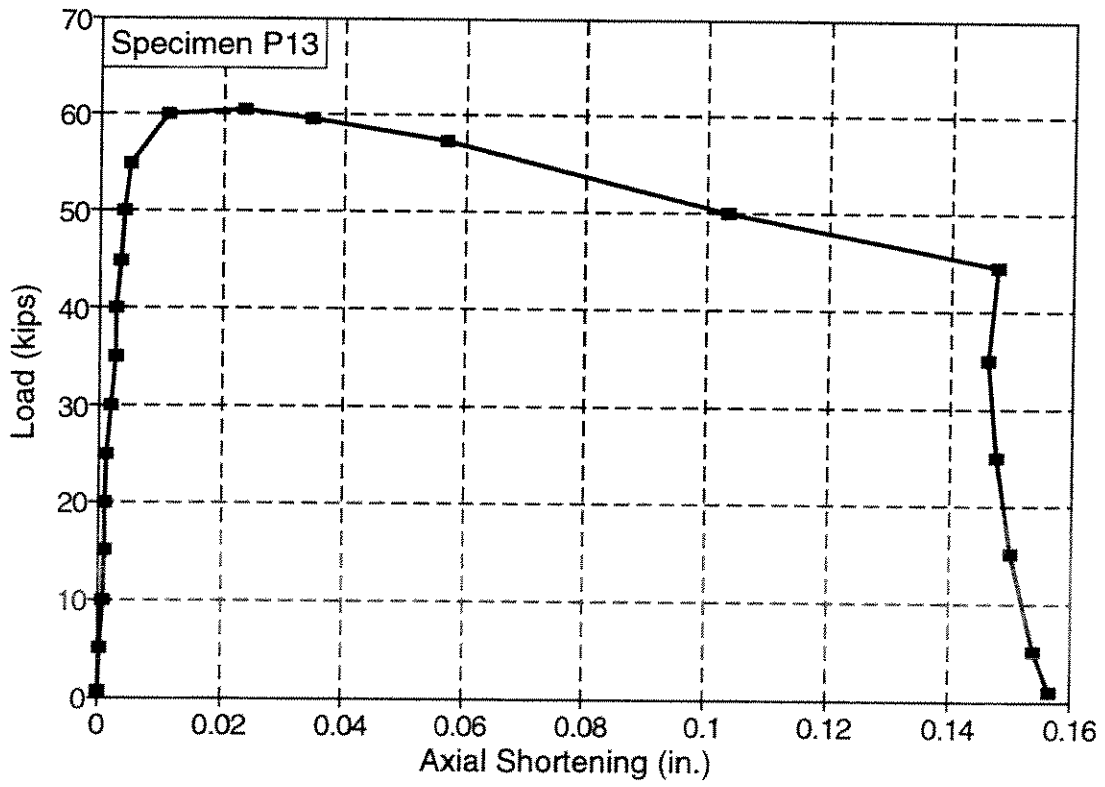


Figure 11-18 Load-Shortening for Specimen P13

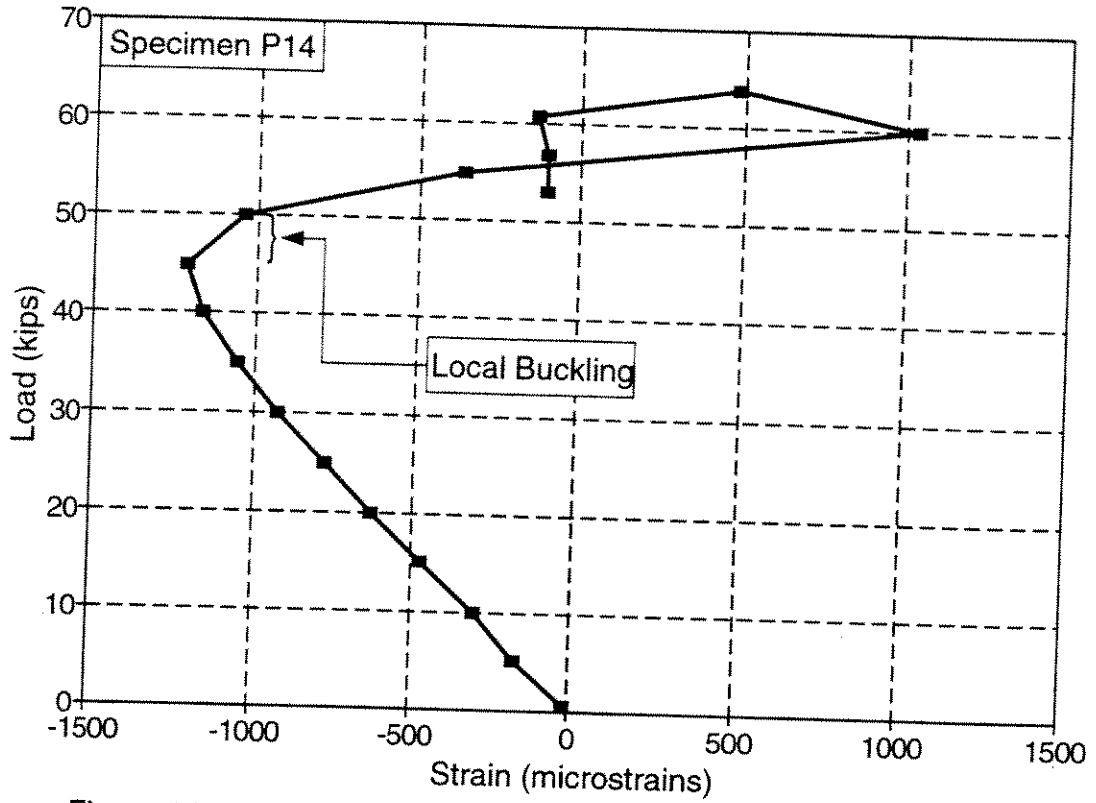


Figure 11-19 Strain in Corrosion Patch (Gage 7) for Specimen P14

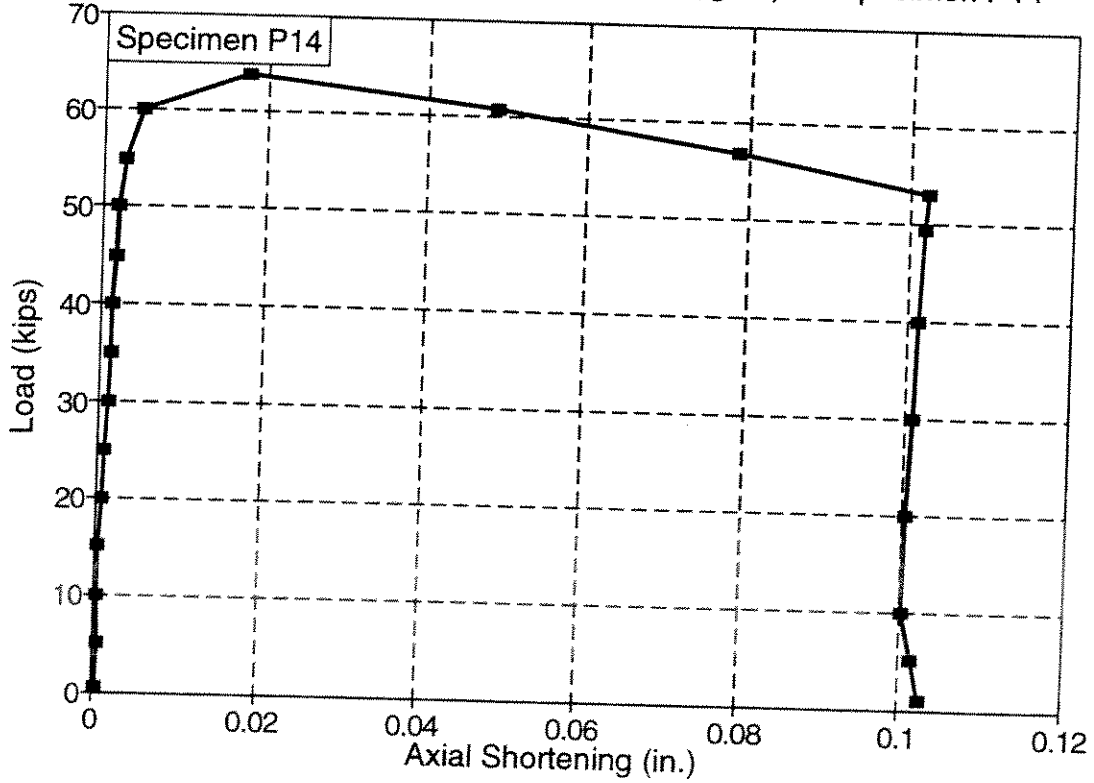


Figure 11-20 Load-Shortening for Specimen P14

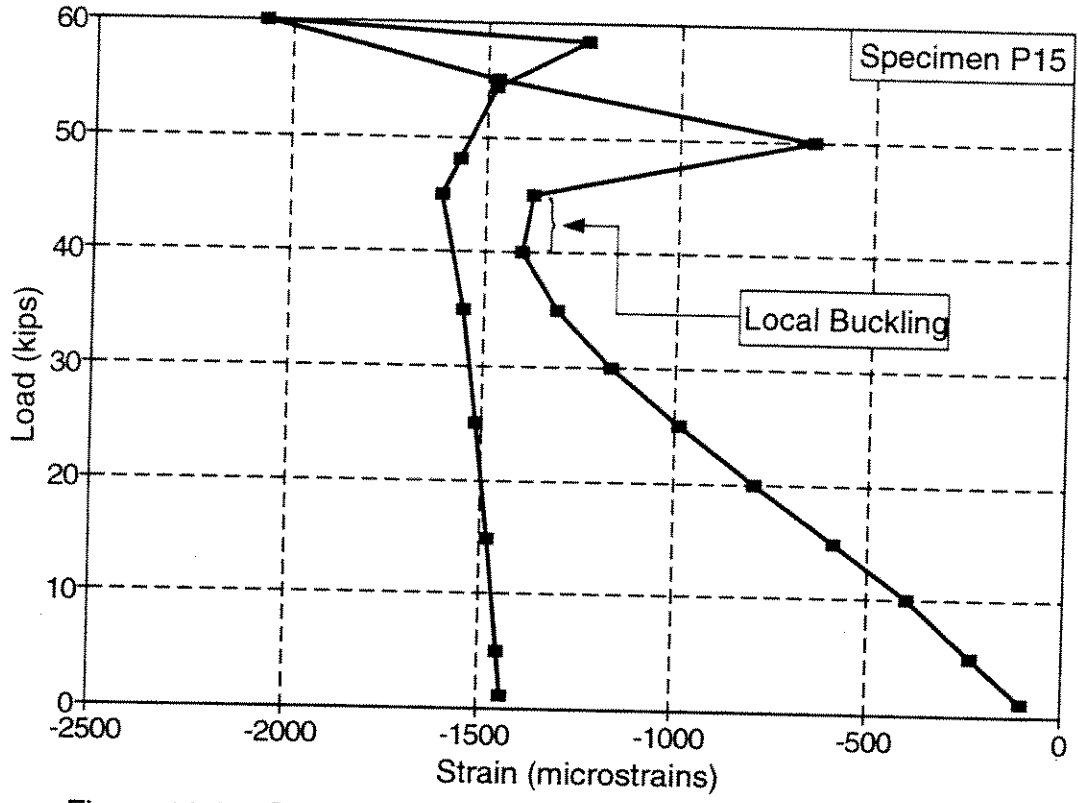


Figure 11-21 Strain in Corrosion Patch (Gage 7) for Specimen P15

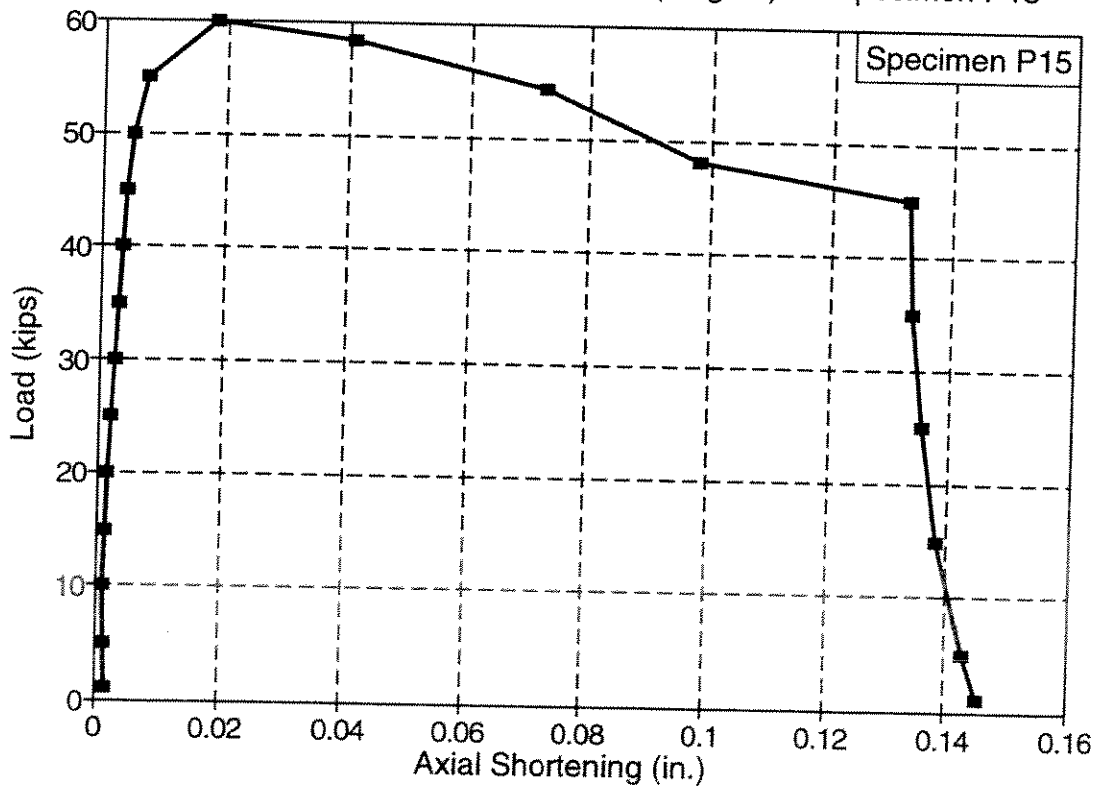


Figure 11-22 Load-Shortening for Specimen P15

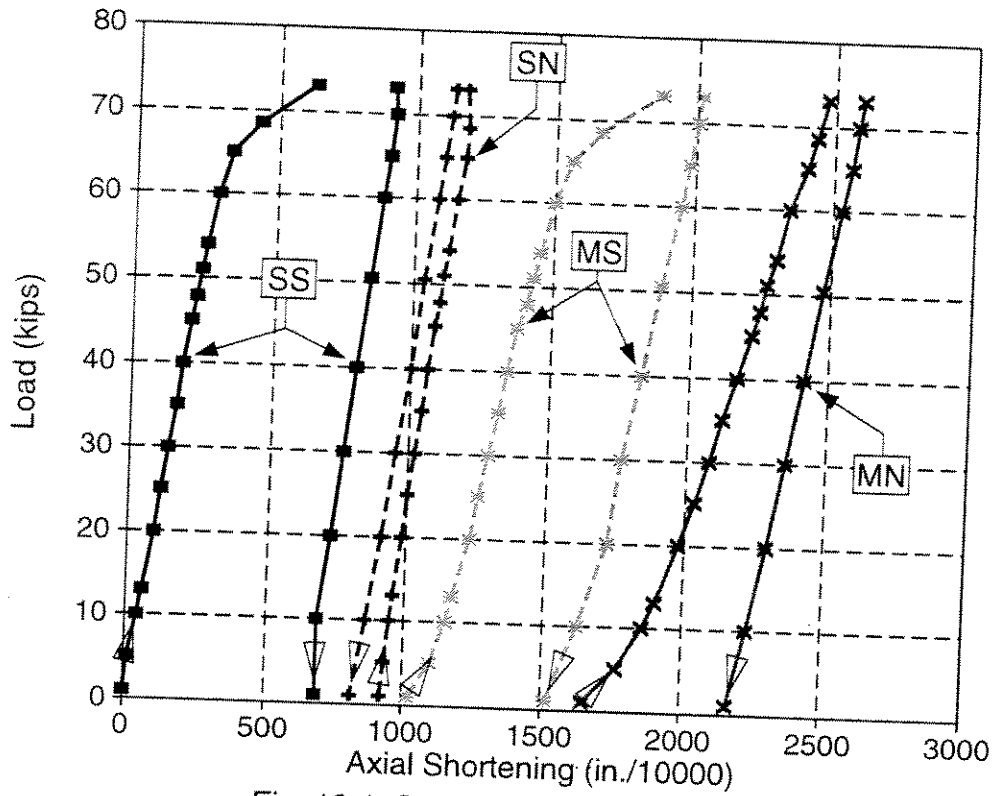


Fig. 12-1 Specimen P6 -- Dial Gages

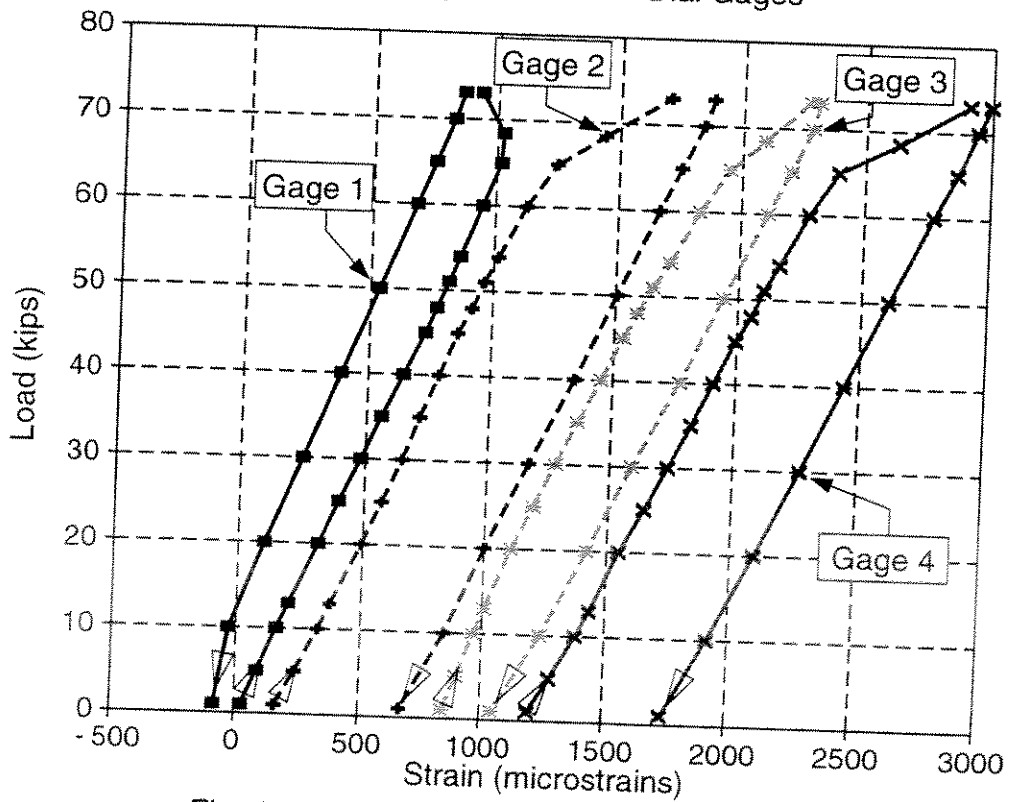


Fig. 12-2 Specimen P6 -- Strain Gages 1 to 4

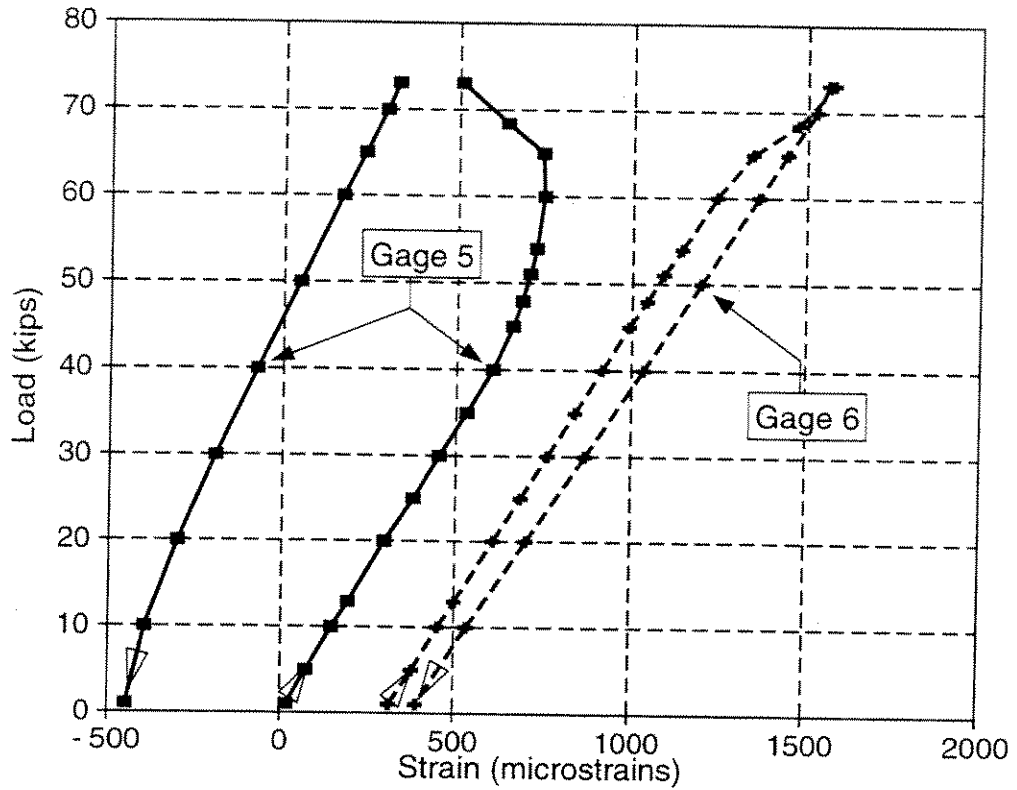


Fig. 12-3 Specimen P6 -- Strain Gages 5 and 6

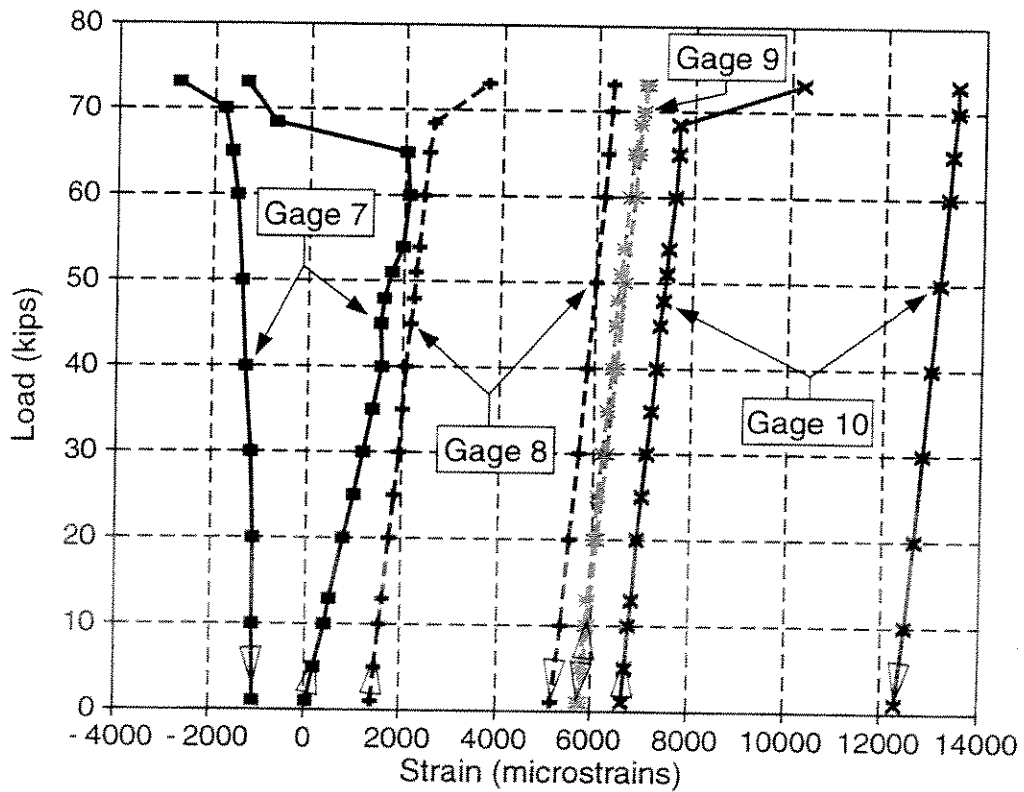


Fig. 12-4 Specimen P6 -- Strain Gages 7 to 10

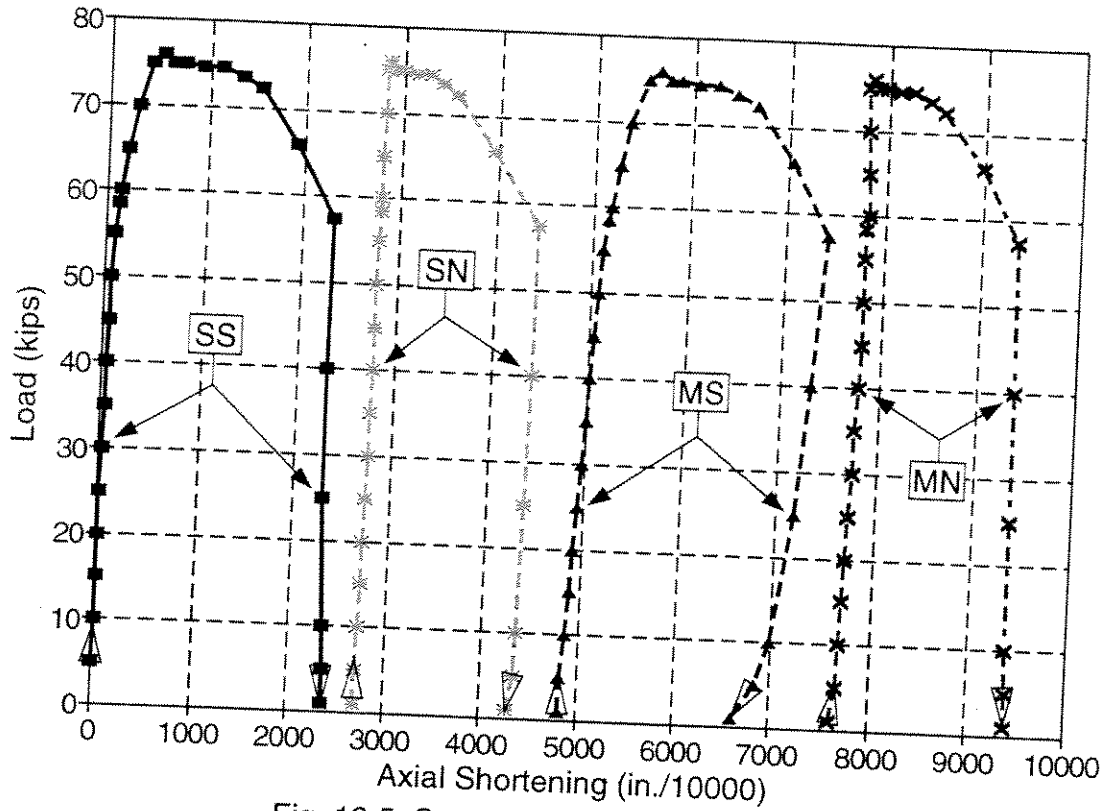


Fig. 12-5 Specimen P10 -- Dial Gages

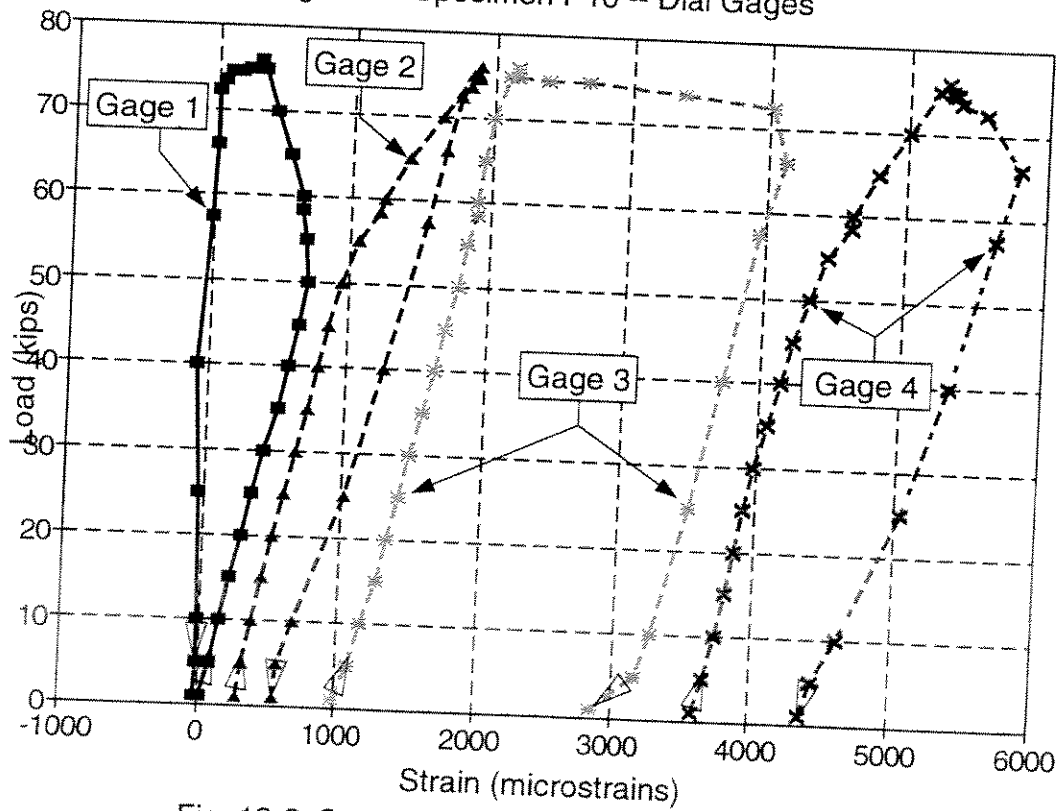


Fig. 12-6 Specimen P10 -- Strain Gages 1 to 4

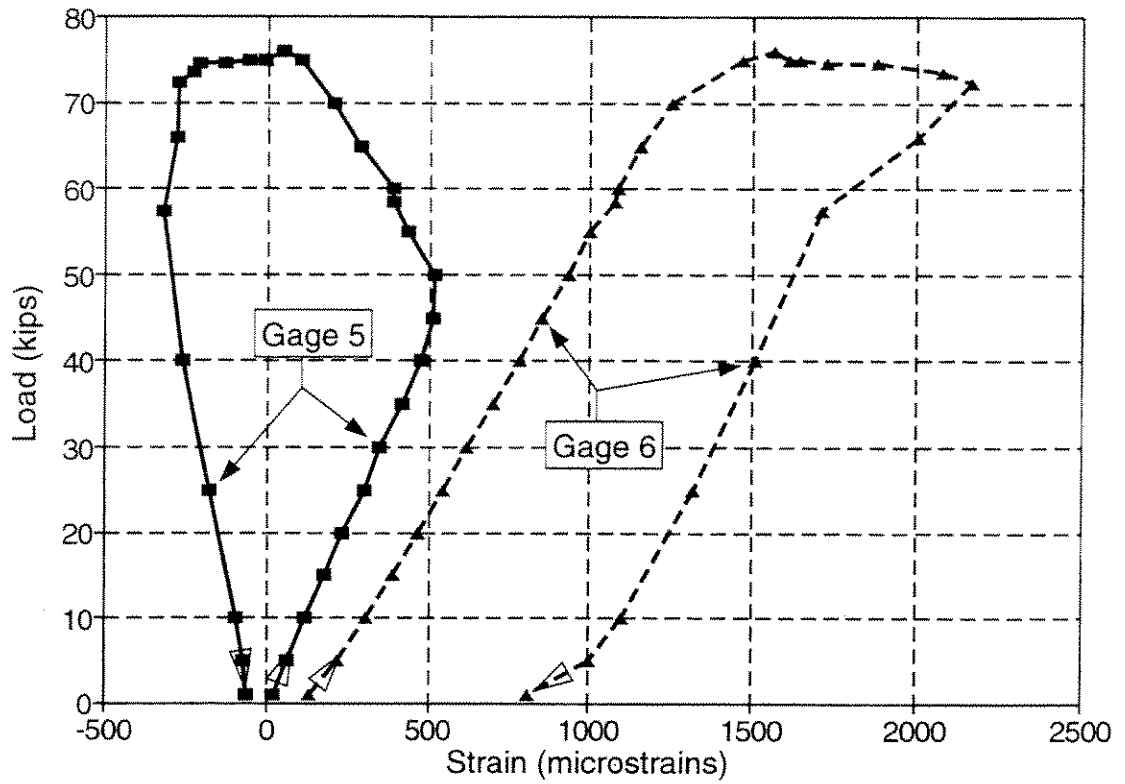


Fig. 12-7 Specimen P10 -- Strain Gages 5 and 6

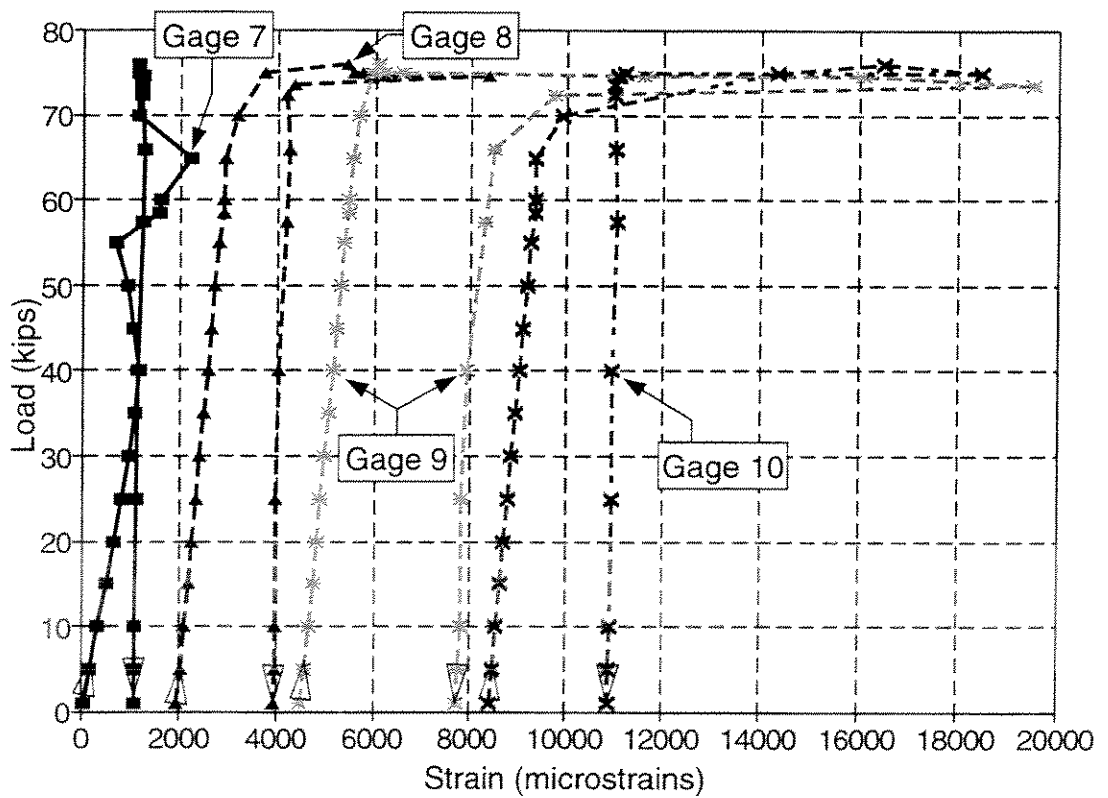


Fig. 12-8 Specimen P10 -- Strain Gages 7 to 10

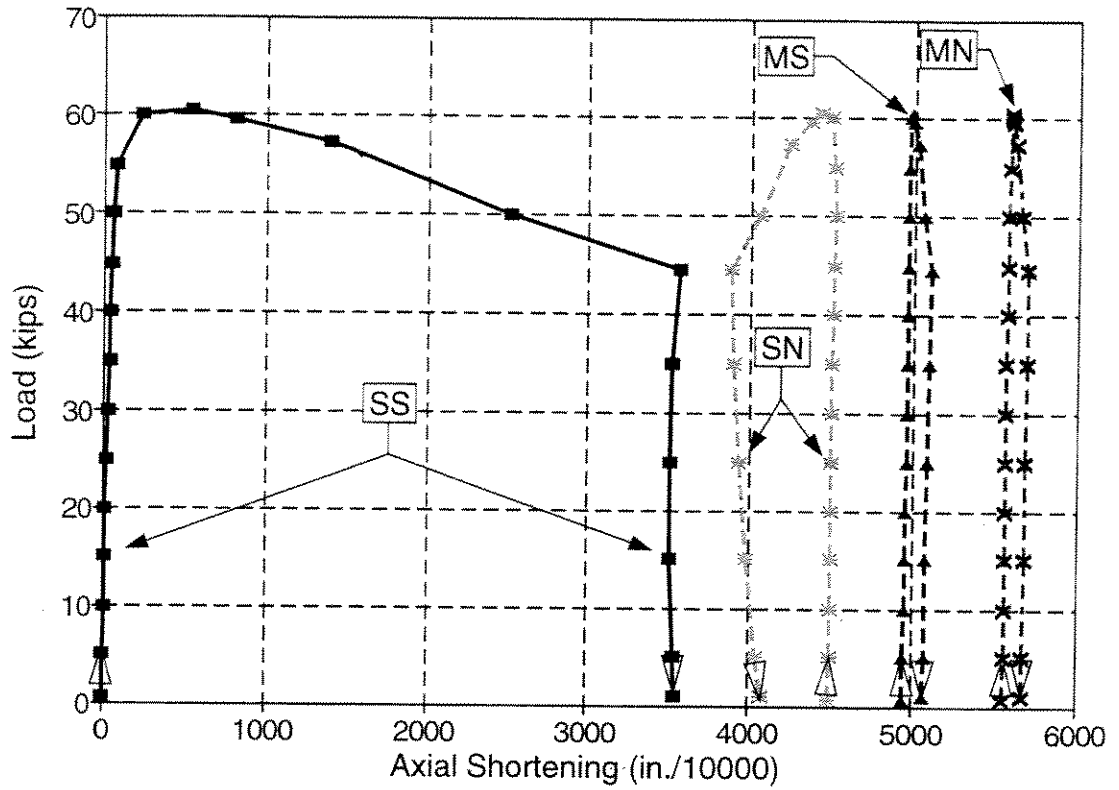


Fig. 12-9 Specimen P13 -- Dial Gages

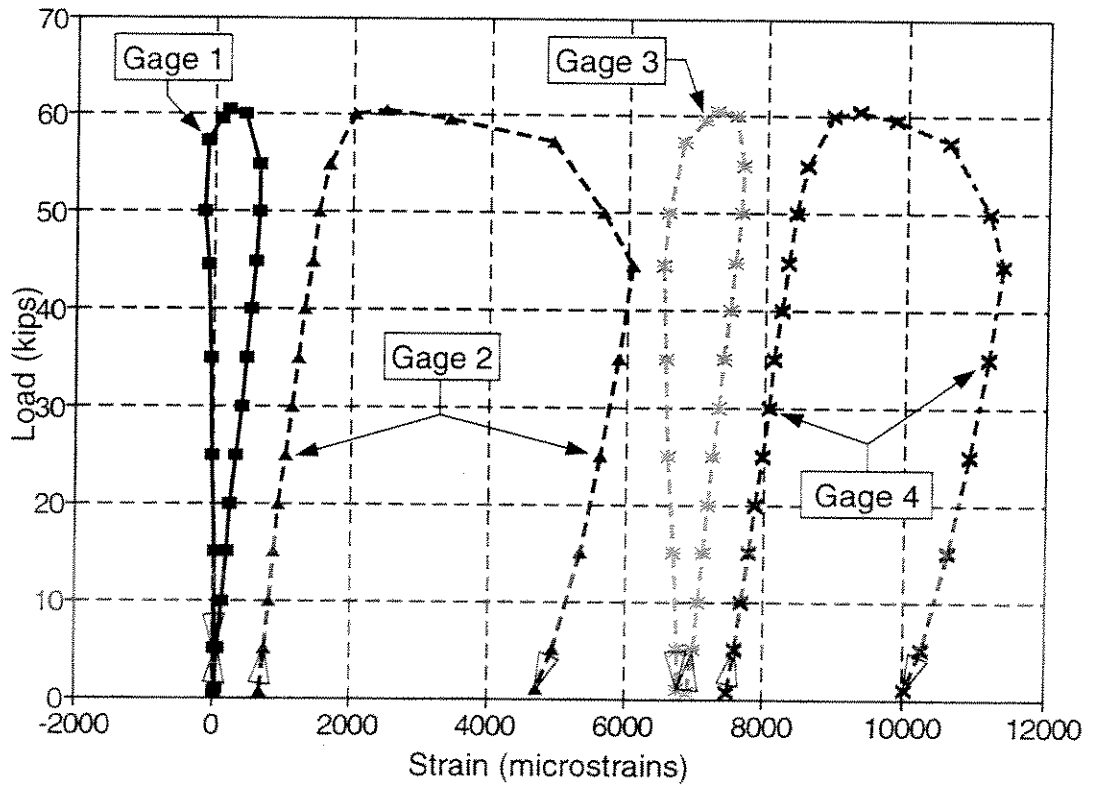


Fig. 12-10 Specimen P13 -- Strain Gages 1 to 4

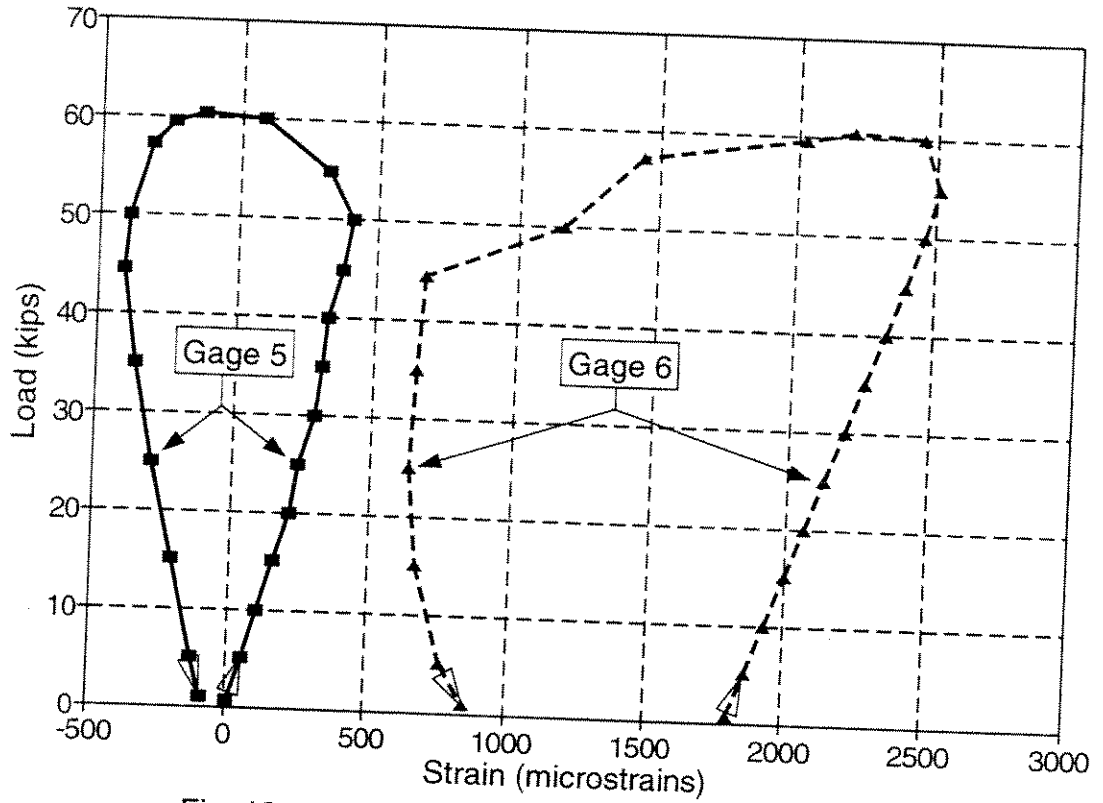


Fig. 12-11 Specimen P13 -- Strain Gages 5 and 6

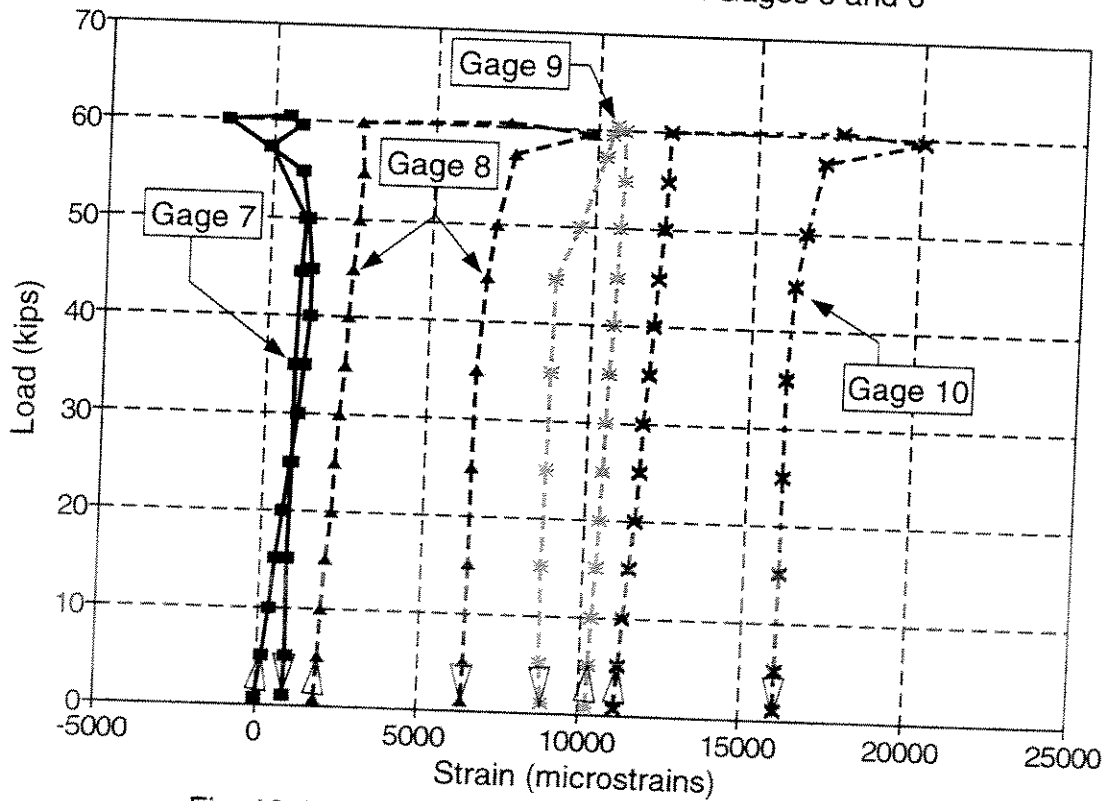


Fig. 12-12 Specimen P13 -- Strain Gages 7 to 10

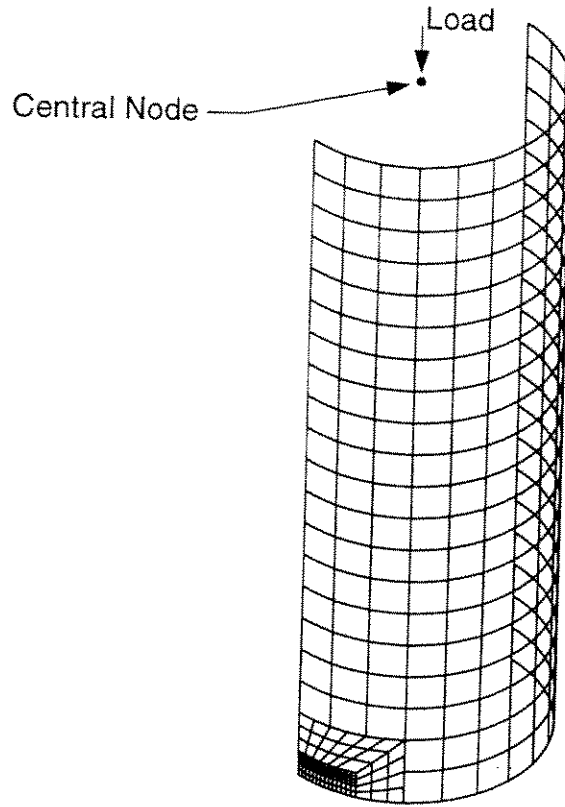


Fig. 13-1 Typical FE Model for Specimens P5 to P9

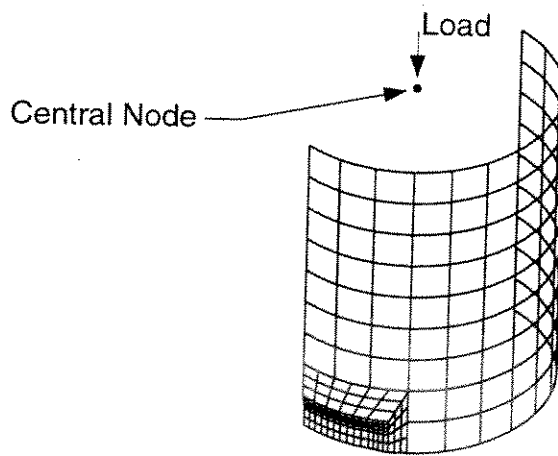


Fig. 13-2 Typical FE Model for Specimens P10 to P15

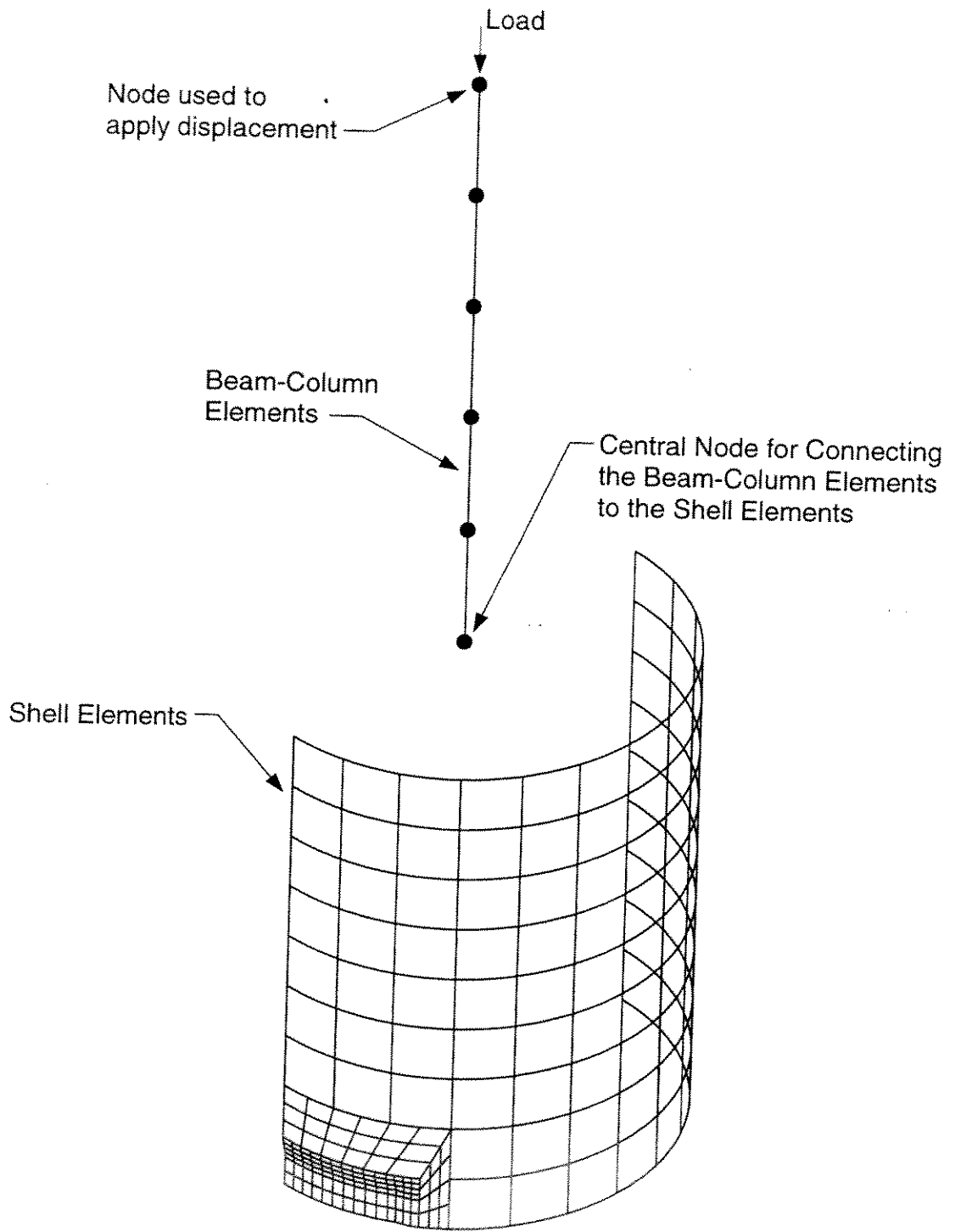


Fig. 13-3 Typical FE Model for a Combined Specimen

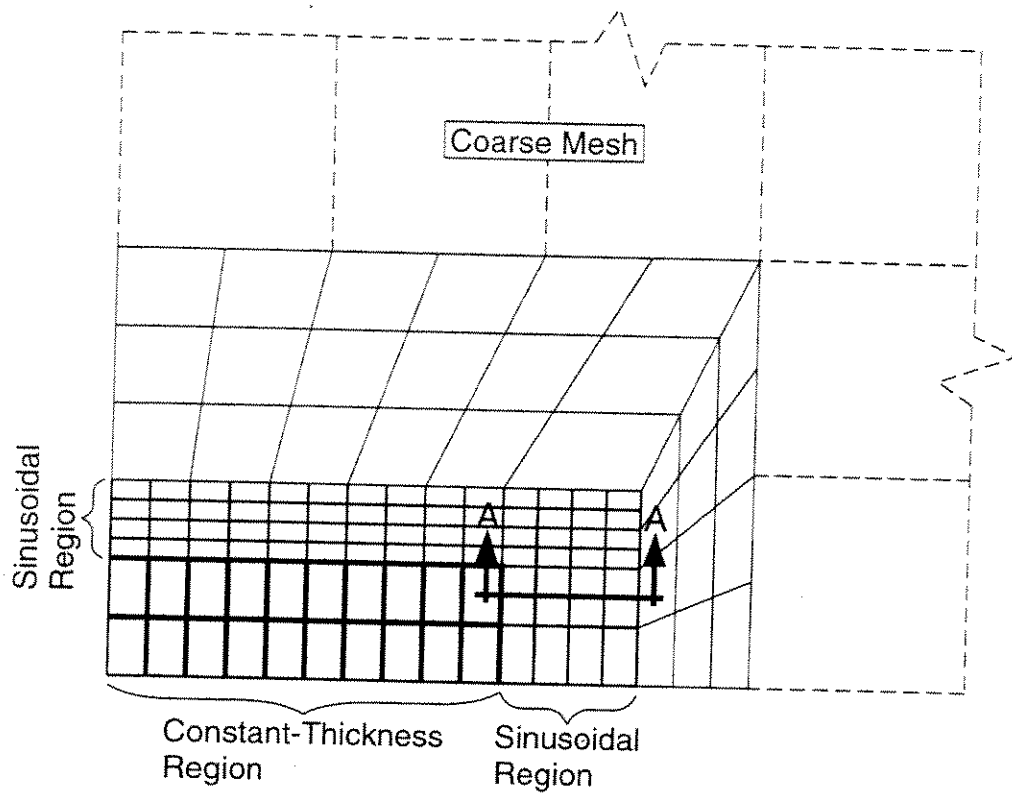


Fig. 13-4 Unfolded View of Corrosion Patch Mesh

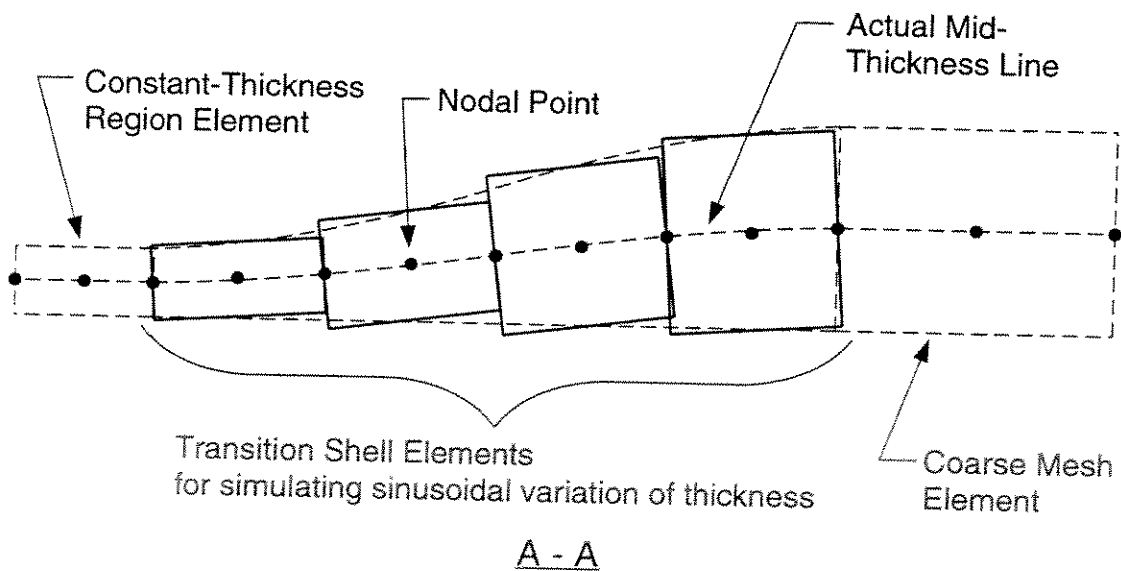


Fig. 13-5 Modeling of the Sinusoidal Transition Region

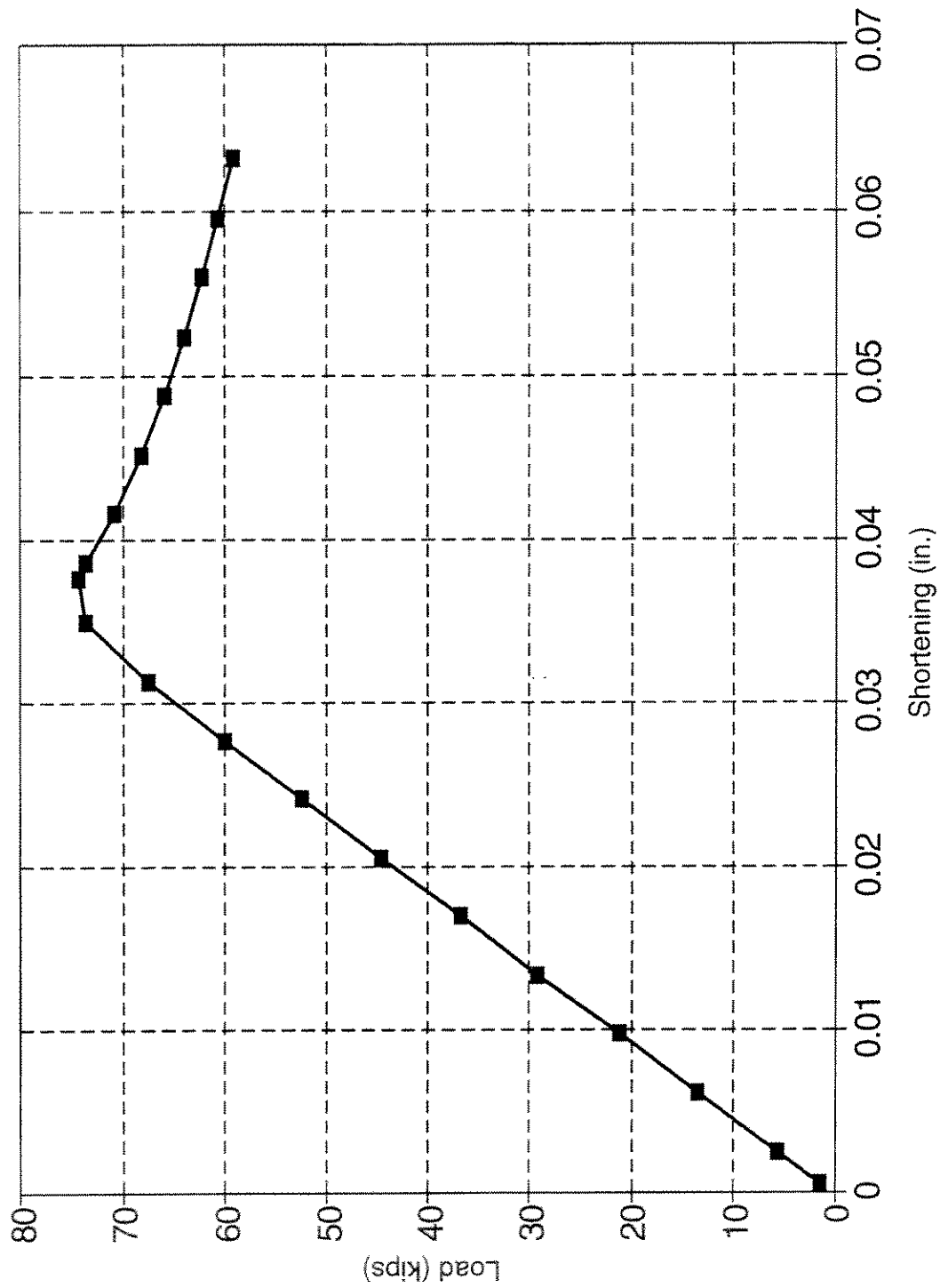
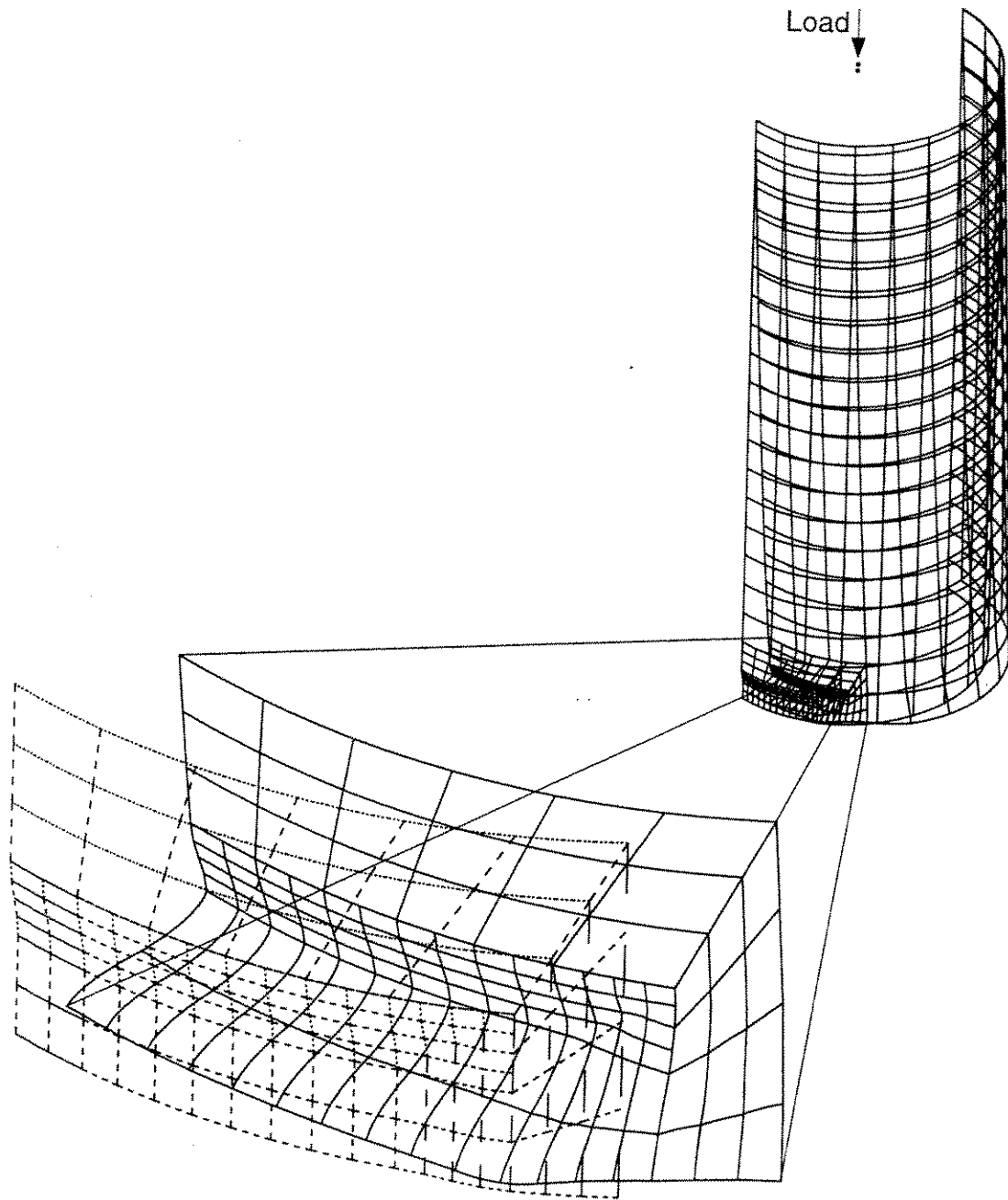


Fig. 13-6 Typical Load-Shortening Curve from FE Analysis (Specimen P5)



Dotted/Dashed Lines -- Original
Solid Lines -- Deformed

Fig. 13-7 Final Deformed Configuration for a Typical Pin-Ended Specimen
(Specimen P9)

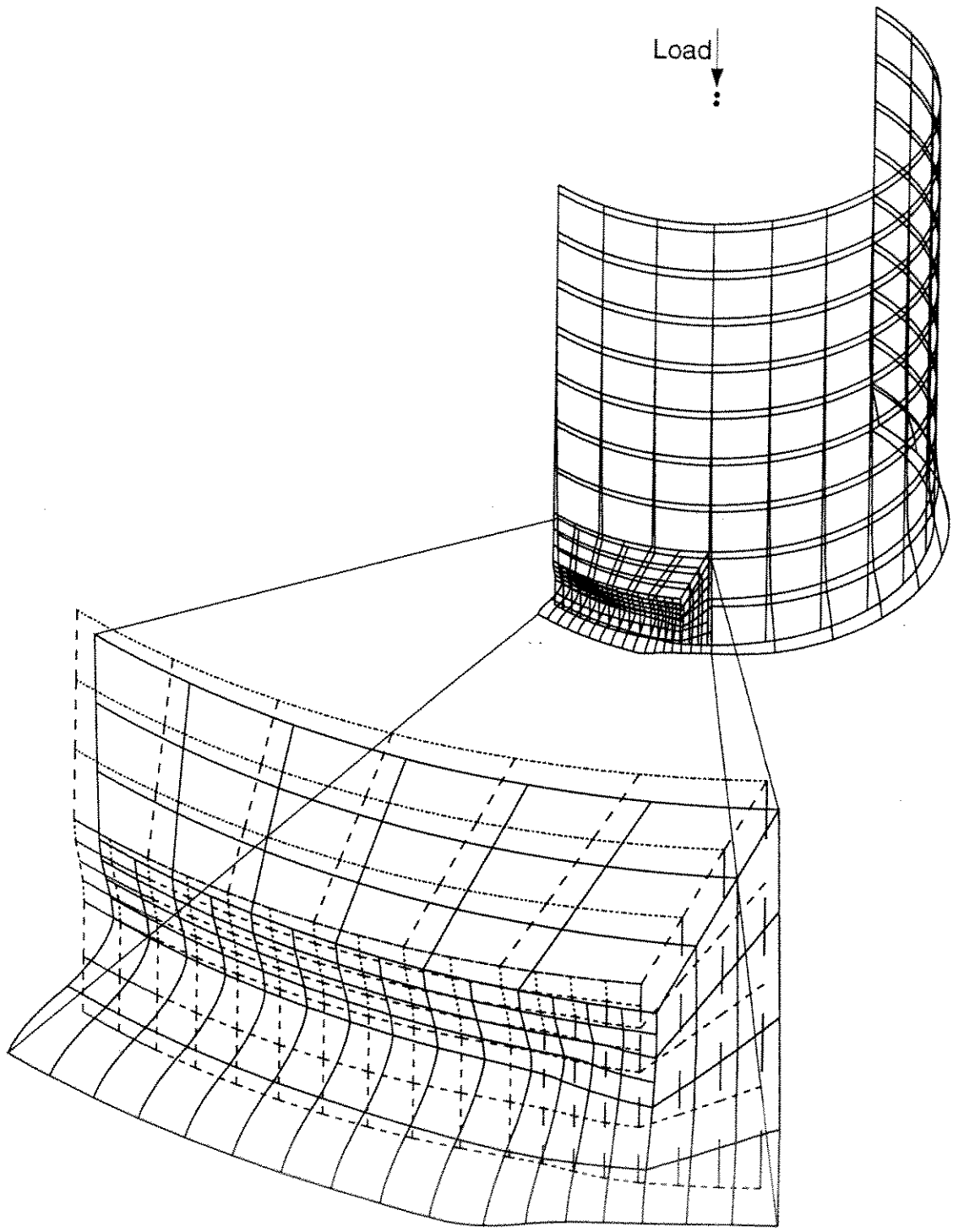


Fig. 13-8 Final Deformed Configuration for a Typical Fixed-End Specimen (Specimen P10)

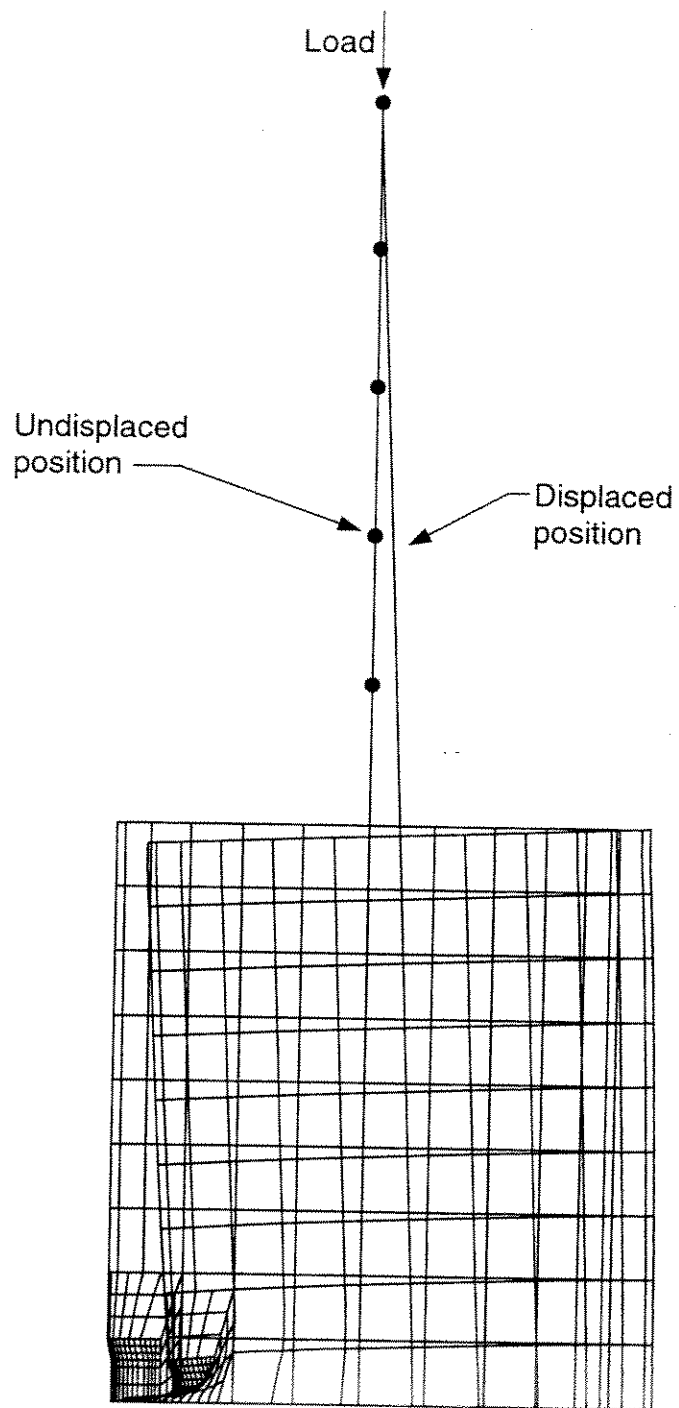


Fig. 13-9 Deformation Configuration of a Combined Model
(Specimen P13)

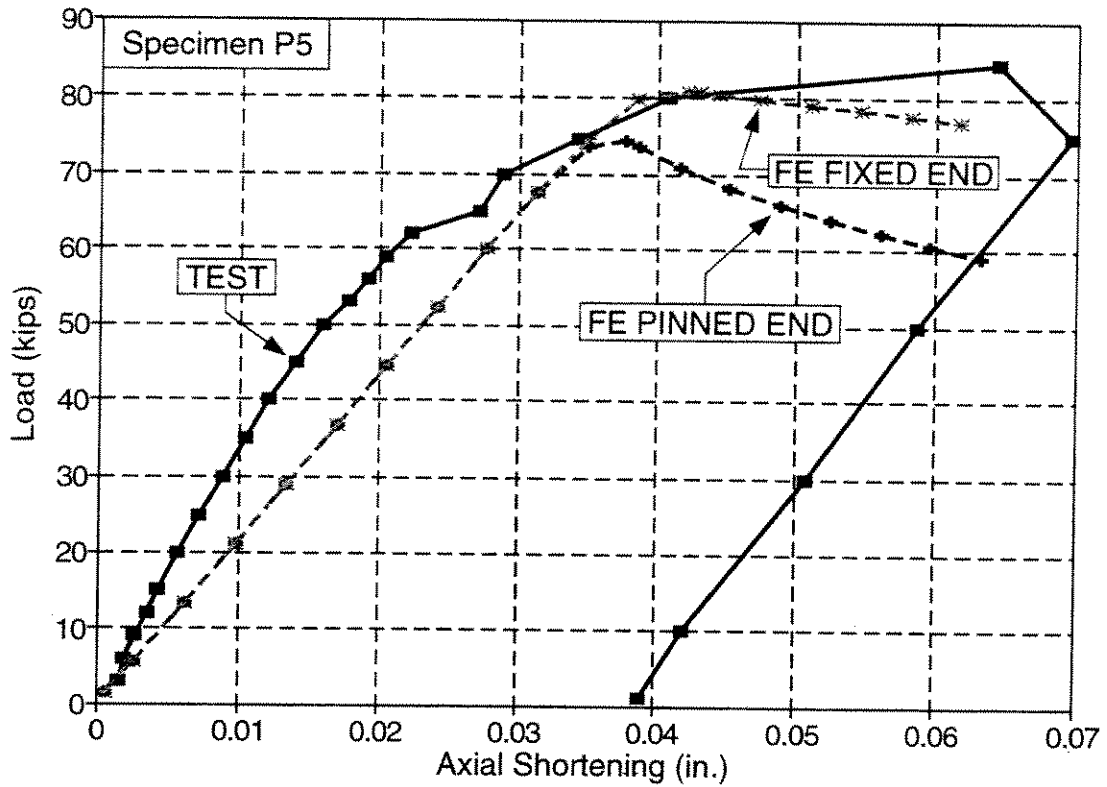


Figure 13-10 Specimen P5 -- Load-Shortening from Test and FE Analysis

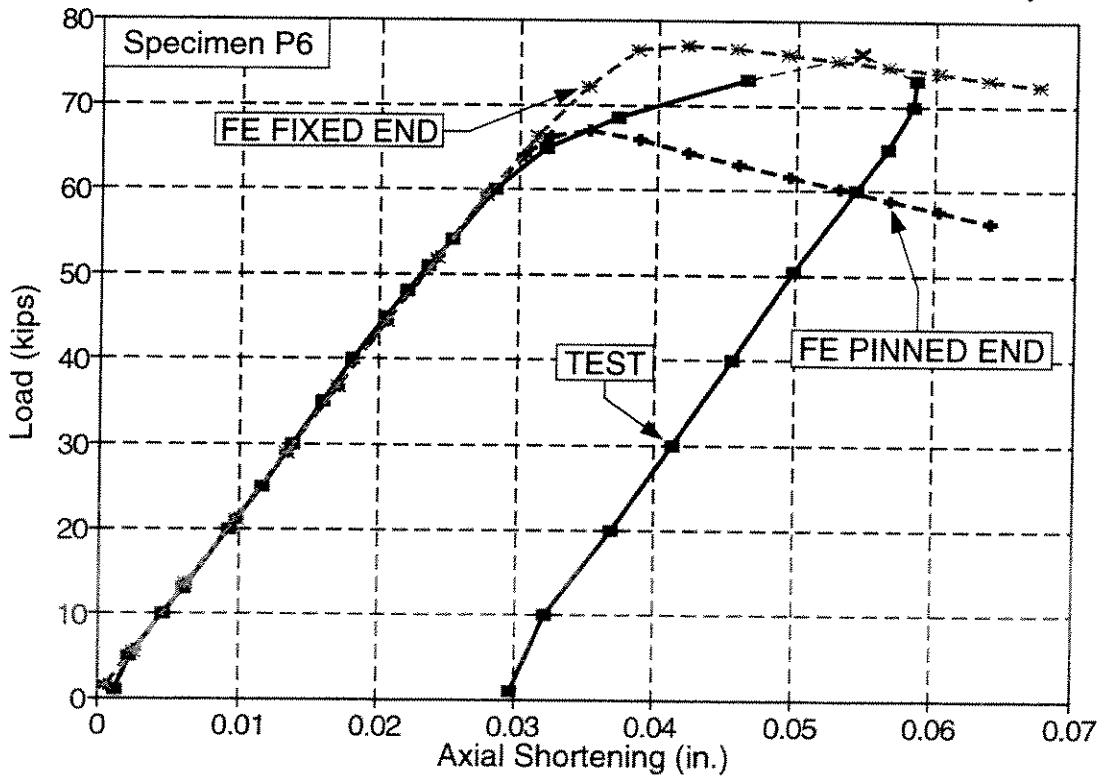


Figure 13-11 Specimen P6 -- Load-Shortening from Test and FE Analysis

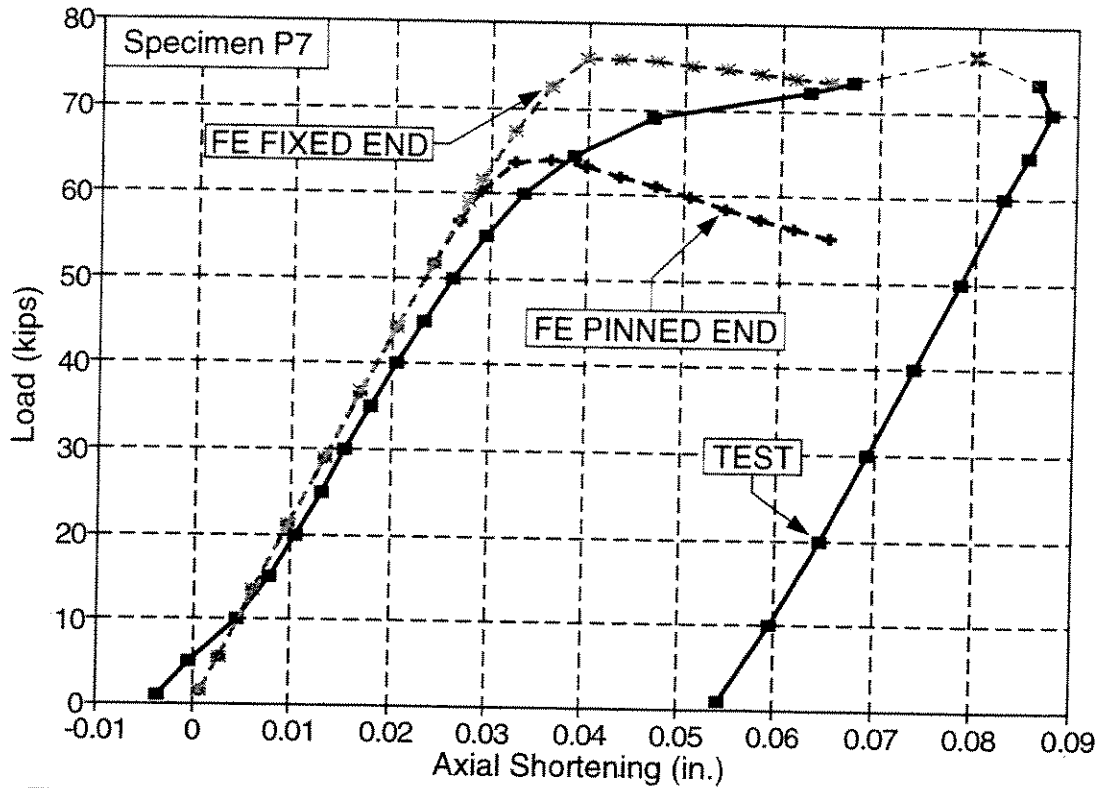


Figure 13-12 Specimen P7 -- Load-Shortening from Test and FE Analysis

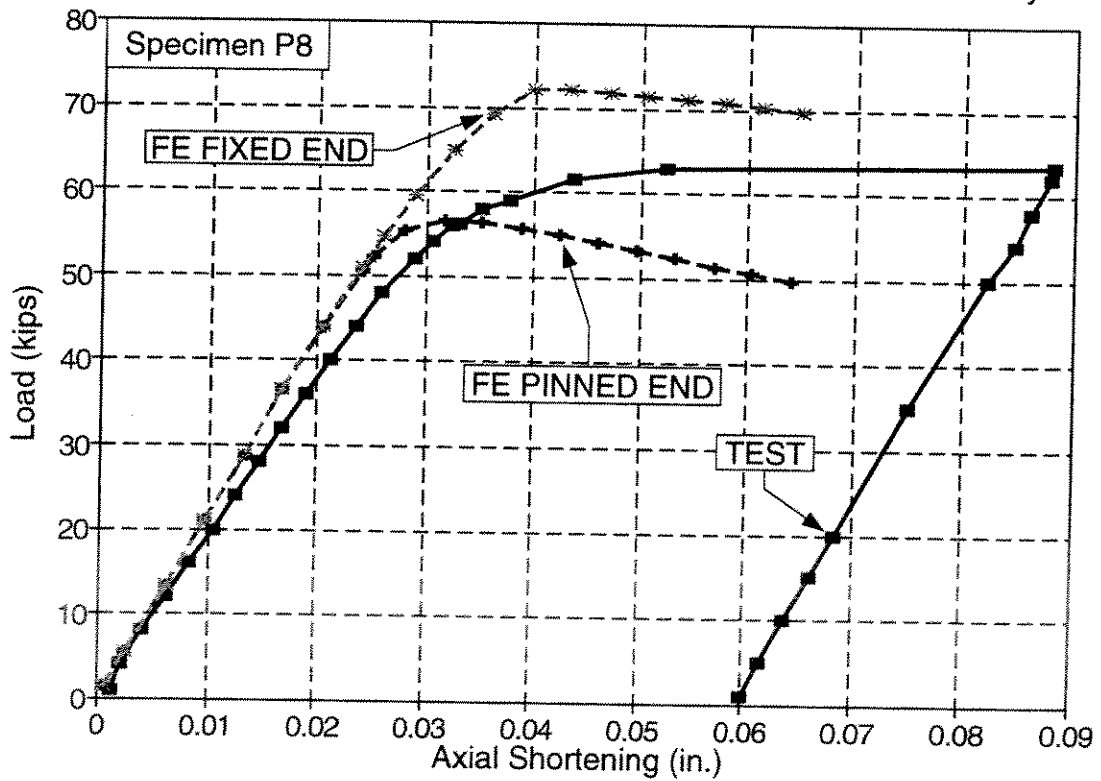


Figure 13-13 Specimen P8 -- Load-Shortening from Test and FE Analysis

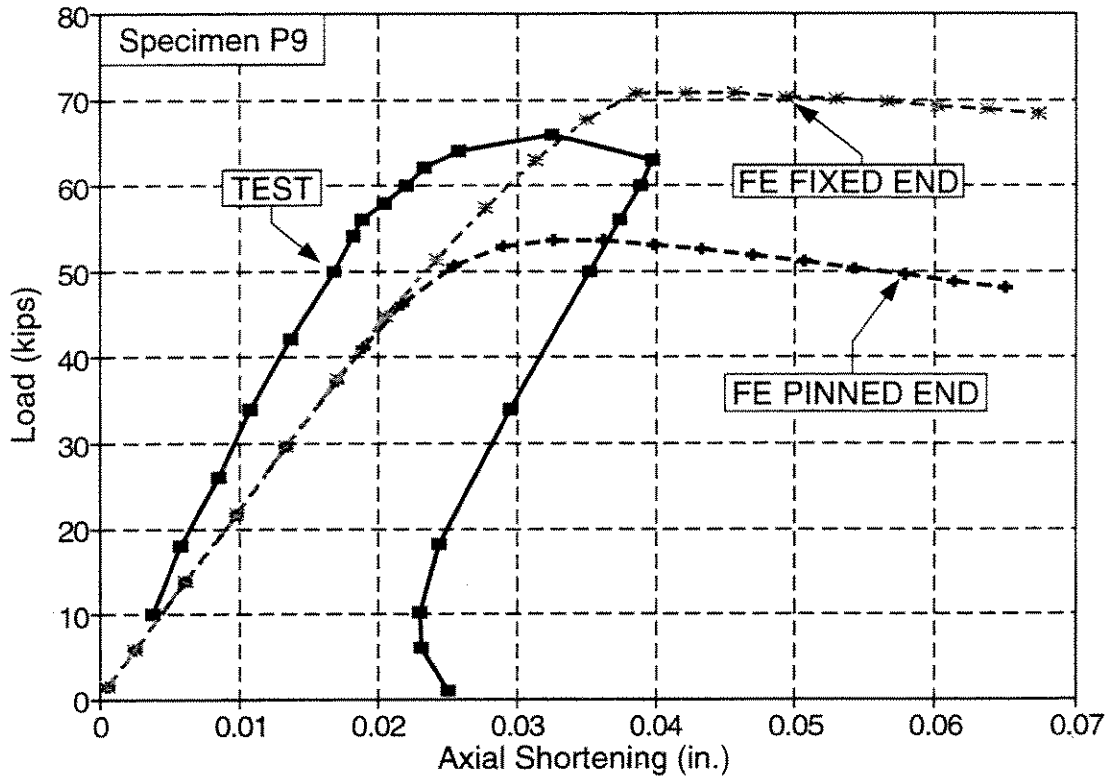


Figure 13-14 Specimen P9 -- Load-Shortening from Test and FE Analysis

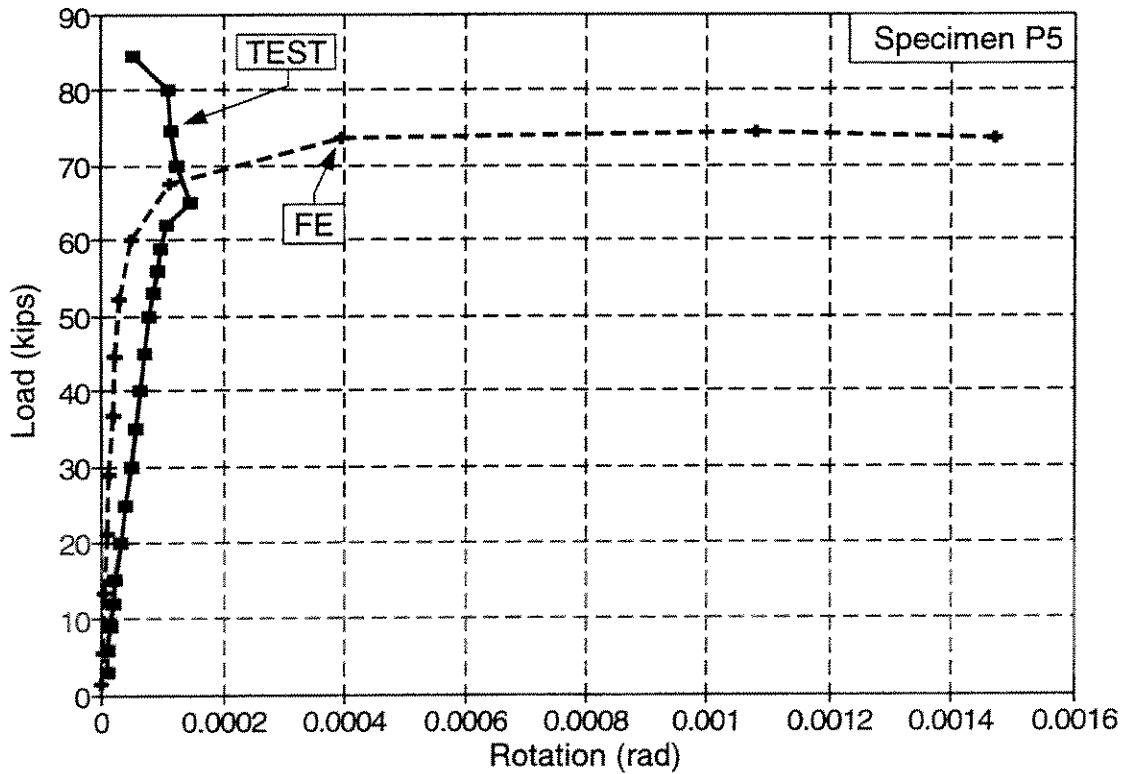


Figure 13-15 Specimen P5 -- End Rotation from Test and FE Analysis

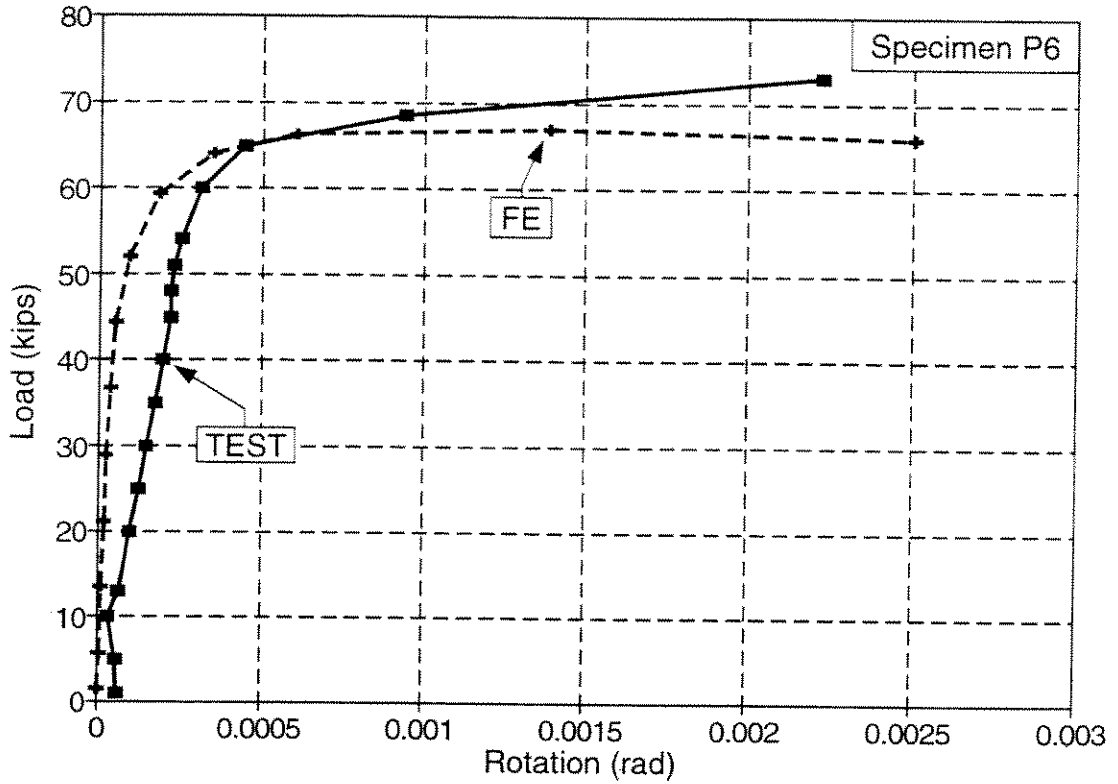


Fig. 13-16 Specimen P6 -- End Rotation from Test and FE Analysis

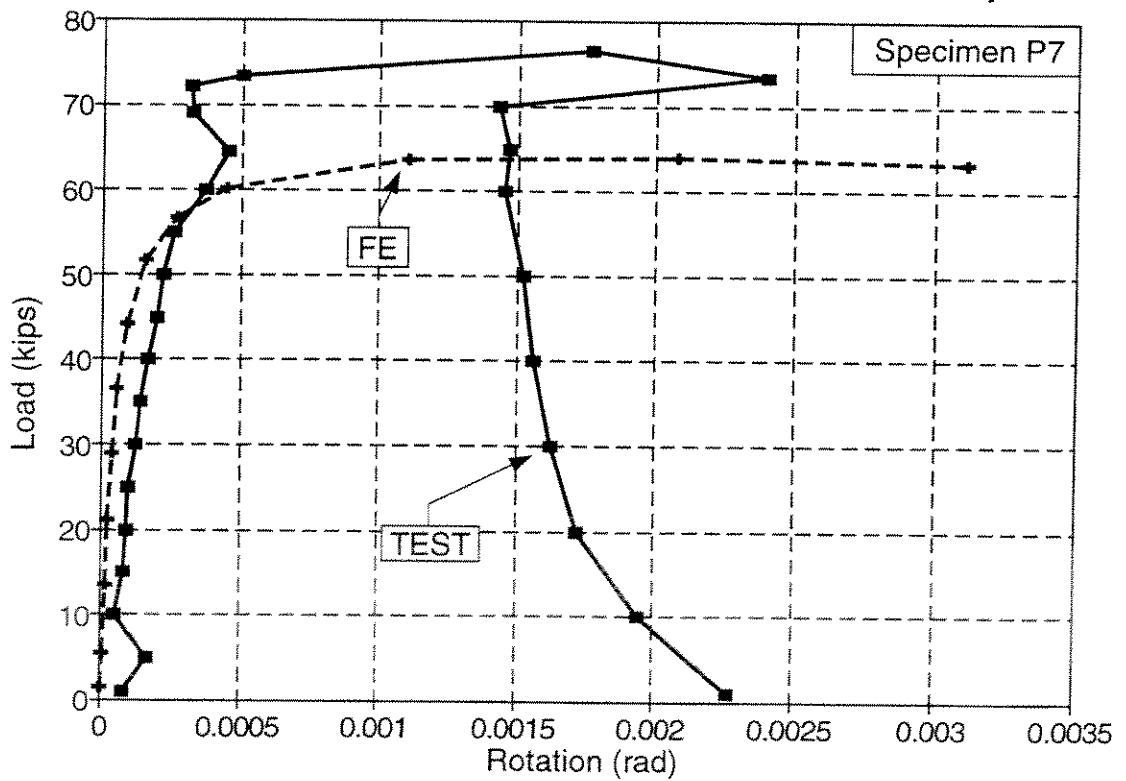


Fig. 13-17 Specimen P7 -- End Rotation from Test and FE Analysis

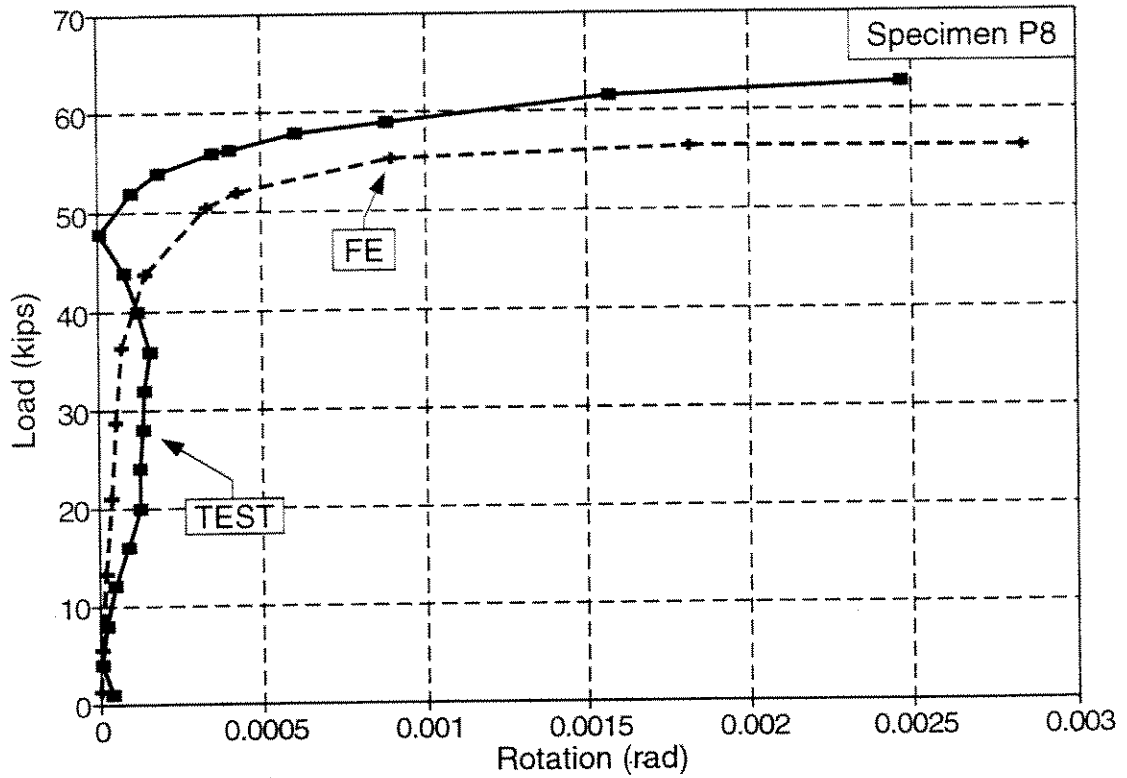


Fig. 13-18 Specimen P8 -- End Rotation from Test and FE Analysis

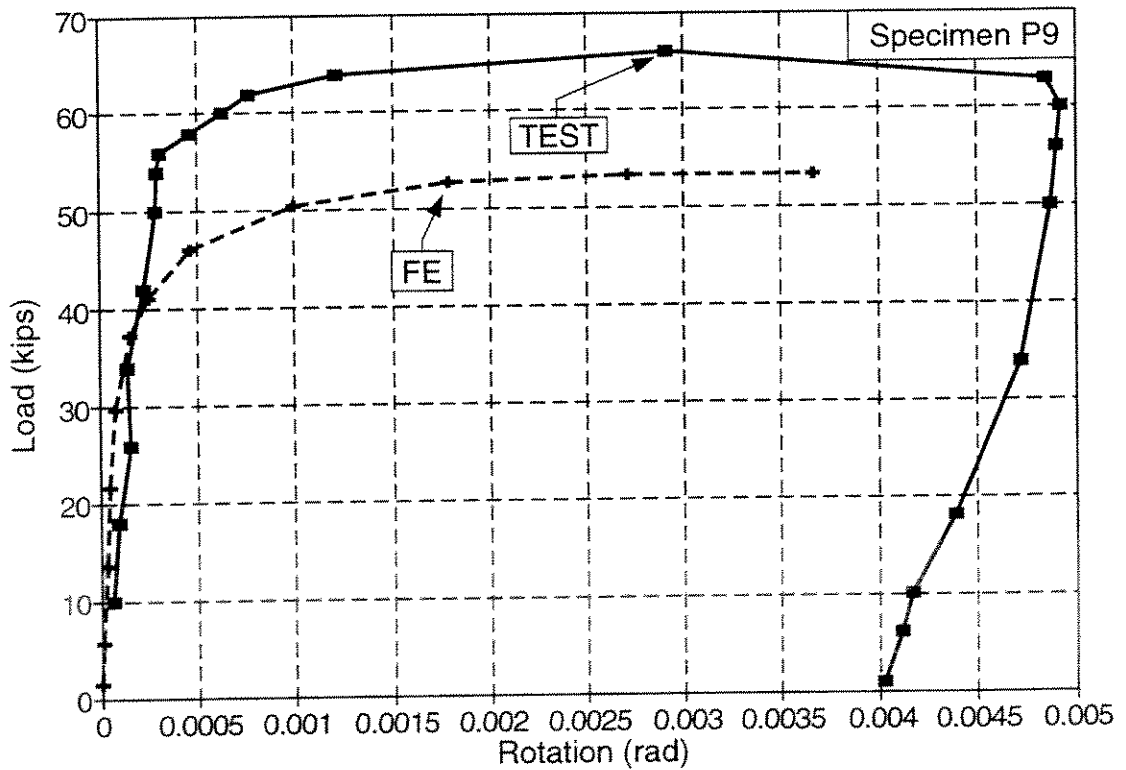


Fig. 13-19 Specimen P9 -- End Rotation from Test and FE Analysis

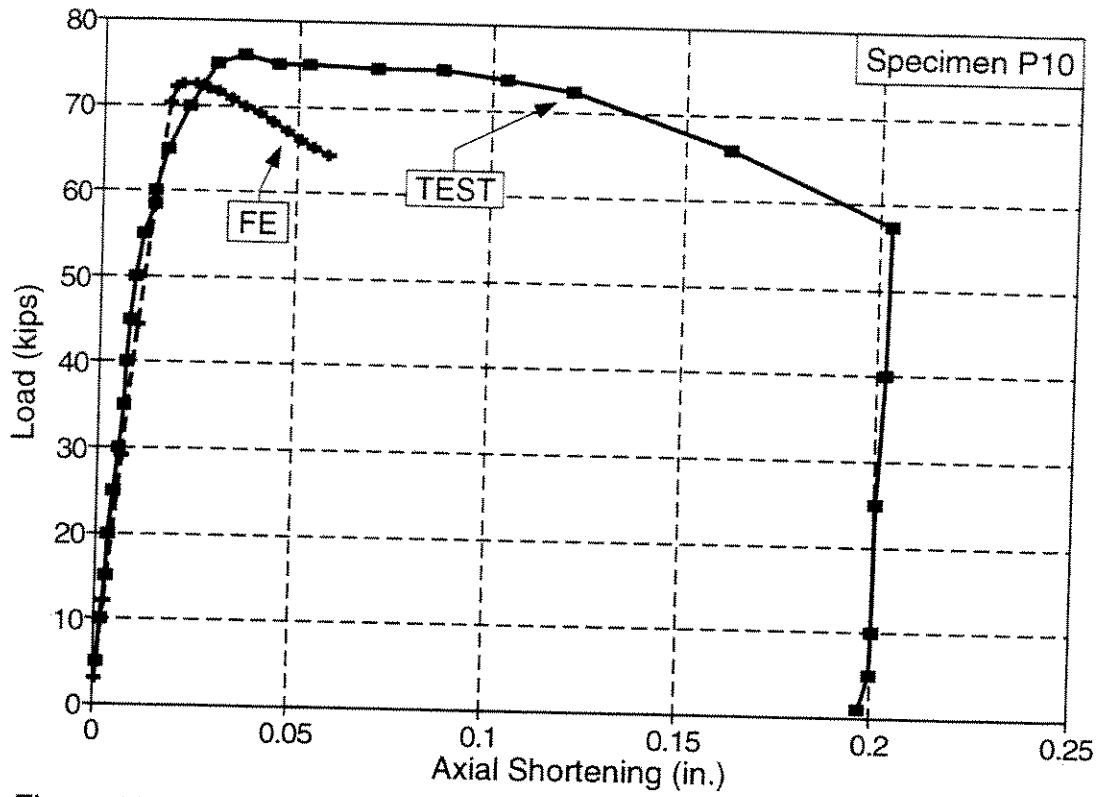


Figure 13-20 Specimen P10 -- Load-Shortening from Test and FE Analysis

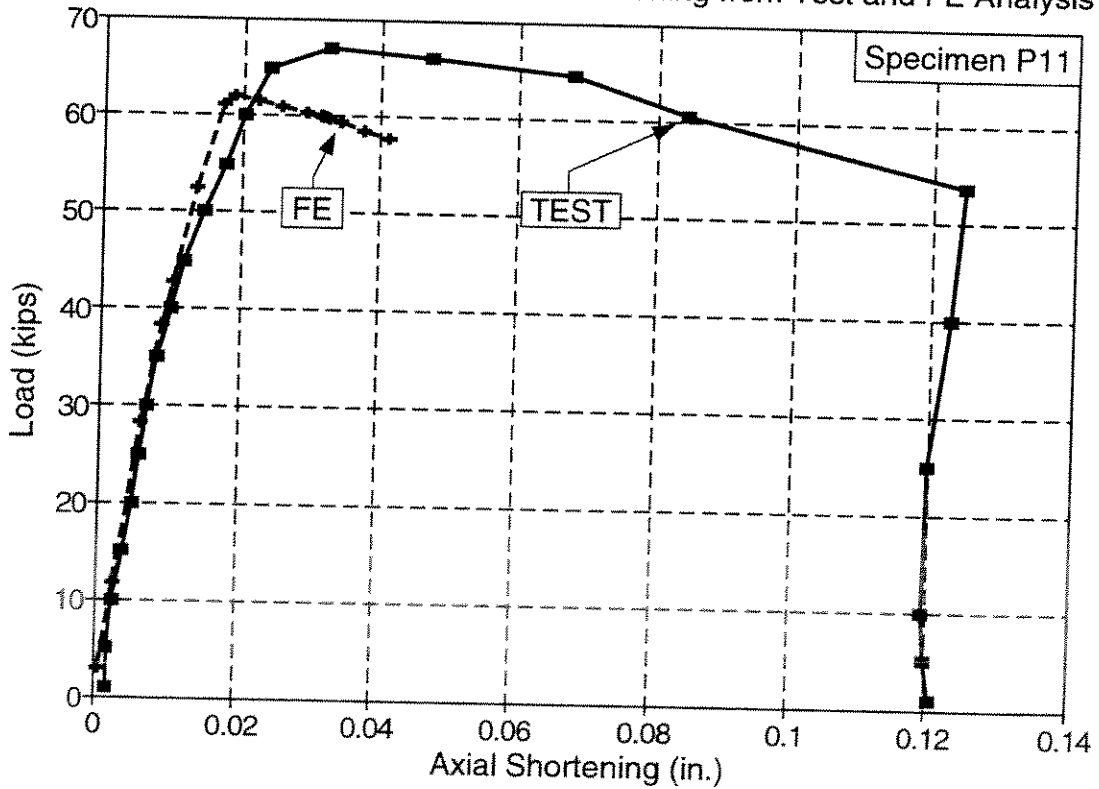


Figure 13-21 Specimen P11 -- Load-Shortening from Test and FE Analysis

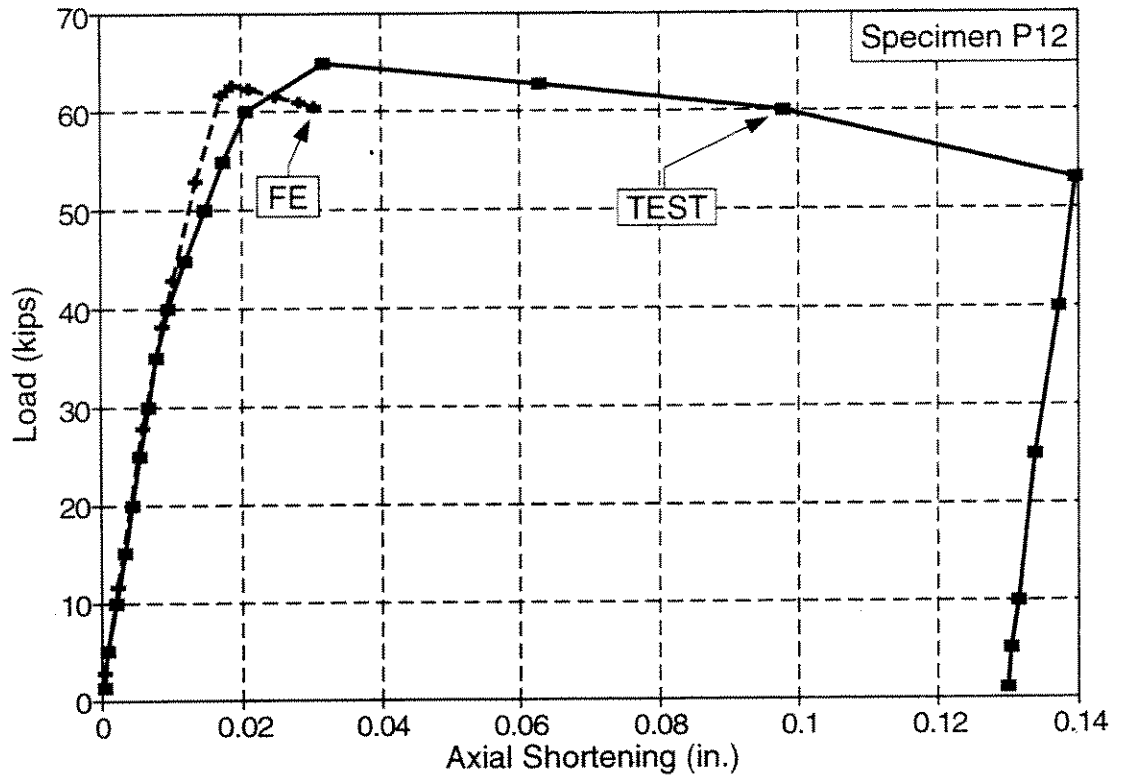


Figure 13-22 Specimen P12 -- Load-Shortening from Test and FE Analysis

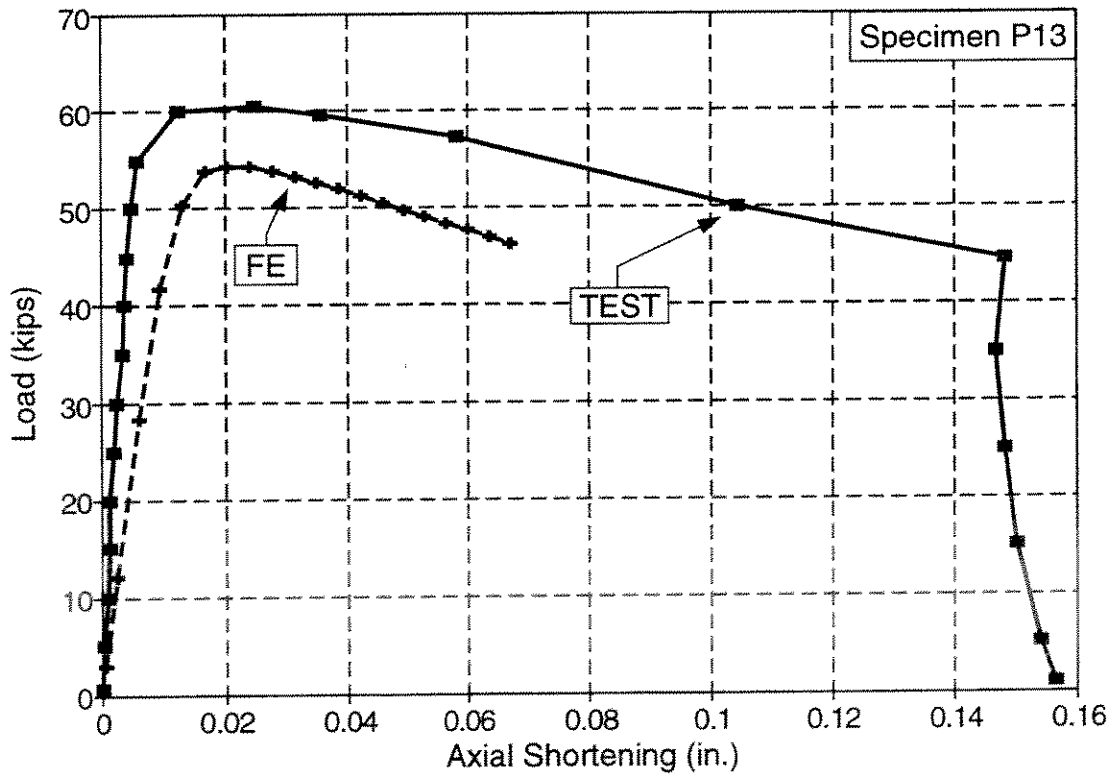


Figure 13-23 Specimen P13 -- Load-Shortening from Test and FE Analysis

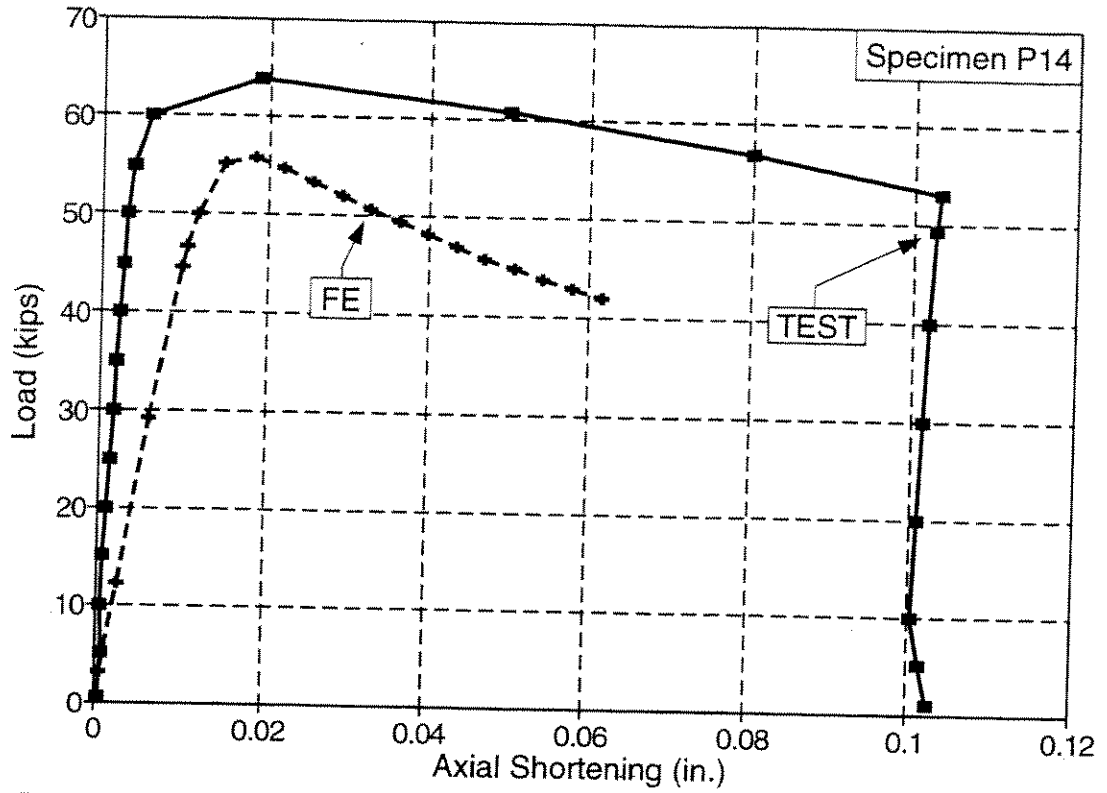


Figure 13-24 Specimen P14 -- Load-Shortening from Test and FE Analysis

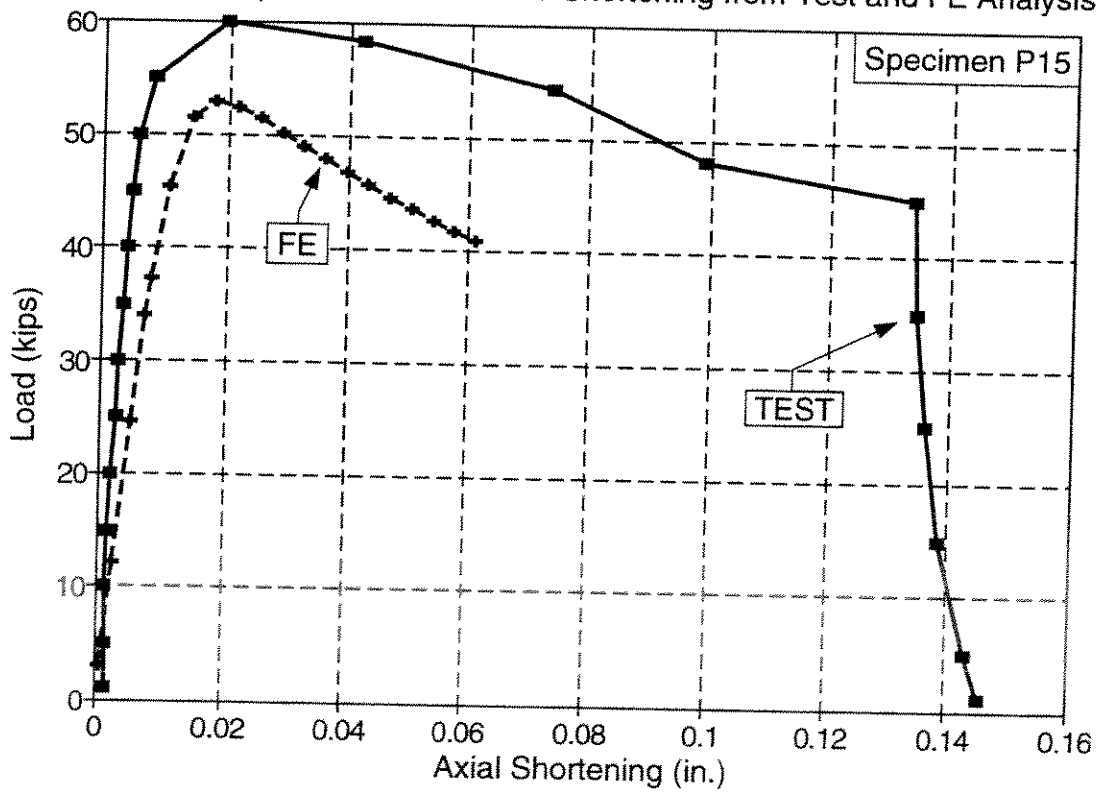


Figure 13-25 Specimen P15 -- Load-Shortening from Test and FE Analysis

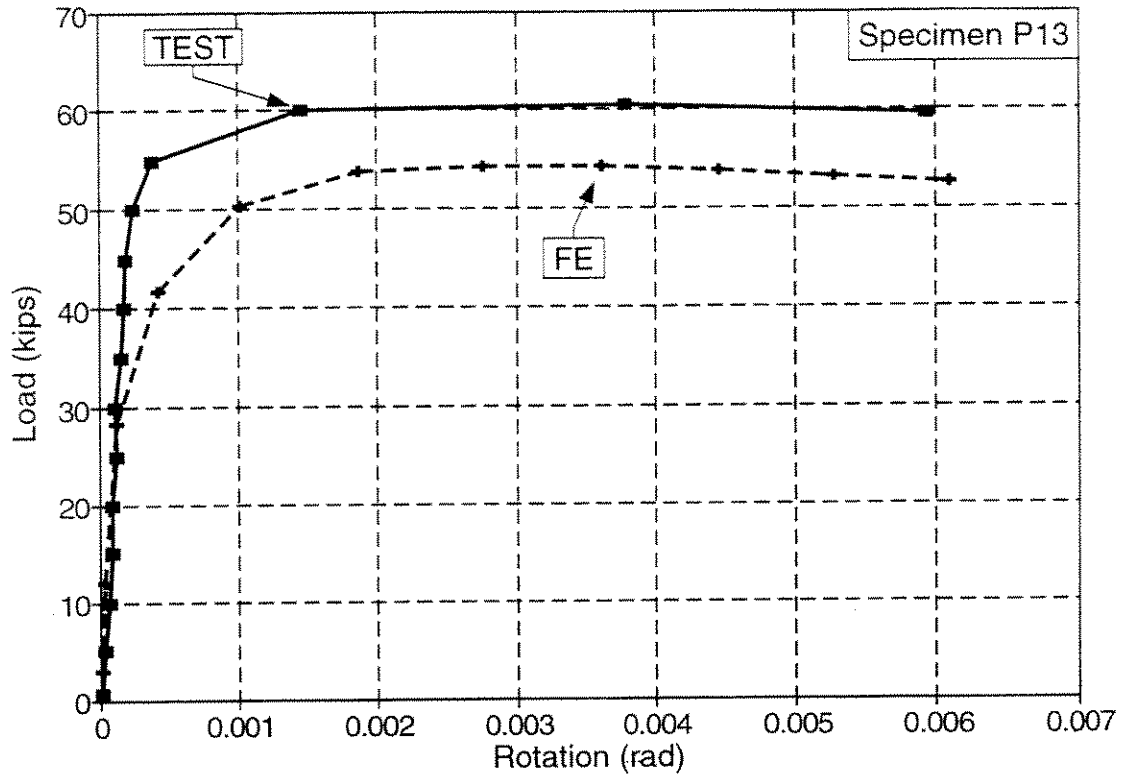


Fig. 13-26 Specimen P13 -- End Rotation from Test and FE Analysis

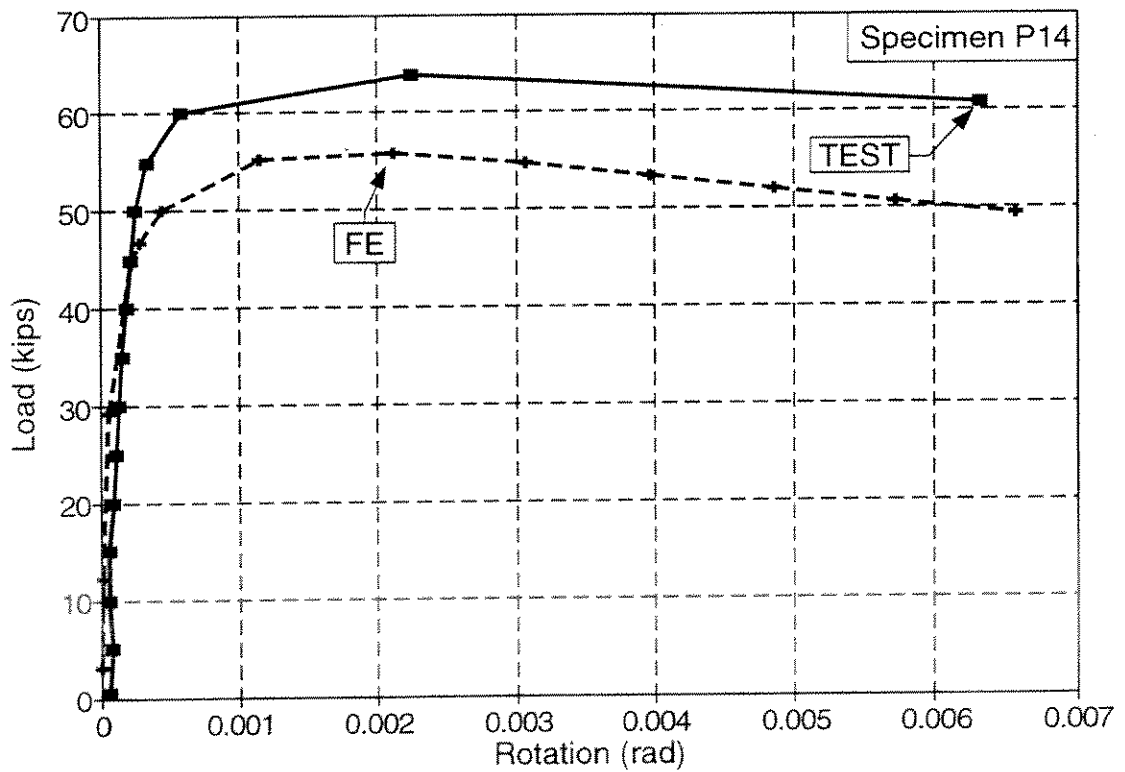


Fig. 13-27 Specimen P14 -- End Rotation from Test and FE Analysis

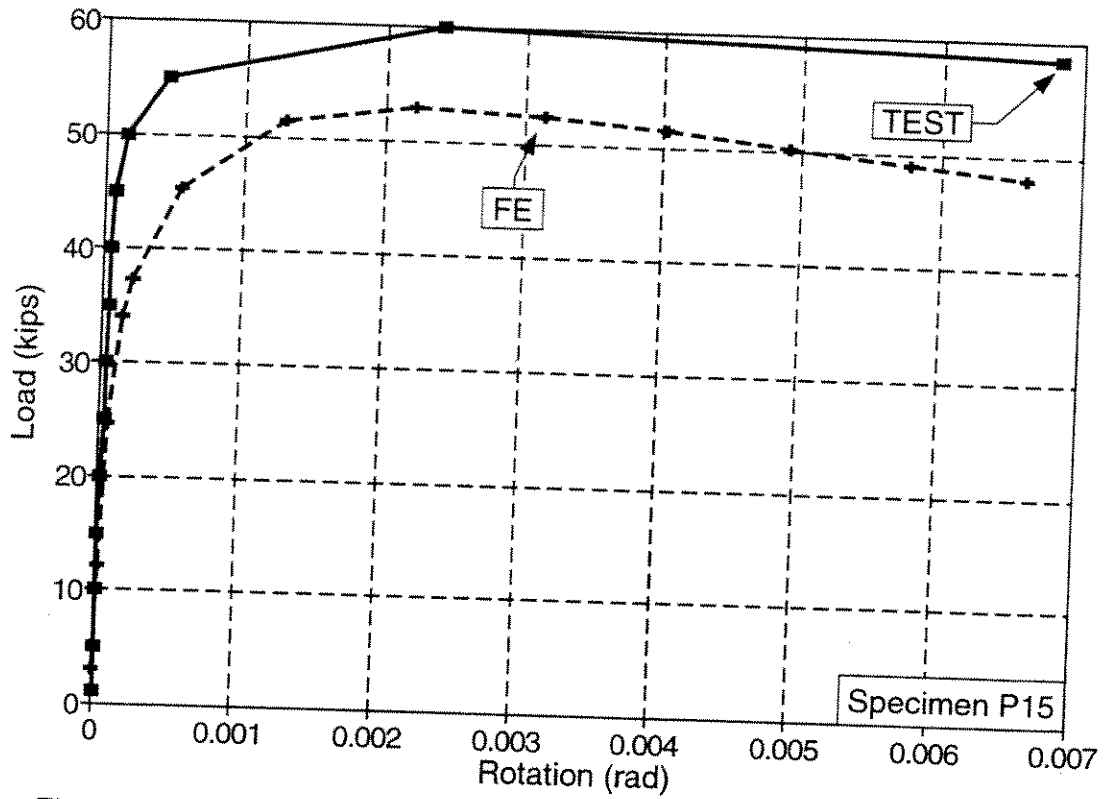


Figure 13-28 Specimen P15 -- End Rotation from Test and FE Analysis

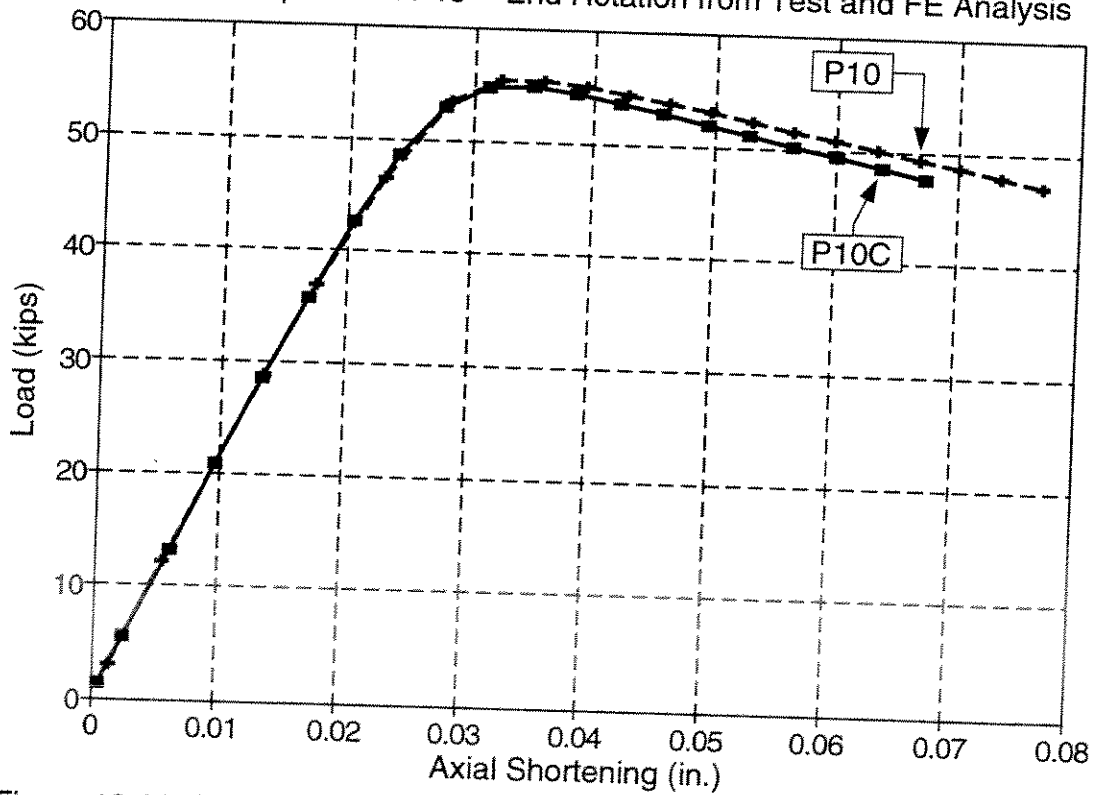


Figure 13-29 Specimens P10 and P10C -- Load-Shortening from FE Analysis

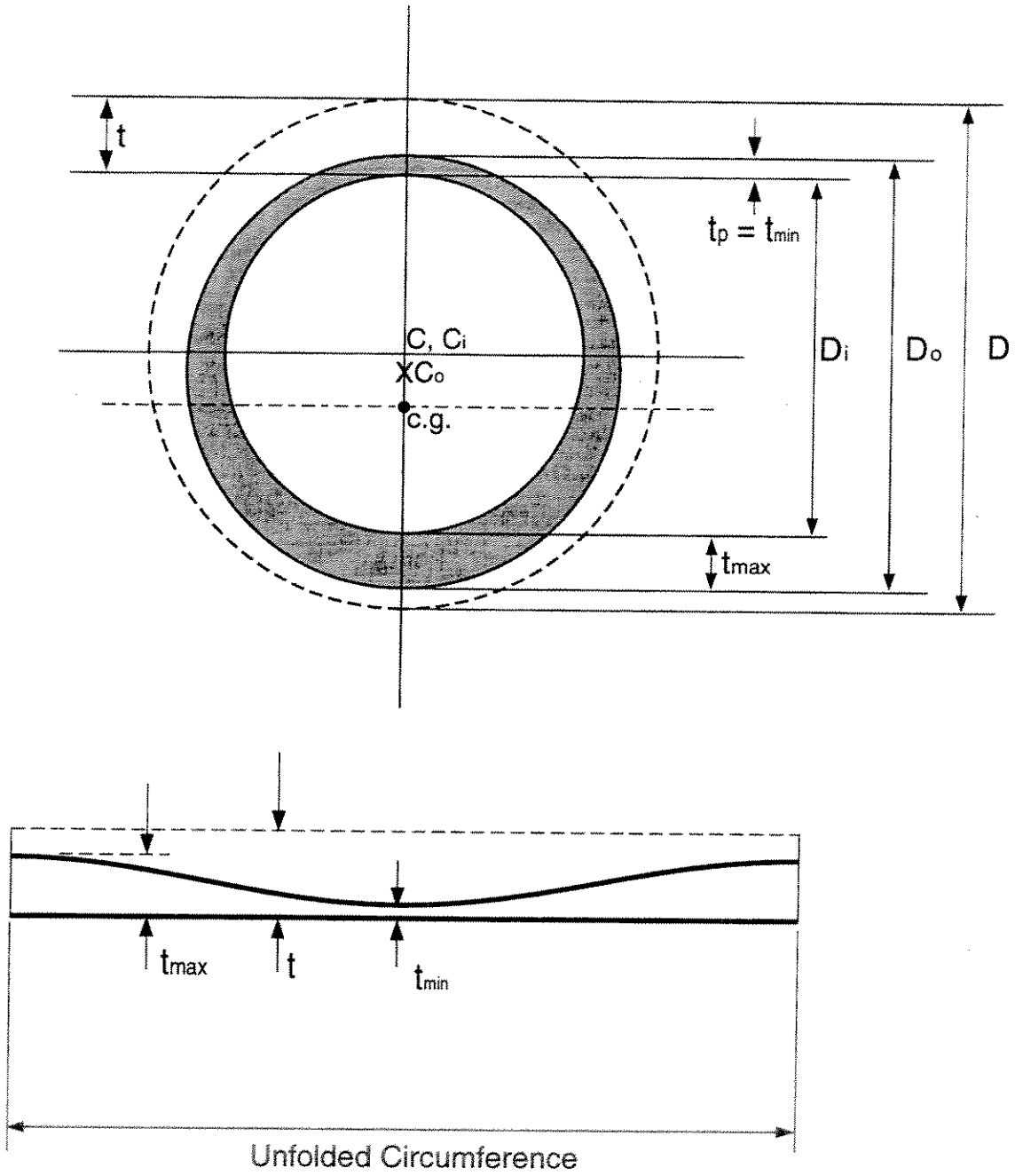


Figure 14-1 " Shifted Circle" Model of Thickness Variation Around Circumference [8]

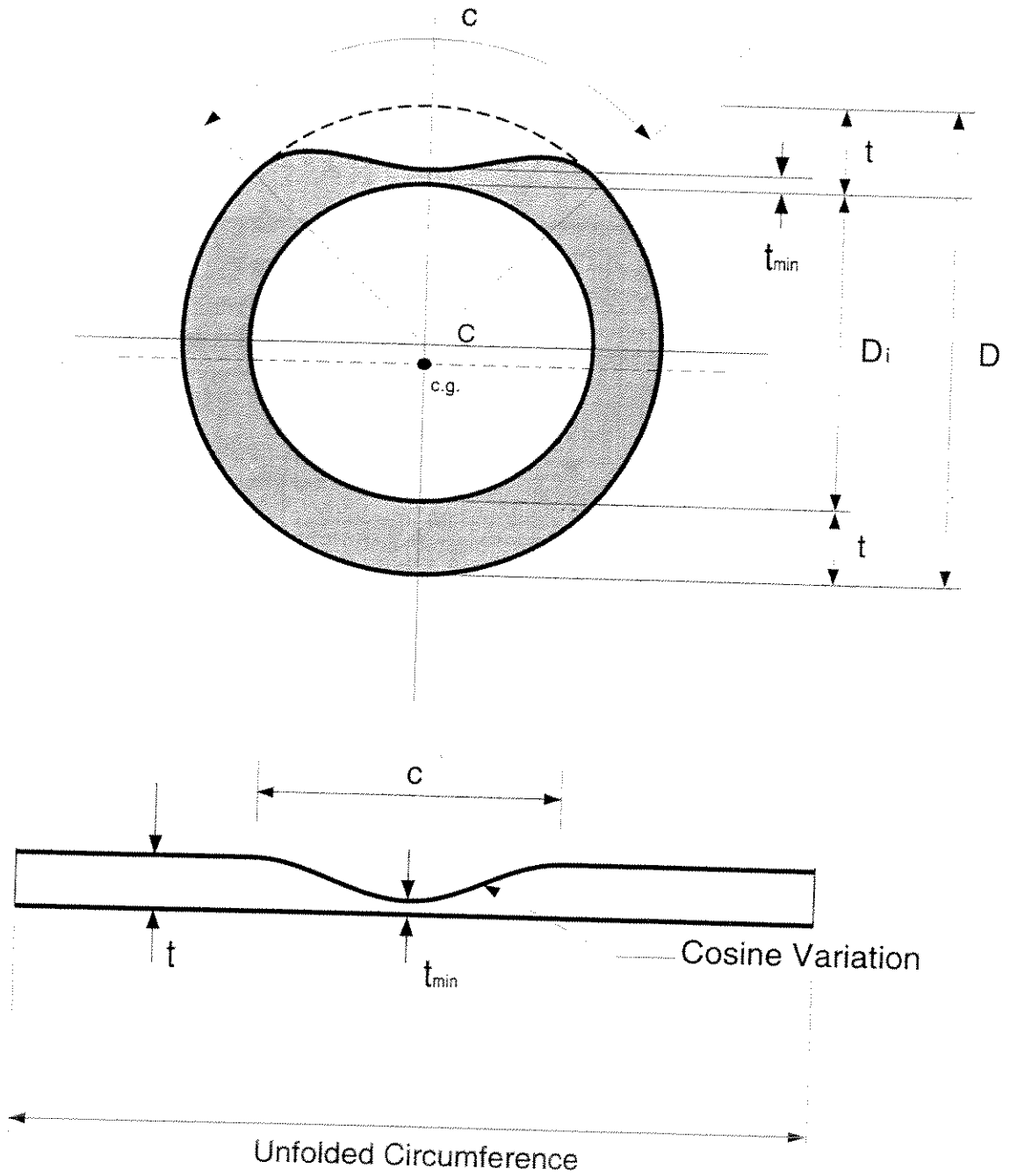


Figure 14-2: "Cosine Patch" Model of Thickness Variation Around Circumference. (From Ref. 5,10)

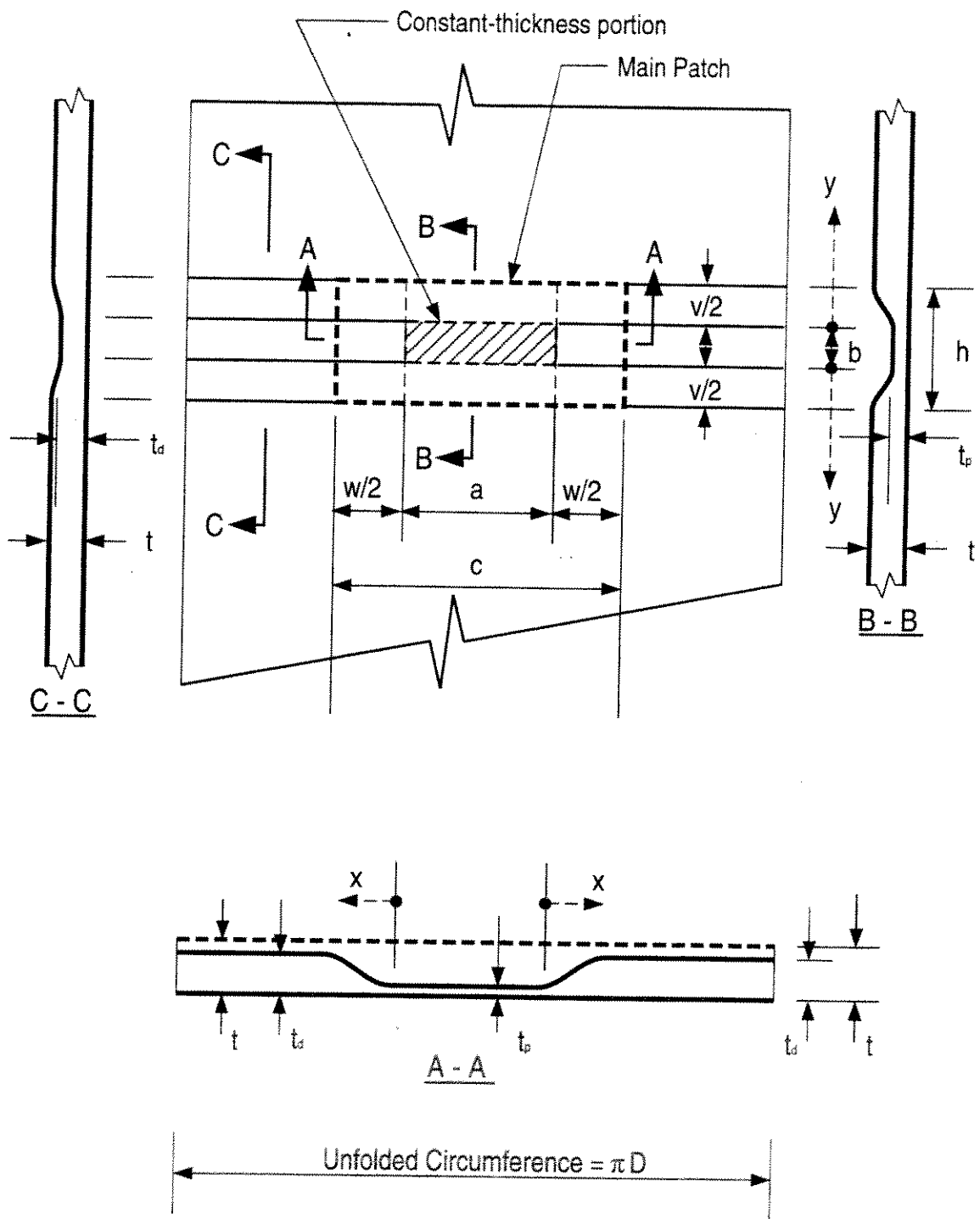


Figure 14-3 "Constant-Thickness Patch" Model of Thickness Variation in Corrosion Patch

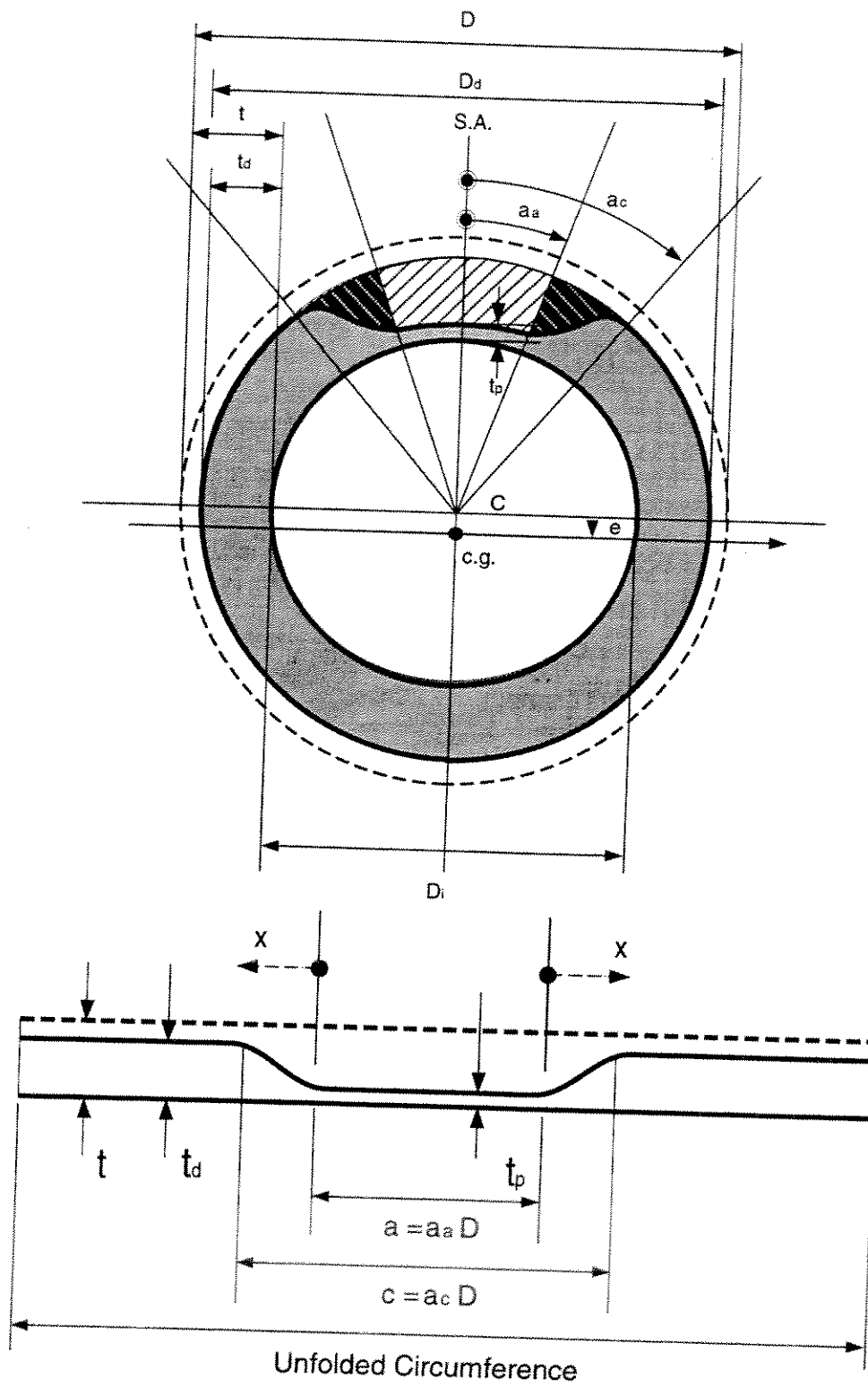


Figure 14-4 "Constant-Thickness Patch" Model of Thickness Variation Around Circumference

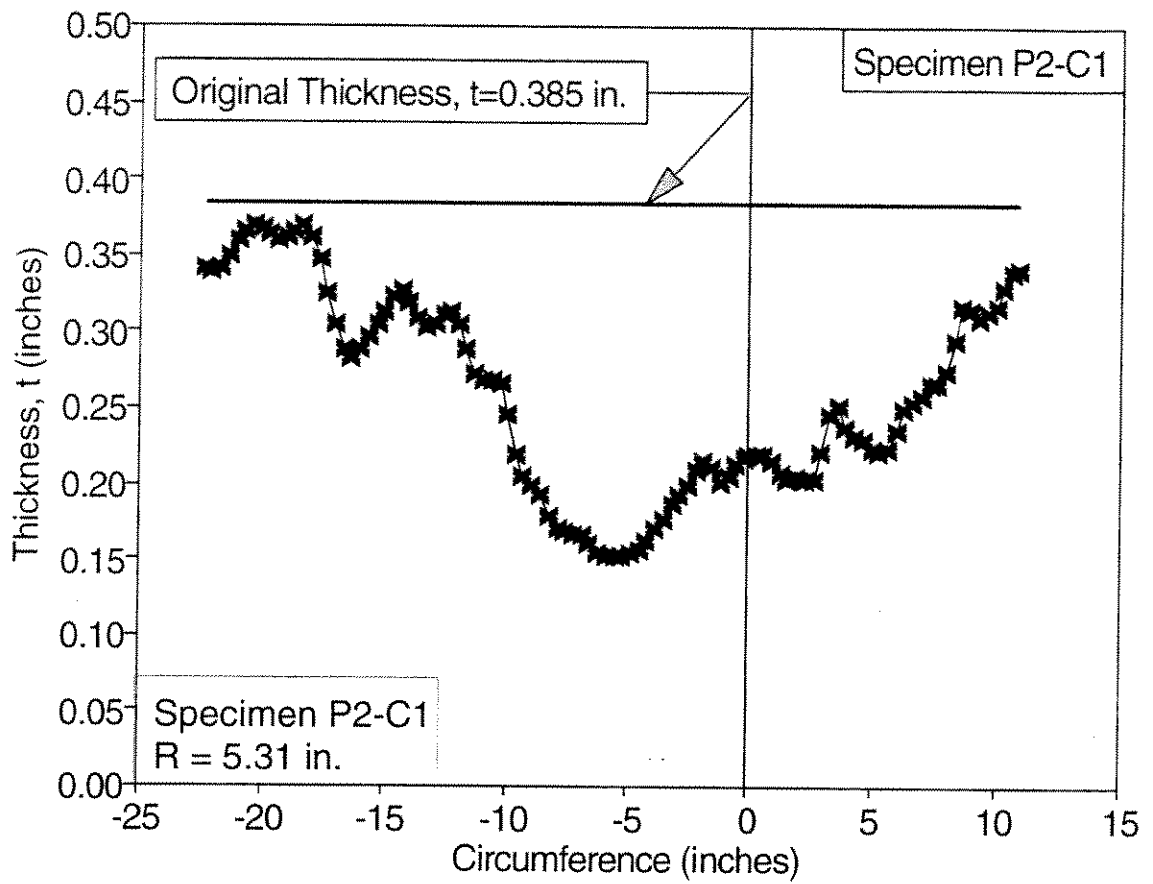


Figure 14-5: Irregular Thickness Variation at Location of Buckle 3.
Specimen P2-C1.

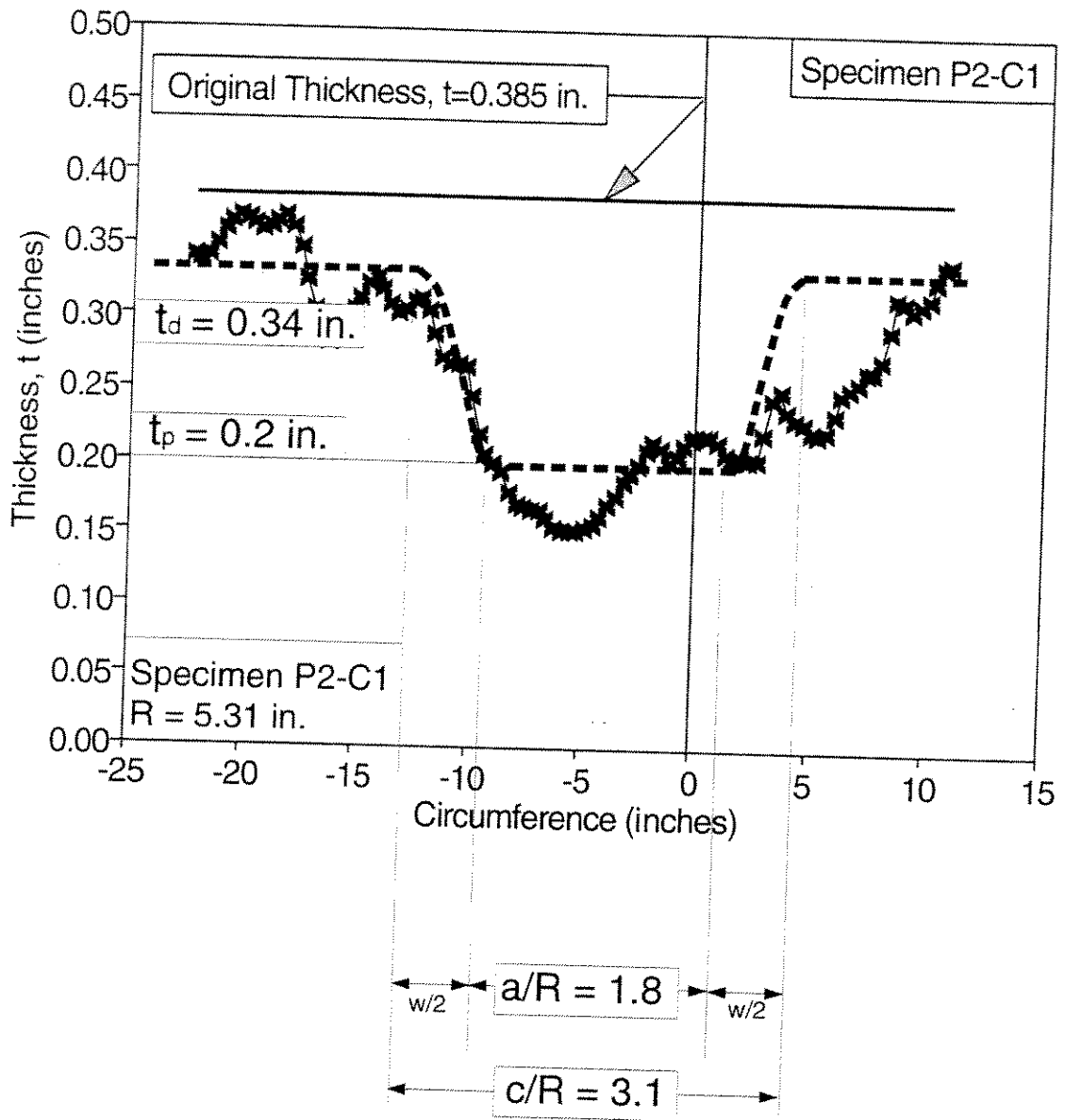


Figure 14-6: Modelling of Thickness Variation at Location of Buckle 3. Specimen P2-C1.

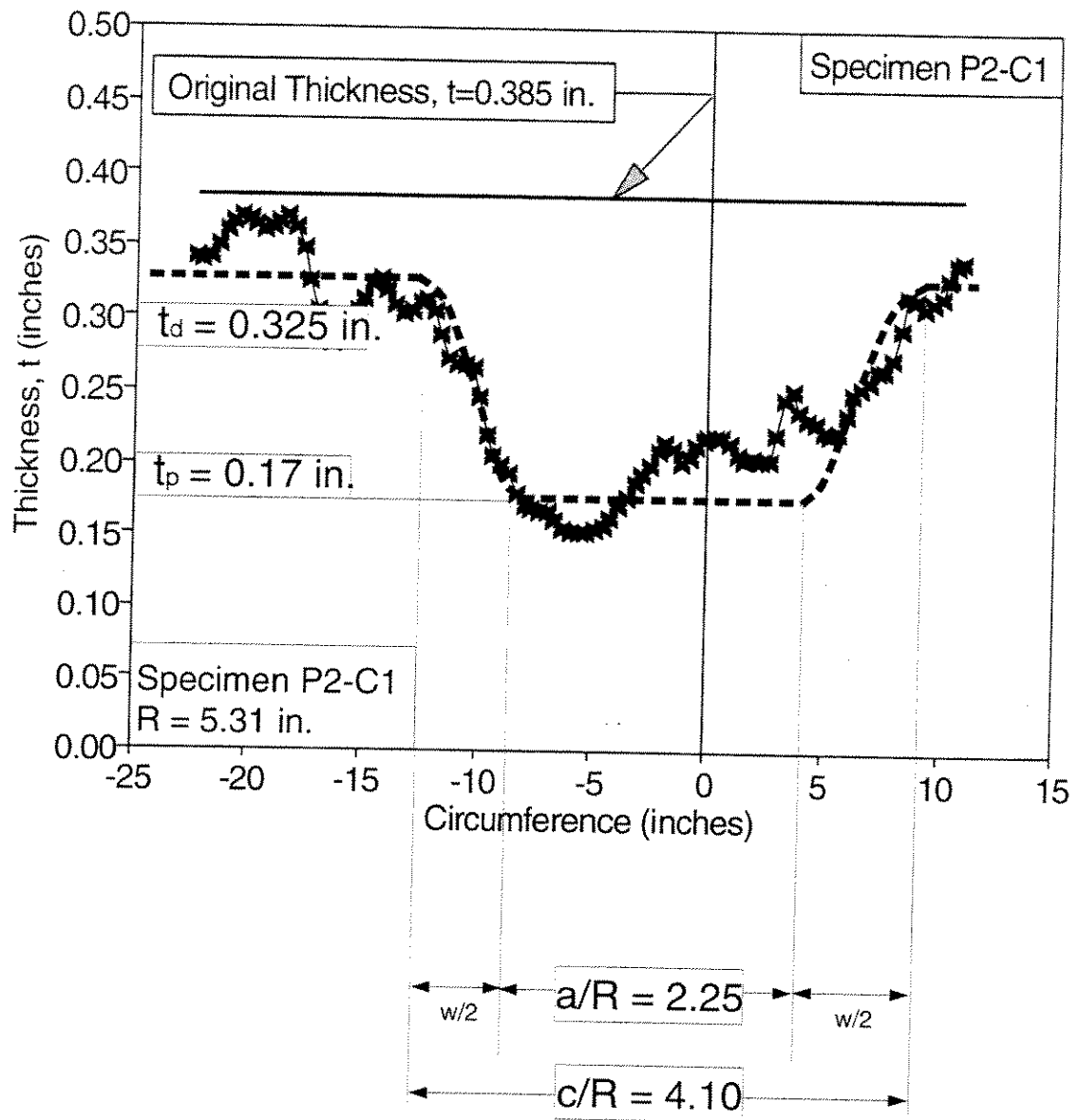


Figure 14-7: Modelling of Thickness Variation at Location of Buckle 3. Specimen P2-C1.

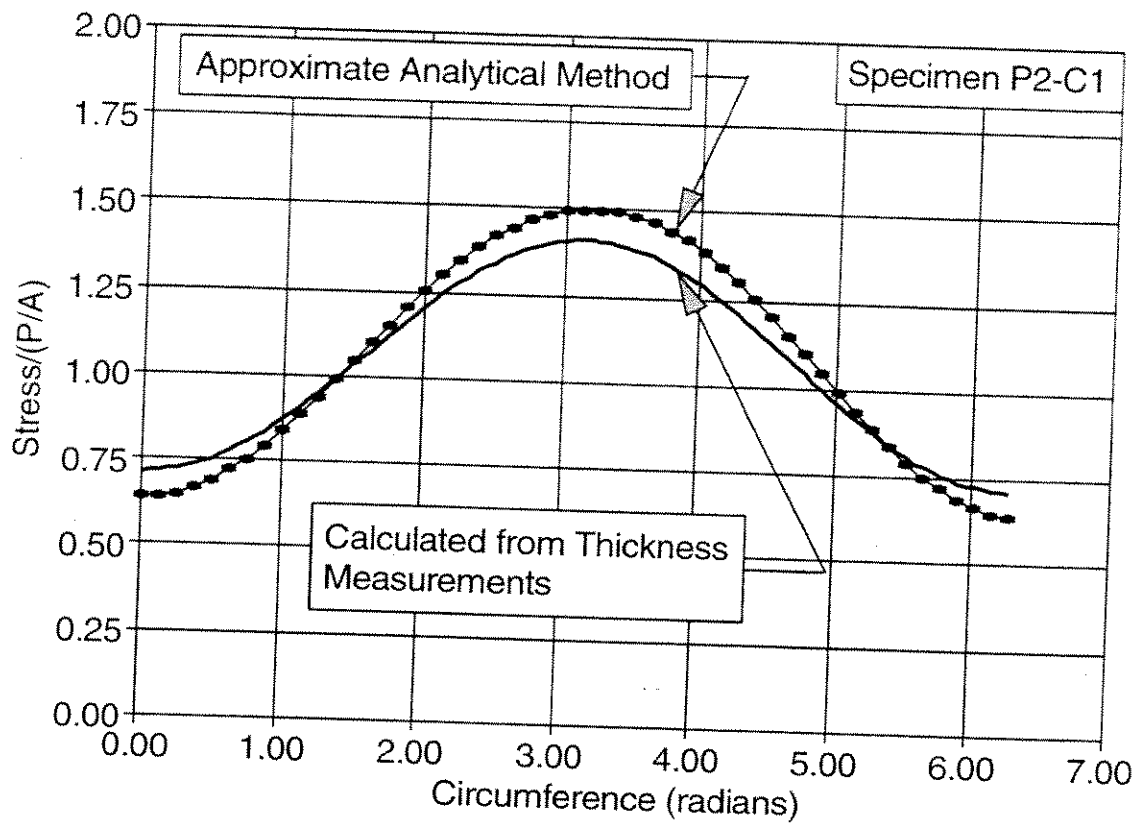


Figure 14-8: Buckle 2, Specimen P2-C1 -- Stress Distribution around Tube Circumference. (Nondimensionalized with respect to the stress at the centroid.)

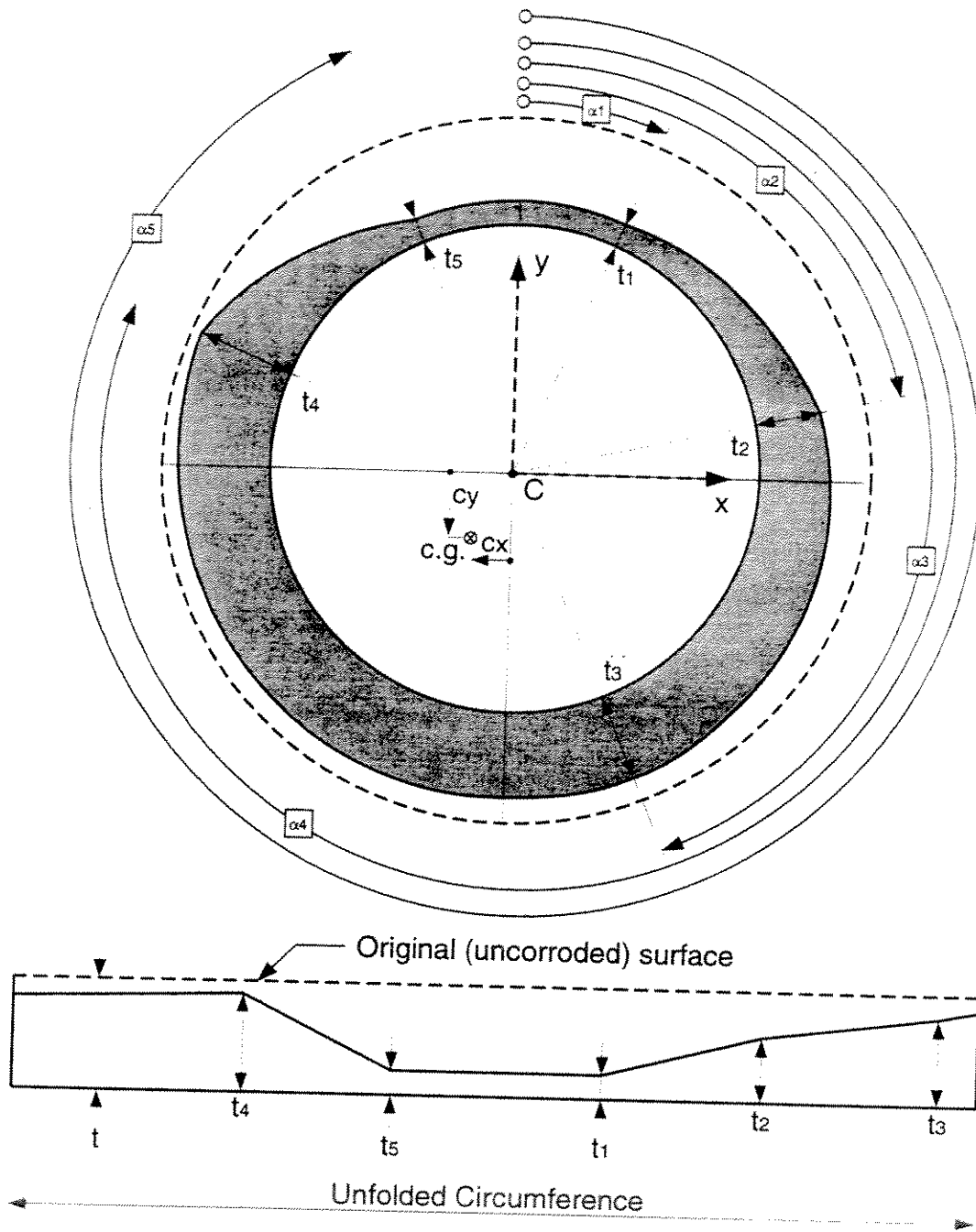


Figure 14-9 "Linear Segments" Model for Approximating Corroded Section

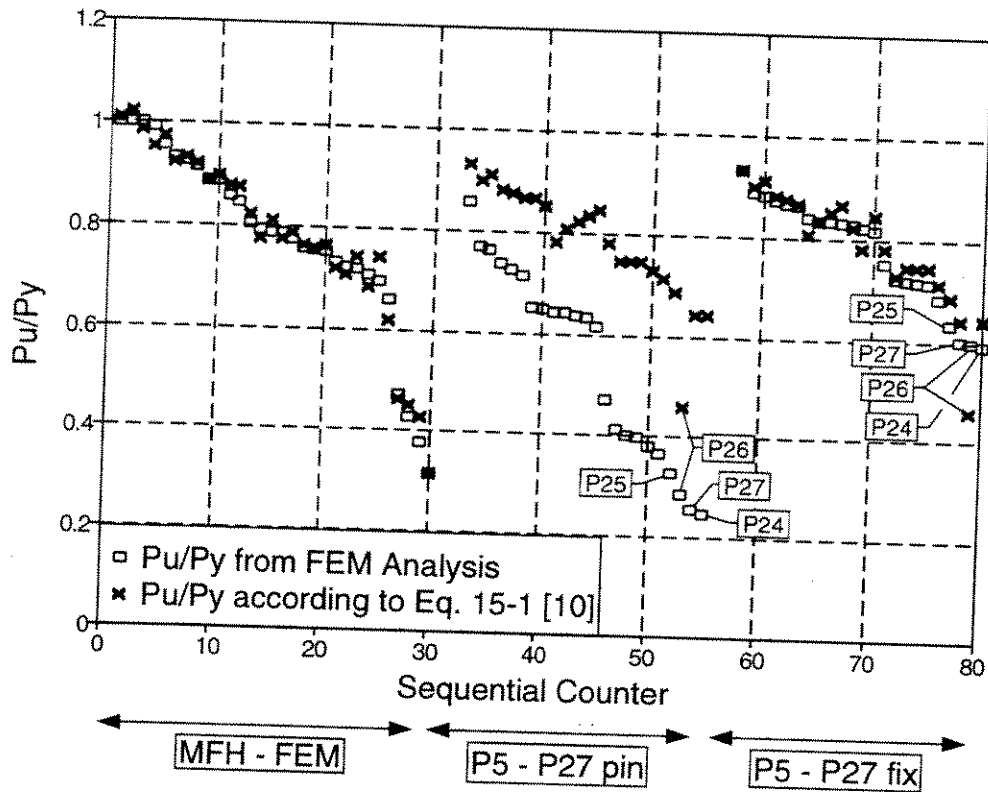


Figure 15-1 Formula by Hebor and Ricles [10] Compared with FEM Values from [5] and this Project

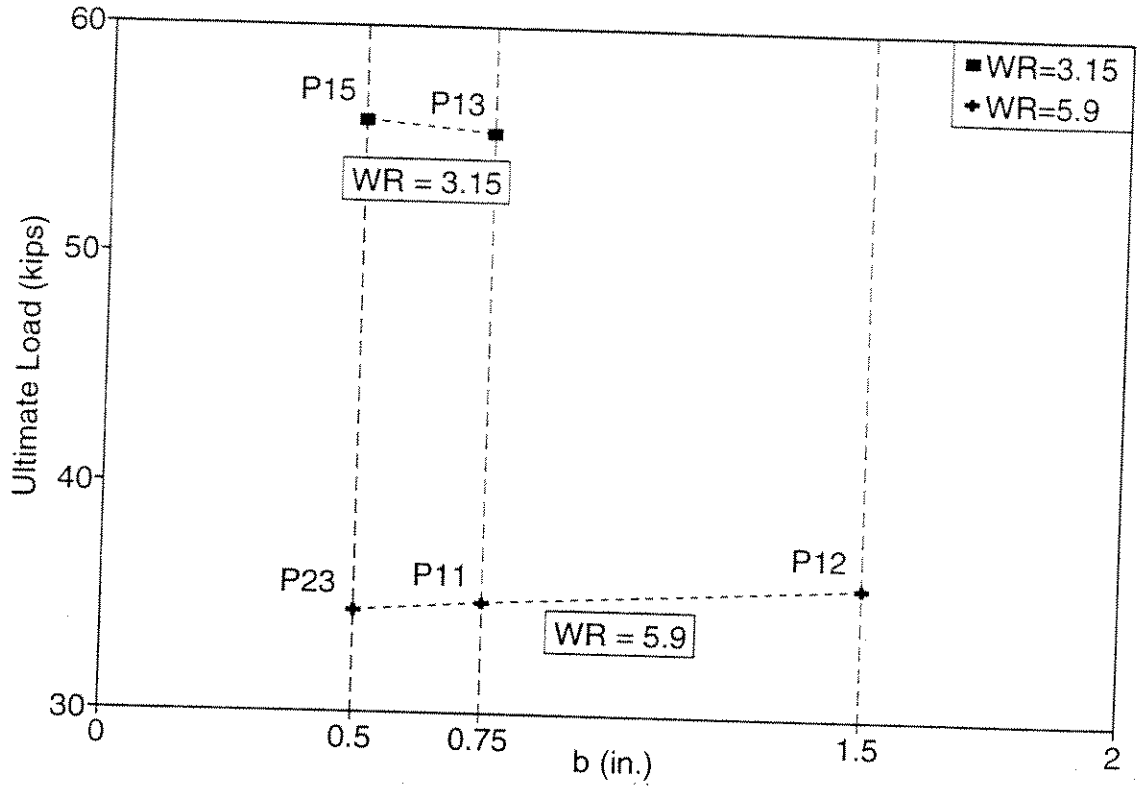


Fig. 15-3 Ultimate Load vs. b

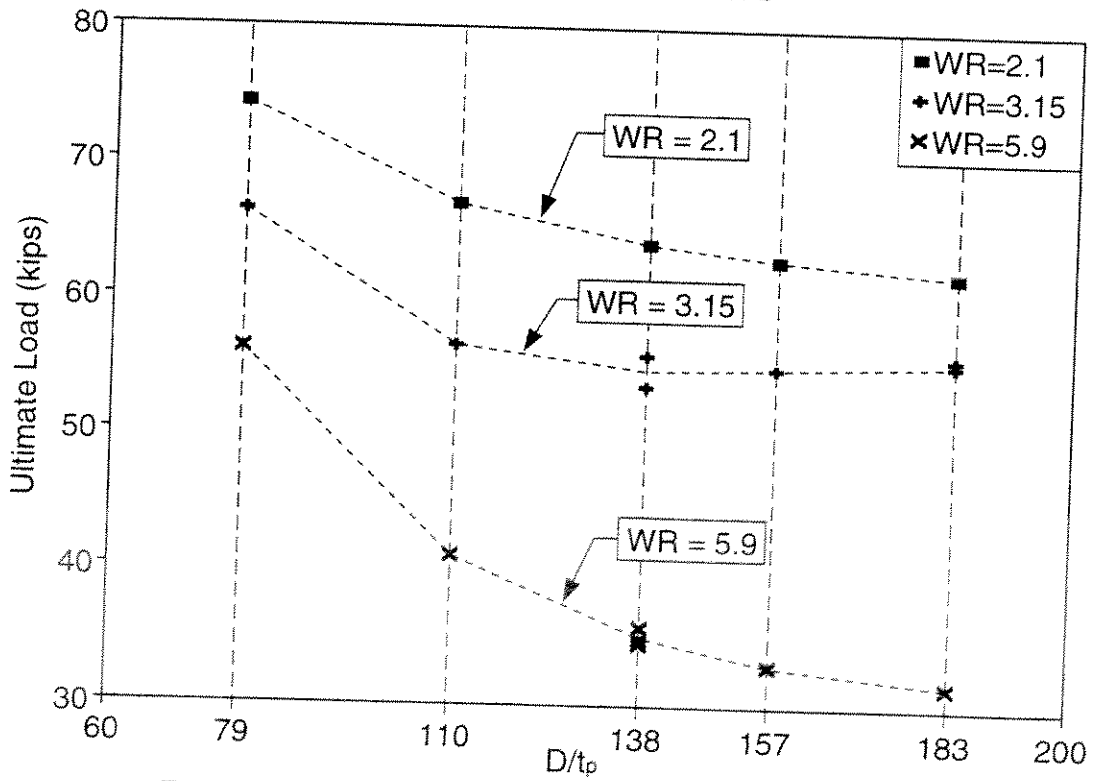


Fig. 15-4 Ultimate Load vs. D/t_p --Specimens P5 to P23

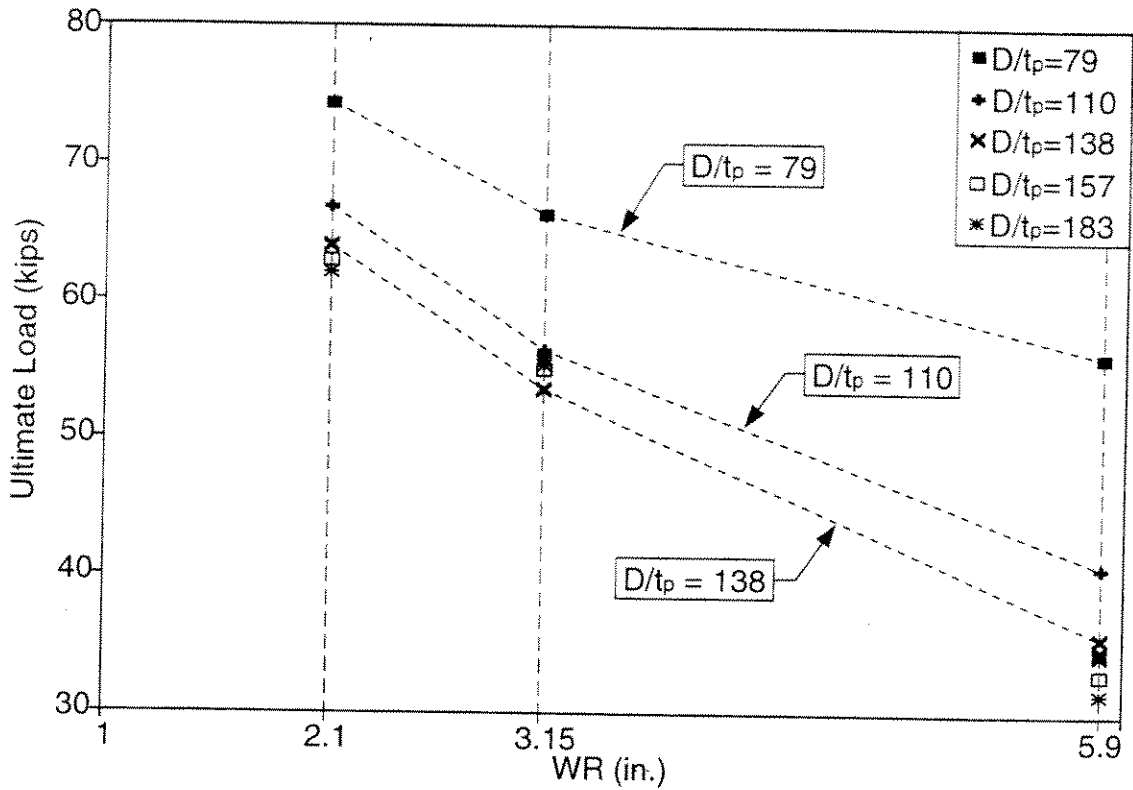


Fig. 15-5 Ultimate Load vs. WR--Specimens P5 to P23

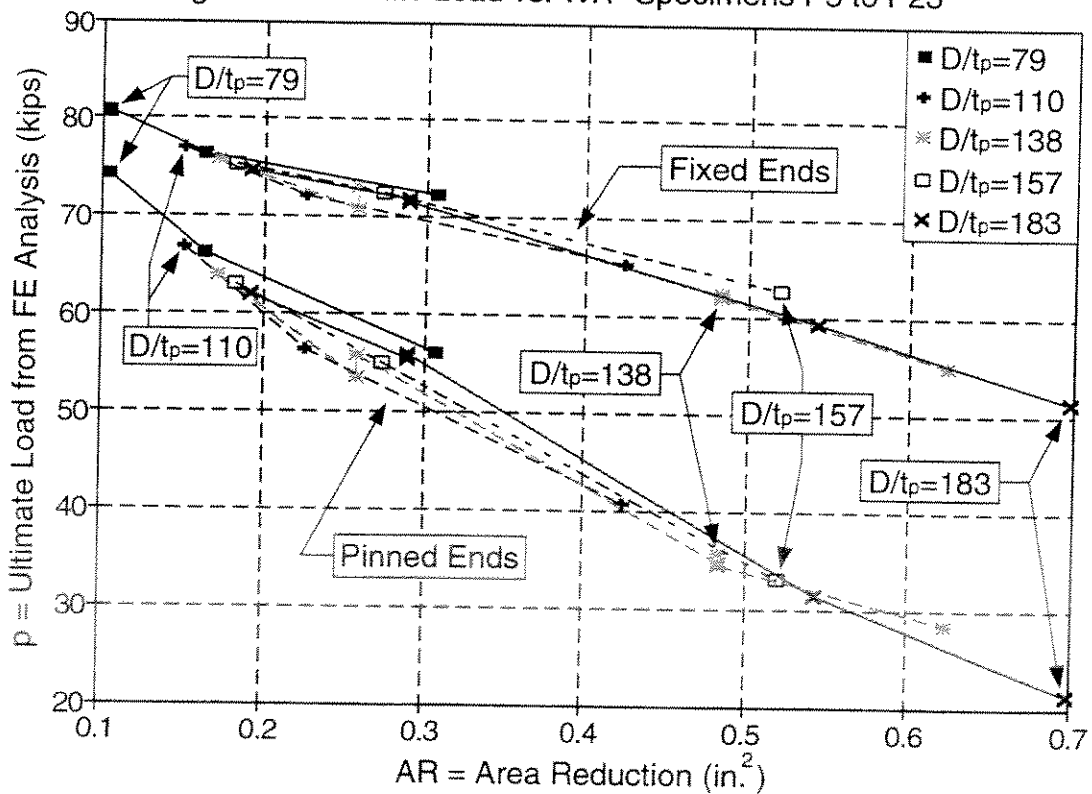


Fig. 15-6 p vs. AR--Specimens P5 to P25

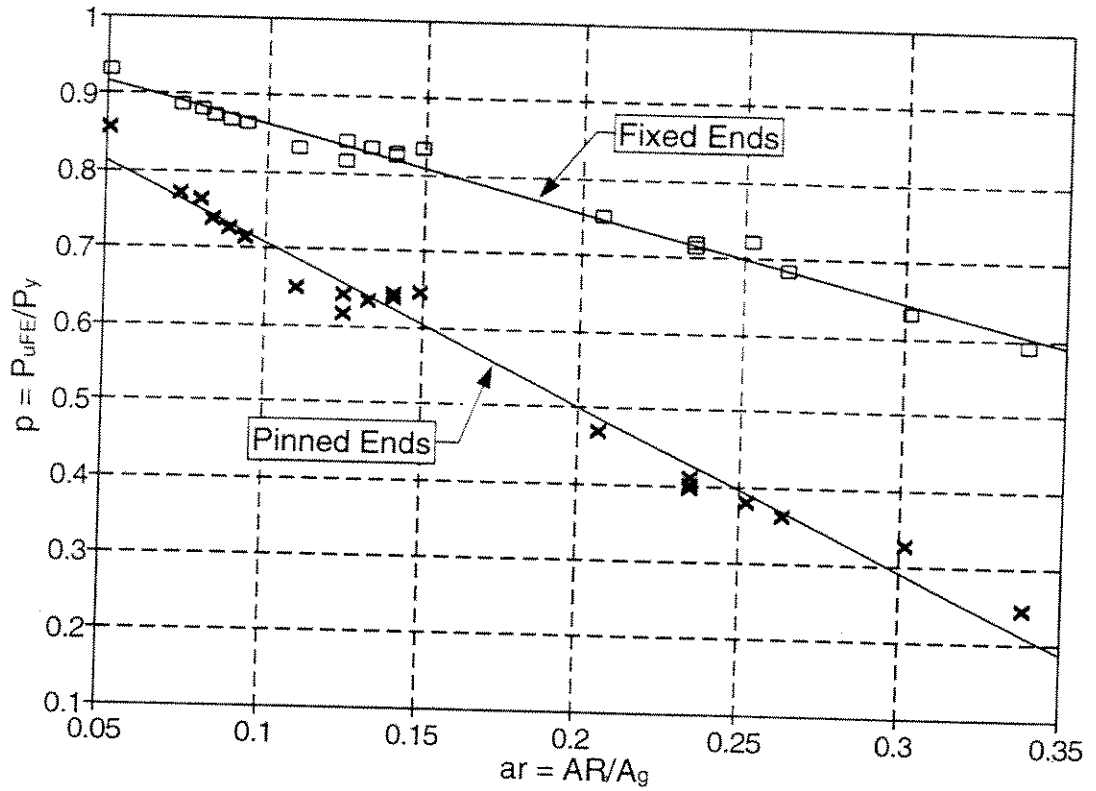


Fig. 15-7 p vs. ar --Specimens P5 to P25

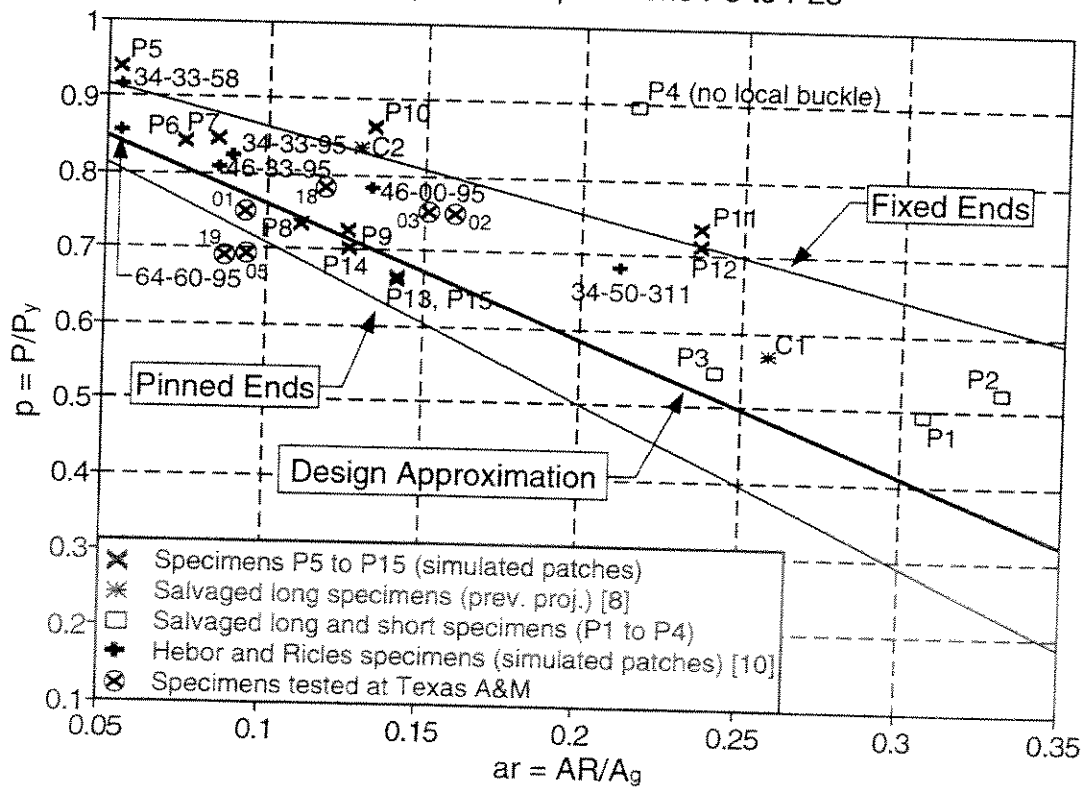


Fig. 15-8 p vs. ar --Test Specimen Comparison

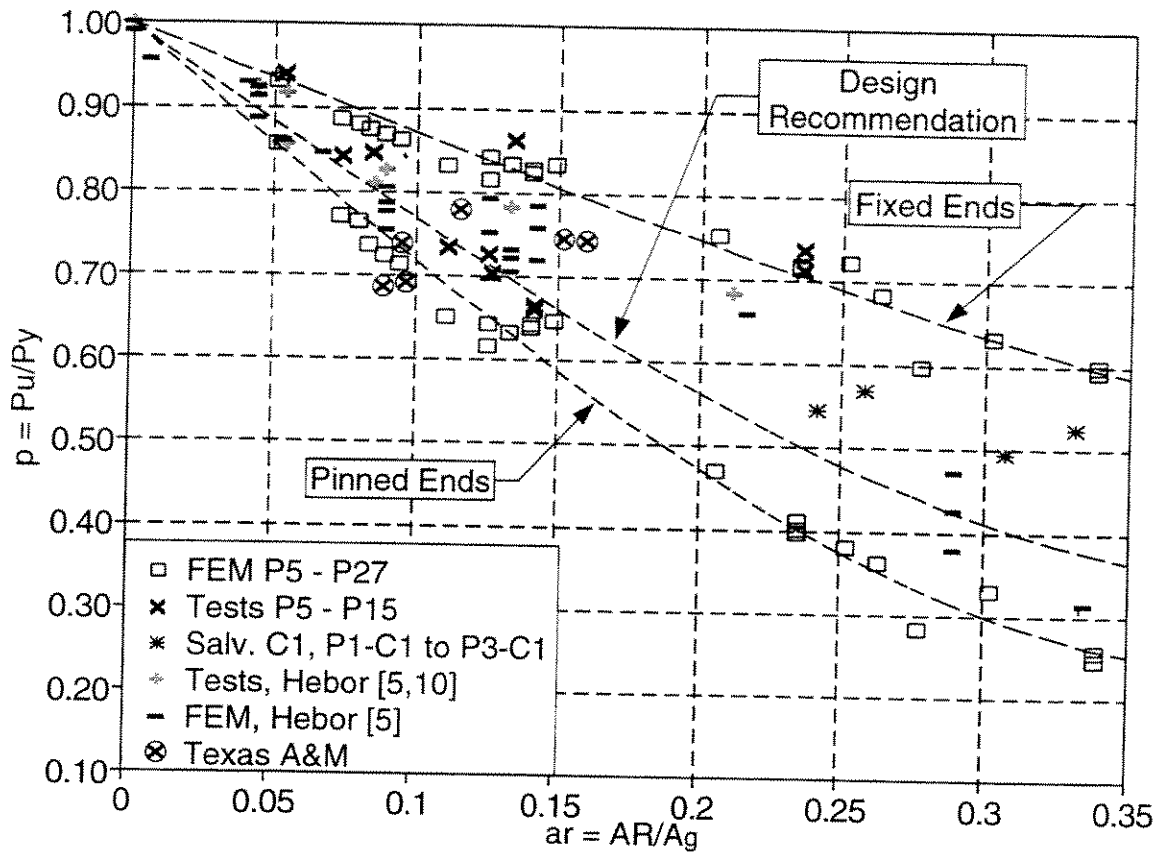


Fig. 15-9 Cubic Approximation

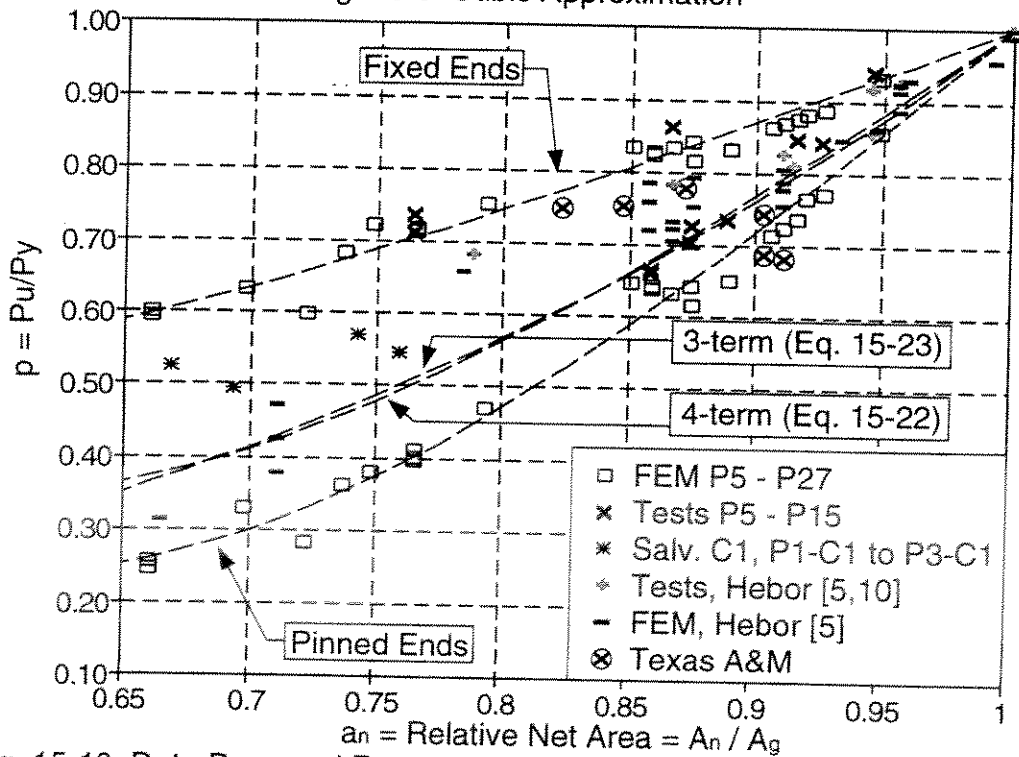


Fig. 15-10 Data Base and Regression Approximations for Ultimate Strength as Function of Relative Net Area a_n

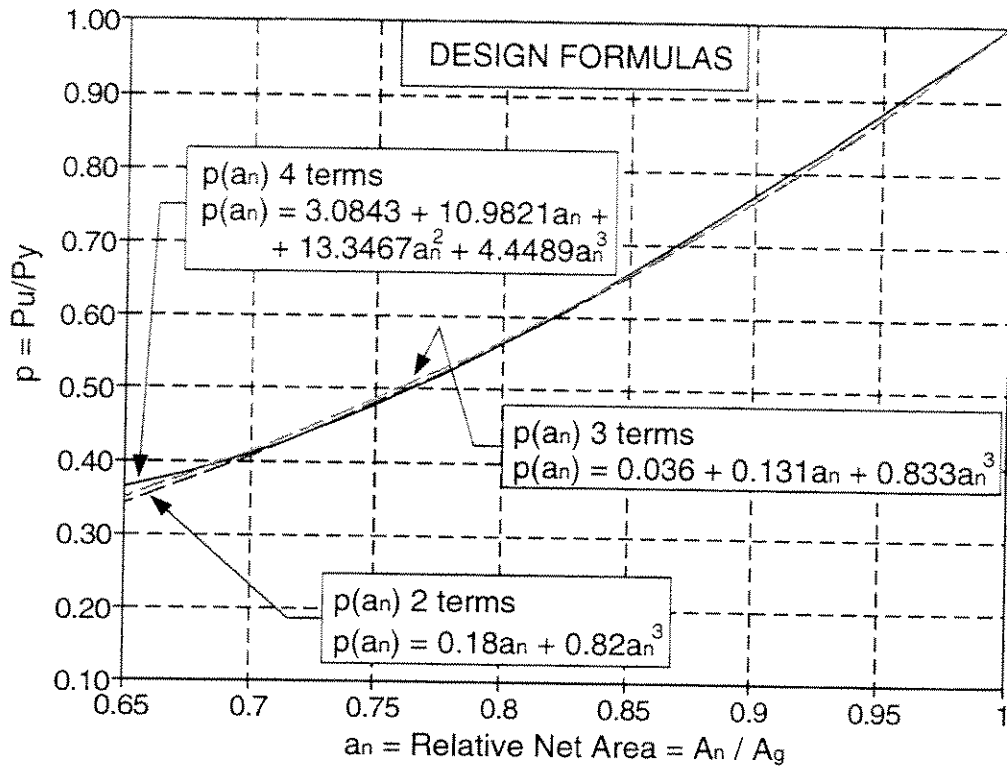
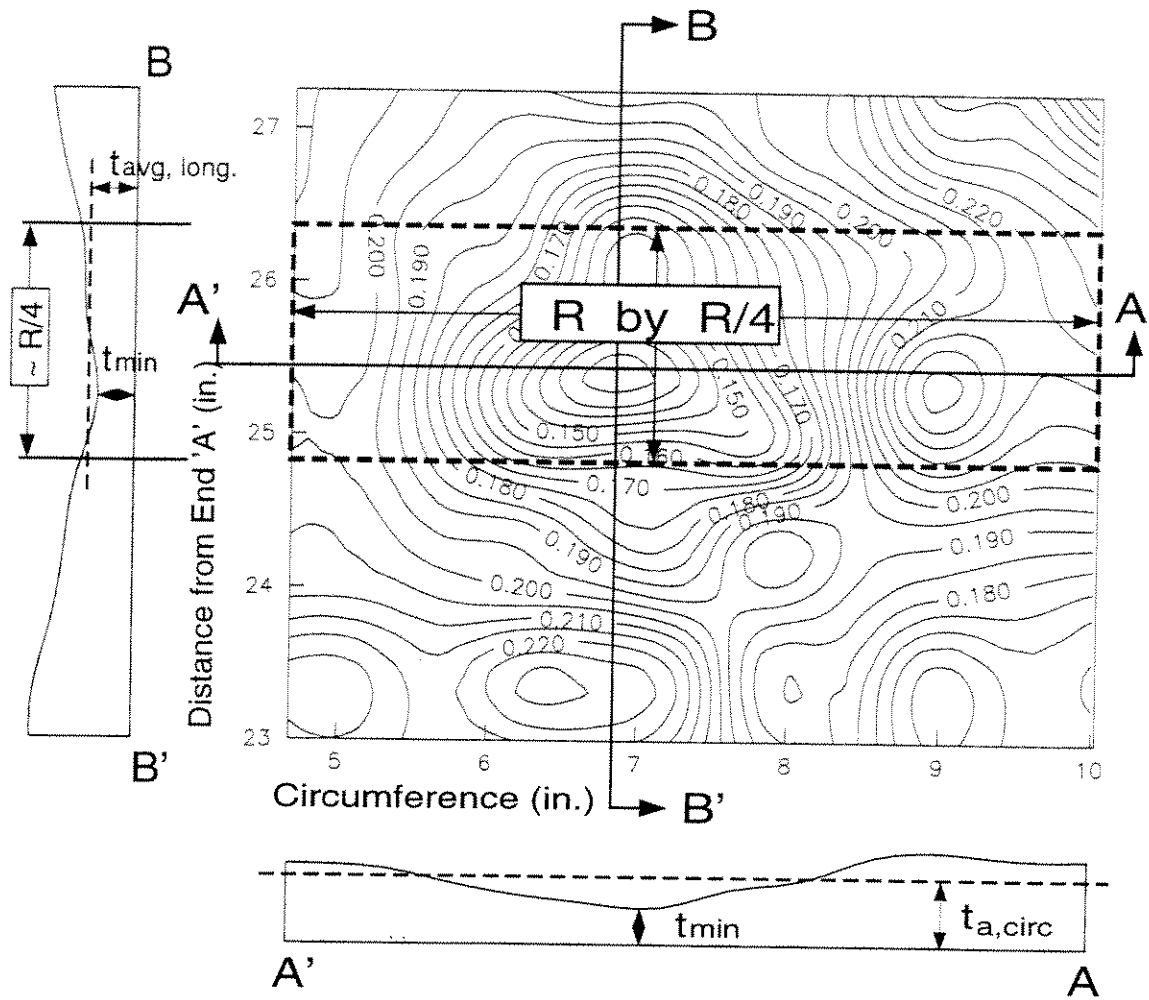


Fig. 15-11 Comparison of Suitable Formulas for Ultimate Strength as Functions of Relative Net Area a_n



$$t_a = \left(\frac{t_{a, long}}{t_{min}} \right) t_{a, circ}$$

Fig. 16-1 Determination of Thickness Parameter, (Specimen P3-C1, Buckle 1)

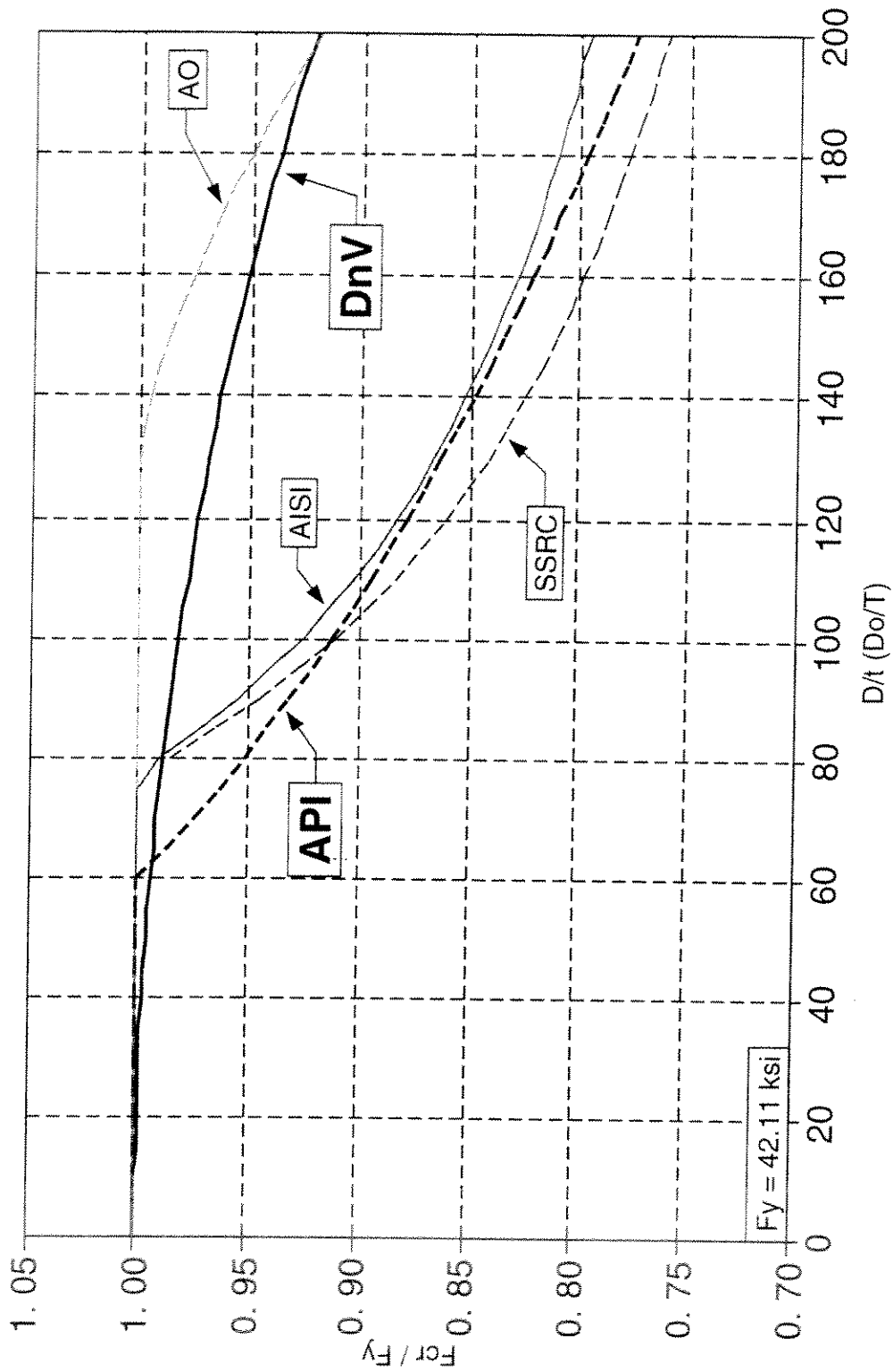


Fig. 16-2 Local Buckling Formulas for Various Specifications (Eqs. 16-2 to 16-7)

PHOTOGRAPHS

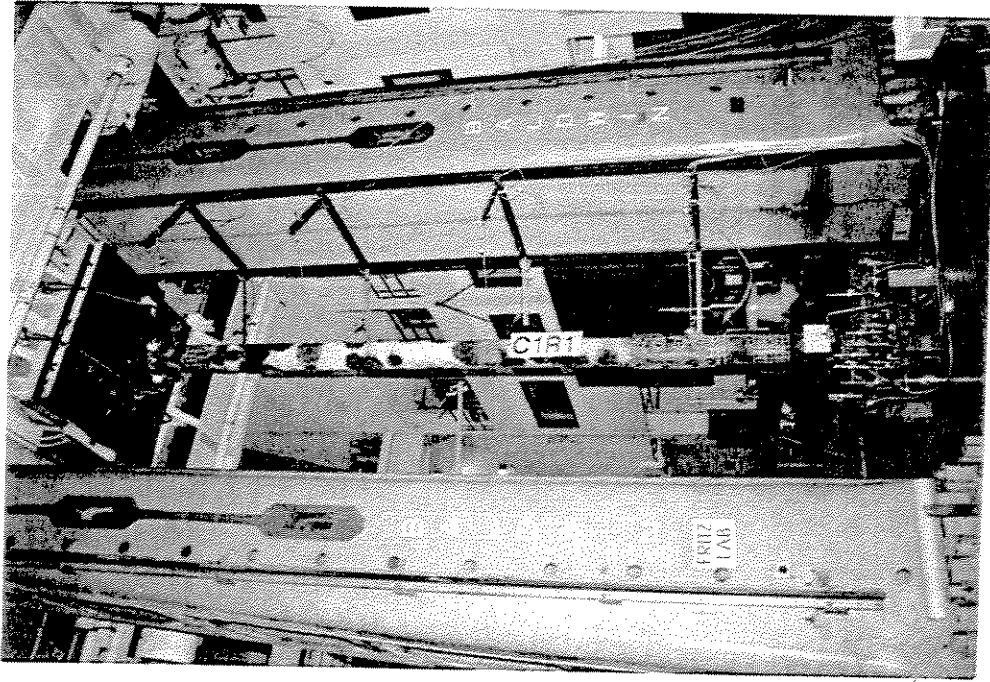


Photo 2-1(a): Overall View of Specimen P1-C1.

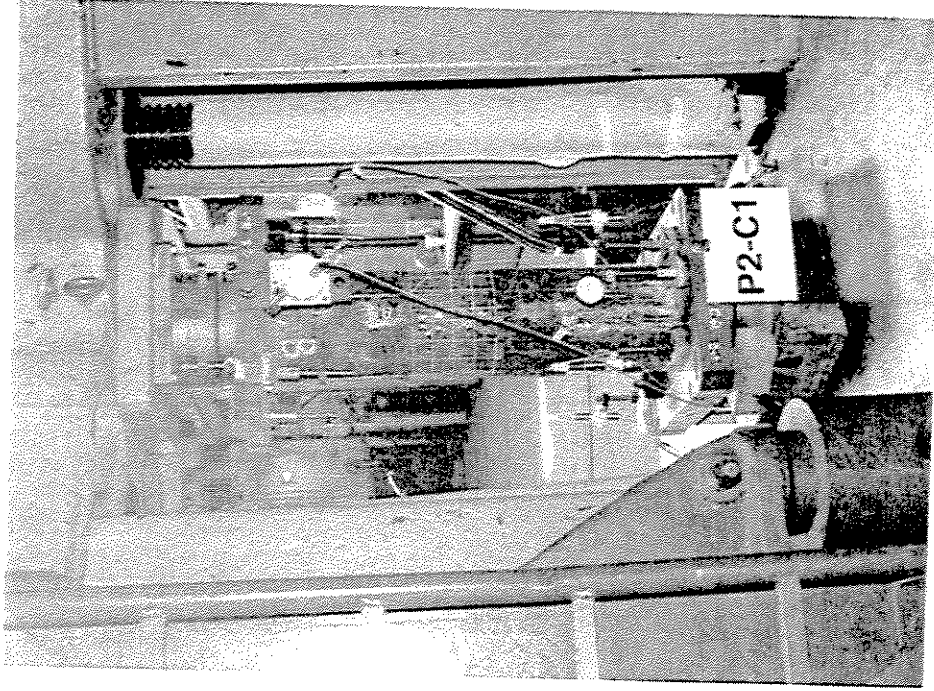


Photo 2-1(b): Overall View of Specimen P2-C1.

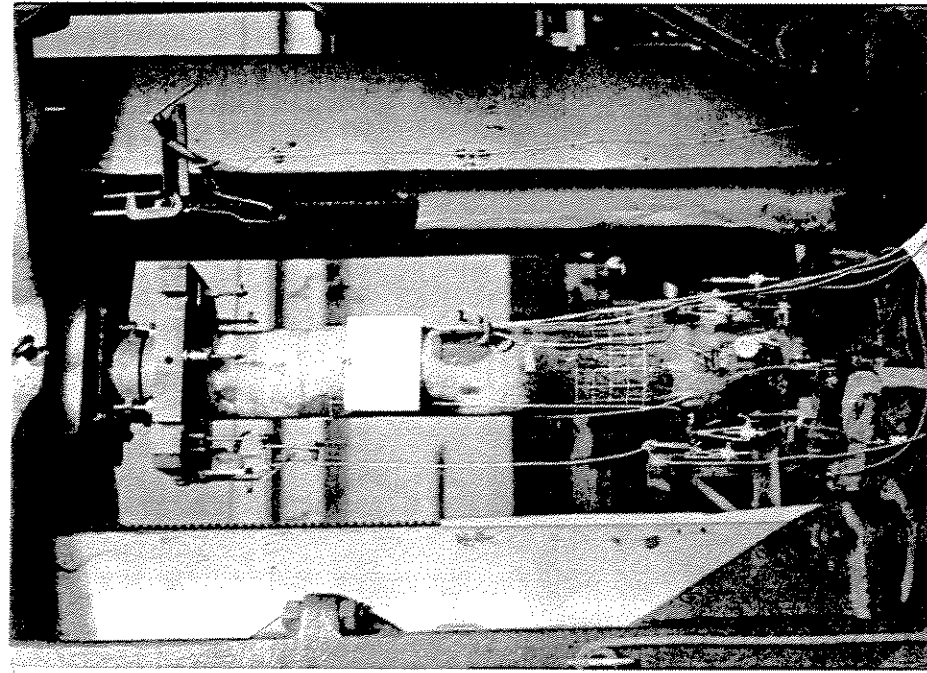


Photo 2-1(c): Overall View of Specimen P3-C1.

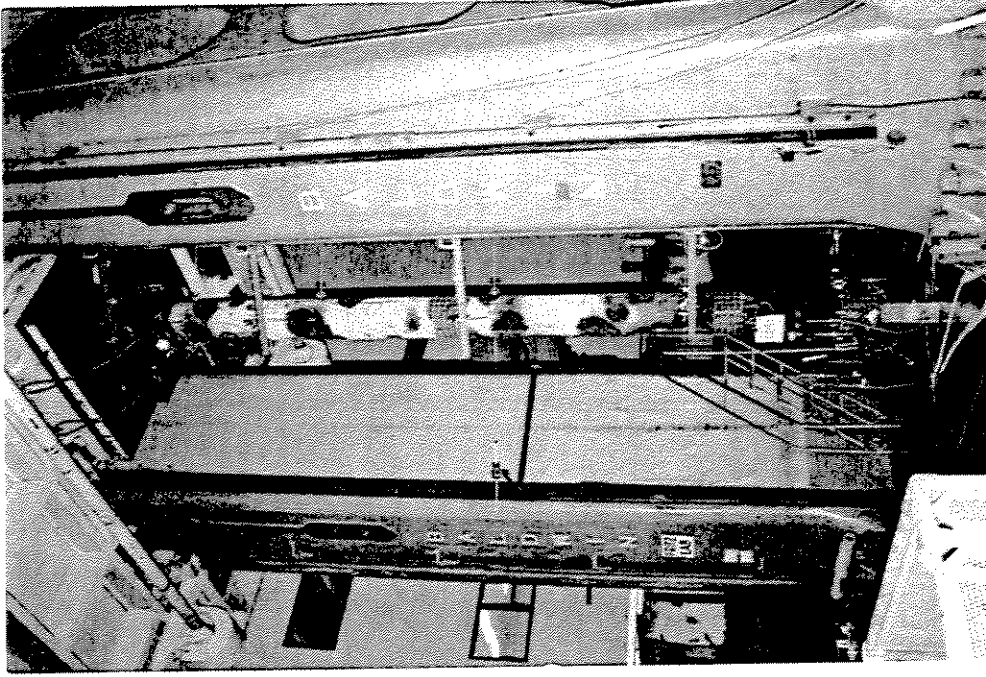


Photo 2-1(d): Overall View of Specimen P4-C2.

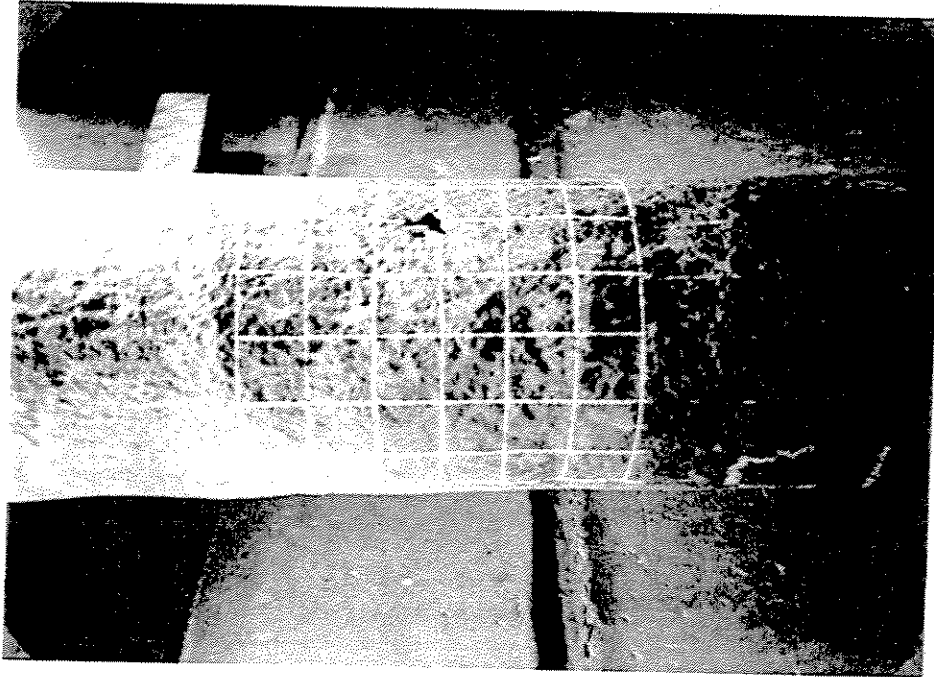


Photo 2-2: View of Hole and Typical Grid.
(Specimen P1-C1)

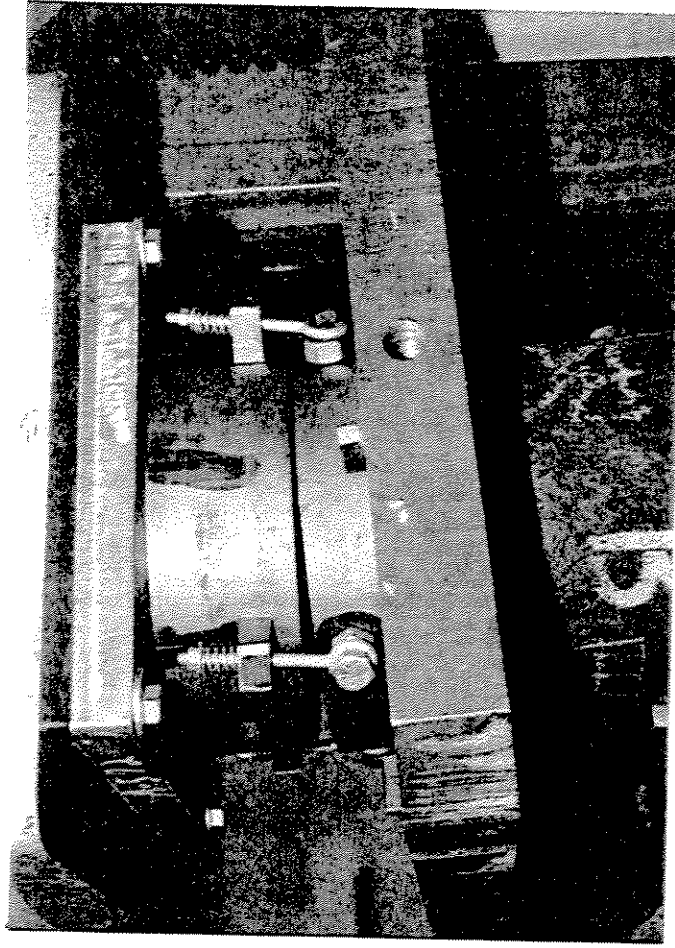


Photo 4-1: Spherical Bearing End Fixtures Used for
All Specimens.

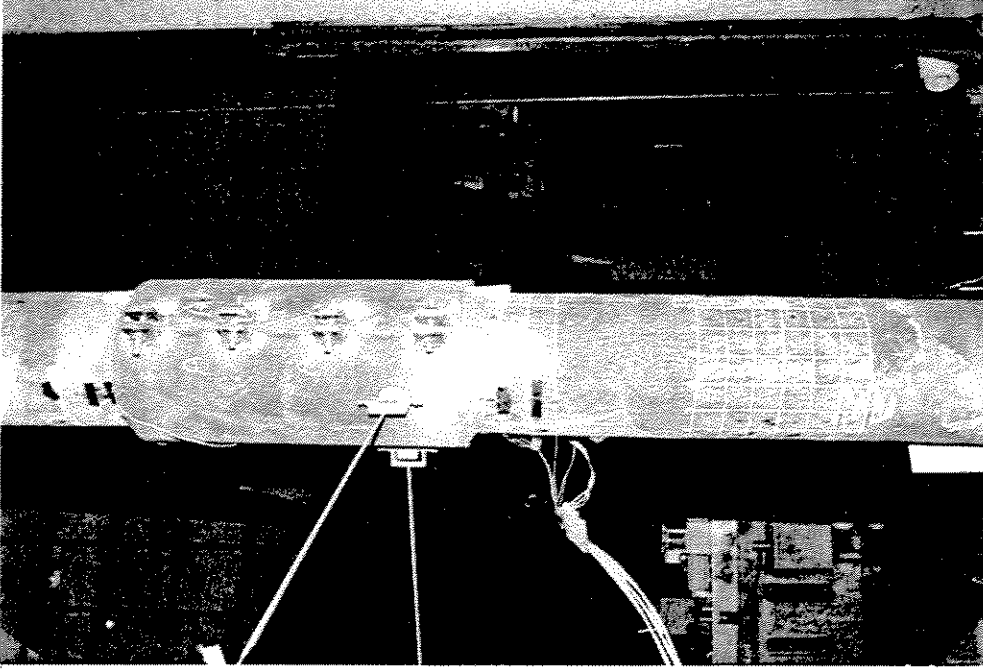


Photo 4-3: View of Epoxy Sleeve after Repair.
(Specimen P1-C1)

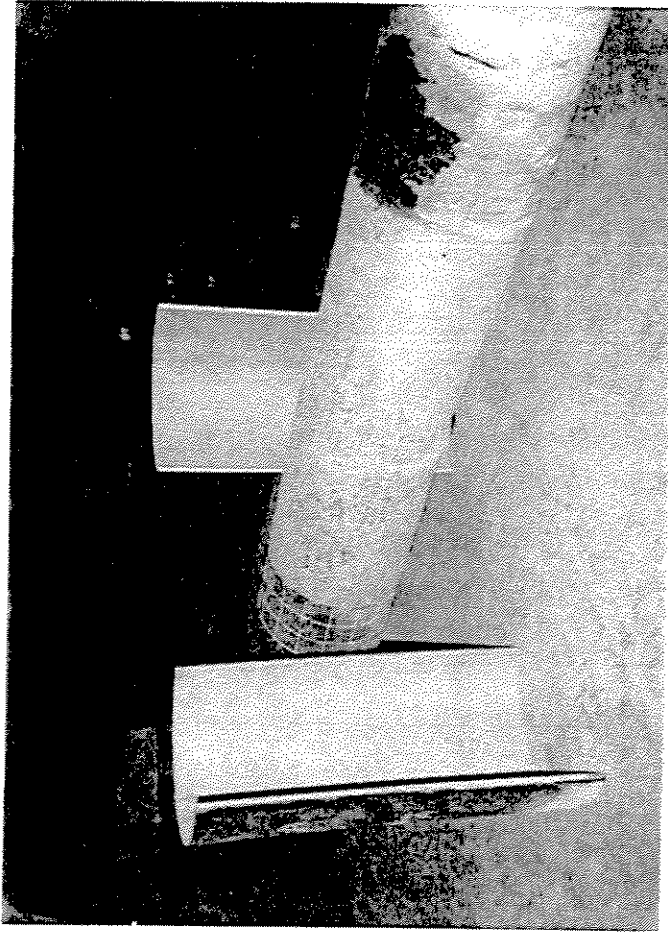
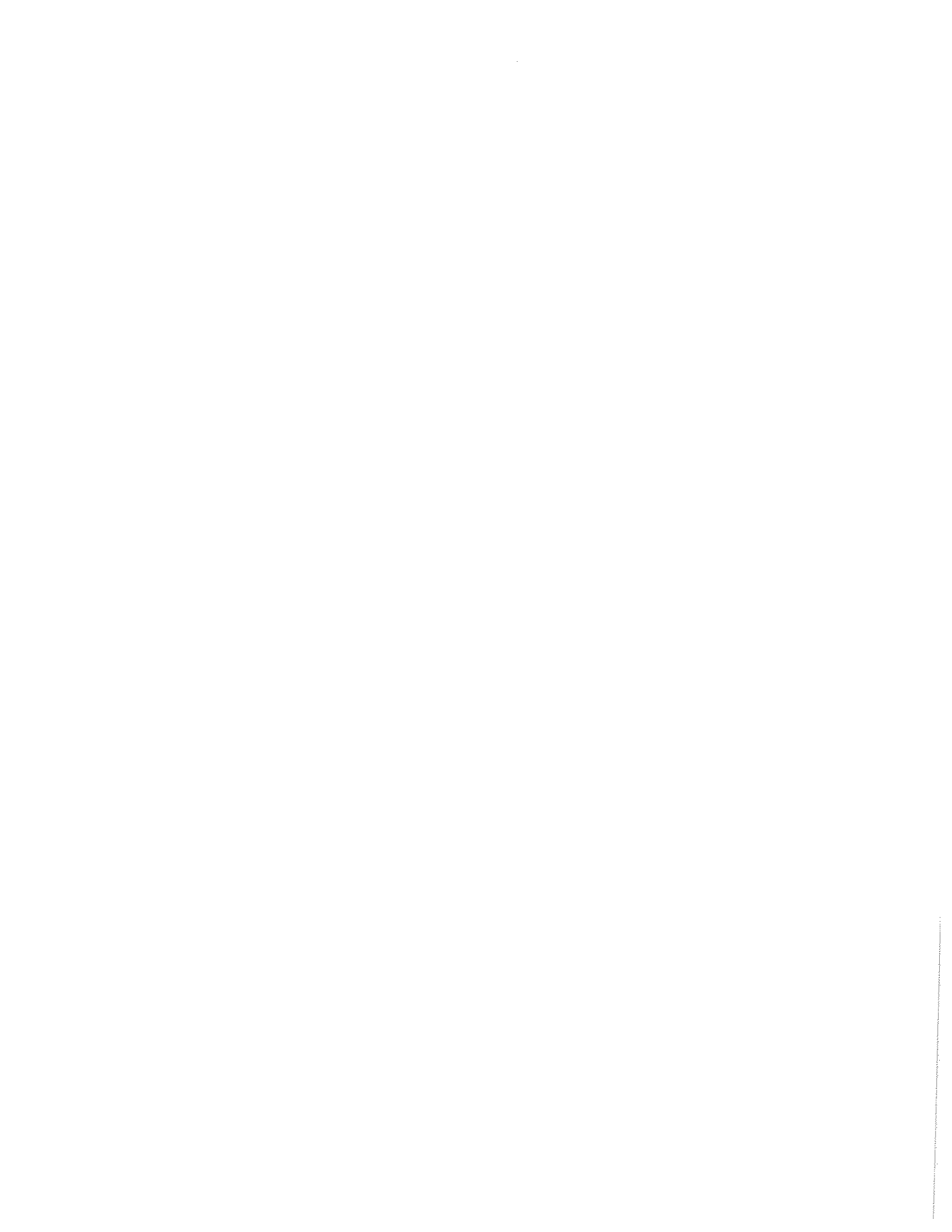


Photo 4-2: View of Sandblasted Sleeves and
Tube Surface in Buckled Area of
Specimen P1-C1 before Epoxy Repair.



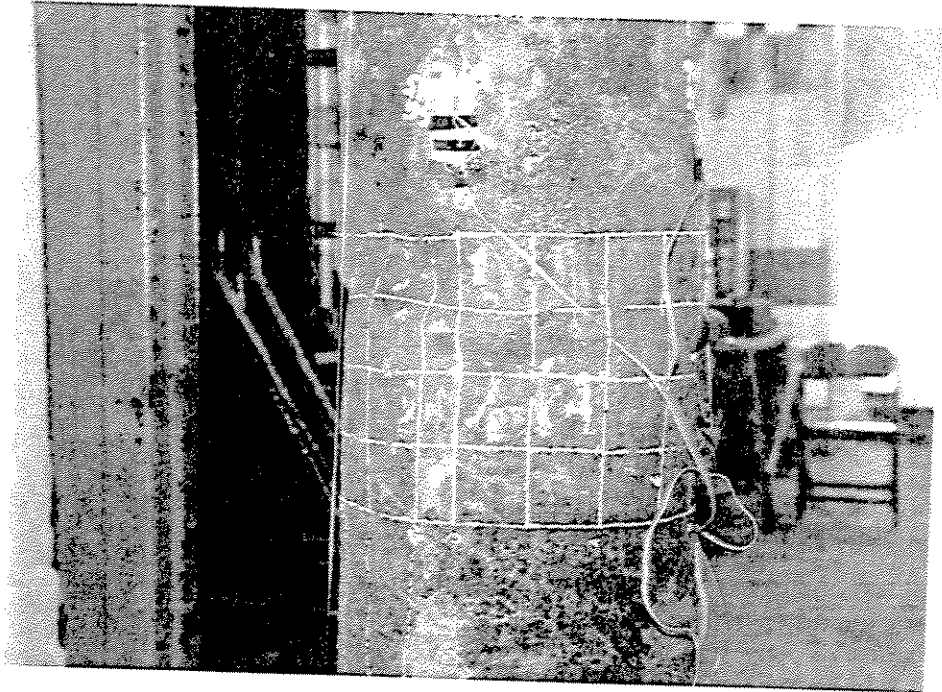


Photo 5-1: View of Local Buckles in Area 'E' for Specimen P2-C1.

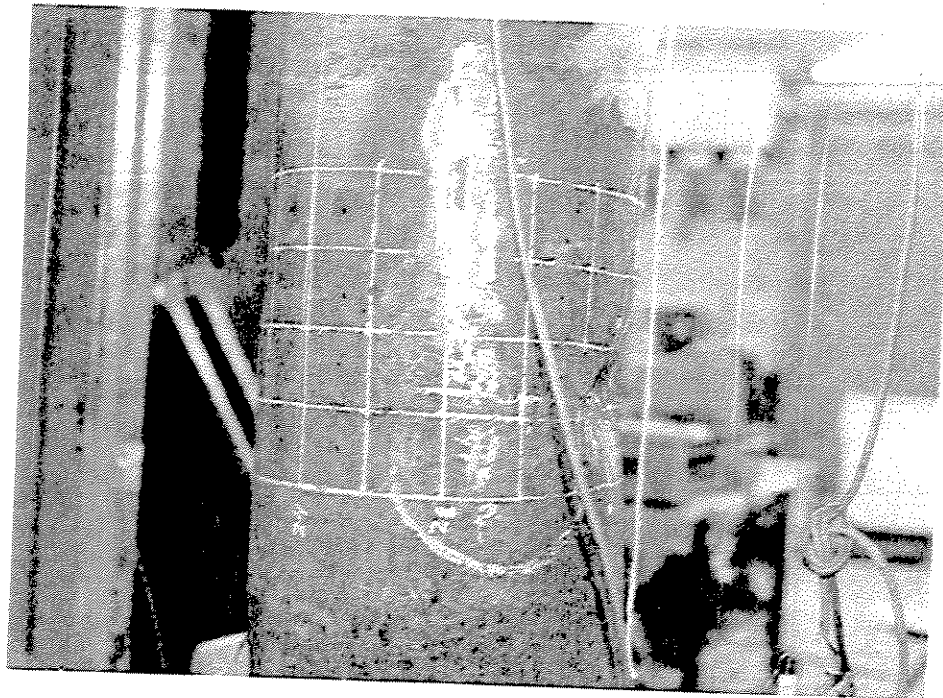


Photo 5-2: View of Local Buckles in Area 'C' for Specimen P3-C1.



Photo 5-3: View of Local Buckles in Area 'B' for Specimen P1-C1.



Photo 8-1: 'Lathe' Method for Diameter Measurements of Specimens P8 to P15

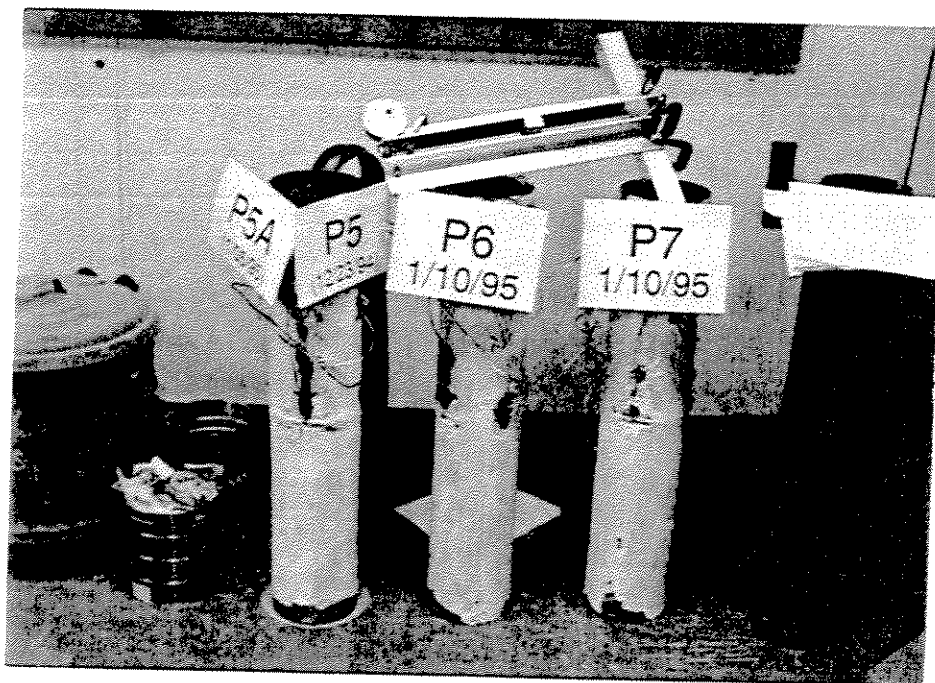


Photo 9-1: Specimens P5 (P5A), P6 and P7 after Testing and the Fork Tool for Measuring Depth of Patch

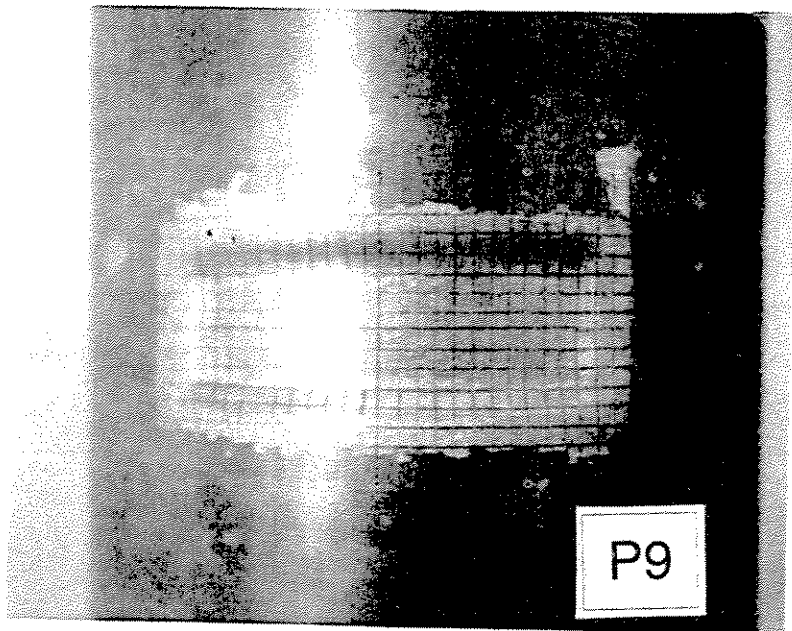


Photo 9-2: Grid for Final Thickness Measurements in Specimen P9

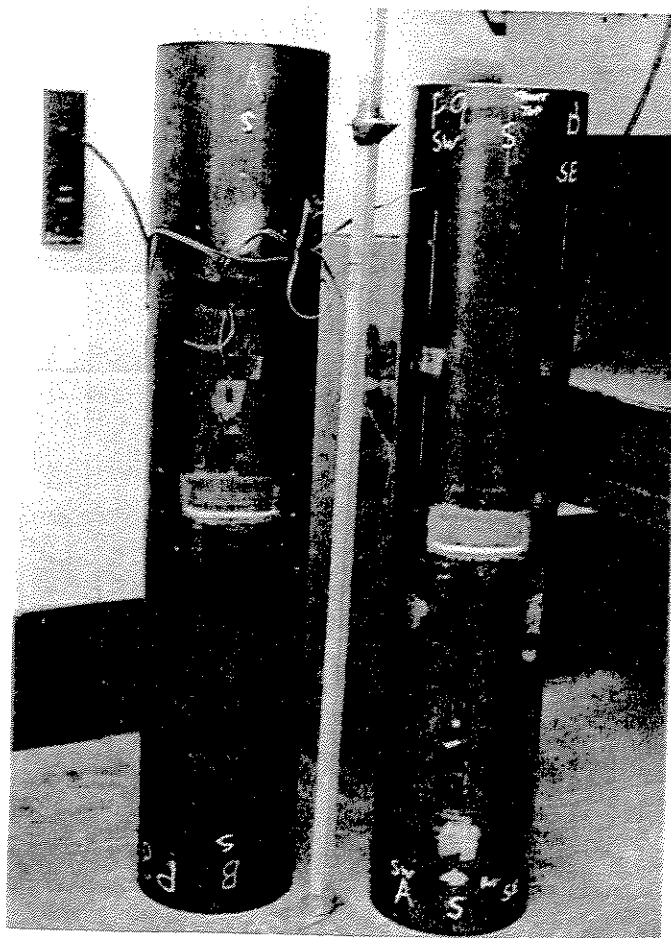


Photo 9-3: Specimens P8 and P9 after Completion of Corrosion Patches

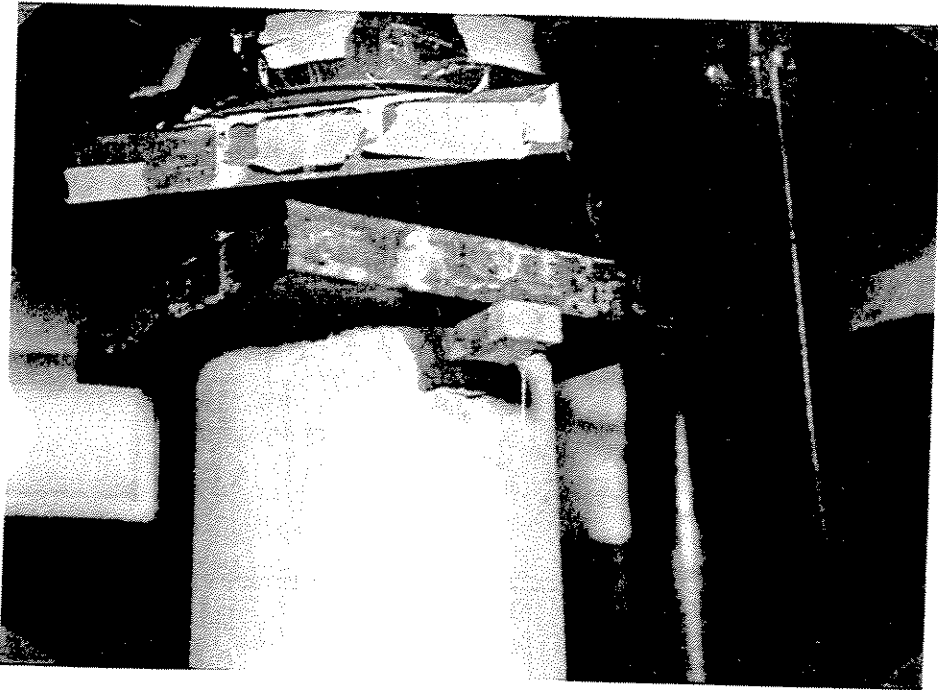


Photo 10-1(a): Arrangement of Cylindrical Bearing
Fixture at the Top

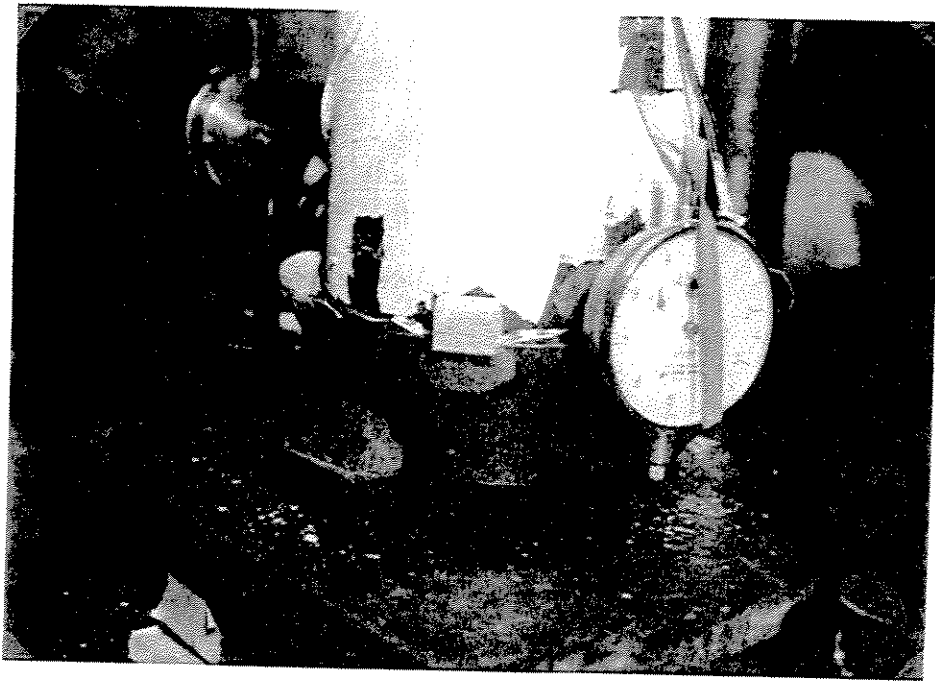


Photo 10-1(b): Arrangement of Cylindrical Bearing
Fixture at the Bottom

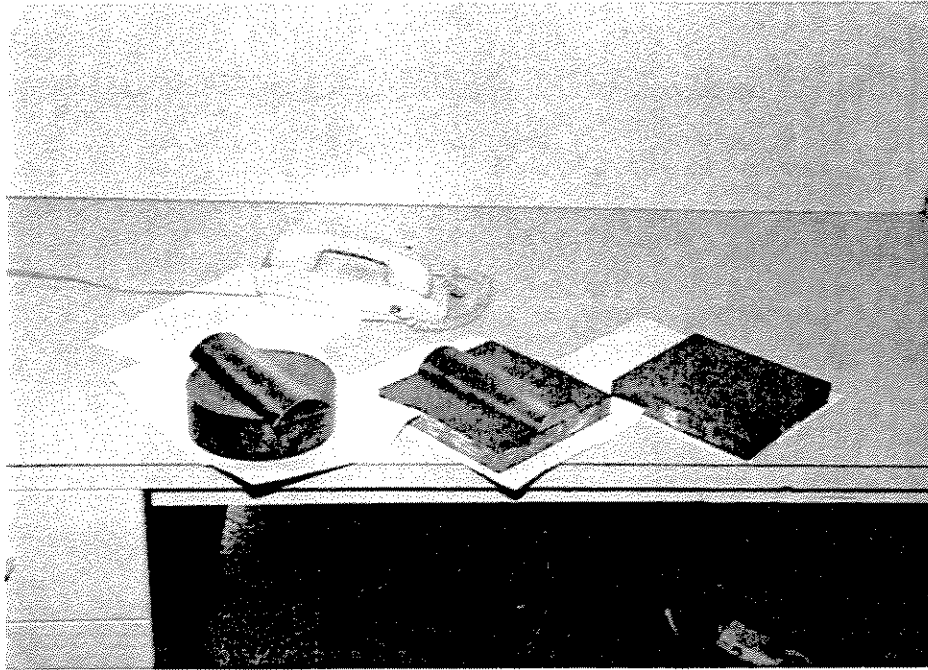


Photo 10-2: Principal Components of Cylindrical Bearing Fixtures

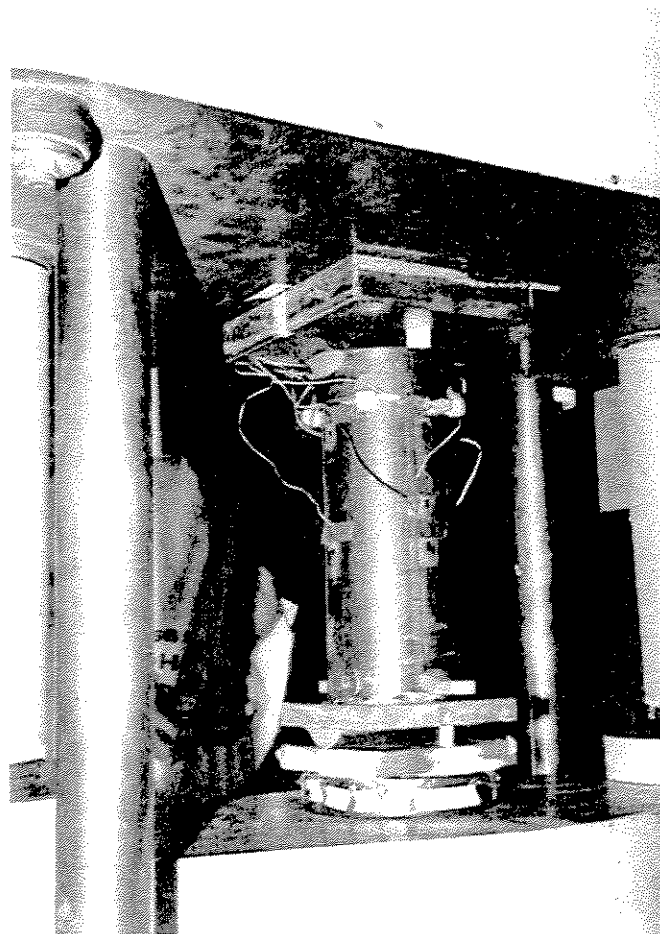


Photo 10-3: Specimen with Cylindrical Bearing Fixtures (P13) Ready for Connecting Instrumentation

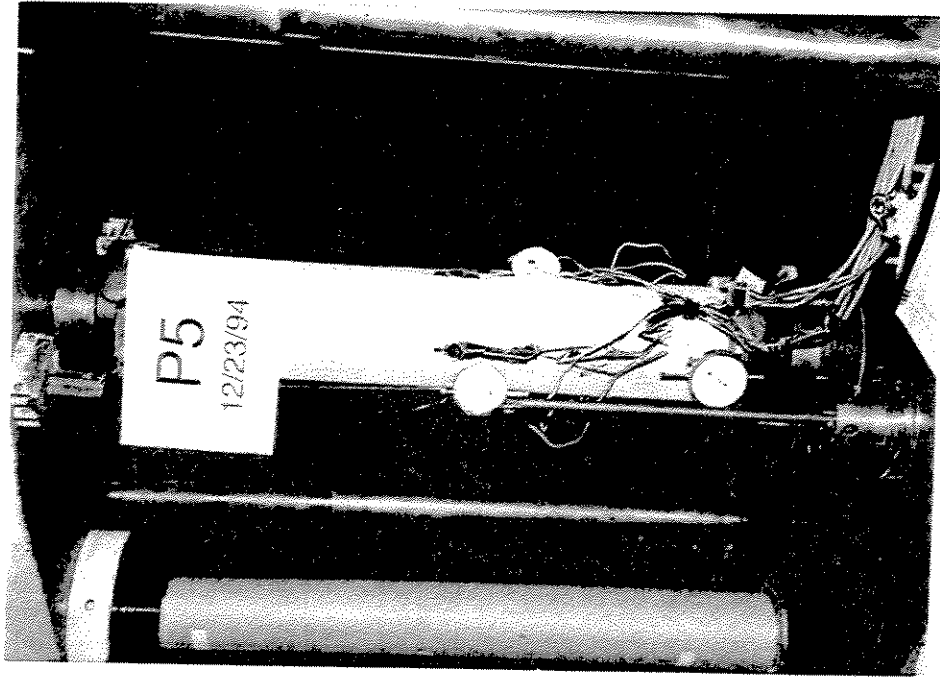


Photo 10-4: Specimen P5 Ready for Testing

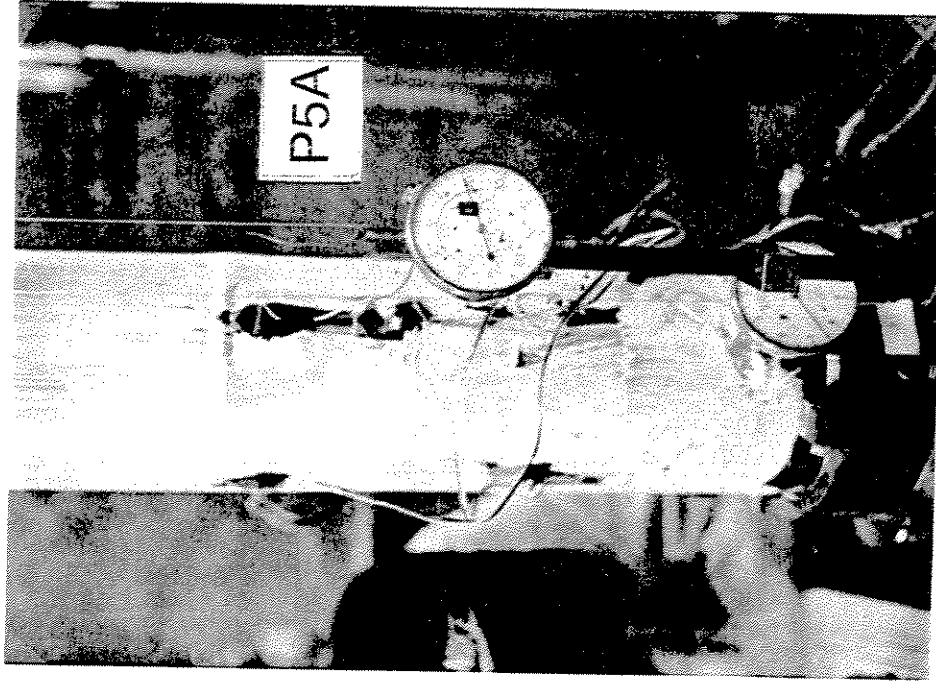


Photo 11-1: Specimen P5A with a Local Buckle in the Patch before Testing

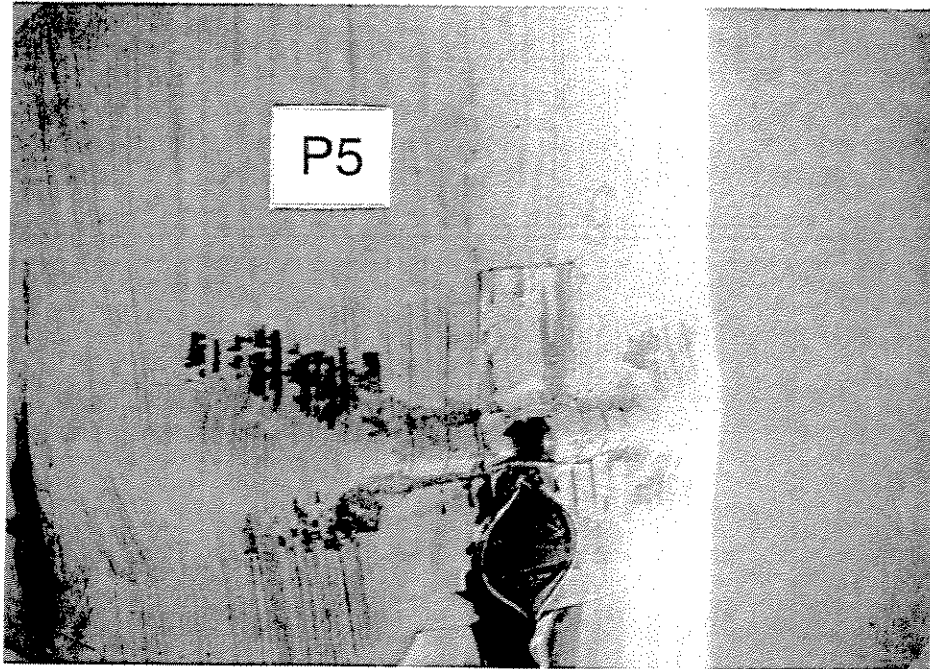


Photo 11-2: Final Local Buckle in the Patch of Specimen P5 (P5A)

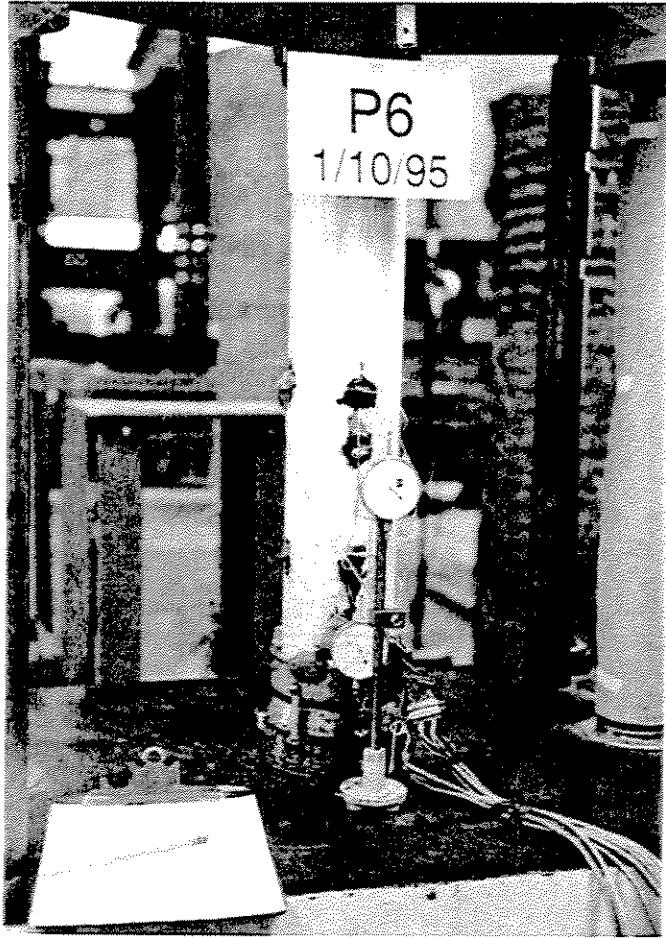


Photo 11-3: Specimen P6 before Testing

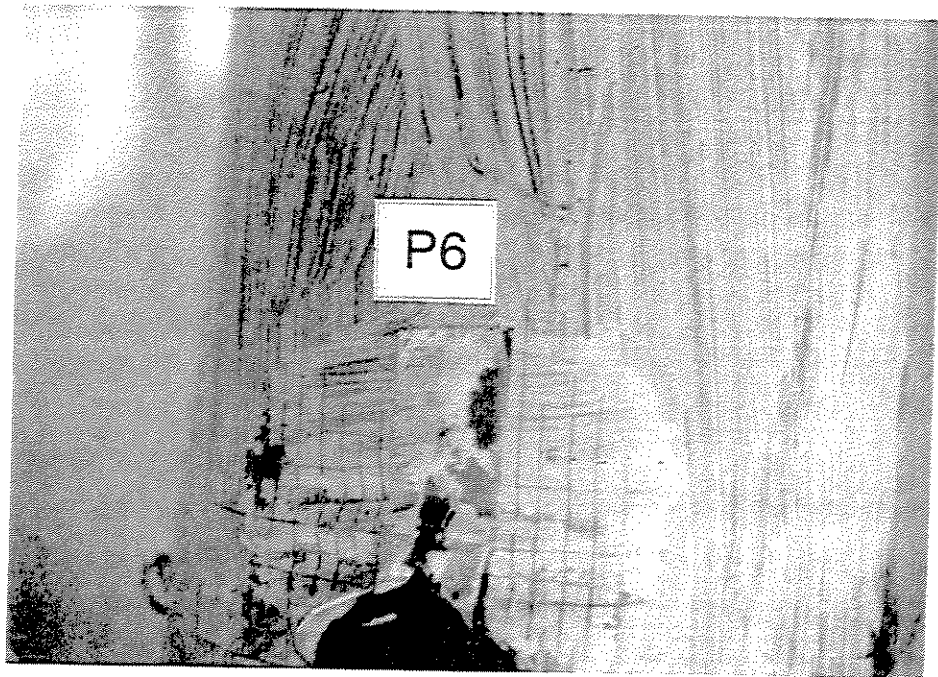


Photo 11-4: Final Local Buckle in the Patch of Specimen P6

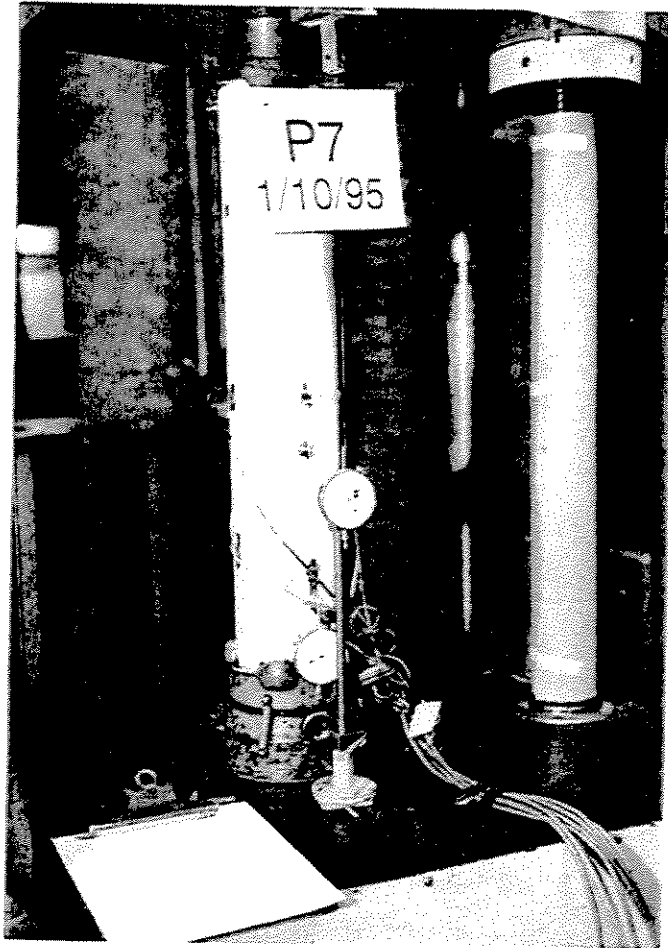


Photo 11-5: Specimen P7 before Testing

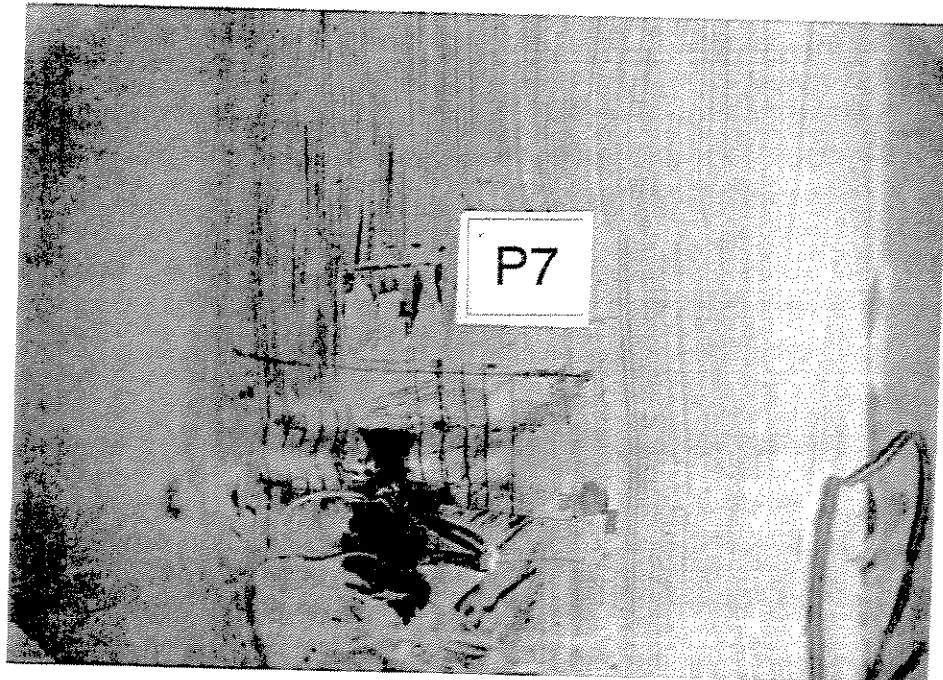


Photo 11-6: Final Local Buckle in the Patch of Specimen P7

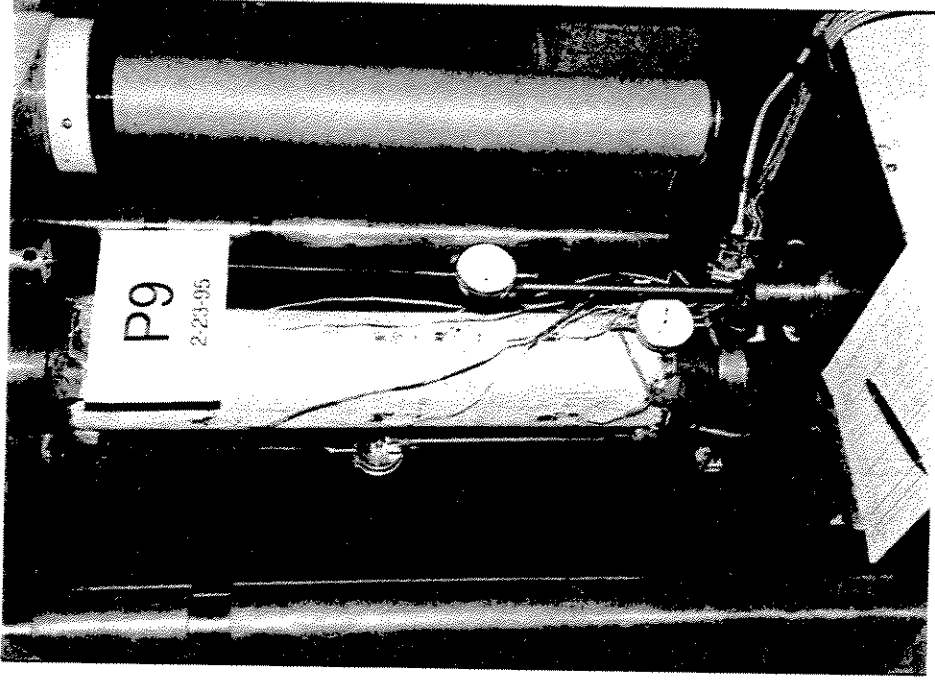


Photo 11-8: Specimen P9 before Testing

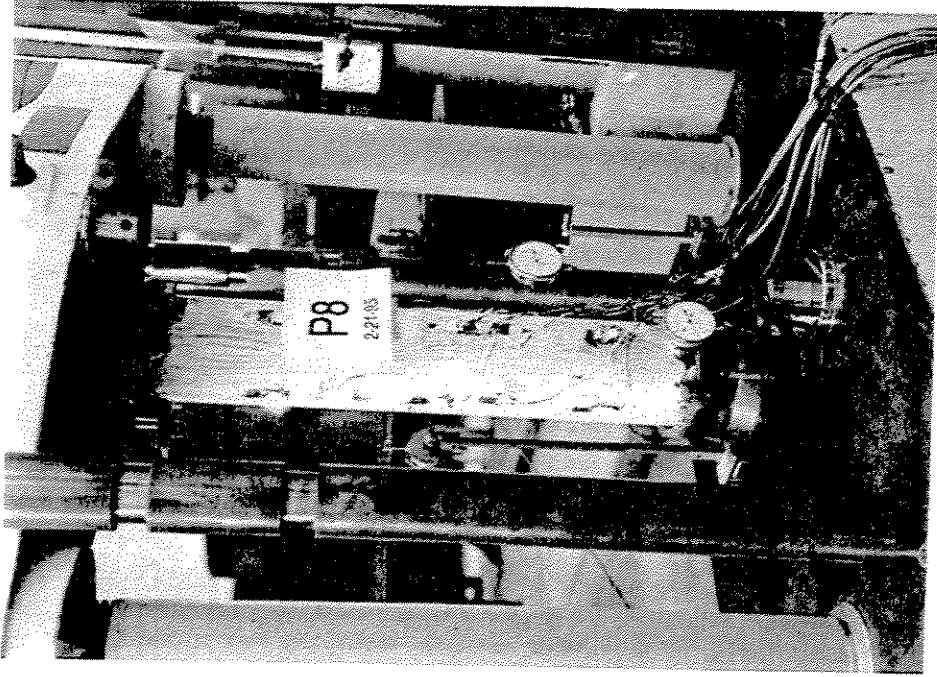


Photo 11-7: Specimen P8 during Testing



Photo 11-9: Final Local Buckle in the Patch of Specimen P10

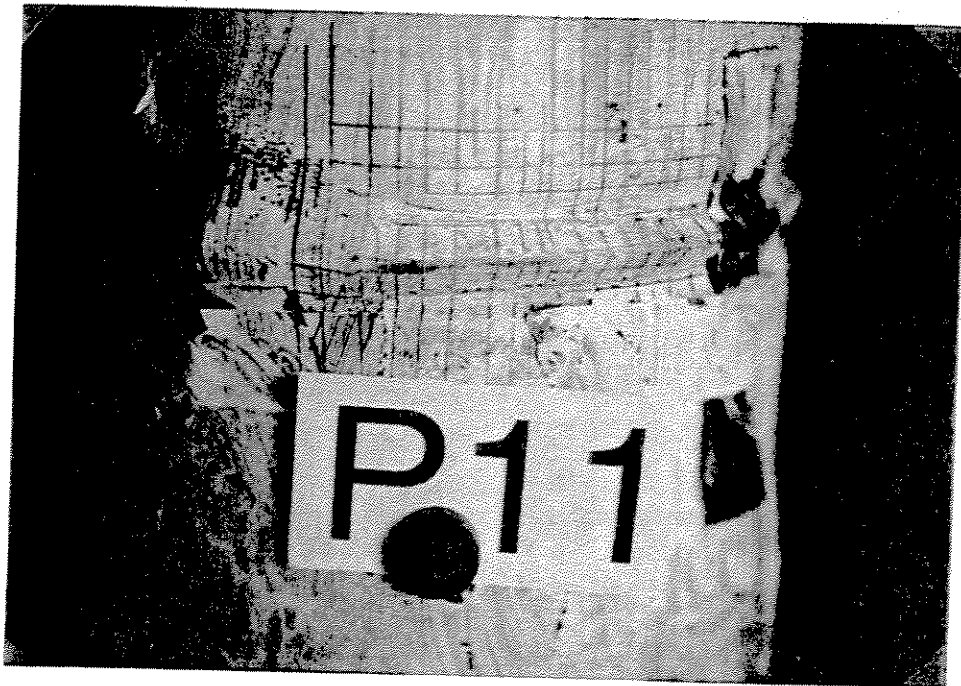


Photo 11-10: Final Local Buckle in the Patch of Specimen P11

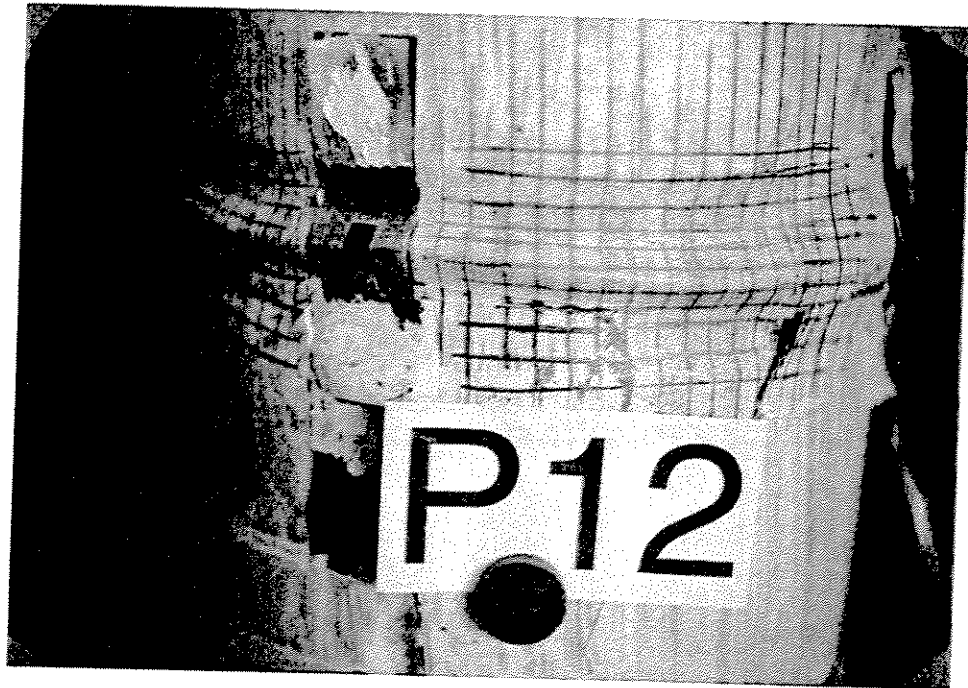


Photo 11-11: Final Local Buckle in the Patch of Specimen P12

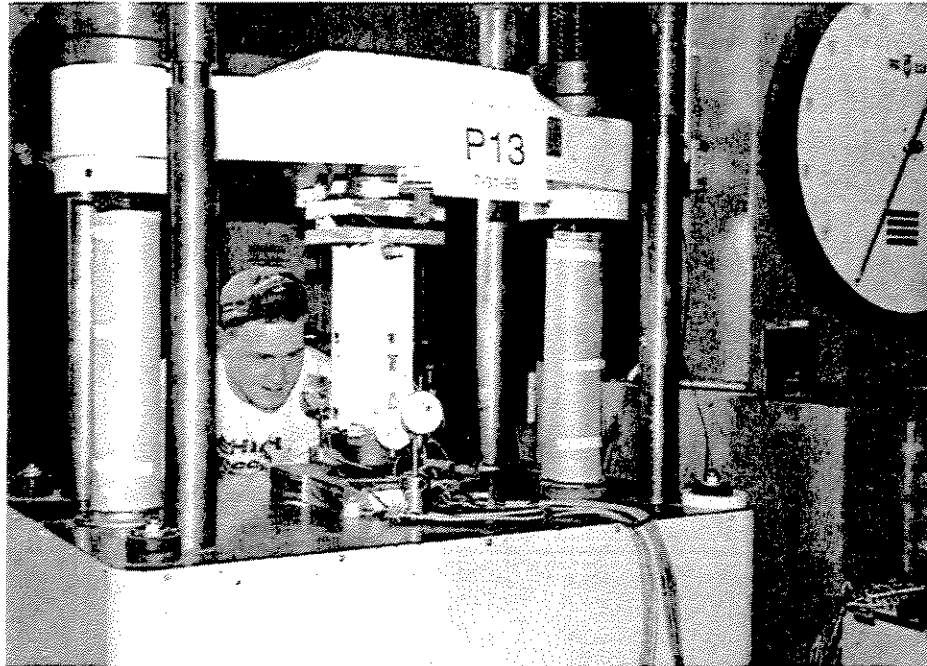


Photo 11-12: Specimen P13 during Testing

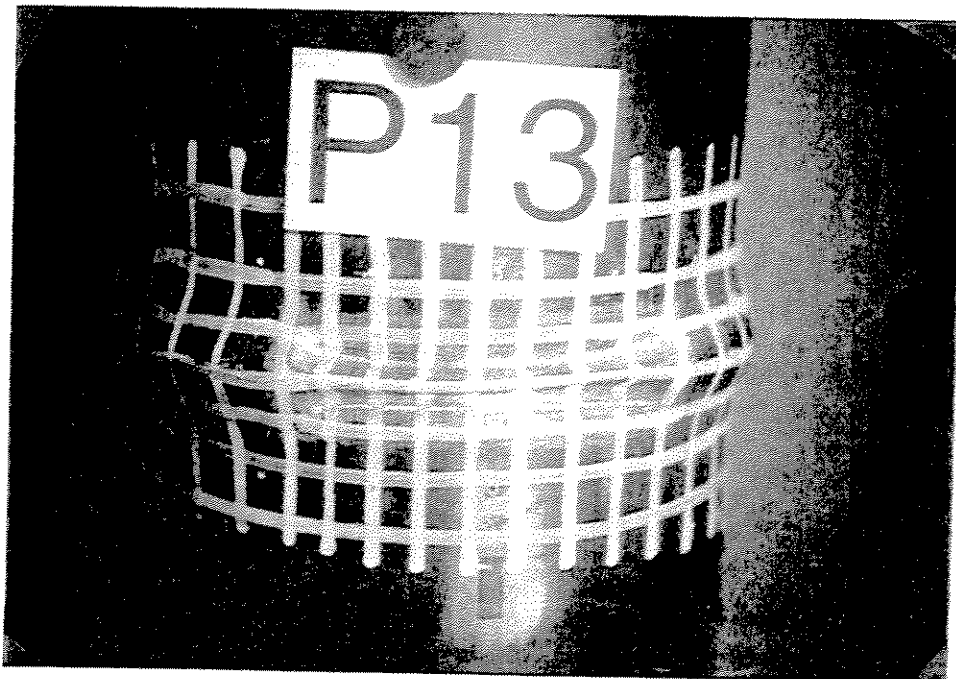


Photo 11-13: Final Local Buckle in the Patch of Specimen P13

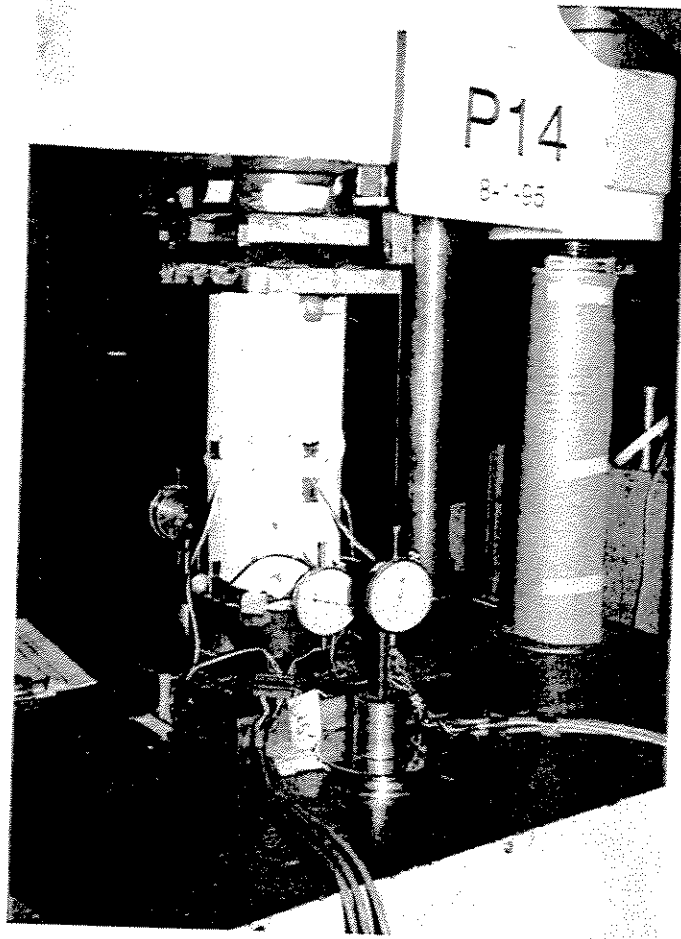


Photo 11-14: Specimen P14 after Testing



Photo 11-15: Final Local Buckle in the Patch of Specimen P14

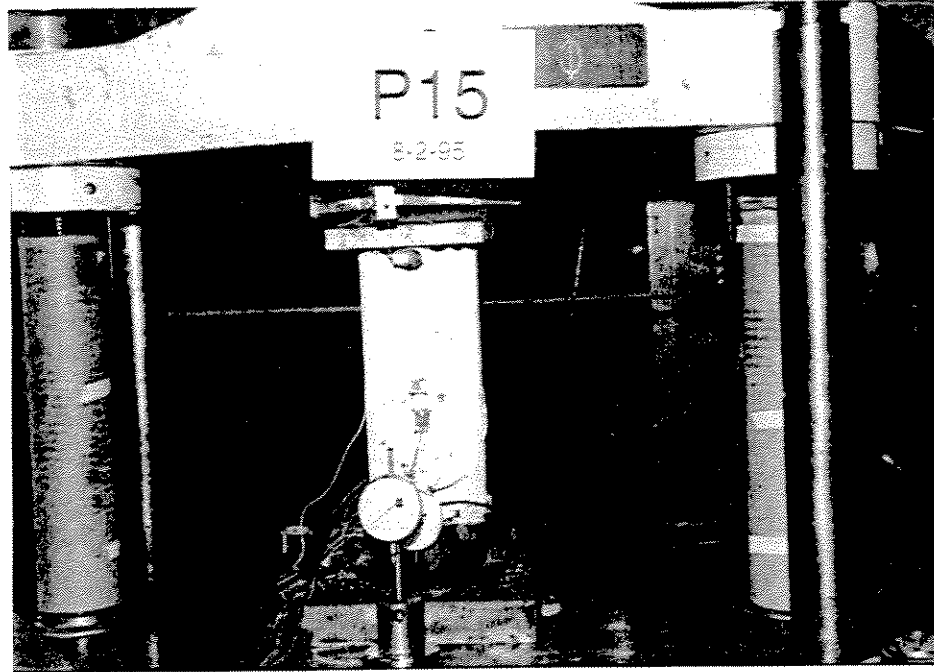


Photo 11-16: Specimen P15 before Testing



Photo 11-17: Final Local Buckle in the Patch of Specimen P15

APPENDIX A. FORTRAN-77 PROGRAM CXS.for

(CXS stands for Corroded Cross (X) Section)

A1. Introduction

The FORTRAN-77 program CXS.for was written for computing the cross-sectional properties and strength of corroded tubular circular sections with the thickness varying linearly between N points around the circumference.

The load capacities (strength) are computed for the following limiting states:

- 1) First yielding at the point of maximum stress, P_{yld} .
- 2) Local buckling in the area of smallest thickness according to the API specification, P_{api} [3].
- 3) Local buckling in the area of smallest thickness according to the DnV specification, P_{dnv} [4].
- 4) Ultimate ("Design") load according to the proposed formula, P_{des} [Eq. 15-24].
- 5) Ultimate load according to the proposed formula for pin-ended members, P_{pin} [Eq. 15-23a].

The procedure of the computer program is shown by the flow chart in Sect. A5 and the code is listed in Sect. A6.

A2. Input

The first step in running the program is to input the data, and this can be done either from the keyboard or from an external data file¹. If the data file is used, it has to be

¹Also, a sample set of input data is built into the program in order to facilitate the learning process.

properly formatted (an example is shown in Sect. A2.3). For keyboard entry, the program provides prompts and sample input values.

A2.1 Input Units

The units for angles can be either degrees or radians. (If the value of the largest angle of the input is less than $6.3 (\approx 2\pi)$, the angles are considered to be in radians.)

Other units should be consistent, therefore:

- a) inches, kips (load) and ksi (stress)
- or b) mm, Newtons (not kN, load) and MPa (stress).

A2.2 Input from Keyboard

The input procedure from the keyboard is as follows:

1. Section/Specimen name.
2. Flag to indicate the type of units used: **C** for "customary" - U.S. or **M** for "metric" - S.I.
3. Inside radius of the section.
4. N_p which is the sequential number of the point at which the thickness is the smallest, thus, a potential location of local buckling.
5. N which is the total number of points where thickness is given.
6. The angle to each of the N points measured clockwise in radians or degrees from the upward y -axis of the section with respect to the center of the circle.
7. The thickness at each of the N points.
8. The distances to the point of load application in the x and y directions, that is, load eccentricities e_x and e_y . If the load is not applied eccentrically, zero must be entered for both.

9. Ultimate test (or FE) load if available. If the load is not known, a value should still be entered, and the program suggests 100.
10. Yield stress.
11. Adjusted-thickness-ratio, TATP, which is the average thickness over a portion of the circumference which includes the point of minimum thickness and is estimated to be sufficient to develop a local buckle (usually 0.8 of the inside radius). The value would normally be from 1.0 and up. To use the default value of 1.05, a zero value is entered.

A2.3 Input from External File

The input items in an external file are arranged in the same sequence as for the input from the keyboard except that the flag (Item 2) is put as the last item. The section name (first item) and the flag (last item) should be in single quotes, and individual items on a line should be separated by a comma or a blank space(s). The sample input file shown below is put in four lines.

Line 1 gives items (1) to (4) of the keyboard input listing.

Line 2 contains the N angle values. If necessary more lines can be added to list the angles when they do not all fit on one line.

Line 3 contains the N thickness values corresponding to the angles on Line 2. As for Line 2, more lines may be needed to list thickness for all points.

Line 4 has the load eccentricities, e_x and e_y , the test load, the yield stress, the TATP value, and the flag for the type of units ('C' for Customary U.S., 'M' for Metric - S.I.).

Sample Input File

```
'P3B-10K', 4.9998,1, 10
0. 0.944 1.272 1.792 2.082 2.544 3.064 4.038 4.279 5.657
0.161 0.282 0.256 .264 .327 .357 .353 .347 .286 .220
0. 0. 275. 40.89 1.05 'C'
```

A3. Output

The output is given in several ways:

- 1) To the screen only.
- 2) To the screen and to a separate external output file for each set of input data.
- 3) To the screen for each set of input data and to an external cumulative output file which tabulates the principal results for several sets of input data, one set per line.

A3.1 Output Units

The angles are output in degrees and the remaining output is again in consistent units:

- a) inches (centroid, area, moments of inertia), kips (loads),
- or b) mm (centroid, area, moments of inertia), kN (loads).

A3.2 Output to Screen and Separate File

The output to the screen and separate file gives the following:

1. Name of section, inside radius, N_p and N .
2. The distances to the centroid from the center of the circle, X_c and Y_c .
3. Net area and Gross area ($A_g = \pi (2 R_i + t_{max}) t_{max}$).
4. Moments and product of inertia: I_x , I_y and I_{xy} .
5. Stress amplification factor K_p at $T_{min} = T_p$ at mid-thickness.
6. Principal moments of inertia I_{maj} and I_{min} .
7. Angle to the major principal axis (CW from the upward y-axis), Z_{maj} [degrees].

8. The angle and the stress amplification factor, Z_{max} and K_{max} , for the point of maximum stress on the outside surface.
 9. $f = (P_{test}/A * K_p)/F_y$ which is the stress in the patch due to the test load P_{test} divided by the yield stress.
 10. $D/T_a = D/T_{adj}$, the ratio of the diameter to the adjusted thickness in the patch. This is the slenderness parameter for computing the local buckling stress according to the API and DnV specifications.
 11. The local buckling stresses according to the API and DnV specifications divided by the yield stress.
 12. The load for first yielding at the point of maximum stress, P_{yld} .
 13. The ultimate loads that would cause local buckling according to P_{api} and P_{dnv} .
 14. The ultimate DESIGN load according to the proposed formula, P_{des} .
 15. The ultimate load according to the proposed formula for pinned ends, P_{pin} .
- Finally, the program asks the user if there is another section to analyze.

A sample output for the input example of Sect. A2.3 is given below.

Sample Output File

```

Specimen: P3B-10K      , R= 4.99980      , Np= 1, N= 10
                Xc=  0.06276
                Yc= -0.76764
A (Net Area)=  8.98255      Ix=  114.071
AG(GrossArea)= 11.6154      Iy=  118.386
Ta/Tp=1.050000      Ixy=  1.73819
Principal Moments of Inertia and the angle to
the major principal axis (CW from upward y-axis)
                Imaj= 118.999
                Imin= 113.458
                Zmaj=160.57148
Amplification factor at Tmin=Tp, Kp= 1.35435
Angle and ampl fact for max stress: Zmax= 353.62345  Kmax= 1.36117
f=(Ptest/A*Kp)/Fy=1.014 D/Ta= 61.152 Fapi/Fy=0.9968 Fdnv/Fy=0.9942

```

Test Load= 275.000
Ld for first yieldng at pnt of max stress, Pyld= 269.839
Load according to API Specification, Papi= 270.335
Load according to DnV Specification, Pdnv= 269.614
Load acc to propos formula, DESIGN recomm Pdes= 246.232 (Note,an>=0.65)
Load acc to propos formula, pinned ends Ppin= 202.464 (Note,an>=0.65)

A3.3 Output to Screen and Cumulative File

The cumulative output file can be made in either of two formats: Long format and Short format. In both cases the file is arranged so that it can be directly imported into a spreadsheet (QuattroPro or Lotus 1-2-3).

The Long format lists the following on one line:

Section/Specimen name, Area, I_x , I_y , I_{xy} , Stress Amplification factors for the patch and maximum stress: K_p and K_{max} , and loads P_{yld} , P_{api} and P_{des}

However, the Long format provides the listing only when the values are in the hundreds, thus, it is suitable mainly when the units are inches, kips, and ksi (not mm, kN and MPa).

The Short format lists the name of the Section/Specimen and the six ultimate loads, and it has enough space for using the metric (S.I.) units.

A4. Special Cases

A4.1 Sections with a Hole or Holes

The special case of sections with a hole(s) is readily analyzed except that the loads controlled by local buckling are not given since they cannot be computed.

A4.2 Undamaged Sections

When the section is undamaged, that is, all values of thickness are the same, the computer will display the following message on the screen:

NOTE:

The section is centrally symmetrical, that is, the moments of inertia about any centroidal axis are the same and the product of inertia is equal to zero, $I_{xy} = 0$.

This message IS NOT saved in the output file!

Information of the final results of the solution will be shown in the same arrangement as for other cases, both on the screen and in the output file.

A4.2.1 Load Applied at the Center

When the load is applied at the center, the properties can be obtained by specifying the angles and the same thickness at some two (or even one) arbitrary points. The message shown above will be followed by another message:

NOTE:

Stresses in the section are uniform and, thus, $K_m = 1.0$. Z_m is set to Z_P and $T_m = T_P$ to indicate the location of potential local buckling.

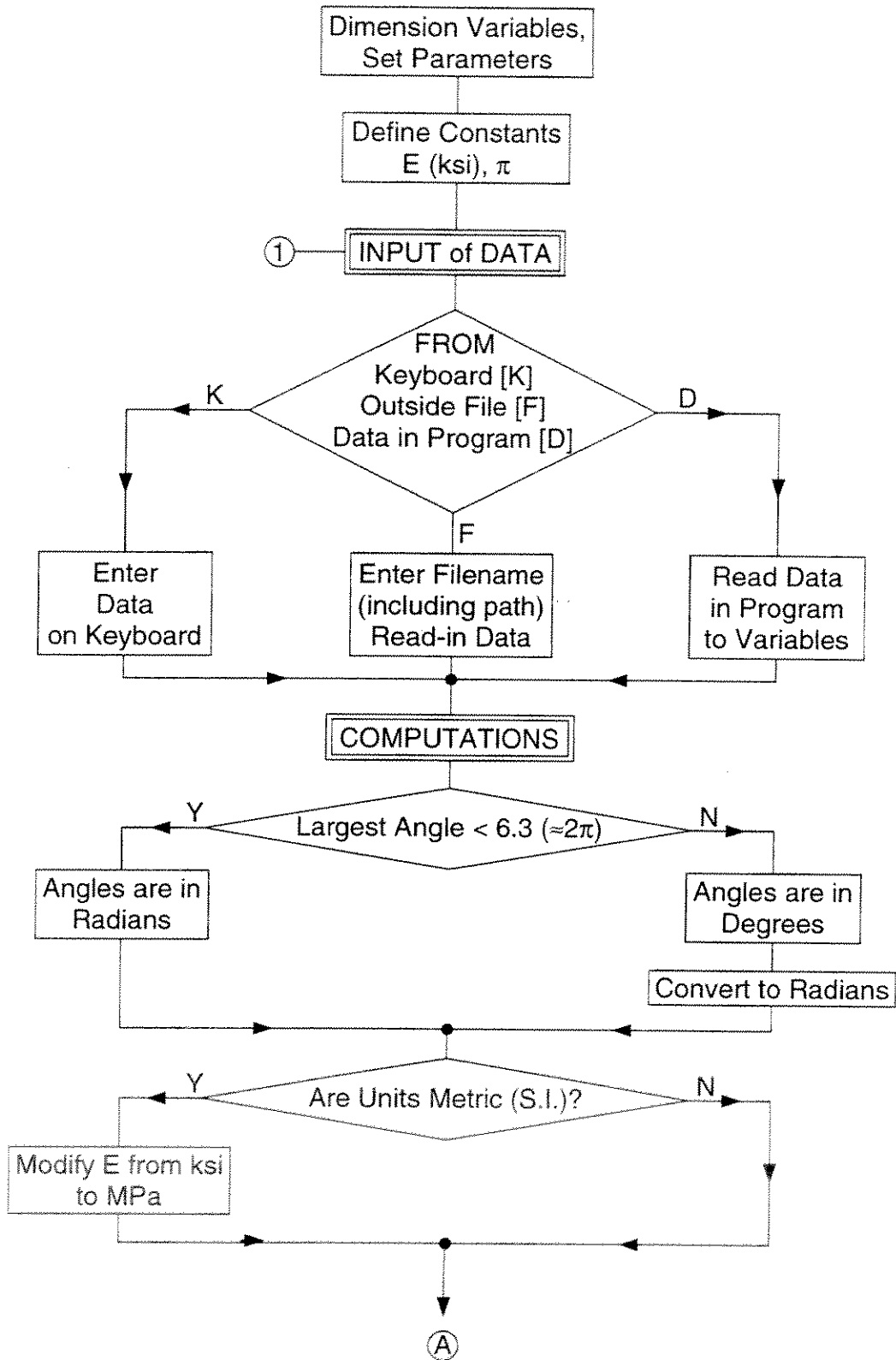
Again this message is displayed on the screen and is not put into the output file.

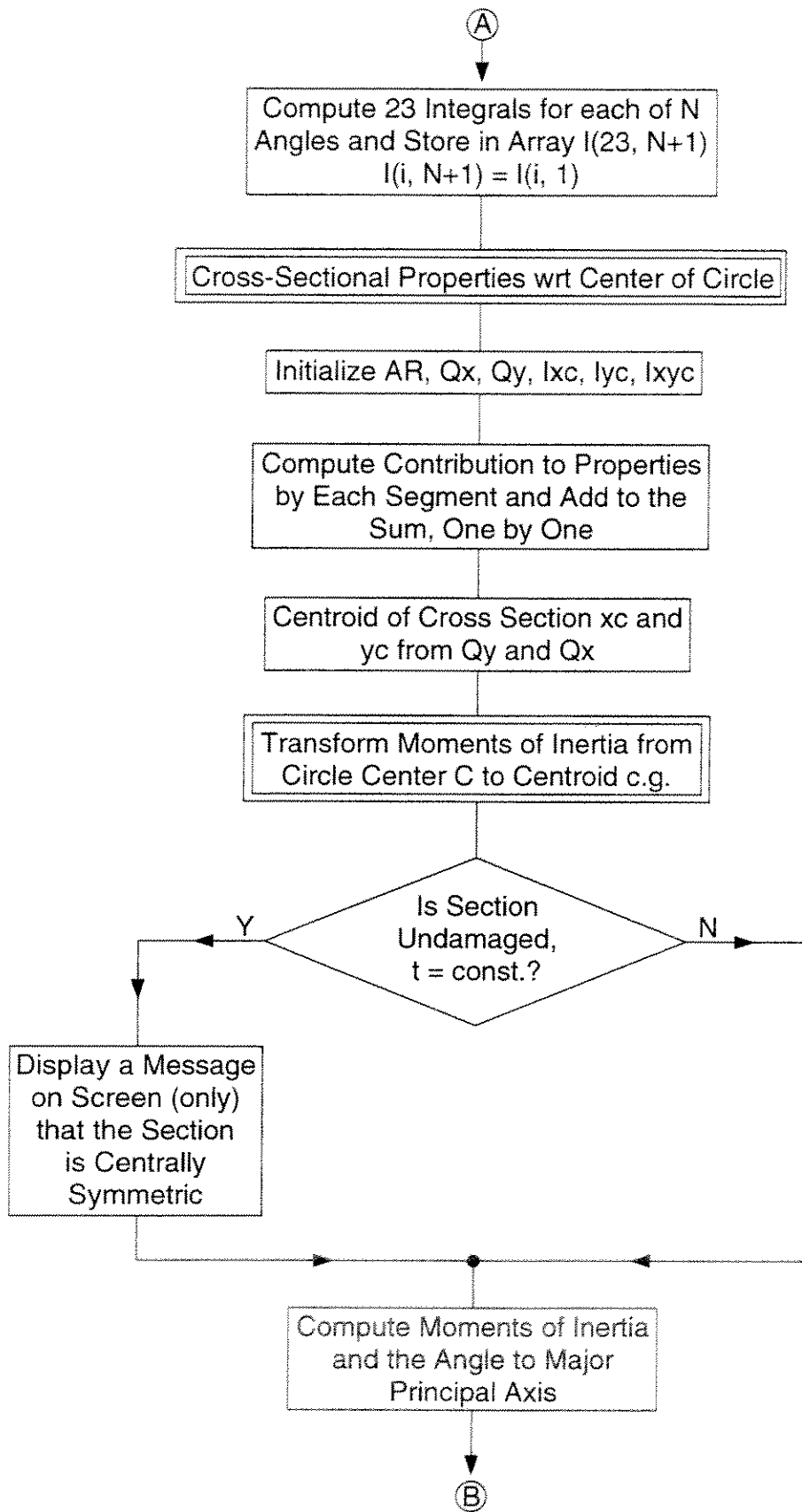
A4.2.2 Load Applied with Eccentricities e_x and e_y

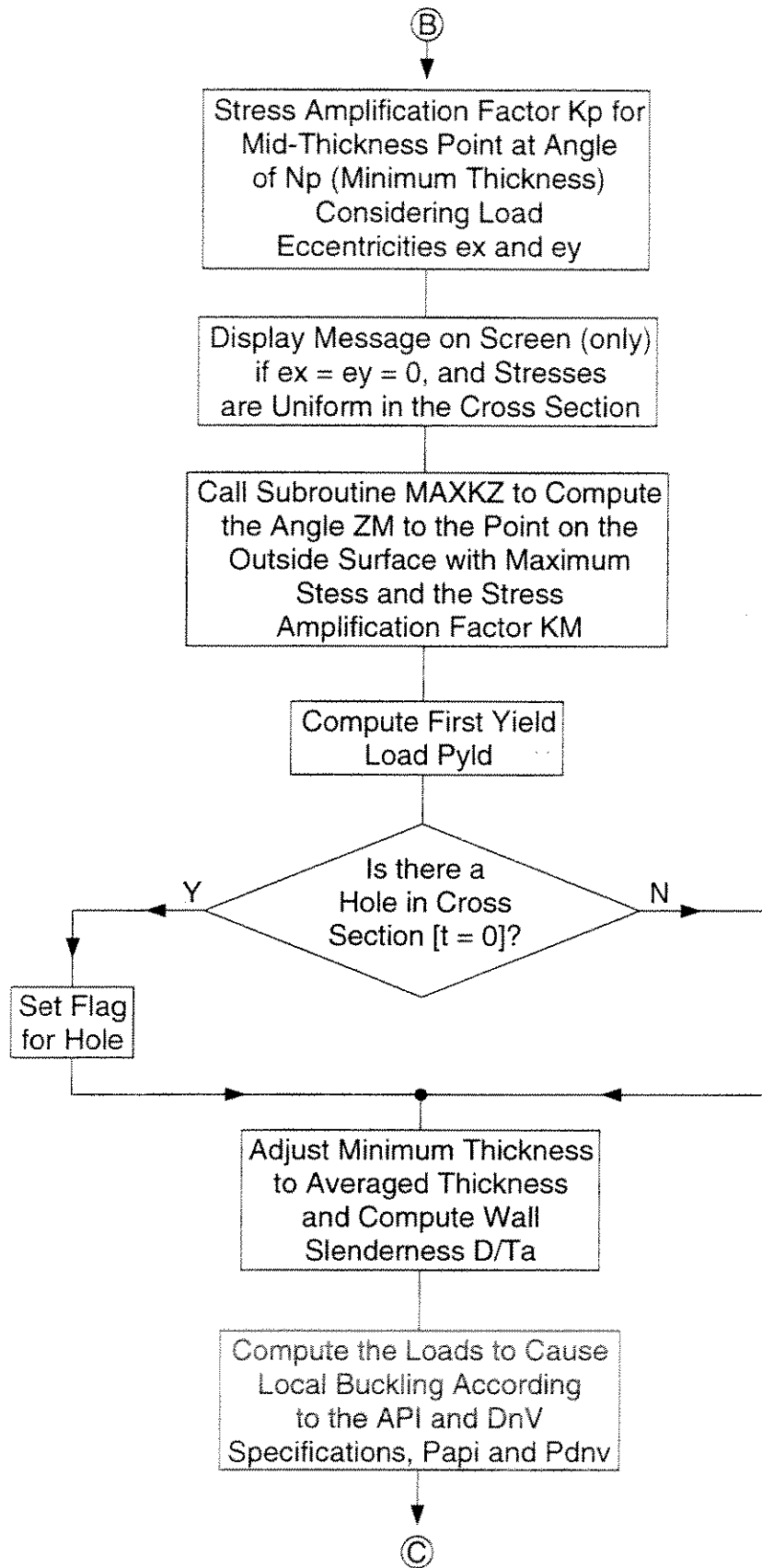
When the load is applied with eccentricities e_x and e_y , select some two diametrically opposite points, say at angles 0° and 180° , and use the given thickness at both. Run the program. Then, use the angle to the maximum stress as the assigned location for N_p (patch

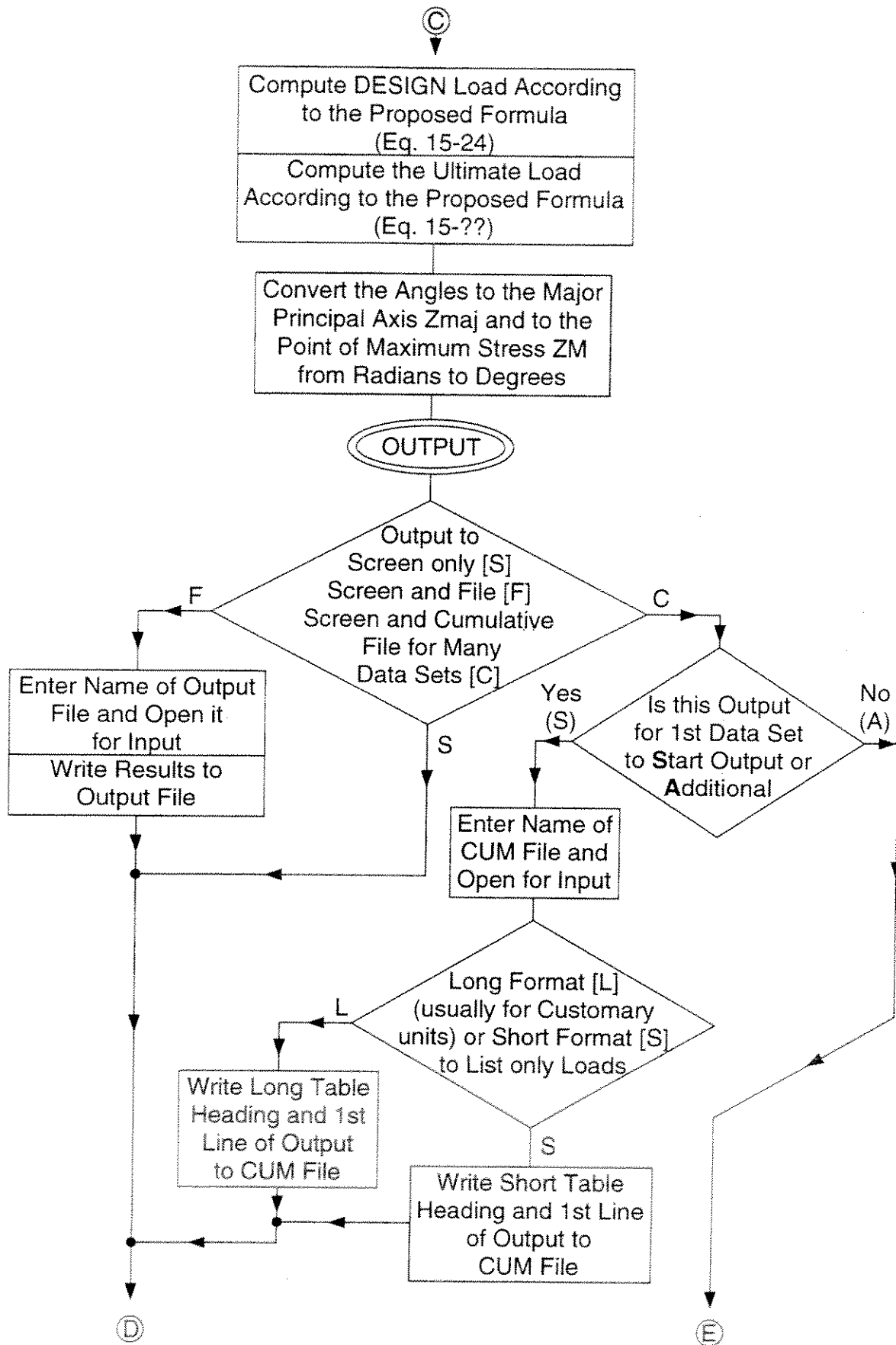
location) and some other angle approximately diametrically opposite to N_p (e.g., N_p angle + 180°) and re-run the program. The reason for re-running the program is that the initial selection would give the local buckling loads for the initial N_p point, not for the point of maximum stress.

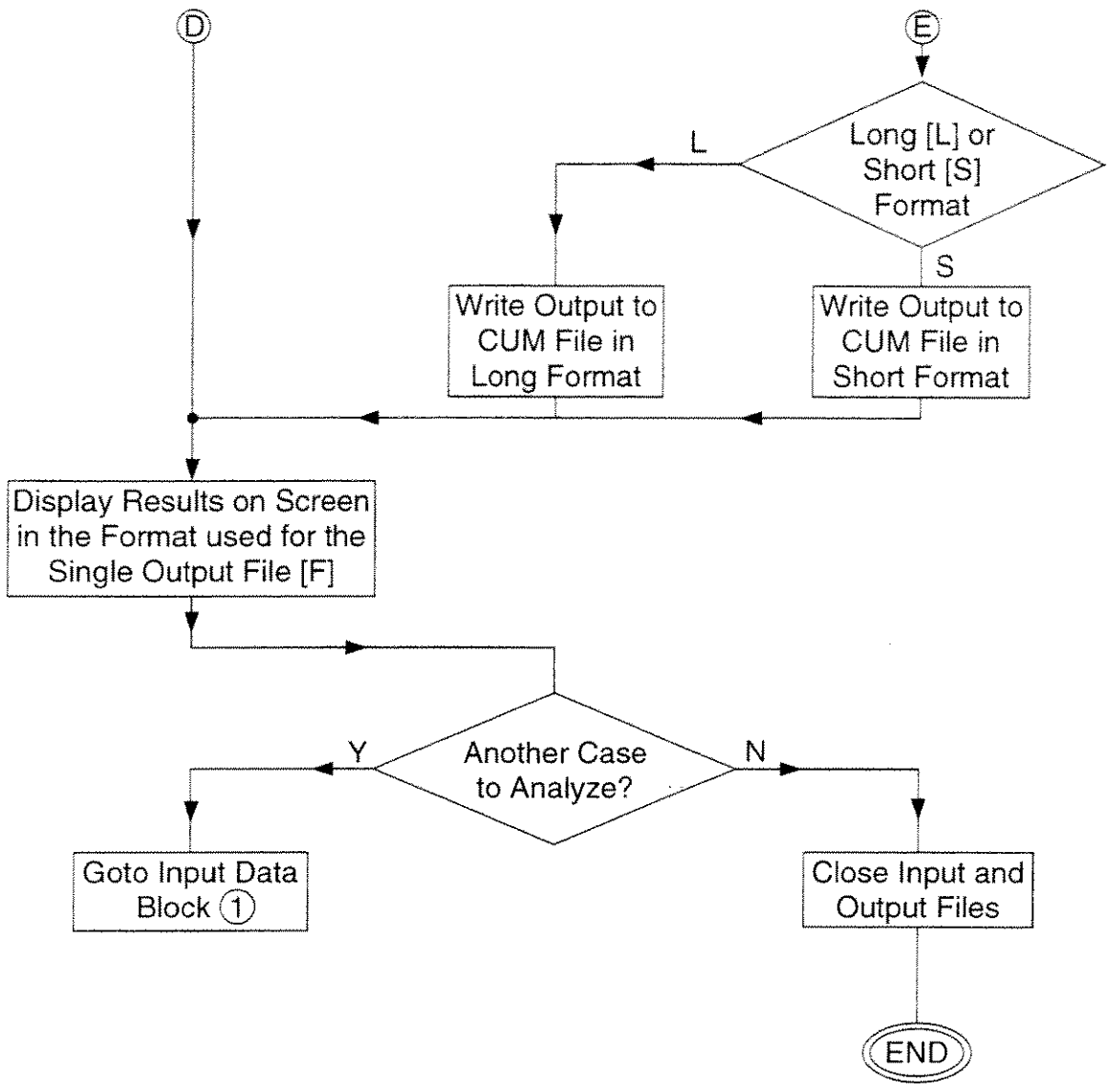
A5. FLOW CHART for Program CXS.for

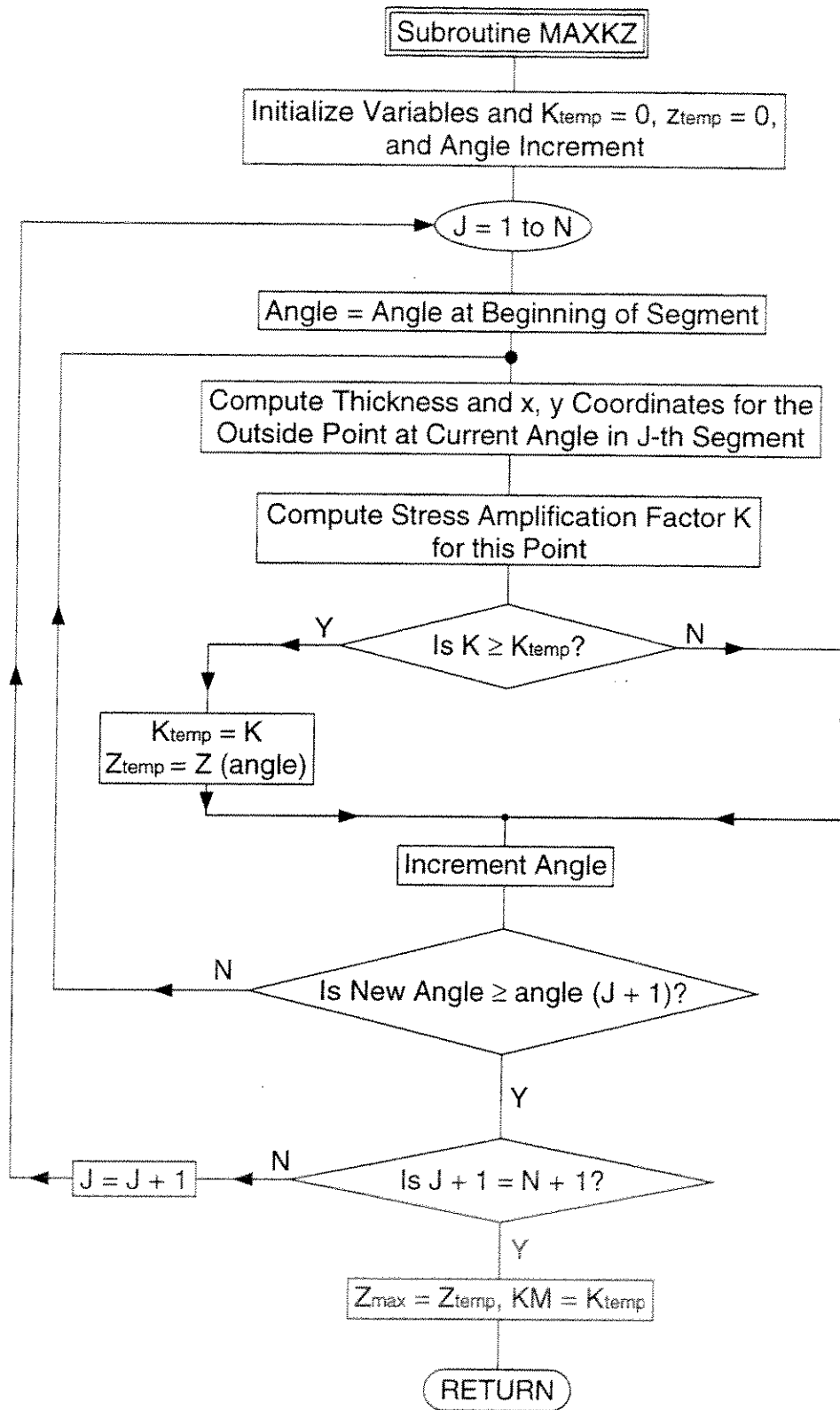












A6. Listing of Program CXS.for

```
PROGRAM CXS
* WF77 Program: Model X(Cross) Section Corroded Pipe
*   with N Thickness Parameters
*   by A.Ostapenko; 8294;3246;4256,4276,4306
*
* 3216; CXS.FOR fr.MXSL.for, some editing
* 3246; CXSa.FOR,fr.CXS, dele redundant material, edit
* 3276; CXSb.FOR,fr.CXSA,modify check on const thickness.Some editing.
* 4276,4256; CXSC.FOR,fr.CXSB,revise output to CUM file of SHORT format
* 4286; CXSD.for fr.CXSC, streamline decision logic.
* 4306; CXS.for renamed from CXSD.for, some editing
*
*           VARIABLES
* Character Variables
* FIN      File with input data
* FOUT     File for output of results
* FCOUT    File for cumulative output of several sets of input data.
* QIN, QOUT Question flags for input and output, respectively
* SPEC     Section or Specimen name
*
* Integer Variables
* J        Counter
* M        M=N+1
* N        Number of thickness values in cross section
* NP       Label for the point in corroded section with minimum thickness
* QH       Flag for presence of a hole in corrosion patch
*
* Double Precision Variables
* A,B      Constants for a particular segment
* AR,AG    Net or Gross cross-sectional area
* AN       Relative net area = AR/AG
* AQ,BQ,CQ,DQ Constants for Qx and Qy of a segment
* DT       D/t ratio wrt Tadj in corrosion patch
* EE       Modulus of elasticity (set to 29500 ksi)
* EX,EY    Load eccentricities wrt the center of the circle in x and y
*           directions, respectively
* I(1,J) to I(23,J) Values of 23 integrals for M ZZ(J) values. All stored
*           in M columns of the I(23,151) array.
* E,F,G,H,II Constans for Ix,Iy and Ixy of a segment.
* KP,KM    Stress amplification factors: Stress in patch, max stress in sect.
* IX,IY,IXY Moments of inertia wrt the centroid.
* IXC,IYC,IXYC Moments of inertia wrt the center of circle.
* PYLD,PAPI,PDNV,PDES,PPIN Loads for various capacity limits.
```

* T,TP,TATP Thickness:wall, patch, ratio of averaged adjusted to TP.
*

```
IMPLICIT DOUBLE PRECISION (A-Z)
COMMON T,ZZ
INTEGER J,M,N,NP,QH
CHARACTER*20 FIN,FOUT,FCOUT,QIN,QOUT,QC,QL,QR,SPEC,U
DIMENSION T(151),ZZ(151)
DIMENSION I(23,151)
PI=3.141592653589793D+0
```

* Modulus of elasticity in ksi, for SI units (MPa) modified later.
EE=29500D+0

```
PRINT*
PRINT*
PRINT 1
PRINT*, '          FORTRAN-77 Program   CXS.FOR'
PRINT*
PRINT*, ' Computation of Properties and Strength'
PRINT*, '   of a corroded tubular circular section using'
PRINT*, '   N segments (max 150) with linear thickness variation'
PRINT*, '(Loads to cause first yielding Pyld, Loads to cause local'
PRINT*, ' buckling according to API and DnV Specifications, and'
PRINT*, 'Lds accord to propsd formulas for DESIGN and pinned ends)'
PRINT*
PRINT*, '          by A. Ostapenko      March 1996'
PRINT*
PRINT*, '[Default adj. thickness for local buckling analysis is'
PRINT*, ' Tadj=1.05(Tmin=Tp), i.e, (Ta/Tp=TATP=1.05).]'
PRINT*, ' Other values of Ta/Tp are entered via the '
PRINT*, ' last but one numeric entry in input data.]'
PRINT 1
1  FORMAT(1X,71('*'))
```

***** INPUT OF DATA *****

```
3  CONTINUE
5  PRINT*
PRINT*, '      Is the data to be INPUT from:      KEYBOARD <K>'
PRINT*, '                                          an external FILE <F>'
PRINT*, '                                          or sample DATA (in this program) <D>?'
PRINT*
PRINT*, '      Enter the corresponding letter: '
PRINT*
READ (*,'(A)') QIN
IF (QIN.NE.'K'.AND.QIN.NE.'k'.AND.QIN.NE.'F'.AND.QIN.NE.'f'
+ .AND.QIN.NE.'D'.AND.QIN.NE.'d') THEN
```

```

PRINT*, 'YOU have ENTERED an INCORRECT LETTER, PLEASE RE-ENTER'
GO TO 5
END IF

```

```

IF (QIN.EQ.'K'.OR.QIN.EQ.'k') THEN
PRINT*, '    INPUT DATA FOR THE SECTION'
PRINT*
PRINT*, '    Enter Section/Specimen Name (w/o quotes):'
PRINT*, '    (Example: Sect1)'
PRINT*
READ(*, '(A)')SPEC
PRINT*
PRINT*, 'Indicate the system of units used by entering '
PRINT*, '    <C> for Customary U.S. (in.,kip,ksi)'
PRINT*, ' or <M> for Metric - S.I. (mm, kN, MPa).'
PRINT*, '    Enter C or M (w/o quotes!)'
PRINT*, '    (Example: C )'
PRINT*
READ (*, '(A)') U
IF (U.NE.'c'.AND.U.NE.'C'.AND.U.NE.'m'.AND.U.NE.'M') THEN
PRINT*, 'YOU have ENTERED an INCORRECT LETTER, PLEASE RE-ENTER'
GO TO 4
END IF
PRINT*
PRINT*, '    Enter the Inside Radius. (Example: 5.0)'
PRINT*
READ*, R
PRINT*
PRINT*, 'Enter the sequential counter Np of the angle for Tmin'
PRINT*, '    (Example: 1)'
PRINT*
READ*, NP
PRINT*
PRINT*, 'Enter N, the number of Thickness Values.(Maximum N=150)'
PRINT*, '    (Example: 5)'
PRINT*
READ*, N
PRINT*
PRINT*, 'Enter N Angle Values (in DEGREES or RADIANS, measured CW'
PRINT*, '    from upward vertical axis y)'
PRINT*, ' [Angles are assumed to be in Degrees, unless the largest'
PRINT*, '    value is less than 6.3. Then, angles are in Radians.]'
PRINT*
PRINT*, '    (Example:    0.4,2.5,4.,4.8,6.0)'
PRINT*
READ*(ZZ(J), J=1,N)

```

```

PRINT*
PRINT*, ' Enter N Thickness Values'
PRINT*, ' (Example:      0.1, .2, .18, .23, .1)'
PRINT*
READ*, (T(J), J=1, N)
PRINT*
PRINT*, ' Enter load eccentricities Ex and Ey measured'
PRINT*, ' from center of circle in x and y directions.'
PRINT*, '      (Example: 0.1, -0.15) '
PRINT*
READ*, EX, EY
PRINT*
PRINT*, ' Enter the ultimate test load P (kips or kN) and '
PRINT*, ' The yield stress Fy (ksi or MPa).'
PRINT*, ' [If the test load P is not known, enter the ultimate'
PRINT*, ' load from FE analysis or use, say 100]'
PRINT*, '      (Example: 160., 40.)'
PRINT*
READ*, P, FY
PRINT*
PRINT*, ' Enter the Adjusted-Thickness-Ratio Tadj/Tp.'
PRINT*, ' [ (Tadj/Tp) >= 1.0 ]'
PRINT*, ' (Example: 1.15 (To use Default of 1.05, enter 0.))'
PRINT*
READ *, TATP
GO TO 100
END IF

```

* INPUT FROM a DATA FILE

```

PRINT*
IF (QIN.EQ.'f'.OR.QIN.EQ.'f') THEN
PRINT*
PRINT*, '      Enter the name of the INPUT DATA File:'
PRINT*
READ (*, '(A)') FIN
OPEN (UNIT=10, FILE=FIN)
READ(10, *) SPEC, R, NP, N, (ZZ(J), J=1, N), (T(J), J=1, N)
READ(10, *) EX, EY, P, FY, TATP, U
GO TO 100
END IF

```

* INPUT OF SAMPLE DATA IN THIS PROGRAM

```

IF (QIN.EQ.'D'.OR.QIN.EQ.'d') THEN
SPEC = 'P3A-5'
R     = 5.0
NP    = 1

```

```

N      =5
ZZ(1)=0.0
ZZ(2)=0.84
ZZ(3)=2.025
ZZ(4)=3.794
ZZ(5)=5.078
T(1) =0.165
T(2) =0.22
T(3) = .236
T(4) = .372
T(5) =.21
EX    =0.2
EY    =-0.1
P      =245
FY    =40.9
TATP=1.05
U='c'
END IF

```

***** COMPUTATIONS *****

* Check if angles are in Degrees and, if so, convert to Radii.

```

100  IF(ZZ(N).GT.6.3) THEN
      DO 27 J=1,N
27    ZZ(J)=ZZ(J)*PI/180.
      END IF

```

* Check if default value of TATP is to be used.

```

IF (TATP.LT.1.0) TATP=1.05

```

* Check what system of units used and adjust E for S.I.

```

IF (U.EQ.'m'.OR.U.EQ.'M') EE=EE*6.895
      M=N+1
      ZZ(M)=ZZ(1)+2.*PI
      T(M)=T(1)
      ZP=ZZ(NP)
      TP=T(NP)

```

* Computation of all integrals in the I-array

```

DO 10 J=1,M
  Z=ZZ(J)
  I(1,J)=SIN(Z)
  I(2,J)=COS(Z)+Z*SIN(Z)
  I(3,J)=2*Z*COS(Z)+(Z**2-2)*SIN(Z)
  I(4,J)=(Z**3-6*Z)*SIN(Z)+3*(Z*Z-2)*COS(Z)
  I(5,J)=-COS(Z)
  I(6,J)=SIN(Z)-Z*COS(Z)
  I(7,J)=2*Z*SIN(Z)-(Z**2-2)*COS(Z)

```

```

      I(8,J)=3*(Z**2-2)*SIN(Z)-(Z**3-6*Z)*COS(Z)
      I(9,J)=(2*Z+SIN(2*Z))/4
      I(10,J)=(2*Z**2+2*Z*SIN(2.*Z)+COS(2.*Z))/8
      I(11,J)=(2*Z**2-1)*SIN(2.*Z)/8+Z**3/6+Z*COS(2.*Z)/4
      I(12,J)=((Z**4-3*Z**2)+(2*Z**3-3*Z)*SIN(2.*Z)+
+           (6*Z**2-3)*(COS(Z))**2)/8
      I(13,J)=(2*Z**5-10*Z**3+15*Z)/20+(2*Z**4-6*Z**2+3)/8*
+           SIN(2.*Z)+(2*Z**3-3*Z)*(COS(Z))**2/2
      I(14,J)=(2*Z-SIN(2*Z))/4
      I(15,J)=(2*Z**2-2*Z*SIN(2*Z)-COS(2*Z))/8
      I(16,J)=Z**3/6-(2*Z**2-1)*SIN(2*Z)/8-2*COS(2*Z)/4

      I(17,J)=((Z**4+3*Z**2)-(2*Z**3-3*Z)*SIN(2.*Z)-
+           (6*Z**2-3)*(COS(Z))**2)/8
      I(18,J)=(2*Z**5+10*Z**3-15*Z)/20-(2*Z**4-6*Z**2+3)/8*
+           SIN(2.*Z)-(2*Z**3-3*Z)*(COS(Z))**2/2

      I(19,J)=-COS(2*Z)/4
      I(20,J)=(SIN(2*Z)-2*Z*COS(2*Z))/8
      I(21,J)=(2*Z*SIN(2*Z)-(2*Z**2-1)*COS(2*Z))/8
      I(22,J)=((6*Z**2-3)*SIN(2*Z)-(4*Z**3-6*Z)*COS(2*Z))/16
      I(23,J)=((4*Z**3-6*Z)*SIN(2*Z)-(2*Z**4-6*Z**2+3)*COS(2*Z))/8
10  CONTINUE

```

* CROSS-SECTIONAL PROPERTIES wrt CENTER of CIRCLE

* Initialize AR,QX, etc.

```

      AR=0.
      QX=0.
      QY=0.
      IXC=0.
      IYC=0.
      IXYC=0.

```

* Computation of properties, segment by segment

```

      DO 20 J=2,M
          Z1=ZZ(J-1)
          Z2=ZZ(J)
          A=(T(J-1)*Z2-T(J)*Z1)/(Z2-Z1)
          B=(T(J)-T(J-1))/(Z2-Z1)

```

* Computation of Area AR

```

      DAR=(A*(2*R+A)*(Z2-Z1)+B*(R+A)*(Z2**2-Z1**2)
+           +B**2/3*(Z2**3-Z1**3))/2
      AR=AR+DAR

```

* Computation of the static moments Qx and Qy

```

      AQ=A*(2*R+A)**2
      BQ=B*(4*R**2+8*A*R+3*A**2)

```

```

      CQ=B**2*(4*R+3*A)
      DQ=B**3
      DQX=(AQ*(I(1,J)-I(1,J-1))+BQ*(I(2,J)-I(2,J-1))+
+      CQ*(I(3,J)-I(3,J-1))+DQ*(I(4,J)-I(4,J-1)))/4
      DQY=(AQ*(I(5,J)-I(5,J-1))+BQ*(I(6,J)-I(6,J-1))+
+      CQ*(I(7,J)-I(7,J-1))+DQ*(I(8,J)-I(8,J-1)))/4

      QX=QX+DQX
      QY=QY+DQY

```

* Computation of the moments of inertia

```

      R1=R+A
      R2=R+2*A
      R3=2*R+A

      E=A*R3*R3*R3*0.125
      F=B*R2*R3*R3*0.25
      G=R1*R3*B*B*0.75
      H=(R1+R3)*B*B*B*0.25
      I1=B*B*B*B*0.125

      DIX=(E*(I(9,J)-I(9,J-1))+F*(I(10,J)-I(10,J-1))+G*(I(11,J)-
+      I(11,J-1))+H*(I(12,J)-I(12,J-1))+I1*(I(13,J)-I(13,J-1)))
      DIY=(E*(I(14,J)-I(14,J-1))+F*(I(15,J)-I(15,J-1))+G*(I(16,J)-
+      I(16,J-1))+H*(I(17,J)-I(17,J-1))+I1*(I(18,J)-I(18,J-1)))
      DIXY=(E*(I(19,J)-I(19,J-1))+F*(I(20,J)-I(20,J-1))+G*(I(21,J)-
+      I(21,J-1))+H*(I(22,J)-I(22,J-1))+I1*(I(23,J)-I(23,J-1)))

      IXC=IXC+DIX
      IYC=IYC+DIY
      IXYC=IXYC+DIXY

```

20 CONTINUE

* CENTROID and TRANSFORMATION of PROPERTIES to CENTROID

```

      XC=QY/AR
      YC=QX/AR
      IX=IXC-AR*YC**2
      IY=IYC-AR*XC**2
      IXY=IXYC-AR*XC*YC
      PRINT*

```

* Check if the section has constant thickness

```

      TC=T(1)
      DO 30 J=2,N
      IF(ABS(TC-T(J)).GE.5.D-6) GOTO 32

```

```

30  CONTINUE
    WRITE(*,(' NOTE'''' The section has constant thickness. Thus
+ , the moments''/
+ 2X, ''of inertia about any centroidal axis are the same, and''/
+ 2X, ''the product of inertia is equal to zero, Ixy=0.''))
        IMAJ=IX
        IMIN=IX
        ZPA=0.
    PRINT*
    PRINT*
    PAUSE 'Press ENTER to proceed'
    GO TO 50
32  CONTINUE

*   Computation of principal I's from Ix, Iy, Ixy and of Angle ZPA
*   for direction of the Major princ. axis wrt upward y-axis
        W=(IX-IY)/2
        RAD=SQRT(W*W+IXY*IXY)
        IMAJ=(IX+IY)/2+RAD
        IMIN=(IX+IY)/2-RAD
*   Determine the angle of the major principal axis
        ZA=ASIN(IXY/RAD)/2
    IF (IX.GE.IY) THEN
        ZPA=PI/2+ZA
    ELSE IF (IXY.GE.0.) THEN
        ZPA=PI-ZA
    ELSE
        ZPA=-ZA
    END IF
50  CONTINUE

        XCE=XC-EX
        YCE=YC-EY

*   Computation of amplification factor Kp for mid-thickness point Np
*   [Angle=ZZ(NP) at Tmin ]
*   when load acts with eccentricities Ex and Ey wrt to Center C.

        XP=(R+TP/2)*SIN(ZZ(NP))-XC
        YP=(R+TP/2)*COS(ZZ(NP))-YC
        KP=1.-AR*((IX*XCE-IXY*YCE)*XP+(IY*YCE-IXY*XCE)*YP)/(IX*IY-IXY**2)

*   Computation of ANGLE Zm, amplif factor Km and local thickness Tm
*   for the point on outside surface with maximum stress

*   Check if stress is uniform (Km=1.0) and Zm is undefined.

```

```

IF (ABS(XCE)/R.LT.5.D-8.AND.ABS(YCE)/R.LT.5.D-8) THEN
  PRINT*
  WRITE(*,(' NOTE'''' Stresses in the section are uniform and,
+ thus, Km=1.0.''/3X,'ZM is set to ZP and TM=TP to indicate the lo
+ cation''/4X,'of potential local buckling.''))
  KM=1.0
  ZM=ZP
  TM=TP
  PRINT*
  PRINT*
  PAUSE 'Press ENTER to proceed'
  GO TO 60
END IF

CALL MAXKZ(PI,N,AR,IX,IY,IXY,R,XC,YC,XCE,YCE,ZM,KM)

60    CONTINUE

* Comparison of stress at Tmin due to exper ult load, with yield stress
  F=P/AR/FY*KP

* Load to cause first yielding in cross section
  PYLD=AR*FY/KM

* Check if there is a hole (that is t=0.0) in the section and, if so,
* set a flag and bypass computation of Fapi, Fdnv and Papi.
  QH=1
  DO 102 J=1,N
102    IF(T(J).EQ.0.0) QH=0
  IF(QH.EQ.0) GO TO 103

* LOCAL BUCKLING STRESS in PATCH according to API and DNV, and Papi
* Adjusted thickness for buckle wave Tadj and the D/Ta ratio
  TA=TATP*TP
  DT=2*(R/TA+1)

* Critical stress according to API, Fapi/Fy
  IF (DT.LE.60) THEN
    FAPI=1.0
  ELSE
    FAPI=1.64-0.23*(DT**0.25)
  END IF

* Critical stress according to DnV, Fdnv/Fy
  FDNV=1.-(DT*FY*(1.5+DT/1000.)/EE)**2./3.

```

```

*   Ultimate Load Pu for local buckl according to API and DnV
      PAPI=AR*FAPI*FY/KP
      PDNV=PAPI*FDNV/FAP1

103  CONTINUE
*   Comps of Ultimate Load Pprop (PAN) as functn of relat net area AN
*       accord to proposed formula (Eq.15-24)
*
*   Find maximum thickness in section and compute gross area AG.
      TMAX=T(1)
      DO 101 J=2,N
          JMAX=J
          IF (T(J).GE.TMAX) TMAX=T(J)
101  CONTINUE
      AG=PI*(2.*R+TMAX)*TMAX
      AN=AR/AG
*   Pdes according to Eq.15-24
      PDES=(0.18*AN+0.82*AN**3)*AG*FY
*   Ppin according to Eq.15-23a
      PPIN=(0.016143-0.14437*AN+1.128227*AN**3)*AG*FY
      IF (AN.LT.0.65) THEN
          QR=' (Warn,an<0.65)!'
      ELSE
          QR=' (Note,an>=0.65)!'
      END IF

*   Convert angles to degrees for output.
      ZM=ZM*180./PI
      ZPA=ZPA*180./PI

***** OUTPUT *****

      PRINT*
6   PRINT*,'What is the destination of the computed OUTPUT results?'
      PRINT*,'
          To the Screen only <S>'
      PRINT*,' To the Screen and an external FILE for each data set <F>'
      PRINT*,' To Screen and a Cumulative file for many data sets <C>'
      PRINT*
      PRINT*,' Enter the corresponding letter:'
      PRINT*
      READ (*,'(A)') QOUT

      IF (QOUT.NE.'S'.AND.QOUT.NE.'s'.AND.QOUT.NE.'F'.AND.QOUT.NE.'f'
+ .AND.QOUT.NE.'C'.AND.QOUT.NE.'c') THEN
          PRINT*,' YOU ENTERED AN INCORRECT LETTER, PLEASE RE-ENTER'
          GO TO 6

```

END IF

IF (QOUT.EQ.'S'.OR.QOUT.EQ.'s') GO TO 200

* OUTPUT TO AN EXTERNAL FILE

IF (QOUT.EQ.'F'.OR.QOUT.EQ.'f') THEN

PRINT*

PRINT *, ' Enter the name of the OUTPUT File for the results:'

PRINT*

READ (*,'(A)') FOUT

OPEN (UNIT=11,FILE=FOUT)

IF(QH.EQ.0) THEN

* Printout for Specimens with holes

WRITE(11,299)SPEC,R,NP,N,XC,YC,AR,IX,AG,IY,IXY,IMAJ,IMIN,ZPA,KP,

+ ZM,KM,F,P,PYLD,PDES,QR,PPIN,QR,

+ 'Since Tp=0.0(hole),D/Tp,Fapi,Fdnv,Papi and Pdnv are N.A.'

ELSE

* Printout for Specimens without holes

WRITE(11,300)SPEC,R,NP,N,XC,YC,AR,IX,AG,IY,TATP,IXY,IMAJ,IMIN,

+ ZPA,KP,ZM,KM,F,DT,FAP1,FDNV,P,PYLD,PAP1,PDNV,PDES,QR,PPIN,QR

END IF

GO TO 200

END IF

* OUTPUT to a CUMULATIVE file

PRINT*

7 PRINT*,' Is this the first DATA set to Start the Cum file? <S>'
Screen only <S>'

To the

PRINT*,' or an Additional data set to cumulative file? <A>'

PRINT*

PRINT*,' Enter the corresponding letter:'

PRINT*

READ (*,'(A)') QC

IF (QC.NE.'S'.AND.QC.NE.'s'.AND.QC.NE.'A'.AND.QC.NE.'a') THEN

PRINT*,' YOU ENTERED AN INCORRECT LETTER, PLEASE RE-ENTER'

GO TO 7

END IF

IF (QC.EQ.'A'.OR.QC.EQ.'a') GO TO 13

PRINT *, ' Enter the name of the CUM output File:'

PRINT *

READ (*,'(A)') FCOUT

```

OPEN (UNIT=12,FILE=FCOUT)

8 PRINT*
PRINT*, 'SELECT:'
PRINT*, ' L ) LONG format to list Ix, Iy, Kp, etc, and Loads'
PRINT*, '          (Use when I and Load values are expected to be'
PRINT*, '          in the hundreds; usually, for Customary units)'
PRINT*, 'or S ) SHORT format to list only Loads'
PRINT*, '          (Use mainly when I and/or Load values expected
+to'
PRINT*, '          be in the thousands; usually, for SI units.)'
PRINT*
PRINT*, '          Enter L or S'
PRINT*
READ (*, '(A)') QL
IF (QL.NE.'S'.AND.QL.NE.'s'.AND.QL.NE.'L'.AND.QL.NE.'l') THEN
PRINT*, ' YOU ENTERED AN INCORRECT LETTER, PLEASE RE-ENTER'
GO TO 8
END IF

IF (QL.EQ.'L'.OR.QL.EQ.'l') THEN

* Print the heading
350 FORMAT(1X,A9,5X,A5,7X,A2,8X,A2,8X,A3,2(4X,A2),2(4X,A4)/80(' -'))
WRITE(12,350) 'Sct/Spec', 'Area', 'Ix', 'Iy', 'Ixy', 'Kp', 'Km', 'Papi'
+ , 'Pdes'

* CUM OUTPUT file is formatted for Importing to QPro (in Comma & "").

362 FORMAT (1X, ' ', A8, ' ', ' ', F8.4, 3(' ', ' ', F9.4), 2(' ', ' ', F5.3), A7, ' ', ' ', F7.3)
363 FORMAT (1X, ' ', A8, ' ', ' ', F8.4, 3(' ', ' ', F9.4), 2(' ', ' ', F5.3), 2(' ', ' ', F7.3))
IF(QH.EQ.0) THEN
WRITE(12,362)SPEC,AR,IX,IY,IXY,KP,KM,' "N.A." ',PDES
ELSE
WRITE(12,363)SPEC,AR,IX,IY,IXY,KP,KM,PAPI,PDES
END IF
GO TO 200
ELSE

* Print the heading
* Format for Short CUM heading of Short CUM output file
365 FORMAT(1X,A10,6(6X,A5)/80(' -'))
WRITE(12,365) 'Sectn/Spec', 'Ptest', 'Pfyld', ' Papi', ' Pdnv',
+ ' Pdes', ' Ppin'

* CUM OUTPUT file is formatted for Importing to QPro (in Comma & "").

```

```

366  FORMAT (1X,'"',A10,'"',2(',',G10.5),2(A11),2(',',G10.5))
367  FORMAT (1X,'"',A10,'"',6(',',G10.5))
      IF(QH.EQ.0) THEN
          WRITE(12,366)SPEC,P,PYLD,'"N.A."',',','"N.A."',PDES,PPIN
      ELSE
          WRITE(12,367)SPEC,P,PYLD,PAPI,PDNV,PDES,PPIN
      END IF
      GO TO 200
END IF

13  CONTINUE

      IF (QL.EQ.'L'.OR.QL.EQ.'l') THEN
*   Print Additional entry in LONG FORMAT
          PRINT*
          PRINT*,'FCOUT-file is ',FCOUT,' in LONG FORMAT'

          IF(QH.EQ.0) THEN
              WRITE(12,362)SPEC,AR,IX,IY,IXY,KP,KM,'"N.A."',',','"N.A."'
          ELSE
              WRITE(12,363)SPEC,AR,IX,IY,IXY,KP,KM,PAPI,PDNV
          END IF

          ELSE

*   Print Additional entry in SHORT FORMAT
          PRINT*,'FCOUT-file is ',FCOUT,' in SHORT FORMAT'

          IF(QH.EQ.0) THEN
              WRITE(12,366)SPEC,P,PYLD,'"N.A."',',','"N.A."',PDES,PPIN
          ELSE
              WRITE(12,367)SPEC,P,PYLD,PAPI,PDNV,PDES,PPIN
          END IF

          END IF

200      PRINT*

*   FORMAT of printout to screen and indiv file for tubes with holes
299  FORMAT (2X,'Specimen: ',A11,', R=',G12.6,', Np=',I3,
+ ', N=',I3/19X,'Xc= ',F9.5/19X,'Yc= ',F9.5/6X,'A (Net Area)= ',
+ G12.6,T36,'Ix= ',G12.6/6X,'AG(GrossArea)=',G12.6,T36,
+ 'Iy= ',G12.6/8X,'Ta/Tp=1.0 (hole)',T36,'Ixy= ',G12.6/
+ 7X,'Principal Moments of Inertia and the angle to the'//
+ 9X,'major principal axis (CW from upward y-axis)'//
+ 36X,'Imaj=',G12.6/36X,'Imin=',G12.6/36X,'Zmaj=',F9.5//

```

```

+ 7X,'Amplification factor at Tmin=Tp, Kp=' ,F8.5/2X,
+ 'Angle and ampl fact for max stress: Zmax=' ,F10.5,3X,'Kmax=' ,F8.5
+ /2X,'f=(Ptest/A*Kp)/Fy=' ,F5.3//2X,'Test Load=' ,G12.6,' ,Load at fi
+rst yielding Pyl=' ,G12.6/2X, 'Load acc to propos formula, DESIGN
+recomm Pdes=' ,G12.6,A17/2X,'Load acc to propos formula, pinned en
+ds Ppin=' ,G12.6,A17//3X,A60)

* FORMAT of printout to screen and indiv file for tubes w/o holes
300 FORMAT (2X,'Specimen: ',A11,' , R=' ,G12.6,' , Np=' ,I3,
+ ' , N=' ,I3/19X,'Xc= ' ,F9.5/19X,'Yc= ' ,F9.5/4X,'A (Net Area)= ' ,
+ G12.6,T36,'Ix= ' ,G12.6/4X,'AG(GrossArea)=' ,G12.6,T36,'Iy= ' ,
+ G12.6/8X,'Ta/Tp=' ,F8.6,T36,'Ixy= ' ,G12.6/
+ 10X,' Principal Moments of Inertia and the angle to'/
+ 12X,'the major principal axis (CW from upward y-axis)'/
+ 36X,'Imaj=' ,G12.6/36X,'Imin=' ,G12.6/36X,'Zmaj=' ,F9.5/
+ 7X,' Amplification factor at Tmin=Tp, Kp=' ,F8.5/
+ 2X,'Angle and ampl fact for max stress: Zmax=' ,F10.5,3X,'Kmax=' ,
+ F8.5/3X,'f=(Ptest/A*Kp)/Fy=' ,F5.3,' D/Ta=' ,F8.3,' Fapi/Fy=' ,F6.4,
+ ' Fdnv/Fy=' ,F6.4//3X,'Test Load=' ,G12.6/
+ 2X,'Ld for first yielding at pnt of max stress, Pyl=' ,G12.6/
+ 2X,'Load according to API Specification, Papi=' ,G12.6/
+ 2X,'Load according to DnV Specification, Pdnv=' ,G12.6/
+ 2X,'Load acc to propos formula, DESIGN recomm Pdes=' ,G12.6,A17/
+ 2X,'Load acc to propos formula, pinned ends Ppin=' ,G12.6,A17)

* OUTPUT to screen
IF(QH.EQ.0) THEN
* Printout for Specimens with holes
PRINT 299,SPEC,R,NP,N,XC,YC,AR,IX,AG,IY,IXY,IMAJ,IMIN,ZPA,KP,ZM,
+ KM,F,P,PYLD,PDES,QR,PPIN,QR,
+ 'Since Tp=0.0(hole),D/Tp,Fapi,Fdnv,Papi and Pdnv are N.A.'
ELSE
* Printout for Specimens without holes
PRINT 300,SPEC,R,NP,N,XC,YC,AR,IX,AG,IY,TATP,IXY,IMAJ,IMIN,ZPA,
+ KP,ZM,KM,F,DT,FAP,FDNV,P,PYLD,PAPI,PDNV,PDES,QR,PPIN,QR
END IF

PRINT*
15 PRINT*, ' ANOTHER CASE TO ANALYZE? <enter Y or N>'
PRINT*
READ (*, '(A)') QIN
IF (QIN.NE.'Y'.AND.QIN.NE.'y'.AND.QIN.NE.'N'.AND.QIN.NE.'n')
+ THEN
PRINT*, ' You have Entered an INCORRECT LETTER, please RE-ENTER'
GO TO 15
END IF

```

```

IF (QIN.EQ.'Y'.OR.QIN.EQ.'y') THEN
  CLOSE (10)
  CLOSE (11)
  GO TO 3
END IF

END

```

```

***** FUNCT TMZ *****

```

```

FUNCTION TMZ(PI,N,Z)

```

```

* Function TMZ computes the thickness at the angle = Z.

```

```

  IMPLICIT DOUBLE PRECISION (A-Z)
  INTEGER J,M,N
  COMMON T,ZZ
  DIMENSION T(151),ZZ(151)
  M=N+1
  DO 30 J=1,M
30    IF (ZZ(J).GE.Z) GO TO 31
31    CONTINUE
  IF(J.EQ.1) THEN
    ZL=Z+2*PI
    T1=T(N)
    T2=T(M)
    Z1=ZZ(N)
    Z2=ZZ(M)
  ELSE
    ZL=Z
    T1=T(J-1)
    T2=T(J)
    Z1=ZZ(J-1)
    Z2=ZZ(J)
  END IF
  TMZ=T1+(T2-T1)/(Z2-Z1)*(ZL-Z1)
  RETURN
END

```

```

***** SBR MAXKZ *****

```

```

SUBROUTINE MAXKZ(PI,N,AR,IX,IY,IXY,R,XC,YC,XCE,YCE,ZM,KM)

```

```

* SBR MAXKZ determines max KM and ZM by sequential search and parabolic
* interpolation

```

```

  IMPLICIT DOUBLE PRECISION (A-Z)

```

```

        INTEGER J,N,FL
        COMMON T,ZZ
        DIMENSION T(151),ZZ(151)
* The angle increment DZ=0.035 corresponds to approx. 2 degrees
c      DZ=0.01
        DZ=0.02
c      DZ=0.035
* Initialize the variables for computing KM and ZM
        M=N+1
        ZM1=0.
        ZM=0.
        Z3=0.
        KM1=0.
        KM=0.
        K3=0.
DO 10 J=1,N
        PRINT*, ' J=',J
DO 10 Z=ZZ(J),ZZ(J+1),DZ
        TT=TMZ(P1,N,Z)
        X=(R+TT)*SIN(Z)-XC
        Y=(R+TT)*COS(Z)-YC

        K=1.-AR*((IX*XCE-IXY*YCE)*X+(IY*YCE-IXY*XCE)*Y)/(IX*IY-IXY**2)

        IF (J.EQ.1.AND.Z.EQ.ZZ(1)) THEN
                Z2=ZZ(1)
                ZM=Z2
                ZZ1=ZZ(1)+2*PI
                K2=K
                KM=K
                KZ1=K
                FL=1
                GO TO 15
        ENDIF

        IF(K.LT.KM) THEN

                IF(J.EQ.1.AND.Z.EQ.(ZZ(1)+DZ)) THEN
                        Z13=Z+2.*PI
                        K13=K
                ENDIF
                IF(FL.EQ.1) THEN
                        Z3=Z
                        K3=K
                ENDIF
                Z1=Z2

```

```

        Z2=Z
        K1=K2
        K2=K
        FL=0
    ELSE
        ZM1=Z2
        ZM=Z
        Z1=Z2
        Z2=Z
        KM1=K2
        KM=K
        K1=K2
        K2=K
        FL=1
    ENDIF

15    CONTINUE
10    CONTINUE

        IF(KM.EQ.KZ1.AND.ZM.EQ.ZZ(1)) GO TO 20
        IF((ZZ1-ZM).LT.DZ) THEN
            Z3=ZZ1
            K3=KZ1
        ENDIF

* Computation of max K by parabolic interpolation from three points
        X1=ZM1-ZM
        X3=Z3-ZM
        Y1=KM1-KM
        Y3=K3 -KM
        A=KM
        D=X1*X3*(X3-X1)
        B=(Y1*X3*X3-Y3*X1*X1)/D
        C=(X1*Y3-X3*Y1)/D
        XM=-B/(2*C)
        KM=A+B*XM+C*XM*XM
        ZM=ZM+XM
        IF(ABS(ZM-2.*PI).LE.7D-4) ZM=0.0
        IF(ZM.GE.2*PI) ZM=ZM-2*PI

20    CONTINUE
    RETURN
    END

```